Hydrodynamics of gas-liquid flows in Slug Flow regime

Tiago Sotto Mayor Moura Santos

PhD Dissertation in Chemical and Biological Engineering

Supervision

João Bernardo Lares Moreira de Campos
Alexandra Maria Pinheiro da Silva Ferreira Rodrigues Pinto

March, 2007

Abstract

The main goal of the present thesis was the experimental and numerical study of co-current continuous vertical slug flow in Newtonian liquids.

The experimental and numerical studies were enabled by the development of a non-intrusive image analysis technique and a slug flow simulation code, respectively.

The experimental investigation focused on slug flow in 0.032 m and 0.052 m internal diameter columns, for water and aqueous glycerol solutions. The study covered operating conditions leading to the three scenarios possible in slug flow: the fully turbulent and the fully laminar scenarios (in the main liquid and in the near-wake bubble region) and the mix scenario (laminar regime in the main liquid and turbulent regime in the near-wake bubble region). Correlations for bubble motion and interaction were obtained for each scenario.

The aforementioned correlations were used to develop a slug flow simulation code which addresses several features of the slug flow pattern, including the gas expansion along the column. The latter feature has enabled the study of the influence of such phenomenon on the evolution of several flow parameters.

The simulator was used to study the entrance length of slug flow for each of the three scenarios. Ranges of 50-70*D*, 50-80*D* and 70-100*D* were found for the fully turbulent, the mix and the fully laminar scenarios, respectively.

The influence of the superficial gas and liquid velocities on the evolution along the column of bubble velocity, bubble length and liquid slug length was studied thoroughly, for the three scenarios. General expressions are given for the prediction of these parameters as a function of the superficial gas and liquid velocities, column diameter and vertical coordinate along the column.

The influence of the column outlet configuration on the gas expansion rate and gas hold-up in the column was studied via simulation. The expansion rate was found to oscillate over time and to depend on the configuration of the outlet system.

The results reported in this thesis are relevant for the design, optimization and operation of applications containing slug flow in Newtonian liquids.

Sumário

O objectivo principal da presente dissertação foi o estudo experimental e numérico do escoamento vertical em regime de bolhas tubulares, em contínuo e co-corrente, em líquidos Newtonianos.

O estudo experimental e numérico foi possibilitado, respectivamente, pelo desenvolvimento de uma técnica de análise de imagem não intrusiva e de um código de simulação numérica do regime de bolhas tubulares.

A investigação experimental foi levada a cabo em colunas com diâmetro interno de 0,032 m e 0,052 m, para água e soluções aquosas de glicerina. O estudo abrangeu condições de operação conducentes aos três cenários possíveis em regime de bolhas tubulares: os cenários totalmente turbulento ou totalmente laminar (no líquido principal e na região da esteira da bolha) e o cenário misto (regime laminar no líquido principal e regime turbulento na região da esteira da bolha). Para cada um deles foram obtidas correlações para o movimento e interacção das bolhas.

As correlações mencionadas anteriormente foram utilizadas para desenvolver um código de simulação do regime de bolhas tubulares, que considera várias das características do padrão de escoamento, incluindo a expansão da fase gasosa ao longo da coluna. Este facto permitiu estudar a influência da expansão sobre a evolução de vários parâmetros do escoamento.

O simulador foi usado para estudar o comprimento de entrada do regime de bolhas tubulares para cada um dos três cenários. Obtiveram-se, respectivamente, comprimentos de entrada de 50-70D, 50-80D e 70-100D para os cenários totalmente turbulento, misto e totalmente laminar.

Para cada cenário foi estudada a influência das velocidades superficiais de gás e de líquido sobre a variação da velocidade das bolhas, comprimento das bolhas e distância entre as mesmas, ao longo da coluna. Apresentam-se expressões gerais para a previsão destes parâmetros em função das velocidades superficiais de gás e de líquido, do diâmetro da coluna e da coordenada vertical ao longo da mesma.

Usando o simulador, estudou-se a influência do sistema de saída (no topo da coluna) sobre a taxa de expansão da fase gasosa e sobre a retenção de gás dentro da coluna. Verificou-se que a taxa de expansão oscila ao longo do tempo e depende da configuração do sistema de saída.

Os resultados apresentados nesta tese são relevantes para o dimensionamento, optimização e operação de sistemas envolvendo escoamento em regime de bolhas tubulares, em líquidos Newtonianos.

Résumé

L'objectif principal de cette thèse était l'étude expérimentale et numérique de l'écoulement vertical continu et co-courant de bulles de Taylor dans des liquides Newtoniens.

Les études expérimentales et numériques ont été permises par le développement d'une technique non-intrusive d'analyse d'image et d'un code de simulation (d'écoulement de bulles de Taylor), respectivement.

La recherche expérimentale s'est concentrée sur l'écoulement de bulles de Taylor dans les colonnes de diamètre interne de 0.032 m et de 0.052 m, en utilisant de l'eau et des solutions aqueuses de glycérol. L'étude a couvert des conditions de fonctionnement menant aux trois scénarios possibles dans l'écoulement de bulles de Taylor: les scénarios entièrement turbulent et entièrement laminaire (dans le liquide principal et dans le sillage de la bulle) et le *mix* scénario (régime laminaire dans le liquide principal et régime turbulent dan le sillage de la bulle). Des corrélations pour le mouvement et l'interaction entre bulles ont été obtenues pour chaque scénario. Ces corrélations ont été employées pour développer un code de simulation pour l'écoulement de bulles de Taylor qui adresse plusieurs phénomènes caractéristiques de cet écoulement diphasique, y compris l'expansion du gaz tout au long de la colonne qui a permis l'étude de l'influence de ce phénomène sur l'évolution de plusieurs paramètres d'écoulement.

Le simulateur a été utilisé pour étudier la longueur d'entrée de l'écoulement de bulles de Taylor pour chacun des trois scénarios. Des gammes de 50-70D, de 50-80D et de 70-100D ont été trouvées pour les scénarios entièrement turbulent, *mix* et entièrement laminaire, respectivement. L'influence de la vitesse superficiel du gaz et du liquide sur l'évolution au long de la colonne de la vitesse des bulles, de la longueur des bulles et de la distance entre bulles ont été étudiées, pour les trois scénarios. Des expressions générales sont données pour la prévision de ces paramètres en fonction des vitesses du gaz et du liquide, du diamètre de la colonne et de la coordonnée verticale tout au long de la colonne.

L'influence de la configuration de sortie de la colonne sur le taux d'expansion de gaz et sur la rétention de gaz dans la colonne a été étudiée en utilisant le simulateur. Les résultats obtenus montrent que le taux d'expansion oscille avec le temps et dépend de la configuration du système de sortie.

Les résultats présentés dans ce travail sont déterminants pour la conception, l'optimisation et l'opération de plusieurs applications concernant l'écoulement de bulles de Taylor à travers des liquides Newtoniens.

à Inês

aos meus pais

à minha irmã

Acknowledgments

During the four-year research period I have contacted, interacted and learned with so many people that it is impossible to mention them all. I would like, though, to single out a few to whom I feel especially grateful for they have helped me grow both professionally and personally. For all the others, my sincere thank you.

I would like to express my deep gratitude to my supervisors Professor João Campos and Professor Alexandra Pinto for suggesting this work to me and for their encouraging support and guidance during the last four years. It was an honour and a pleasure to work and to learn with them.

I thank my colleague Victor Ferreira for the help during the experimental work. He was of a tremendous assistance in 'mastering' and 'controlling' the seven-metre high experimental facility.

I wish to thank all my friends and colleagues at FEUP for the companionship, fruitful discussions and… memorable laughter.

I am grateful to my family for being always present, tolerant and understanding, in all stressful periods, particularly during the preparation and writing of the thesis.

And last, but definitely not least, I am truly indebted to Inês for her unconditional love, support and encouragement throughout the last five years. Her smile is an inspirational force.

This work was supported by Fundação para a Ciência e a Tecnologia with fellowship SFRH/BD/11105/2002.

Thesis layout

This thesis is organized into six Chapters and three Appendixes, most of which are based on scientific papers prepared by the author as a result of his research work (Chapters 2-5 and Appendixes A-C). The content of each of these Chapters/Appendixes is given in brief below.

Chapter 1 describes the previous contributions to the research on slug flow. From the motion of one Taylor bubble to the interaction between consecutive Taylor bubbles, a review of the main findings and eventual shortcomings is presented.

Chapter 2 focuses on experimental study of the hydrodynamics of gas-liquid vertical slug flow in turbulent regime, using a non-intrusive image analysis technique developed for the purpose.

Chapter 3 presents a simulation study on turbulent slug flow, based on a slug flow simulator developed by building on the bubble motion/interaction correlations described in Chapter 2.

The image analysis technique and the slug flow simulator mentioned in Chapters 2 and 3, respectively, were used to experimentally and numerically study the hydrodynamics of vertical slug flow in laminar regime. Chapter 4 presents the corresponding approach and findings.

Chapter 5 describes an approach that follows a similar strategy, but focuses on the characteristics of slug flow in operating conditions leading to turbulent regime in the bubble wake and laminar regime in the main liquid (a mix scenario). A comparison with the fully turbulent and fully laminar regime data is presented.

Chapter 6 summarizes the main conclusions of the work and provides some suggestions for future work.

Appendix A presents a study on the gas expansion and gas hold-up along vertical slugging columns for different column outlet configurations.

Appendix B examines the uncertainty associated with the study of slug flow pattern characteristics, using the proposed image analysis technique.

Appendix C provides a discussion on the advantages of the use of simulation tools such as the proposed slug flow simulator for educational purposes.

The scientific papers that constitute the majority of the Chapters/Appendixes of this thesis were submitted to peer-reviewed Journals during the last stage of the four-year research period. For this reason, there was a need to include brief descriptions of simulator assumptions and approaches in some of the later papers (e.g. Chapters 4, 5 and Appendix A), which are better and

more thoroughly described in Chapter 3. Although leading to a slight overlap, the inclusion of this information is aimed at providing an easier understanding of the global approach pursued in each of the papers individually, as well as to address some of the reviewers' suggestions and requests.

Contents

List of Figures

List of Tables

1 Introduction

This Chapter presents a review of the research on Slug flow, emphasizing the main findings and eventual shortcomings. At the end of the Chapter, the main contributions of the present work are highlighted.

1.1 Two-phase flow patterns in vertical pipes

Gas and liquids flowing through pipes display several temporal and spatial characteristics/distributions that are often referred to as flow patterns. Examples of flow patterns occurring for increasing ratios of gas/liquid flow rates are: Bubble, Slug, Churn and Annular flows. A schematic representation of these flow patterns is shown in Figure 1.1.

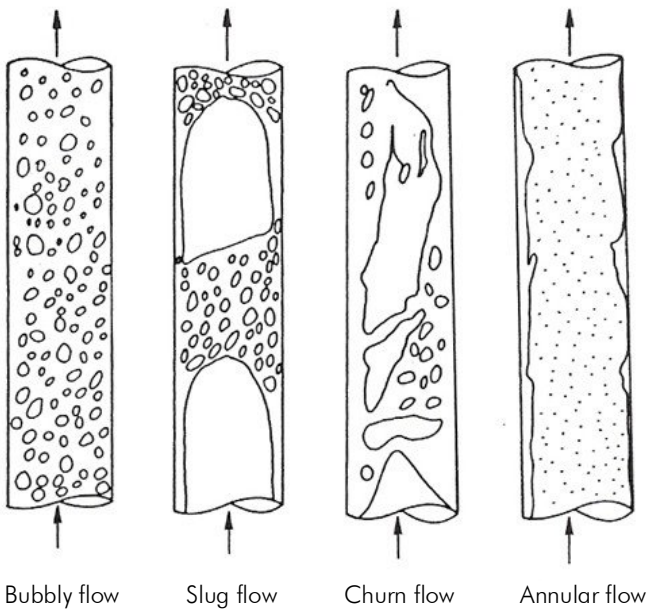

Figure 1.1 – Main two-phase flow patterns for increasing ratios of gas/liquid flow rates (left to right); image taken from Taitel et al. (1980)

Bubbly flow occurs for low gas and liquid flow rates and is characterised by a continuous liquid phase spread with a spread of small gas bubbles. These are only few millimetres in diameter and quite uniformly distributed. As gas flow rate increases, bubbles start to randomly collide and coalesce, forming a number of somewhat larger individual bubbles. These feature spherical caps similar to those of slug flow Taylor bubbles (after G.I. Taylor, as in Davies and Taylor (1950)), but they still have dimensions smaller than the pipe internal diameter (ID). With further increases in the gas flow rate, a point is reached where the dispersed bubbles become so closely packed that the rate of collision and agglomeration increases sharply. Taitel et al. (1980) mentions a figure of 0.25 for this critical void fraction (bubble volume fraction), based on the assumption of a maximum distance between bubbles of approximately half of their radius. The generalised agglomeration of bubbles marks the onset of the Slug flow pattern.

In Slug flow, most of the gas is located in large bullet-shaped bubbles which occupy most of the pipe cross-sectional area. These are the aforementioned Taylor bubbles. The liquid between Taylor bubbles is known as the liquid slug. Expressions like Plug or Piston flow have also been used while referring to Slug flow, namely for low flow rates where the gas-liquid boundaries are very well-defined. In general, liquid slugs are of a more or less aerated nature.

As gas flow rate increases, Taylor bubbles elongate and accelerate. The aeration level of the liquid slugs increases up to a point where its structure becomes less defined. Bubble shape is no longer stable with lumps of liquid being pushed back and forth continuously. The flow becomes chaotic, frothy and disordered. This oscillating flow pattern is referred to as Churn flow.

Further increases in the gas flow rate results in the onset of the Annular flow. The gas phase continuum moves along the pipe core and the liquid phase moves upward, partly as wavy liquid films and partially in the form of drops entrained in the gas core. This flow pattern has also been referred to as wispy-annular, namely when large lumps or “wisps” of liquid are entrained in the gas phase.

1.2 Vertical Slug flow

Slug flow is a complex and intermittent two-phase flow pattern which can be found in several industrial applications such as air-lifts, nuclear and chemical reactors, geothermal power plants, membrane and crystallisation processes, hydrocarbon production and transportation and even in natural volcanic phenomena such as at Stromboli volcano.

Figure 1.2 represents an instant in the motion of Taylor bubbles through a stagnant or flowing liquid. As bubbles move upward, the liquid is forced to flow around them in a thin annular film, whose weight is totally supported by the shear forces at the column wall (a free-falling film).

As the liquid film drains past the tail of the Taylor bubble it penetrates the liquid slug creating a relatively confined flow, the bubble wake, with forms varying from a closed well-defined recirculation region to an open random-like circulation region (laminar and turbulent wakes, respectively). The entrainment of small gas bubbles at the Taylor bubble wake contributes to the more or less aerated nature of the liquid slug region.

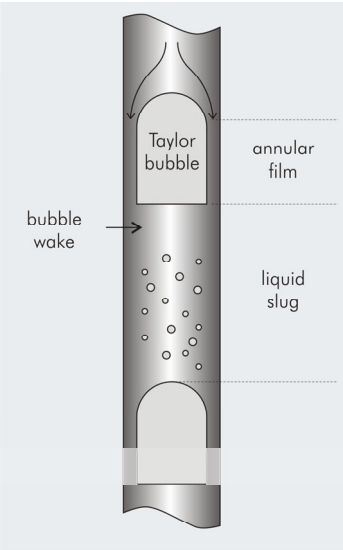

Figure 1.2 – Schematic representation of Slug Flow

Slug flow pattern has often been addressed on the basis of the "unit cell" concept, developed by Fernandes et al. (1983) for vertical slug flow. The intrinsically complex structure of such flow is taken as a series of unit cells, each consisting of a Taylor bubble and the liquid slug below, rising along the column at different velocities. Following on from this idea, the slug flow pattern is said to be undeveloped when there is relative motion between consecutive unit cells (i.e. Taylor bubbles interacting, approaching and eventually coalescing). This condition is associated with strong changes in the flow pattern characteristics (e.g. bubble lengths, velocities and frequency). As the distance between consecutive bubbles escalates, the relative motions dissipate and the flow reaches its fully developed condition. The work reported here focuses on undeveloped Slug flow.

The successful operation, simulation and optimisation of industrial applications containing Slug flow greatly depends on the knowledge one has about the relevant flow pattern regimes (in the main liquid and in the bubble wake region), the governing correlations (for bubble motion and interaction) and the flow pattern characteristics. The following sections describe the main contributions to the development of knowledge on these issues.

1.3 Rise of Taylor bubbles in stagnant liquids

Dumitrescu (1943) and Davies and Taylor (1950) were the first to treat theoretically the rise of a Taylor bubble in a vertical tube containing a stagnant ideal fluid (i.e one without viscosity or surface tension). Using potential flow theory, both researchers concluded that the dimensionless group $U_\infty/\sqrt{gD}$ (known as the *Froude* number, after William Froude) has a constant value. In that ratio, U_∞ stands for the terminal upward velocity of the bubble in a column of diameter D and g denotes the acceleration of gravity. Dumitrescu (1943) obtained a figure of 0.351 and Davies and Taylor (1950) a figure of 0.328, although using a more severe truncation of the series equations arising in the solutions. Other researchers (e.g. Nicklin et al. (1962b)) argued that the solution of Davies and Taylor was not unique but tended to the limiting value of 0.346. The validity of these estimates does not extend, however, for high viscosity liquids (as found experimentally by Brown (1965)). For that scenario, the findings of other researchers such as those of White and Beardmore (1962) should be considered. In an extensive experimental investigation, these researchers addressed the rise of air Taylor bubbles in several different liquids and for a wide range of properties. They concluded that three dimensionless numbers can be used to correlate the Taylor bubble velocity. These are the *Froude* number, the *Eötvös* number (after Loránd *Eötvös*) and the *Morton* number. Their definitions are given in Table 1.1.

Table 1.1 – Dimensionless groups definitions

Dimensionless group	Symbol	Definition[1]	Representation
Froude number	*Fr*	$\frac{U_\infty}{\sqrt{gD}}$	Inertia vs. gravity forces
Eötvös number	*Eo*	$\frac{\rho g D^2}{\sigma}$	Buoyancy vs interfacial forces
Morton number	*Mo*	$\frac{g\mu^4}{\rho\sigma^3}$	Viscosity vs. surface tension

Depending on the relevance of the several types of forces involved, different forms of correlations were expected:

1) where viscous, inertial and interfacial forces are relevant: $Fr = \phi(Eo, Mo)$
2) where viscous forces are unimportant: $Fr = \phi(Eo)$
3) where interfacial forces are unimportant: $Fr = \phi(Eo^3/Mo)$
4) where both viscous and interfacial forces are unimportant: Fr = constant.

[1] In the definitions of the *Eötvös* and *Morton* numbers, the density of the gas is considered much smaller than that of the liquid. Furthermore, this simplification is considered throughout the whole chapter.

The results of the work of White and Beardmore (1962) are condensed in the chart of Figure 1.3.

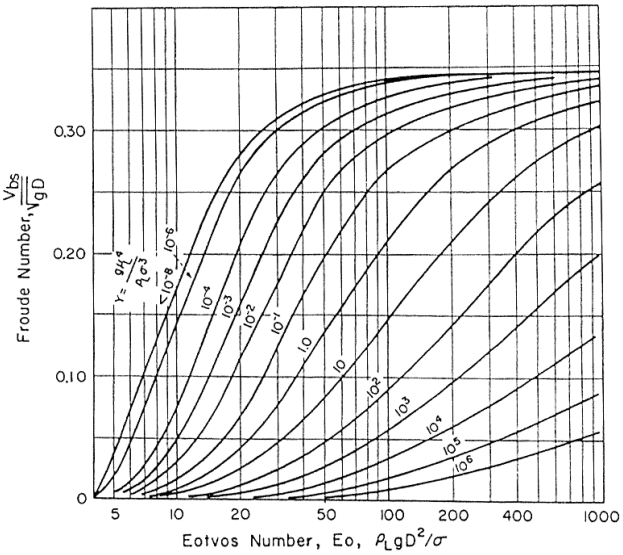

Figure 1.3 – *Froude* number as a function of *Eotvos* and *Morton* numbers (taken from White and Beardmore (1962))

An alternative empirical correlation for the dimensionless bubble rise velocity (or *Froude* number) was proposed by Wallis (1969) for the full range of viscous, inertial and interfacial forces shown in Figure 1.3:

$$Fr=0.345\left[1\text{-}\exp\left(-\frac{0.01N_f}{0.345}\right)\right]\left[1\text{-}\exp\left(\frac{3.37\text{-}Eo}{m}\right)\right] \tag{1.1}$$

where N_f is the dimensionless inverse viscosity,

$$N_f=\left(\frac{Eo^3}{Mo}\right)^{1/4}=\frac{\rho\left(gD^3\right)^{1/2}}{\mu} \tag{1.2}$$

and m a parameter dependent on the value of N_f:

$N_f < 18$	=>	$m = 25$
$18 < N_f < 250$	=>	$m = 69N_f^{-0.35}$
$N_f > 250$	=>	$m = 10$

More recently, Viana et al. (2003) proposed yet another expression to compute the dimensionless bubble rise velocity. Using a set of power laws in *Eo*, the authors obtained a

universal correlation based on all experimental data previously published. This correlation has been shown to perform well for most experimental results.

The theoretical works of Dumitrescu (1943) and Davies and Taylor (1950) mentioned at the beginning of this section fall on the fourth scenario of White and Beardmore results (item 4). This scenario, often referred to as the inertia-controlled regime, occurs, according to White and Beardmore (1962), when $Eo > 70$ and $\sqrt{Eo^3/Mo} > 3 \times 10^5$ ($N_f > 550$). Wallis (1969) refers to slightly different limits namely $Eo > 100$ and $N_f > 300$.

For inertia-controlled regime, the *Froude* number equals 0.345 and the rise velocity of a Taylor bubble (the drift velocity) can be calculated as:

$$U_\infty = 0.345\sqrt{gD} \tag{1.3}$$

Several other experimental and simulation studies on this asymptotic regime provide very similar estimates of dimensionless bubble rise velocity (Nicklin et al. (1962b), Zukoski (1966), Mao and Dukler (1991)).

Most results presented in this work fall on the inertia-controlled regime (limits after White and Beardmore (1962)). The exception is the fully laminar regime results, with the more viscous solution, for which the *Froude* number was obtained using the correlations of Figure 1.3.

Although beyond the scope of the present work, other studies are worthy of mention for their contribution to the understanding of the effects of surface tension, viscosity and inclination angle on the motion of Taylor bubbles. These are Zukoski (1966), Bendiksen (1984), Nickens and Yannitell (1987) and Campos (1991).

1.4 Rise of Taylor bubbles in flowing liquids

The motion of Taylor bubbles in a flowing liquid depends on the velocity of the liquid flowing upstream as well as on the rise due to buoyancy. Nicklin et al. (1962b) conducted experimental work on the motion of individual air bubbles in co-current flowing water and suggested the following expression for bubble rise velocity (U_B):

$$U_B = U_\infty + CU_L \tag{1.4}$$

where U_L is the superficial liquid velocity and C an empirical parameter depending on the flow regime in the liquid. The authors reported $C \approx 1.2$ for fully established turbulent flow (Reynolds numbers higher than 8000), suggesting that the bubble follows the maximum liquid velocity ahead of it. Bendiksen (1984) conducted experiments on the motion of Taylor bubbles in inclined tubes

and confirmed C≈1.2 for turbulent flow (vertical tube; Reynolds numbers in the range 6000-104000). Polonsky et al. (1999a) obtained the same figure for Reynolds numbers in the range 2300-6300.

Collins et al. (1978b) presented theoretical predictions for U_B for both turbulent and laminar velocity profiles of the form:

$$U_B = U_C + (gD)^{\frac{1}{2}} \varnothing \left\{ \frac{U_C}{(gD)^{\frac{1}{2}}} \right\} \tag{1.5}$$

where U_C is the liquid velocity at the centreline (axis of the tube) and $\varnothing$ is a functional relationship. For turbulent velocity profile in the liquid, Collins obtained:

$$U_B = U_L \left[\frac{\ln Re_{U_L} + 0.089}{\ln Re_{U_L} - 0.74} \right] + 0.347 (gD)^{\frac{1}{2}} \varnothing \left\{ \frac{U_L}{(gD)^{\frac{1}{2}}} \frac{1.81}{\ln Re_{U_L} - 0.74} \right\} \tag{1.6}$$

in which the coefficient of U_L expresses the dependence of U_C / U_L on Re_{U_L}. The experimental results of Nicklin et al. (1962b) for turbulent regime (Eq. (1.4) with C=1.2) are in good agreement with the previous equation (when considering the relevant operating conditions). For laminar velocity profile in the liquid, Collins obtained:

$$U_B = 2U_L + 0.347 (gD)^{\frac{1}{2}} \varnothing \left\{ \frac{2.39 U_L}{(gD)^{\frac{1}{2}}} \right\} \tag{1.7}$$

Eq. (1.7) was found to be in good agreement with experimental data from the authors only when the parabolic (laminar) velocity profile in the liquid was fully established, i.e. when the experimental data was free from entrance effects. Recall that the column length along which these effects can be observed is proportional to the Reynolds number, the constant of proportionality being variously quoted as 0.028 (experimental, Govier and Aziz (1972)) and 0.06 (theoretical, White (1999)). Later on, Mao and Dukler (1991) reported simulation work whose results represent remarkably well the Collins' laminar flow data, provided that a laminar velocity profile is enforced in the simulation algorithm. For these operating conditions a figure of 1.89 was obtained for the empirical parameter C (in Eq. (1.4)). Polonsky et al. (1999a) obtained a figure of 1.86 for a Reynolds number of 220.

There are some doubts, however, regarding the Reynolds numbers at which the transition in bubble rise velocity occurs. Fréchou (1986) reports experimental results (Figure 1.4) showing that the empirical parameter C starts decreasing for Reynolds numbers much lower than 2100, the characteristic Reynolds number for the onset of transition in the flow regime.

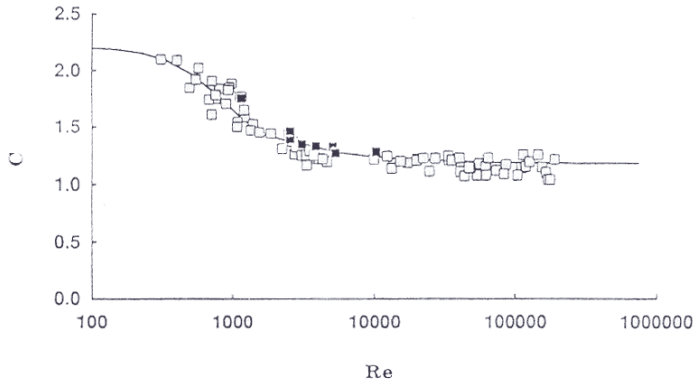

Figure 1.4 – Experimental values of empirical parameter C plotted against the mixture Reynolds (figure taken from Fabre and Liné (1992b)); correlation of Fréchou (1986): solid line; experiments of Fréchou (1986): open squares; numerical simulations of Mao and Dukler (1991): solid squares

Pinto et al. (2005) report a study on the motion of individual bubbles in liquids of low to moderate viscosities (0.002-0.0065 Pa s), in which laminar velocity profiles ahead of the bubbles were observed for Reynolds numbers in the liquid (based in U_L) lower than 2100, and the bubble rise velocities were, still, lower than expected (Eq. (1.4) with C=2). The authors reported decreasing Reynolds numbers for the onset of transition in bubble velocity as increasingly viscous solutions were considered, and therefore argued that the parameter C is not a unique function of Re_{U_L}. They still observed that a single curve was obtained when plotting the parameter C against $Re_{U_L} We_{U_\infty}^{0.21} \left(U_L/U_\infty\right)^{0.28}$, as shown in Figure 1.5.

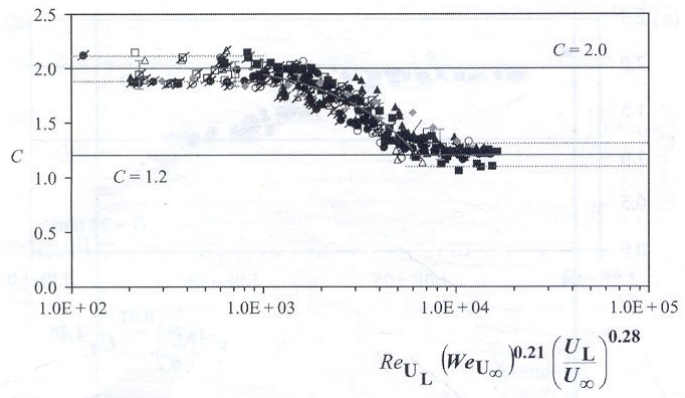

Figure 1.5 – Experimental values of empirical parameter C plotted against $Re_{U_L} We_{U_\infty}^{0.21} \left(U_L/U_\infty\right)^{0.28}$ (figure taken from Pinto et al. (2005))

The representation is only applicable, however, for a short range of liquid viscosities. Fabre and Liné (1992b) argue, for instance, that it is likely that the occurrence of turbulence in the liquid slugs is dependent on the turbulence in the falling film as well on the length of the slugs. This thus remains as an open issue.

1.5 Flow field around the Taylor bubbles

Consider the motion of a Taylor bubble through a stagnant liquid. In a moving reference frame (one attached to the bubble), the liquid ahead of the bubble is "seen" flowing downward at a given velocity. As the liquid approaches the bubble nose, the axial and radial components of the velocity start to change. The fluid elements flowing along the axis slowdown as they reach the nose of the bubble, the stagnation point (where velocity is null). The remaining elements develop a radial velocity as they move away from the pipe centreline to detour the bubble.

Brown (1965) suggested the flow around a Taylor bubble should be divided into two zones: one near its nose and another further below (see Figure 1.6).

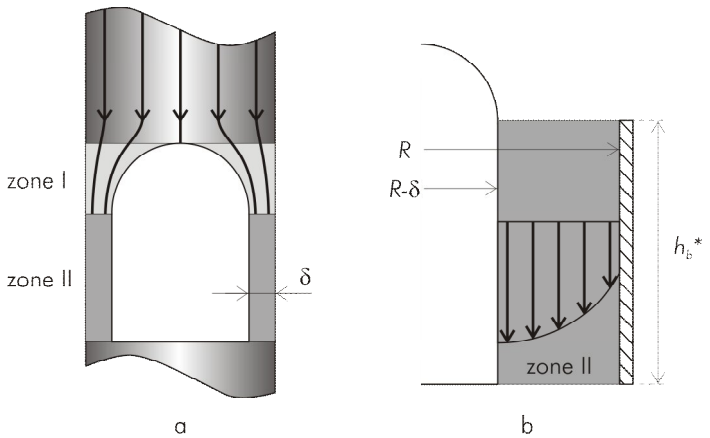

Figure 1.6 – Zones I and II of the liquid flow around a Taylor bubble (in a moving reference frame)

In the first zone (zone I in Figure 1.6a), the thickness of the liquid film decreases as the fluid elements accelerate. The shear stress at the column wall starts to induce a velocity gradient in the adjoining fluid elements. The growing boundary layer is, however, still very thin and thus the velocity profiles in the liquid are mainly affected by the pressure field induced by the bubble (an isobaric region since the gas density is negligible when compared to the liquid's). As the axial distance from the bubble nose increases, the boundary layer thickens and the velocity profiles become increasingly affected by the viscosity forces. This process continues until the boundary layer reaches the gas-liquid interface, at which point the liquid film stabilises in its minimum thickness (δ). This marks the onset of zone II (Figure 1.6b). From this point onward, the velocity profile in the

liquid is fully developed and the film is said to be in a free-falling condition. Its weight is totally supported by the shear stress at the wall and the film can be considered, as the gas bubble, an approximately isobaric region.

In order to obtain the velocity profile in the stabilised liquid film, Brown (1965) performed a balance between gravitational and shear stress forces acting on an infinitesimal cylindrical film element (see Figure 1.7), for a fixed reference frame:

$$\tau_{r+\delta r} S_{r+\delta r} h_b^* - \tau_r S_r h_b^* - \rho g v_{\delta r} h_b^* = 0 \tag{1.8}$$

where h_b^* is the length of the stabilised liquid film, τ_r is the shear stress at the radial coordinate *r*, S_r is the surface (lateral) area of a cylinder with radius *r* and *v* is the volume of the infinitesimal cylindrical (annular) film element. By further substitution of *S* and *v*, one obtains:

$$\tau_{r+\delta r} 2\pi (r+\delta r) h_b^* - \tau_r 2\pi r h_b^* - \rho g 2\pi r \delta r h_b^* = 0 \tag{1.9}$$

which, by simplification and when $\delta r \to 0$, reduces to:

$$\frac{\partial(\tau r)}{\partial r} - \rho g r = 0 \tag{1.10}$$

Integrating the previous equation for the film region (from the bubble interface, $r=R-\delta$, to a general radial coordinate, *r*) one obtains:

$$\tau = \frac{\rho g}{2}\left[r - \frac{(R-\delta)^2}{r} \right] \tag{1.11}$$

For a Newtonian fluid in laminar flow

$$\tau = \mu \left| \frac{du}{dr} \right| \tag{1.12}$$

where *u* is the liquid velocity in the annular film and μ the liquid dynamic viscosity. Thus, by substitution of τ in Eq. (1.11) according to Eq. (1.12), and integrating for the film region (from the wall, where $r=R$ and $u=0$, to a general radial coordinate *r*), one obtains an expression for the velocity profile in the liquid film:

$$u = \frac{\rho g}{\mu}\left[\frac{R^2 - r^2}{4} - \frac{(R-\delta)^2}{2}\ln\frac{R}{r}\right] \tag{1.13}$$

Now, integrating the previous equation along the flow cross-section, S_δ, as $u_\delta = \int u dS_\delta / S_\delta$, one obtains an expression to compute the average velocity in the liquid film, in a fixed reference frame:

$$u_\delta = \frac{\rho g}{\mu}\left(\frac{R^4}{R^2 - (R-\delta)^2}\right)\left[\frac{2}{3}\left(\frac{\delta}{R}\right)^3\left(1-\frac{\delta}{R}\right) + \frac{1}{10}\left(\frac{\delta}{R}\right)^5 + \frac{1}{60}\left(\frac{\delta}{R}\right)^6 + \ldots\right] \tag{1.14}$$

Notice that the previous equations are valid for both stagnant and flowing (upward) liquid conditions (U_L=0 or U_L>0, respectively).

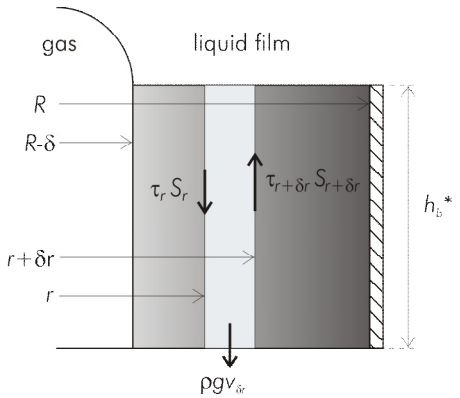

Figure 1.7 – Force balance in an infinitesimal cylindrical element of fluid in the fully developed annular film

Let us now consider the general scenario depicted in Figure 1.8 of a Taylor bubble moving upwards with velocity U_B, in a liquid flowing with velocity U_M (average superficial mixture velocity, i.e. U_L+U_G). Note in particular the average velocity patterns at the planes A and B, i.e. ahead of Taylor bubble and in the fully developed annular film, respectively. In a moving reference frame (Figure 1.8b), the liquid ahead of the bubble (at plane A) moves downward with velocity U_B - U_M, whereas the liquid in the annular film (at plane B) moves downward with velocity $U_B + u_\delta$. Flow continuity requires consistency between the liquid flow rates at planes A and B, thus, one can write:

$$\pi R^2 (U_B - U_M) = \pi\left[R^2 - (R-\delta)^2\right](U_B + u_\delta) \tag{1.15}$$

where πR^2 and $\pi\left[R^2 - (R-\delta)^2\right]$ are the column and annular film cross-sectional area, respectively. Now, by substitution of u_δ in Eq. (1.15) according to Eq. (1.14), one obtains an expression relating the upward bubble velocity (U_B) with the average superficial mixture velocity (U_M) and the thickness of the annular liquid film (δ), as follows:

$$U_B = \frac{\rho g}{\mu}\frac{R^2}{(1-\delta/R)^2}\left[\frac{2}{3}\left(\frac{\delta}{R}\right)^3\left(1-\frac{\delta}{R}\right)+\frac{1}{10}\left(\frac{\delta}{R}\right)^5+\frac{1}{60}\left(\frac{\delta}{R}\right)^6+\ldots\right]+\frac{U_M}{(1-\delta/R)^2} \tag{1.16}$$

After some algebraic transformation this equation yields:

$$\frac{\delta}{R} = \left\{\left(\frac{\mu}{\rho g R^2}\left[(1-\delta/R)^2 U_B - U_M\right]-\frac{1}{10}\left(\frac{\delta}{R}\right)^5-\frac{1}{60}\left(\frac{\delta}{R}\right)^6-\ldots\right)\frac{3}{2(1-\delta/R)}\right\}^{1/3} \tag{1.17}$$

an expression that allows to predict δ given U_B and U_M. Note that, for individual Taylor bubbles flowing through stagnant liquid (U_G=U_L=U_M=0), Eq. (1.17) reduces to the expression obtained by Brown (1965). An approximated version of Eq. (1.17) can be obtained by neglecting the fifth and higher power terms of δ/R, yielding:

$$\frac{\delta}{R} = \left\{\frac{3\nu}{2g(R-\delta)}\left[(R-\delta)^2 U_B - R^2 U_M\right]\right\}^{1/3} \tag{1.18}$$

where ν is the kinematic viscosity. Note that following on from the assumptions for deriving it, this equation is valid only for fully laminar flow in the annular film.

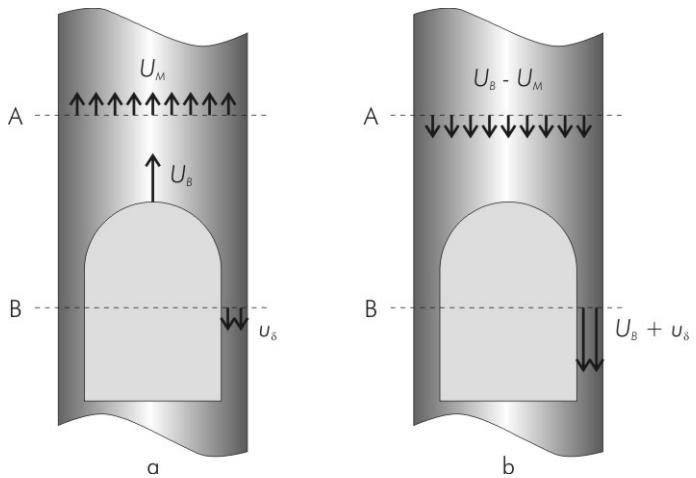

Figure 1.8 – Average velocity patterns in the liquid at planes A and B, (a) in a fixed reference frame and (b) in a moving reference frame

The problem of fully turbulent flow in thin liquid films has not been frequently addressed in the literature, probably because of the great complexity of the flow processes involved. Nearly all treatments of turbulent film flow build on the assumption that the film can be regarded as smooth,

and that some form of the dimensionless velocity profile valid for single-phase flow (pipe flow) can be applied to the flow of films. For instance, Dukler and Bergelin (1952) used the universal velocity profile equations of Nikuradse (1933):

$$u^+ = y^+ \qquad 0 \le y^+ \le 5 \quad \text{(laminar sublayer)} \tag{1.19}$$

$$u^+ = -3.05 + 5.0 \ln y^+ \qquad 5 < y^+ \le 30 \quad \text{(buffer layer)} \tag{1.20}$$

$$u^+ = 5.5 + 2.5 \ln y^+ \qquad 30 < y^+ \le b^+ \quad \text{(turbulent zone)} \tag{1.21}$$

where $u^+ \left(= u/u^*\right)$ is the dimensionless velocity, $y^+ \left(= yu^*/\upsilon\right)$ is the dimensionless distance from the wall, $b^+ \left(= \delta u^*/\upsilon\right)$ is the dimensionless film thickness, $u^* \left(= \sqrt{\tau_w/\rho}\right)$ is the friction velocity and τ_w is the shear stress at the column wall (Eq. (1.11) with r=R). Dukler and Bergelin integrated the dimensionless velocities over the film thickness and obtained, for turbulent flow ($b^+ > 30$)

$$Re_{u_\delta} = b^+ \left(3.0 + 2.5 \ln b^+\right) - 64 \tag{1.22}$$

where Re_{u_δ} is the Reynolds number based on the average velocity in the liquid film in a fixed reference frame, u_δ (retrieved from Eq. (1.15)), and on the film thickness, δ, i.e.:

$$Re_{u_\delta} = \frac{\rho u_\delta \delta}{\mu} \tag{1.23}$$

This expression follows that used for a liquid flowing in a wetted wall column, a scenario very similar to the free-falling annular film. Hence, knowing all physical properties required to define b^+, Eq. (1.22) allows to compute δ for any value of Re_{u_δ}, for turbulent flow conditions. However, in a recent study using Particle Image Velocimetry (a non-intrusive technique), Nogueira et al. (2006a) report liquid film thicknesses for Taylor bubbles flowing through water, clearly smaller than those predicted by Eq. (1.22) (error about 30%), thus casting doubt on the applicability of such predictions.

In a review paper on the flow in thin films, Fulford (1964) presents the results of several researchers regarding the critical Reynolds numbers (Re_{u_δ}) for the onset of turbulence in the films. Several of these researchers mention an upper and lower critical values, enclosing a transition region. The bulk of evidence seems to support a lower value in the region of 250-400, and a less well-marked upper value of about 800. These ranges are wide, supporting the idea that the transition to turbulence in the films is a gradual and complex process, one that might be affected, for instance, by small interface oscillations in the liquid film or by column surface irregularities.

The experimental work developed in this thesis covered both laminar and turbulent film conditions (experiments with viscous solutions and water, respectively). For the experiments leading to laminar films, the film thickness was predicted using Eq. (1.18). For the experiments leading to turbulent films, the findings of Nogueira et al. (2006a) (for Re_{υ_δ} similar to those of the experiments reported here, i.e.1400 and 1500-1700, respectively) advise caution in the use of Eq. (1.22) to predict δ. Indeed, for the turbulent film experiments, the estimates of δ obtained with Eq. (1.18) (derived for laminar films) are still better than those obtained with Eq. (1.22) (derived for turbulent films), when compared to the relevant experimental results of Nogueira et al.. In light of this, preference was given to Eq. (1.18) for the prediction of the liquid film thickness for all experiments reported here.

1.6 Flow field in the wake of Taylor bubbles

The dynamics in the wake of a Taylor bubble affects the velocity profiles along the liquid slug, which ultimately determine the extent of the interaction between consecutive bubbles. Several authors have studied the flow field in the wake of Taylor bubbles in past decades.

In a comprehensive study on the development of slug flow, Moissis and Griffith (1962) measured the velocity profiles behind a plastic Taylor bubble using a Pitot tube, and used that information to formulate the problem of the rise velocity of a trailing bubble.

Maxworthy (1967) confirmed the existence of wakes behind Taylor bubbles using a flow-visualization technique based on photographs of bubbles moving from a highly concentrated dye region into a clear water region.

Shemer and Barnea (1987) performed a visualization study of the velocity profiles behind Taylor bubbles using the hydrogen bubble technique. They observed two zones in the liquid slug: a mixing zone where the annular jet enters slug (the bubble wake), and a zone of fully developed velocity profile.

Campos and Guedes de Carvalho (1988a) reported a study on the motion of Taylor bubbles rising in stagnant liquids, with particular emphasis on the characteristics and dynamics of the wake region. They argued that the flow pattern in the wake of Taylor bubbles, the dimensionless wake volume (v_w) and the dimensionless wake length (l_w) depend on the dimensionless inverse viscosity N_f ($=\rho(gD^3)^{1/2}/\mu$), on the *Eötvös* number and on the length of the Taylor bubble (h_b). The last two relations are, however, negligible for tubes larger than about 20 mm and bubbles long enough to allow for the development of fully-established liquid films. Thus, depending on the values of N_f, the authors discerned three different types of bubble wakes: laminar wakes (closed axisymmetric wake as in Figure 1.9a; $N_f<500$), transitional wakes (closed

unaxisymmetric wake as in Figure 1.9b; $500<N_f<1500$) and turbulent wakes (opened wake flow as in Figure 1.9c; $N_f>1500$).

By visually inspecting the laminar wakes, Campos and Guedes de Carvalho (1988a) were able to determine empirical correlations for the estimation of the dimensionless wake length and volume:

$$\frac{l_w}{D} = 0.30 + 1.22\times10^{-3}N_f \tag{1.24}$$

and

$$\frac{v_w}{D^3} = 7.5\times10^{-4}N_f \tag{1.25}$$

A different approach was developed to determine the length of the turbulent wakes given their opened nature. Campos and Guedes de Carvalho (1988b) proposed a method based on the study of the mixing induced by the wake of Taylor bubbles moving along vertical columns (in which each wake is considered as a perfectly mixed vessel).

In a study on the coalescence of pairs of bubbles rising in co-current flowing liquid, Pinto et al. (1998) proposed a change in the relevant dimensionless group in which to base the assessment of the flow regime in the wake flow pattern, namely from the inverse viscosity number (N_f) to a sort of Reynolds number based on the downward liquid velocity as seen by the bubble (V_S). The relative velocity V_S was defined as follows:

$$V_S = U_B - U_L \tag{1.26}$$

which yields, after substitution of U_B according to Eq. (1.4) and rearranging:

$$V_S = U_\infty + (C-1)U_L \tag{1.27}$$

In the study of Campos and Guedes de Carvalho (1988a) there was no net liquid flow ($U_L=0$), so, for those conditions, $V_S = U_\infty = 0.35\sqrt{gD}$, which results in:

$$Re_{V_S} = \frac{\rho V_S D}{\mu} = \frac{0.35\rho\sqrt{gD^3}}{\mu} = 0.35N_f \tag{1.28}$$

Thus, using the boundary values of N_f (500 and 1500) proposed by Campos and Guedes de Carvalho (1988a) in the previous equation, Pinto et al. (1998) obtained the ranges of Re_{V_S} for which the three wake flow patterns can be observed:

$$Re_{V_S} < 175 \tag{1.29}$$

for laminar wakes,

$$175 < Re_{V_S} < 525 \tag{1.30}$$

for transitional wakes, and

$$Re_{V_S} > 525 \tag{1.31}$$

for turbulent wakes. The boundary values of N_f and Re_{V_S} for the transition in the wake flow patterns (for stagnant and flowing liquid, respectively) were later confirmed by Nogueira et al. (2006b) in an experimental study using Particle Image Velocimetry (PIV). These boundary values are used as reference for discerning the wake flow patterns for all experiments described in this document.

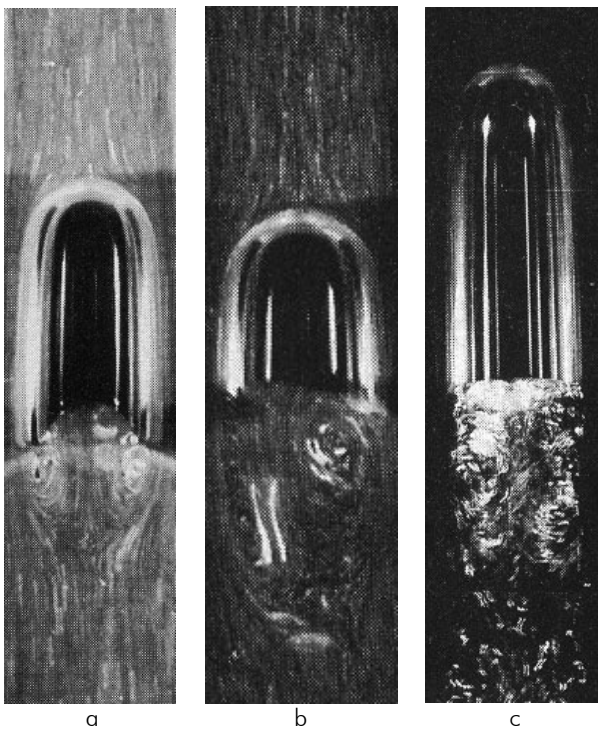

Figure 1.9 – Snapshots of bubble wake flow patterns (taken from Campos and Guedes de Carvalho (1988a)): (a) closed axisymmetric wake, N_f<500; (b) closed unaxisymmetric wake, 500<N_f<1500; (c) opened wake with recirculatory flow, N_F>1500

Nakoryakov et al. (1999) performed a study on the instantaneous velocity fields in vertical slug flow using an electrochemical velocity probe. They observed that the vortex ring in the mixing zone behind a Taylor bubble affects significantly the flow structure in the slug and that its length, found independent of the liquid flow rates, is approximately 2*D* long.

In a visualization study on the motion of Taylor bubbles in vertical pipes, Polonsky et al. (1999a) report that the dominant frequency of the bubble bottom oscillations is nearly constant, but their amplitude increases strongly with the bubble length as well as with the liquid velocity.

Van Hout et al. (2002b) used PIV to perform an experimental investigation on the velocity field around individual Taylor bubbles rising in stagnant water (wake flow pattern: turbulent). The authors observed a distinct vortex up to 2*D* below the bubble, and a secondary, much weaker vortex, between 2*D* and 5*D* below the bubble.

Bugg and Saad (2002) used PIV to study the velocity field around a Taylor bubble rising in a stagnant viscous fluid. They observed that the axial velocity along the tube centreline falls off with increasing distance from the bottom of the bubble (e.g. at 0.77*D* below the bubble, the axial velocity was as low as 10% of the bubble velocity; wake flow pattern: laminar).

Using Laser Doppler Velocimetry (LDV), Sotiriadis and Thorpe (2005) performed an investigation on the liquid recirculation in turbulent flow conditions, behind a cylindrical bluff body and a ventilated cavity attached to a sparger. They reported that the characteristics of the vortexes observed in the two geometries are very similar (the vortexes are 1.3*D* and 1.35*D* long, and their eyes, i.e. the axial locations at which the average radial and axial velocities are zero, were found at the axial locations 0.72*D* and 0.78*D*, respectively). Furthermore, the authors report that the CFX simulations (Thorpe et al. (2001)) performed for the bluff body, the ventilated cavity and the Taylor bubble rising in stagnant liquid (Van Hout et al. (2002b)) compare favourably with the corresponding experimental results, when correlating the results in the appropriate form.

1.7 Interaction between consecutive Taylor bubbles

Two or more Taylor bubbles flowing in the column can interact, approach and eventually coalesce. The relative velocity between consecutive bubbles depends on the extent of the flow disturbances induced by the wake of the leading bubble. Several authors have addressed this issue in past decades.

Zukoski (1966) states that when two Taylor bubbles rise with a short separation, the flow disturbances in the wake of the leading bubble can cause large-scale distortions of the trailing bubble, which may lead to an increase in the rise velocity of the trailing bubble and result in the coalescence of the bubbles.

Moissis and Griffith (1962) report that a bubble rising in the wake of another loses the stable profile characteristic of Taylor bubbles. Its nose distorts, becomes alternately eccentric on one side or another, and leans over to one side of the tube. The authors propose an empirical correlation for the rise velocity of a trailing Taylor bubble as a function of the distance to the leading Taylor bubble. The correlation, valid only for turbulent regime, is of the form:

$$\frac{U^{\text{trail}}}{U_B} = 1 + 8e^{-1.06\frac{h_s}{D}} \tag{1.32}$$

where U^{trail} is the trailing bubble velocity, U_B is upward bubble velocity in fully developed slug flow (as in Eq. (1.4)) and h_s the distance between bubbles (i.e. the length of the liquid slug).

In the study of Shemer and Barnea (1987) a correlation is suggested between the random and alternate movements of the trailing bubble nose and the velocity profiles in the liquid ahead of it. The authors suggest that the rise velocity of a trailing bubble matches the maximum instantaneous velocity in the liquid and assert that the variation of the maximum instantaneous velocity along the liquid slug is the responsible for the merging of bubbles. Furthermore, building on the idea that the stable slug length is that required to obtain a fully developed velocity profile in the liquid, the authors propose a simple expression to predict that parameter. A figure of 20D is obtained for turbulent pipe flow.

Pinto and Campos (1996) report an experimental study on the coalescence of pairs of gas bubbles rising in vertical columns through stagnant liquids of several viscosities. A technique based on pressure transducers was used to compile data on the trailing bubble velocity as a function of the separation distance and on the minimum distance between Taylor bubbles above which no interaction is expected (l_{min}). The latter parameter is, obviously, a synonym of the stable slug length introduced by Shemer and Barnea (1987). Different correlations are reported for l_{min} according to the flow regime in the bubble wake (or ranges of N_f):

Laminar wakes

$$\frac{l_{\min}}{D} = 1.46 + 4.75\times10^{-3}N_f \qquad 100 < N_f < 500 \tag{1.33}$$

Transitional wakes

$$\frac{l_{\min}}{D} = 6.92\times10^{-1} + 7.90\times10^{-3}N_f \qquad 500 < N_f < 1500 \tag{1.34}$$

Turbulent wakes

$$\frac{l_{min}}{D} = 12.5 \qquad N_f > 1500 \qquad (1.35)$$

The same authors observed that, regardless of the flow regime in the bubble wake, the ratios between the values of l_w (wake length) obtained by Campos and Guedes de Carvalho (1988a), Campos and Guedes de Carvalho (1988b) and the estimates of l_{min} obtained by Eqs. (1.33)-(1.35) are approximately constant (≈0.24). They then suggested that the distance over which two Taylor bubbles interact (d) may be approximately divided into two zones: one occupied by the bubble wake ($0<d<0.24l_{min}$) and another along which the liquid coming from the wake evolves to its motionless initial state ($0.24l_{min}<d<l_{min}$). Thus, different expressions were proposed to compute the trailing bubble velocity as a function of the distance between bubbles, for each of these zones:

$$\frac{U^{trail}}{U_B} = -11.4\frac{d}{l_{min}} + 4.24 \qquad \frac{d}{l_{min}} < 0.24 \qquad (1.36)$$

$$\frac{U^{trail}}{U_B} = 2.01 - 1.96\frac{d}{l_{min}} + 0.95\left(\frac{d}{l_{min}}\right)^2 \qquad \frac{d}{l_{min}} > 0.24 \qquad (1.37)$$

Pinto et al. (1998) extended the study of the coalescence of pairs of gas bubbles for co-current flowing liquid, covering laminar and turbulent flow conditions. They report that for turbulent regime in the main liquid and in the bubble wake region $l_{min}\approx 5D$. However, when the flow regime in the main liquid is laminar, a peculiar result is observed for certain operating conditions: the trailing bubbles rise slower than the leading bubbles. The authors relate these events to the velocity profile in the bubble wake region resulting from the competition between the downward velocity of the plunging liquid film (u_δ) and the upward velocity of the main liquid (U_L). They observed that when the ratio between these velocities (u_δ / U_L) is higher than 25 the bubbles approach and there is coalescence (and $l_{min}\approx 10D$). When the ratio is lower than 25 and the initial distance between bubbles is greater than the wake length of the leading bubble, the trailing bubble does not approach the leading one and thus no coalescences takes place.

Tudose and Kawaji (1999) studied the total drag force acting on a stationary solid model of a Taylor bubble placed in a downward flowing stream. They observed a significant decrease in the drag force for Taylor bubbles featuring deformed noses or flowing laterally displaced (eccentrically). Using a dual-bubble model, they found that the drag force on the trailing bubble

increases gradually with the increasing separation distance up to 2*D*, and remains approximately constant beyond that region. Thus, the trailing bubble acceleration could not be justified simply by the decrease in the drag force along the liquid slug. They suggest that the wake of a leading Taylor bubble can have two effects on the motion of a trailing bubble: a direct effect, very near the leading bubble rear (up to 2*D* below), due to the low pressure field because of large vortices and intense mixing, and an indirect effect related to the small-scale residual eddies remaining far below the rear of the leading Taylor bubble (2*D*-6*D* below the bubble rear).

In a study on the interaction between two consecutive Taylor bubbles rising in stagnant water, Aladjem Talvy et al. (2000) report increasing oscillation of the trailing bubble velocity as the trailing bubble approaches the leading bubble. Furthermore, the velocity of the trailing bubble is said to be affected by the vortical velocity field in the wake of the leading bubble for distances exceeding 50*D*. However, Van Hout et al. (2002b) (using also stagnant water) report that the average liquid velocity at the pipe axis becomes negligible much closer to the bubble (12*D* below the bubble, in a moving reference frame).

As a logical next step in the study of the coalescence of Taylor bubbles several reports followed addressing the interaction between consecutive bubbles in continuous (gas and liquid) co-current slug flow. The following section describes the main contributions.

1.8 Continuous co-current slug flow experimentation and simulation

Several authors have studied the slug flow pattern in co-current flowing conditions, both experimentally and numerically.

Barnea and Taitel (1993) propose a model for the prediction of the slug length distributions at any desired position along the pipe. The model assumes a random slug length distribution at the pipe inlet and computes its evolution along the pipe, based on an input relation correlating the trailing bubble velocity with the length of the slug between bubbles. The authors adopted a correlation of the form:

$$\frac{U^{\text{trail}}}{U_B} = 1 + \alpha e^{-\beta \frac{h_s}{l_{\min}}} \tag{1.38}$$

Based on their simulation results, the authors report that, for fully developed slug flow, the mean and the maximum slug lengths are about 1.5 and 3 times the minimum stable slug length (l_{min}), respectively. No information is given, however, on the characteristics of the bubble length distributions, probably because the simulation approach does not take into consideration the expansion of the gas phase along the pipe.

Hasanein et al. (1996) report a study on co-current slug flow in laminar regime. The authors studied the development of slug flow pattern in air-kerosene mixtures by manually inspecting video recordings of the flow. They observed that the correlation of Moissis and Griffith (1962) (Eq. (1.32), for turbulent regime) did not adequately represent their laminar experimental data and proposed

$$\frac{U^{\text{trail}}}{U_B} = 1 + 3e^{-0.85\frac{h_s}{D}} \tag{1.39}$$

to correlate the variation of the trailing bubble velocity with the distance between bubbles. Using this equation as input to a simulation code, they obtained predictions for the slug length distributions at the column outlet in good agreement with the experimental data. However, their experimental study covered only very low superficial gas and liquid velocities. In addition, for simulation purposes, the gas bubbles were taken as non-deforming solid particles, thus, not undergoing expansion along the column.

Pinto et al. (2001) report a study that extends their previous work on the interaction of Taylor bubbles (Pinto et al. (1998)) to co-current slug flow conditions. Based on a 0.032 m internal diameter tube, the study addresses operating conditions leading to turbulent regime in the near-wake bubble region and turbulent or laminar regime in the main liquid. The authors observed that the minimum distance between bubbles above which there is no interaction (l_{min}) is about 5-6D, for both flow regimes. In addition, when the flow regime in the main liquid is turbulent, the upward undisturbed bubble velocity (U_B) was found to follow the Nicklin relation with C=1.2 and U_L substituted by U_M, the superficial mixture velocity:

$$U_B = U_\infty + CU_M \tag{1.40}$$

When the flow regime in the main liquid is laminar, the values of U_B obtained were, however, considerably lower than expected (Eq. (1.40) with C=2). The authors ascribed this latter result to a flat velocity profile in the liquid emerging from the bubble wake, due to the competition between the downward annular film and the upward main liquid (in agreement with previous findings from the same authors). Still, the reported data were obtained using a relatively inaccurate technique (based on the analysis of the pressure fluctuations induced by the passage of the Taylor bubbles past pressure transducers) and, additionally, there was not a deep analysis of the flow pattern characteristics or even bubble interaction laws, in particular for the operating conditions leading to laminar regime in the liquid.

Van Hout et al. (2001) report a study on co-current slug flow along vertical pipes for air-water mixtures. The authors used optical fibre probes (sensitive to the change in the refractive index of the surrounding medium) to study the evolution of the flow pattern characteristics along 10 m long columns of two diameters (0.024 m and 0.054m), for three pairs of superficial gas and liquid velocities. They obtained slug and bubble length distributions for several coordinates along the columns and proposed correlations, relating the variation of the trailing bubble velocity with the length of the slug between bubbles, of the form:

$$\frac{U^{\text{trail}}}{U_B} = a + 8e^{-1.5h_s/D} + \frac{1}{h_s/D} \tag{1.41}$$

where a=1 for the narrower column and a=1.2 for the larger. The authors observed that the experimental U_B was in good agreement with Nicklin's predictions (Eq. (1.40)) only for the narrower column. For the larger column, the experimental results were clearly under-predicted. They ascribed this discrepancy to the less developed nature of the flow and to the high aeration level of the liquid slugs. Using the correlation (1.41) as input to the model of Barnea and Taitel (1993) they obtained predictions for the slug length distributions along both columns. The model under-predicted the experimental data for the larger column, whereas, for the narrower column, only a moderate agreement was obtained. Moreover, the experimental technique employed is intrusive (a set of optical fibre probes placed inside the column) and the operating conditions cover only three pairs of superficial gas and liquid velocities.

The same authors report another study (Van Hout et al. (2002a)) in which the aforementioned intrusive method is applied together with an image processing technique, to investigate the hydrodynamics of continuous slug flow along pipes (0.024 m and 0.054m) with inclinations ranging from 0° to 90° relative to horizontal. Based on their findings they suggest that the application of the drift velocity of single Taylor bubbles to continuous slug flow is inappropriate, particularly for the larger column, due to the high aeration level of the liquid slugs in continuous operation. Building on the same experimental data, Van Hout et al. (2003) propose correlations (such as Eq. (1.41)) for the variation of the trailing bubble velocity with the length of the slug between bubbles, for different inclination angles (but only for the narrower column). These were introduced into the model of Barnea and Taitel (1993), to obtain predictions of the slug length distributions along the column, for each inclination angle. A general good agreement between the experimental data and the model predictions is claimed. Still, at the pipe exit, the predicted distributions are wider than the experimental ones, and the corresponding means and modes are over-estimated. Moreover and as mentioned previously, one of the experimental techniques is intrusive (the fibre-probe based) and the image processing technique, although non-intrusive, was

applied in continuous slug flow conditions to only a small sample of elongated bubbles (30-40). Additionally, the simulation model used (after Barnea and Taitel (1993)) does not consider the gas phase expansion along the column, with effect over the length and velocity of the bubbles inside the column. Still, it is an interesting contribution upon which to base the development of more complex simulation strategies.

1.9 Contribution of the present work

Several works in the literature describe approaches to the experimental and numerical study of co-current continuous slug flow. They provide valuable insight into the characteristics of slug flow pattern but suffer still from some shortcomings. As outlined in the previous section, some of the experimental studies are based in relatively intrusive techniques whereas others address only few values of superficial gas and liquid velocities (or cover narrow ranges of operating conditions). Moreover, the previous approaches to the simulation of co-current continuous slug flow do not tackle thoroughly the problem of the gas expansion along the column (some attempts discard it in the prediction of bubble length and velocity, while others simply consider an averaging correction strategy for the prediction of the effective volumetric gas flow rate along the pipe). The present work is an attempt to answer these questions/problems. From a non-intrusive image analysis technique (for the experimental study), to an enhanced slug flow simulation strategy (for the numerical study), the present work provides information on the characteristics, features and governing rules of co-current continuous vertical slug flow, for all possible flow regimes (in the main liquid and in the near-wake bubble region). Both the experimental and the numerical studies cover wide ranges of operating conditions (several column diameters, fluid properties and gas and liquid flow rates). Finally, the expansion of the gas phase along the column was tackled and implemented in the simulation approach. This has enabled a thorough investigation about the influence of this phenomenon on the evolution of several flow parameters.

1.10 Notation

Roman symbols

a	dimensionless fit parameter	
b^+	dimensionless film thickness ratio ($= \delta u^*/u$)	
C	empirical coefficient	
d	distance along which two bubbles can interact ($d < l_{min}$)	[m]
D	column internal diameter	[m]
g	acceleration of gravity	[m/s^2]

h_b^*	stabilized length of gas bubble	[m]
h_s	length of liquid slug	[m]
l_{min}	minimum distance between bubbles for negligible interaction	[m]
l_w	length of bubble wake	[m]
m	dimensionless parameter (dependent on N_f)	
r	radial coordinate	[m]
R	column internal radius	[m]
S_δ	cross-sectional area of the annular film region (from $r=R-\delta$ to $r=R$)	[m^2]
S_r	surface (lateral) area of a cylinder with radius r	[m^2]
u	liquid velocity in the annular film, in a fixed reference frame	[m/s]
u_δ	average liquid velocity in the annular film, in a fixed reference frame	[m/s]
u^+	dimensionless velocity ratio ($= u/u^*$)	
u^*	friction velocity ($=[\tau_w/\rho]^{1/2}$)	[m/s]
U_B	upward bubble velocity (according to Nicklin's equation)	[m/s]
U_G	superficial gas velocity	[m/s]
U_L	superficial liquid velocity	[m/s]
U_M	superficial mixture velocity ($= U_L + U_L$)	[m/s]
U_∞	upward bubble velocity in a stagnant liquid (drift velocity)	[m/s]
U^{trail}	trailing bubble velocity	[m/s]
$v_{\delta r}$	volume of an infinitesimal cylindrical (annular) film element with thickness δr	[m^3]
v_w	volume of bubble wake	[m^3]
V_S	liquid velocity relative to the bubble ($=U_B^{exp} - U_M$)	[m/s]
y	distance from the column wall	[m]
y^+	dimensionless distance from the wall ratio ($= yu^*/\upsilon$)	

Greek symbols

α, β	dimensionless fit parameters	
δ	liquid film thickness	[m]
σ	liquid surface tension	[N/m]
μ	liquid dynamic viscosity	[Pa s]
ρ	liquid density	[kg/m^3]
$\varnothing$	functional relationship	
τ	shear stress	[Pa]
τ_r	shear stress at the radial coordinate r	[Pa]
τ_w	shear stress at the column wall	[Pa]
υ	liquid kinematic viscosity ($=\mu/\rho$)	[m^2/s]

Dimensionless groups

Eo	Eötvös number ($= \rho g D^2/\sigma$)
Fr	Froude number ($= U_\infty/\sqrt{gD}$)
Mo	Morton number ($= g\mu^4/\left[\rho\sigma^3\right]$)
N_f	inverse viscosity number ($= \rho[gD^3]^{1/2}/\mu$)
Re_{υ_δ}	Reynolds number based on the liquid velocity in the annular film, in a fixed reference frame ($= \rho\,\upsilon_\delta\,\delta/\mu$)
Re_{U_L}	Reynolds number based on the superficial liquid velocity ($= \rho U_L D/\mu$)
Re_{U_M}	Reynolds number based on the mixture velocity ($= \rho U_M D/\mu$)
Re_{V_S}	Reynolds number based on the liquid velocity relative to the bubble ($= \rho V_S D/\mu$)
We_{U_∞}	Weber number based on the drift velocity ($= \rho\, U_\infty^2 D/\sigma$)

Acronyms

CFD	computational fluid dynamics
CFX	CFD simulator
ID	internal diameter
LDV	laser doppler velocimetry
PIV	particle image velocimetry

1.11 References

Aladjem Talvy, C., Shemer, L. and Barnea, D., 2000. On the interaction between two consecutive elongated bubbles in a vertical pipe. Int. J. Multiphas. Flow 26: 1905-1923.

Barnea, D. and Taitel, Y., 1993. A model for slug length distribution in gas-liquid slug flow. Int. J. Multiphas. Flow 19(5): 829-838.

Bendiksen, K. H., 1984. An experimental investigation on the motion of long bubbles in inclined tubes. Int. J. Multiphas. Flow 10(4): 467-483.

Brown, R. A. S., 1965. The mechanics of large gas bubbles in tubes. I - Bubble velocities in stagnant liquids. Canadian Journal of Chemical Engineering 43: 217-223.

Bugg, J. D. and Saad, G. A., 2002. The velocity field around a Taylor bubble rising in a stagnant viscous fluid: numerical and experimental results. Int. J. Multiphas. Flow 28: 791-803.

Campos, J. B. L. M., 1991. Mixing induced by air slugs rising in an inclined column of water. Chem. Eng. Sci. 46(8): 2117-2122.

Campos, J. B. L. M. and Guedes de Carvalho, J. R. F., 1988a. An experimental study on the wake of gas slugs rising in liquids. J. Fluid Mech. 196: 27-37.

Campos, J. B. L. M. and Guedes de Carvalho, J. R. F., 1988b. Mixing induced by air slugs rising in narrow columns of water. Chem. Eng. Sci. 43(7): 1569 -1582.

Collins, R., De Moraes, F. F., Davidson, J. F. and Harrison, D., 1978. The Motion of Large Gas Bubble Rising Through Liquid Flowing in a Tube. J. Fluid Mech. 28: 97-112.

Davies, R. M. and Taylor, G. I., 1950. The mechanics of large Bubbles rising through extended liquids and through liquids in tubes. Proc. R. Soc. Lond. A 200: 375-392.

Dukler, A. E. and Bergelin, O. P., 1952. Characteristics of flow in falling liquid films. Chemical Engineering Progress 48(11): 557-563.

Dumitrescu, D. T., 1943. Stromung an Einer Luftblase im Senkrechten Rohr. Z. Angeus. Math. Mec. 23: 139-149.

Fabre, J. and Liné, A., 1992. Modeling of two-phase slug flow. Ann. Rev. Fluid Mech. 24: 21-46.

Fernandes, R. C., Semiat, R. and Dukler, A. E., 1983. Hydrodynamic model for gas-liquid slug flow in vertical tubes. AIChE J. 29(6): 981-989.

Fréchou, D. (1986). Etude de l'écoulement ascendant à trois fluides en conduite verticale. Thèse Inst. Natl. Polytech. Toulouse.

Fulford, G. D., 1964. The flow of liquids in thin films. Adv. Chem. Eng. 5: 151-236.

Govier, W. and Aziz, K. (1972). The flow of complex mixtures in pipes. New York, USA, Van Nostrand Reinhold Edition.

Hasanein, H. A., Tudose, G. T., Wong, S., Malik, M., Esaki, S. and Kawaji, M., 1996. Slug flow experiments and computer simulation of slug length distribution in vertical pipes. AIChE Symposium Series 92(310): 211-219.

Mao, Z. S. and Dukler, A. E., 1991. The motion of Taylor bubbles in vertical tubes II. Experimental data and simulation for laminar and turbulent flow. Chem. Eng. Sci. 46(8): 2055-2064.

Maxworthy, T., 1967. A note on the existence of wakes behind large, rising bubbles. J. Fluid Mech. 27(2): 367-368.

Moissis, R. and Griffith, P., 1962. Entrance effects in a two-phase slug flow. J. Heat Transfer 84: 29-39.

Nakoryakov, V. E., Kashinsky, O. N., Petukhov, A. V. and Gorelik, R. S., 1999. Study of local hydrodynamic characteristics of upward slug flow. Exp. Fluids 7: 560-566.

Nickens, H. V. and Yannitell, D. W., 1987. The effects of the surface tension and viscosity on the rise velocity of a large gas bubble in a closed, vertical liquid-filled tube. Int. J. Multiphas. Flow 13(1): 57-69.

Nicklin, D. J., Wilkes, J. O. and Davidson, J. F., 1962. Two-phase flow in vertical tubes. Transactions of the Institution of Chemical Engineers 40: 61-68.

Nikuradse, J. (1933). Laws of flow in rough pipes, VDI Forschungsheft.

Nogueira, S., Riethmuller, M. L., Campos, B. L. M. and Pinto, A. M. F. R., 2006a. Flow in the nose region and annular film around a Taylor bubble rising through vertical columns of stagnant and flowing Newtonian liquids. Chem. Eng. Sci. 61: 845-857.

Nogueira, S., Riethmuller, M. L., Campos, B. L. M. and Pinto, A. M. F. R., 2006b. Flow patterns in the wake of a Taylor bubble rising through vertical columns of stagnant and flowing Newtonian liquids: an experimental study. Chem. Eng. Sci. 61: 7199-7212.

Pinto, A. M. F. R. and Campos, J. B. L. M., 1996. Coalescence of two gas slugs rising in a vertical column of liquid. Chem. Eng. Sci. 51(1): 45-54.

Pinto, A. M. F. R., Coelho Pinheiro, M. N. and Campos, J. B. L. M., 2001. On the interaction of Taylor bubbles rising in two-phase co-current slug flow in vertical columns: Turbulent wakes. Exp. Fluids 31(6): 643-652.

Pinto, A. M. F. R., Coelho Pinheiro, M. N., Nogueira, S., Ferreira, V. and Campos, J. B. L. M., 2005. Experimental study of the transition in the velocity of individual Taylor bubbles in vertical upward co-current liquid flow. Chem. Eng. Res. Des. 83(A9): 1103-1110.

Pinto, A. M. F. R., Pinheiro, M. N. C. and Campos, J. B. L. M., 1998. Coalescence of two gas slugs rising in a co-current flowing liquid in vertical tubes. Chem. Eng. Sci. 53(16): 2973-2983.

Polonsky, S., Barnea, D. and Shemer, L., 1999. Average and time-dependent characteristics of the motion of an elongated bubble in a vertical pipe. Int. J. Multiphas. Flow 25: 795-812.

Shemer, L. and Barnea, D., 1987. Visualization of the instantaneous velocity profiles in gas-liquid slug flow. Physicochemical Hydrodynamics 8(3): 243-253.

Sotiriadis, A. A. and Thorpe, R. B., 2005. Liquid re-circulation in turbulent vertical pipe flow behind a cylindrical bluff body and a ventilated cavity attached to a sparger. Chem. Eng. Sci. 60(4): 981-994.

Taitel, Y., Barnea, D. and Dukler, A. E., 1980. Modelling flow pattern transitions for steady upward gas-liquid flow in vertical tubes. American Institute of Chemical Engineers Journal 26(3): 345-354.

Thorpe, R. B., Evans, G. M., Zhang, K. and Machniewski, P. M., 2001. Liquid circulation and bubble breakup beneath ventilated gas cavities in downward pipe flow. Chem. Eng. Sci. 56: 6399-6409.

Tudose, E. T. and Kawaji, M., 1999. Experimental investigation of Taylor bubble acceleration mechanism in slug flow. Chem. Eng. Sci. 54: 5761-5775.

Van Hout, R., Barnea, D. and Shemer, L., 2001. Evolution of statistical parameters of gas-liquid slug flow along vertical pipes. Int. J. Multiphas. Flow 27(9): 1579-1602.

Van Hout, R., Barnea, D. and Shemer, L., 2002a. Translational velocities of elongated bubbles in continuous slug flow. Int. J. Multiphas. Flow 28(8): 1333-1350.

Van Hout, R., Gulitski, A., Barnea, D. and Shemer, L., 2002b. Experimental investigation of the velocity field induced by a Taylor bubble rising in stagnant water. Int. J. Multiphas. Flow 28(4): 579-596.

Van Hout, R., Shemer, L. and Barnea, D., 2003. Evolution of hydrodynamic and statistical parameters of gas-liquid slug flow along inclined pipes. Chem. Eng. Sci. 58(1): 115-133.

Viana, F., Pardo, R., Yánez, R., Trallero, J. L. and Joseph, D. D., 2003. Universal correlation for the rise velocity of long gas bubbles in round pipes. J. Fluid Mech. 494: 379-398.

Wallis, G. B. (1969). One dimensional two-phase flow. New York, McGraw Hill Book Co.

White, E. T. and Beardmore, R. H., 1962. The Velocity of Single Cylindrical Air Bubbles Through Liquids Contained in Vertical Tubes. Chem. Eng. Sci. 17: 351-361.

White, F. M. (1999). Fluid mechanics, McGraw-Hill International Editions.

Zukoski, E. E., 1966. Influence of viscosity, surface tension, and inclination angle on motion of long bubbles in closed tubes. J. Fluid Mech. 25(4): 821-837.

2 Hydrodynamics of gas-liquid slug flow along vertical pipes in turbulent regime – An experimental study[2]

2.1 Abstract

An experimental study on free bubbling gas-liquid (air-water) vertical slug flow was developed using a non-intrusive image analysis technique. The flow pattern in the near wake of the bubbles and in the main liquid between bubbles was turbulent. A single correlation for the bubble-to-bubble interaction is proposed, relating the trailing bubble velocity to the length of the liquid slug ahead of the bubble. The proposed correlation is shown to be independent of column diameter, column vertical coordinate, superficial liquid and gas velocities and the velocity and length of the leading bubble. Frequency distribution curves, averages, modes and standard deviations are reported, for distributions of bubble velocity, bubble length and liquid slug length, for each experimental condition studied. Good agreement was found between theoretical predictions and experimental results regarding the upward velocity of undisturbed bubbles, in a 0.032 m internal diameter column. A considerable discrepancy was found, though, for a 0.052 m internal diameter column. The acquired experimental data are crucial for the development and validation of a robust slug flow simulator.

[2] Based on the paper by T. Sotto Mayor, V. Ferreira, A.M.F.R. Pinto and J.B.L.M. Campos, submitted to International Journal of Heat and Fluid Flow (IJHFF)

2.2 Introduction

Slug flow is a highly intermittent and irregular two-phase flow regime observed when gas and liquid flow simultaneously in a pipe, over certain ranges of gas and liquid flow rates. The slug flow pattern is characterised by elongated bullet-shaped gas bubbles, known as Taylor bubbles, separated by liquid slugs which often contain small dispersed bubbles. These long bubbles occupy most of the cross-sectional area of the pipe, forcing the liquid to flow around them, in the opposite direction, in a very thin film where the shear forces tend to balance the body forces (in a free-falling liquid film). At the rear of the bubble, the liquid film expands, creating a separate flow – the bubble wake. Depending on the flow parameters and the liquid's physical properties, the flow in the bubble wake varies from a well-defined recirculation flow (laminar wake) to a turbulent one where small and random recirculation regions can be observed (turbulent wake). In both situations, the liquid in the wake flows upwards at a mean velocity equal to the bubble velocity, thus travelling attached to the rear of the bubble. Below the bubble wake (in a reference frame moving with the bubble) the liquid starts evolving to the undisturbed flow pattern. Interesting contributions on the flow field characterization at the near bubble wake region have been given, for instance, by Van Hout et al. (2002a) or Sotiriadis and Thorpe (2005).

The undisturbed velocity of Taylor bubbles, U_B, has been studied extensively (Nicklin et al. (1962), Collins et al. (1978), among others) and it is generally assumed to be expressed by the sum of the drift velocity (the velocity of the bubble in stagnant liquid, U_∞) and a local contribution of the maximum velocity of the liquid flowing ahead of the bubble nose:

$$U_B = U_\infty + C(U_L + U_G) \tag{2.1}$$

where U_L is the superficial liquid velocity, U_G the superficial gas velocity and C a parameter ranging from approximately 1.2, for fully developed turbulent liquid flow, to 2.0, for laminar liquid flow. For inertial controlled regime (range according to White and Beardmore (1962)) the drift velocity is given by:

$$U_\infty = 0.35\sqrt{gD} \tag{2.2}$$

where g and D are the acceleration of gravity and the column internal diameter, respectively.

When a Taylor bubble flows in the wake of a leading bubble or in the disturbed liquid below it, its velocity tends to increase until it eventually merges with the leading bubble. After the merging process, the bubble length increases. Several authors refer to a minimum liquid slug

length for having a stabilized slug flow pattern (Moissis and Griffith (1962), Pinto and Campos (1996), Pinto et al. (1998), Aladjem Talvy et al. (2000), Van Hout et al. (2001), Van Hout et al. (2002b)). They have suggested empirical correlations relating the velocity of a trailing bubble *i*, U_i^{trail}, with the separation distance between consecutive bubbles, h_s. Pinto and Campos (1996), Pinto et al. (1998), Aladjem Talvy et al. (2000) reported correlations supported in data from controlled bubble injection experiments, while Van Hout et al. (2001) provided a correlation supported by data from naturally occurring continuous gas-liquid slug flow experiments:

$$\frac{U_i^{trail}}{U_B} = a + be^{-c\,h_s/D} + \frac{1}{h_s/D} \tag{2.3}$$

where U_B is the upward bubble velocity as defined by Eq. (2.1), and a, b and c are fitting parameters. However, the dependence of these parameters on gas and liquid flow rates and liquid regimes has not yet been studied thoroughly. Additionally, some discrepancies are reported between the undisturbed bubble velocities observed and theoretical predictions (Eq. (2.1) with C=1.2) for the larger column diameter (0.054 m). The occurrence of highly distorted bubbles (observed along the rise) and highly aerated liquid slugs are suggested to account for these discrepancies. Moreover, correlation (2.3) is based on data acquired through an intrusive method (a set of optical fibre probes placed inside the column).

More recently, Van Hout et al. (2002b) reported a study in which the aforementioned method was applied together with an image processing technique, in order to investigate the hydrodynamics of elongated bubbles in continuous slug flow. The image processing technique, though non-intrusive, was applied in continuous slug flow conditions to a small sample of elongated bubbles (30-40).

The dynamic and complex behaviour of Taylor bubbles creates some difficulties in the development of predictive algorithms capable of providing information about continuous gas-liquid slug flow. In particular, bubble and slug length distributions, bubble velocity distribution, gas entrainment, coalescence rate and minimum pipe length for stabilised flow patterns are all crucial data for the optimal design of slug flow applications.

The main goal of the present work is to acquire more experimental information on free-bubbling gas-liquid slug flow, in order to formulate a robust predictive model. Hydrodynamics and statistical parameters were obtained using a non-intrusive experimental technique (based on image analysis) in two pipe diameters, for a large range of gas and liquid flow rates and in two positions along the pipe. Several hundreds of elongated bubbles (1200-1500) were analysed for each experimental condition. These data allow the thorough analysis of the role played by the gas and liquid flow rates and by the velocity and length of the leading bubble, over the dependence of the

trailing bubble velocity on the length of the liquid slug flowing ahead of it. An empirical bubble-to-bubble interaction correlation is proposed. Experimental values for parameter C and drift velocity are analysed and compared with the values in the literature. The experimental data are compared with the findings of other researchers and serve to support an improved predictive model to be implemented in a robust slug flow simulator.

2.3 Experimental set-up

The experimental apparatus is shown schematically in Figure 2.1. Experiments were performed in acrylic vertical pipes 6.5 m long with internal diameters of 0.032 m and 0.052 m. Tap water was used as flowing medium at superficial velocities up to 0.30 m/s. The flow was set and controlled by a peristaltic pump with damping chambers placed at the pump inlet and outlet to assure a continuous flow. A large open tank with a lateral outlet was mounted at the top of the pipe to minimise free-surface oscillations. The liquid flow rate was measured at the outlet of the tank, before and after each experiment. The liquid temperature was measured by a thermocouple placed inside the tank. Air from a pressure line was introduced laterally at the base of the column through a 3 mm internal diameter injector. The air flow rate was measured by calibrated rotameters at superficial velocities up to 0.30 m/s (at 1 bar and 20°C).

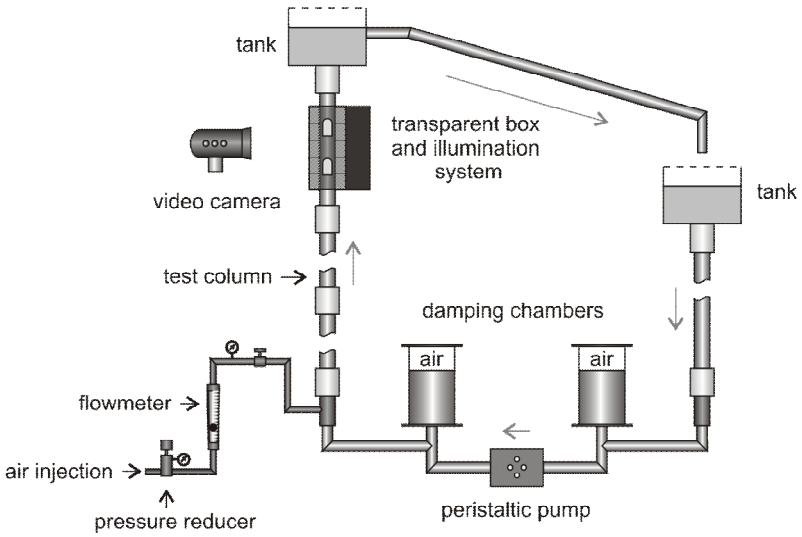

Figure 2.1 – Schematic representation of the experimental facility

Images of slug flow were recorded using a Canon digital video camcorder (model XM1) in two pipe sections comprising the vertical positions 3.25 m and 5.40 m (measured from the base of the column). A rectangular transparent acrylic box filled with water was fitted to the pipe at the measuring sections, in order to reduce image distortion and heating effects from the light source.

The digital video camcorder operated at a frequency of 25 Hz and the exposure times varied from 1/4000s to 1/8000s. A 90° rotation of the camera was chosen for better pixel resolution in the vertical coordinate (non-rotated camera field of view is 720 (width) x 576 (height) pixels). Different camera focal lengths were used according to the flow complexity and the average bubble and liquid slug dimensions, resulting in up to 0.6 m of pipe captured in the camera field of view.

2.4 Image processing

The recorded videos were transferred to a personal computer hard drive using video editing software (Adobe® Premiere).

Stripes containing the test column were extracted from the original videos and further processed using a MATLAB code (The MathWorks (2002)) specially developed for the purpose. Each video file was loaded into MATLAB as a sequence of frames (a frame at each 0.04 s, corresponding to a frequency of 25 Hz). A sequential procedure was then implemented to process each image frame, the outcome of which is shown in Figure 2.2.

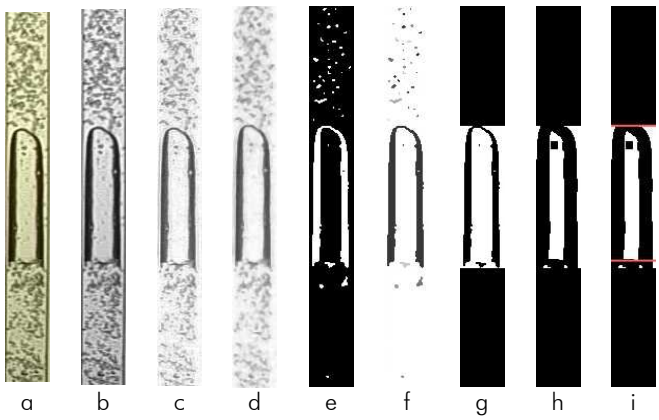

Figure 2.2 – Sequential steps in the image process: (a) RGB image; (b) greyscale image; (c) after background subtraction; (d) after median filter; (e) after conversion to binary mode; (f) after labelling; (g) after object analysis; (h) after erosion; (i) bubble boundaries

Bubble boundary definition is difficult due to the existence of more or less aerated liquid slugs (Figure 2.2a). Thus, a minimum bubble length was defined in order to distinguish between Taylor bubbles and small bubbles in the liquid slug. Depending on the flow complexity and average bubble length, a threshold length between 1*D* and 3*D* was used throughout the analysis of all experiments.

The use of object length as a sorting parameter allowed immediate definition of the Taylor bubble nose as well as a rough estimate of the position of the Taylor bubble rear. This uncertainty

is due to oscillations in the bubble rear as Taylor bubbles flow in the column, and to the small bubbles travelling in the liquid wake. Moreover, as stressed by Nogueira et al. (2003), bubble bottom conformation may also be an issue while defining the positioning of bubble rear (in particular for viscous solutions). These difficulties were lessened by implementing an image erosion procedure to isolate the central white area of each bubble (Figure 2.2h), a region whose lowest white pixel matches the beginning of the bubble wake region (Figure 2.2i). Thus, this strategy allowed for the determination of more accurate bubble length values (discarding the wake region).

2.5 Data analysis from image processing

The image processing procedure was implemented on every video frame. This permitted to gather information about the presence, positioning and dimension of bubbles, in the video frames. Furthermore, by analysing the characteristics of the bubbles (i.e. length and distance) and their displacements (i.e. velocity) along the column, it is possible to compile information about the flow pattern characteristics, for every experimental condition. Two different studies were performed: one describing the flow pattern at a fixed column position (fixed-point data analysis), and another focussing on the bubble-to-bubble interaction as bubbles move along the column (moving-point data analysis).

2.5.1 Fixed-point data analysis

Figure 2.3a-b depicts the camera's field of view in a slug flow experiment (a and b for short and long Taylor bubbles, respectively). Two imaginary reference lines, corresponding to 25% and 75% of the field of view height, were drawn (references 1 and 2). Bubbles are recognized when their noses cross the upper reference line.

If $t_{1,i}$ and $t_{2,i}$ represent consecutive instants, prior and subsequent, respectively, to the passage of the nose of bubble i through the upper reference line, the bubble velocity, U_i, is given by:

$$U_i = \frac{z_{nose,i}^{t_{2,i}} - z_{nose,i}^{t_{1,i}}}{t_{2,i} - t_{1,i}} \tag{2.4}$$

where $z_{nose,i}$ refers to the vertical coordinate of the bubble nose (measured from the base of the camera field of view). If the bubble rear is inside the camera field of view, i.e., for short Taylor bubbles, the bubble length is obtained directly from the position of its boundaries (nose and rear):

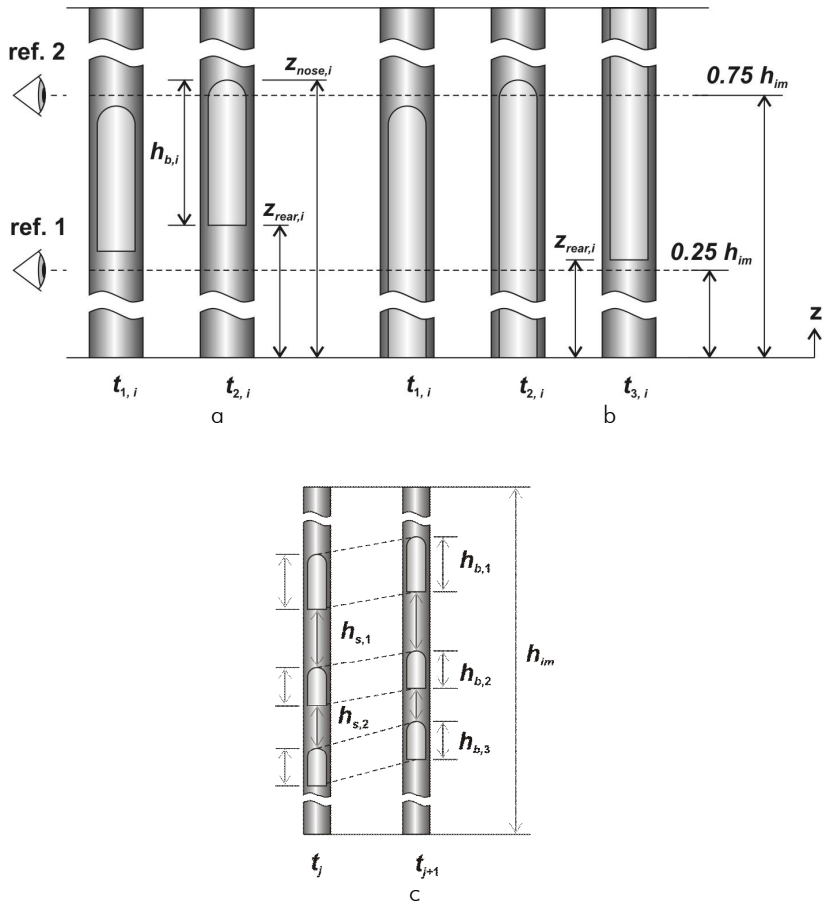

Figure 2.3 – Representation of the camera field of view in fixed-point analysis for (a) short bubbles and (b) long bubbles; (c) representation of camera field of view in moving-point analysis

$$h_{b,i} = z_{nose,i}^{t_{2,i}} - z_{rear,i}^{t_{2,i}} \tag{2.5}$$

The liquid slug length ahead of bubble i, $h_{s,i-1}$, is computed from the coordinate of the rear of the previous bubble (bubble i-1) and the coordinate of the nose of bubble i:

$$h_{s,i-1} = z_{rear,i-1}^{t_{2,i}} - z_{nose,i}^{t_{2,i}} \tag{2.6}$$

The coordinate of the rear of bubble i-1, at instant $t_{2,i}$, can be predicted by:

$$z_{rear,i-1}^{t_{2,i}} = z_{nose,i-1}^{t_{2,i-1}} + (t_{2,i} - t_{2,i-1}) U_{i-1}^{t_{2,i-1}} - h_{b,i-1} \tag{2.7}$$

where $t_{2,i-1}$ refers to the instant at which the nose of bubble i-1 crossed the upper reference line. In the above prediction it is assumed that bubble i-1 has constant upward velocity between instants $t_{2,i-1}$ and $t_{2,i}$. This assumption is reasonable unless the bubble is coalescing, interacting or instantly accelerating or decelerating by the time it passes the upper reference line. In that case, and as a result of the aforementioned assumption, a marginal increase in the occurrence of extreme values

of slug length (either short or long) might take place. Despite this fact, no major effect of this assumption is expected for the most probable value and average for the slug length variable (due to compensation).

A slightly more complex situation occurs when the bubble rear is not inside the field of view by the time the bubble nose crosses the upper reference line (instant $t_{2,i}$ in Figure 2.3b). In that case, the subsequent image frames must be analysed to find the instant $t_{3,i}$, in which the bubble rear crosses the lower reference line (ref. 1). Notice that in the latter instant, $t_{3,i}$, the bubble nose is not inside the camera field of view. Therefore, a prediction of its position must be computed. This parameter can be evaluated using the Eq. (2.8):

$$z_{nose,i}^{t_{3,i}} = z_{nose,i}^{t_{2,i}} + \left(t_{3,i} - t_{2,i}\right) U_i^{t_{2,i}} \tag{2.8}$$

A constant bubble velocity between instants $t_{2,i}$ and $t_{3,i}$ is a reasonable assumption since the time interval is very small for the studied conditions. The bubble length can then be calculated by:

$$h_{b,i} = z_{nose,i}^{t_{3,i}} - z_{rear,i}^{t_{3,i}} \tag{2.9}$$

The above procedure was implemented for each video frame to gather information about every bubble (bubble length, velocity and liquid slug length).

All variables mentioned above have pixel units (or pixel/s in the velocity case). To accomplish their conversion to real length units, the following correction must be computed:

$$variable\left[\text{m or m/s}\right] = variable\left[\text{pixel or pixel/s}\right]\frac{h_{cal.,m}}{h_{cal.,px}} \tag{2.10}$$

where $h_{cal.,m}$ and $h_{cal.,px}$ refer to the height of the calibration element in metres and pixels units, respectively.

2.5.2 Moving-point data analysis

In the moving-point data analysis, the focus is put on bubble-to-bubble interaction. Hence, for higher accuracy, it is important to use an image magnification in which more than one Taylor bubble is visible in the camera field of view. In this scenario, the relation between bubble velocity and liquid slug length ahead of the bubble is achieved without using predictions to compute bubble boundary positioning as in the previous section. Figure 2.3c depicts this situation.

Consecutive instants t_i and t_{i+1} are chosen considering the requirement of frames with equal number of bubbles, and with all bubble boundaries inside the camera field of view (no bubbles entering or exiting the field of view).

Bubble velocities are calculated using the following equation, identical to Eq. (2.4), for every bubble in the chosen frames:

$$U_i = \frac{z_{nose,i}^{t_{i+1}} - z_{nose,i}^{t_i}}{t_{i+1} - t_i} \tag{2.11}$$

Bubble and liquid slug lengths are computed using the following equations:

$$h_{b,i} = z_{nose,i} - z_{rear,i} \tag{2.12}$$

$$h_{s,i-1} = z_{rear,i-1} - z_{nose,i} \tag{2.13}$$

Notice that, for *n* bubbles in a frame, only n-1 liquid slugs are computed. Additionally, the last two equations are applied to each pair of consecutive frames and, therefore, average values for each bubble and liquid slug length are calculated (from every two consecutive frames).

As referred to in the previous section, a correction must be computed to convert the aforementioned variables to real length (or velocity) units (see Eq. (2.10)). An error analysis of the main flow parameters has been performed. The main results are shown in brief in Appendix.

2.6 Experimental data

Several parameters were measured during the analysis of the slug flow experiments in co-current conditions. The flow pattern in the main liquid between bubbles and in the wake of the bubbles was turbulent (Reynolds number in the main liquid in the range 4120-18740, based on the mixture velocity, U_M (= U_G + U_L); Reynolds number in the wake in the range 6230-25830, based on the liquid velocity relative to the bubble, V_S (= U_B^{exp} - U_M); turbulent regime in the wake is acknowledged for Reynolds numbers higher than 525, according to Pinto et al. (1998)).

The main parameters obtained through fixed-point analysis are the distributions of the bubble velocity, bubble length and liquid slug length, and the corresponding average values. Additionally, the experimental average upward bubble velocity, U_B^{exp}, in undisturbed conditions, is also worthy of interest, since it is used in the normalisation procedures described later. Notice that according to the analysis of the slug flow data, only bubbles flowing after long slugs ($h_s \geq$ 8-10D)

are considered undisturbed. Experimental values of parameter C and drift velocity are determined for both columns tested.

The main output of the moving-point analysis is the bubble-to-bubble interaction curve, relating the velocity of the trailing bubble, normalised by U_B^{exp}, to the liquid slug length ahead of the bubble (h_s).

Depending on the flow conditions, 1200-1500 bubbles were processed by the fixed-point data analysis (distribution curves and corresponding averages), and several thousand frames with more than one bubble were considered in the moving-point data analysis (bubble-to-bubble interaction curve). 500-1000 bubbles were taken into account in the calculation of the experimental average upward bubble velocities in undisturbed conditions (U_B^{exp}).

2.6.1 Reproducibility of the method and representativity of the samples

In order to assess the reproducibility of the image analysis method, three independent experiments with equal superficial liquid and gas velocities ($U_L \approx 0.10$ m/s, $U_G \approx 0.085$ m/s, $D = 0.032$ m) were compared. This comparison focussed on the bubble-to-bubble interaction curve, on the frequency distribution curves and on the corresponding average values for several parameters: bubble velocity (U), bubble length (h_b) and liquid slug length (h_s). Figure 2.4a shows this comparison regarding the bubble-to-bubble interaction curve.

The velocities of leading and trailing bubbles (U_i^{lead} and U_i^{trail}), normalised by the experimental average upward bubble velocity in undisturbed conditions (U_B^{exp}), are plotted as a function of their separation distance (h_s or liquid slug length). These results show that the image analysis method, used as a tool to study the slug flow pattern, has considerable reproducibility. Similar conclusions are drawn when focusing on the frequency distribution curves of U, h_b and h_s as well as on the corresponding average values.

In order to evaluate the minimal sample size needed to obtain significant values of the parameters under study, three samples consisting of 500, 1000 and 1500 bubbles were drawn from a general population of 2000 bubbles (as before, $U_L \approx 0.10$ m/s, $U_G \approx 0.085$ m/s, $D = 0.032$ m). The frequency distribution curves of liquid slug length are shown in Figure 2.4b (for a bin size of 1.5D). From this chart it can be concluded that a sample size of 1000 elements assures adequate representation of the parent population. This is based on the reduced changes in the frequency distribution curves for larger samples (for liquid slug length, bubble length and bubble velocity). Nevertheless, a minimum sample size requirement of 1200 bubbles was set for all experiments, for increased representativity.

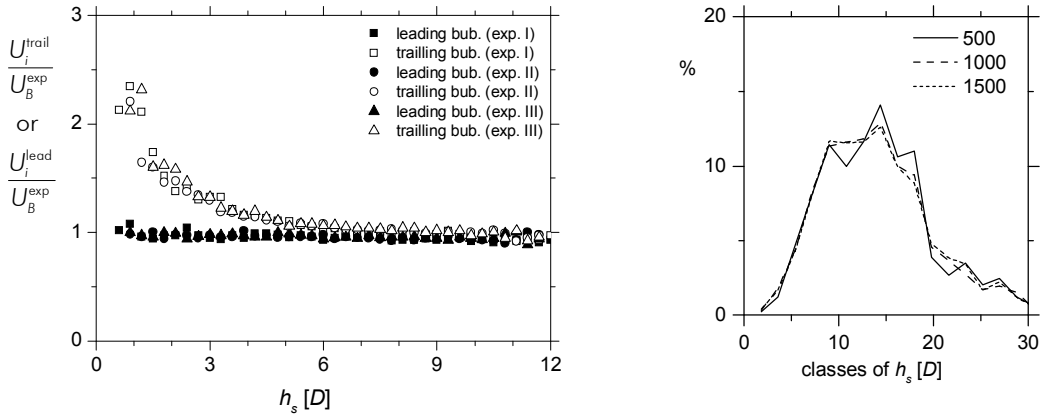

a b

Figure 2.4 – (a) bubble-to-bubble interaction curve for three similar experiments and (b) slug length frequency distribution curves for samples with 500, 1000 and 1500 bubbles; $U_L \approx 0.10$ m/s and $U_G \approx 0.085$ m/s; vertical coordinate: 5.4 m; column diameter: 0.032 m

2.6.2 A systematic study of the bubble-to-bubble interaction curve

Several experimental conditions were studied in order to evaluate the universality of the bubble-to-bubble interaction curve (for turbulent regime). In particular, focus was put on the influence of parameters such as the vertical column coordinate, the superficial liquid and gas velocities, the velocity and length of the leading bubble and the column diameter.

Vertical column position and column diameter

In order to check the universality of the interaction curve along the column, two similar experiments are compared, at different vertical column coordinates (3.25 m and 5.40 m), for the 0.032 m internal diameter column. Superficial liquid and gas velocities are 0.045 m/s and 0.085 m/s, respectively. The superficial gas velocity is at ambient pressure. This reference pressure is used for all gas flow data mentioned in this chapter, unless stated otherwise. Figure 2.5a shows the curve of velocity ratios (U_i^{trail}/U_B^{exp} and U_i^{lead}/U_B^{exp}) plotted against the normalised liquid slug length (h_s).

The acceleration of the trailing bubble towards the leading one occurs at both column coordinates for liquid slugs shorter than 8-10D. Indeed, the entire bubble-to-bubble interaction curve is similar for the two experiments, indicating its independence from the column vertical coordinate.

As referred to in section 2.5.2, for greater accuracy the moving-point data analysis requires that more than one Taylor bubble is visible in the camera field of view. Since this can only be achieved by increasing the distance between the video camera and the test section (or zooming

the image out, with consequent loss in resolution) a balance must be found between image magnification and image resolution. A balance was established for an image magnification covering the movement of two bubbles, at the maximum distance of 11-12*D*. Considering that the bubble-to-bubble interaction occurs over shorter distances (8-10*D*) no limitation is introduced in the analysis by this image magnification/resolution compromise. Notice that, for greater curve smoothness, the velocity ratios are gathered and averaged according to the liquid slug length class (classes of 0.3*D*). Moreover, this averaging approach is used in all the interaction curves presented.

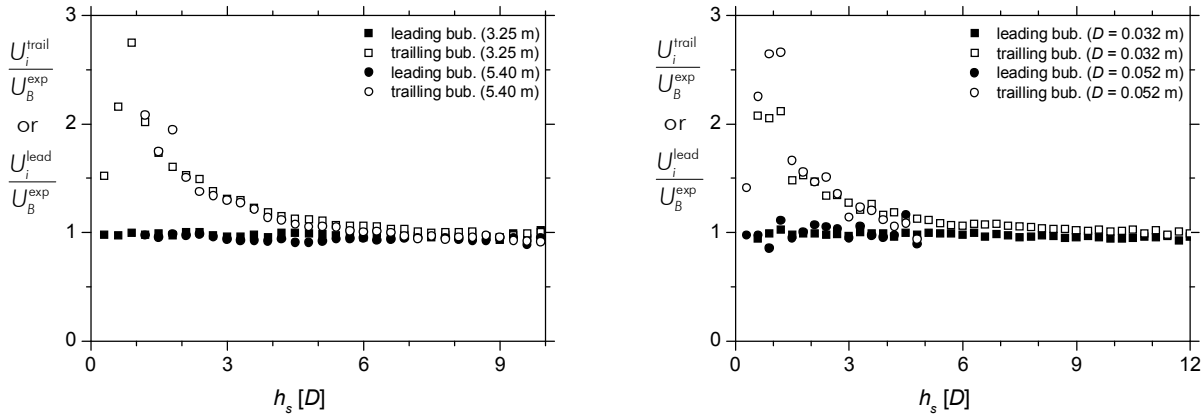

a b

Figure 2.5 – Bubble-to-bubble interaction curves (a) at column vertical coordinates 3.25 m and 5.40 m (U_L≈0.045 m/s, U_G≈0.085 m/s, D=0.032 m), (b) for columns with 0.032 m and 0.052 m of internal diameter (U_L≈0.15 m/s, U_G≈0.10 m/s, respectively; vertical coordinate: 5.4 m)

In order to check the validity of the interaction curve for different column diameters, two experiments with similar superficial gas and liquid velocity (U_L≈0.15 m/s, U_G≈0.10 m/s) were performed in columns with internal diameters equal to 0.032 m and 0.052 m (data were acquired at 5.4 m from the column base). Figure 2.5b shows the curve of velocity ratios plotted against the normalised liquid slug length (h_s). This chart indicates that the bubble-to-bubble interaction curve is similar for both column diameters. Notice that, as a consequence of the two bubbles per frame requirement, different column heights (in normalised form) were captured in the camera field of view (5-6*D* for the 0.052 m column and 11-12*D* for the 0.032 m column). Despite this fact, the aforementioned interaction similarity is clearly perceived. Higher standard deviations are observed for the larger column, due to the higher aeration of the liquid slugs and to the higher turbulence level of the flow (see Reynolds numbers in Table 2.1 and Table 2.2 for relevant operating conditions).

Superficial liquid and gas velocity (U_L and U_G)

In Figure 2.6a, four experiments with increasing superficial liquid velocity are compared (U_L≈0.045, 0.10, 0.15 and 0.21 m/s), for constant superficial gas velocity (U_G≈0.085 m/s). Figure 2.6b regards two experiments with increasing superficial gas velocity (U_G≈0.084m/s and 0.15 m/s) and constant superficial liquid velocity (U_L≈0.10 m/s). The data were acquired in a 0.032 m internal diameter column, at vertical coordinate 3.25 m. It can be seen in these charts that the bubble-to-bubble interaction curve is independent of both the superficial liquid and gas velocities.

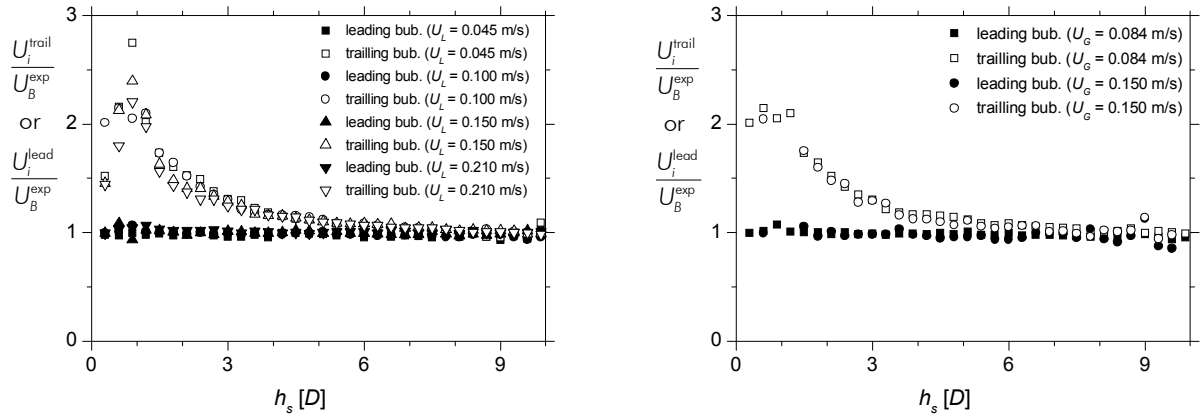

a b

Figure 2.6 – Bubble-to-bubble interaction curve for (a) U_L≈0.045, 0.10, 0.15 and 0.21 m/s; U_G≈0.085 m/s and (b) U_G≈0.084 m/s and 0.15 m/s; U_L≈0.10 m/s; column diameter: 0.032 m

Velocity and length of the leading bubble

In order to assess the influence of the leading bubble velocity and length over the bubble-to-bubble interaction curve, the data from an experiment (U_G≈0.085 m/s and U_L≈0.10 m/s) were thoroughly analysed. In Figure 2.7, two distinct versions of bubble pairs are plotted: one showing data with two different leading bubble velocities (Figure 2.7a) and another showing data with diverse leading bubble lengths (Figure 2.7b). In order to filter the experimental data (pairs of interacting bubbles), the 50th percentiles, of the distributions of the leading bubble velocities and bubble lengths, were used. A value of 12.5 D/s was used to prepare two bubble pair sub-distributions: one with bubble pairs whose leading bubble velocities were higher than 12.5 D/s, and another consisting of bubble pairs whose leading bubble velocities were lower than 12.5 D/s. Likewise, a value of 2.7D was used to prepare two alternative bubble pair sub-distributions: one whose leading bubbles were longer that 2.7D, and another whose leading bubbles were shorter than 2.7D. The comparison of these filtered data is shown in Figure 2.7.

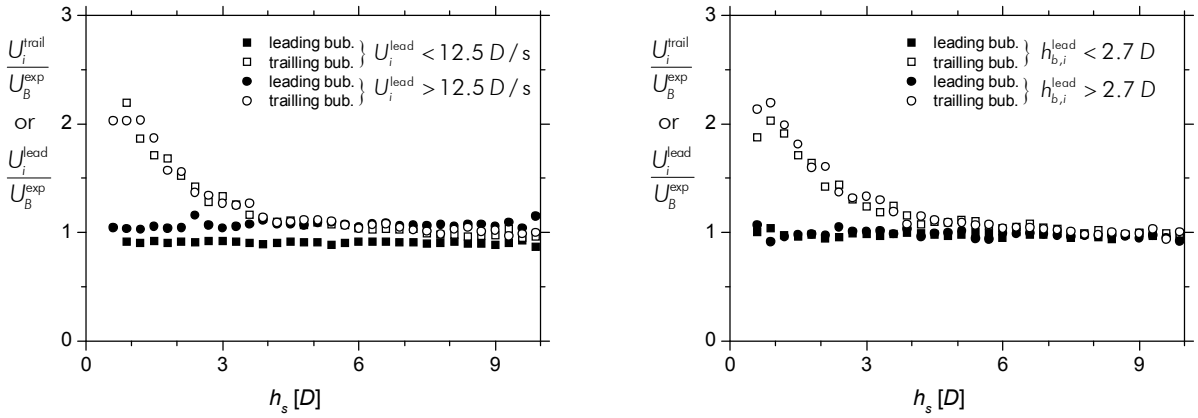

a b

Figure 2.7 – Bubble-to-bubble interaction curve for experiments with (a) different leading bubble velocity and (b) different leading bubble length; $U_G \approx 0.085$ and $U_L \approx 0.10$ m/s; column diameter: 0.032 m

In Figure 2.7a, the different average velocity of the leading bubble, for the two experiments being compared (13.8 *D*/s and 11.7 *D*/s, or 1.07 and 0.91, after normalisation), are clearly perceived. Despite the difference in the leading bubble velocity, a similar acceleration of the trailing bubble occurs at an identical bubble separation distance. Thus, it may be concluded that the interaction curve is unaffected by the velocity of the leading bubble. The chart of Figure 2.7b, for bubble pairs with different leading bubble lengths, indicates that the interaction curve is also independent from this parameter.

2.6.3 Approaching the coalescence phenomenon – the bubble-to-bubble interaction curve

As shown in the previous sections, the bubble-to-bubble interaction curve is independent of several flow parameters, for turbulent regime in the liquid and in the bubble wake. Indeed, it is possible to model the interaction between two consecutive bubbles by expressing the normalised trailing bubble velocity as a function of the liquid slug length ahead of it. Figure 2.8a represents the bubble-to-bubble interaction curve for several experiments, with superficial liquid and gas velocities as shown in Table 2.1.

By averaging the normalised velocities represented in Figure 2.8a, for each slug length class, the smoother bubble-to-bubble interaction curve shown in Figure 2.8b is obtained. Error bands corresponding to a 95% confidence level are also represented in the chart of Figure 2.8b.

Table 2.1 – Superficial liquid and gas velocities used in several experiments and corresponding Reynolds numbers (based on U_G at ambient pressure and U_B^{exp}); internal diameter: 0.032 m

			Reynolds number	
			liquid	wake
	U_L [m/s]	U_G [m/s]	Re_{U_M}	Re_{V_S}
a	0.044	0.084	4122	8526
b	0.047	0.084	4169	7386
c	0.047	0.084	4169	7386
d	0.097	0.149	7885	7204
e	0.098	0.085	5876	8378
f	0.100	0.083	5849	7067
g	0.102	0.088	6056	8281
h	0.152	0.084	7525	6916
i	0.208	0.084	9336	6726
j	0.208	0.150	11452	6233

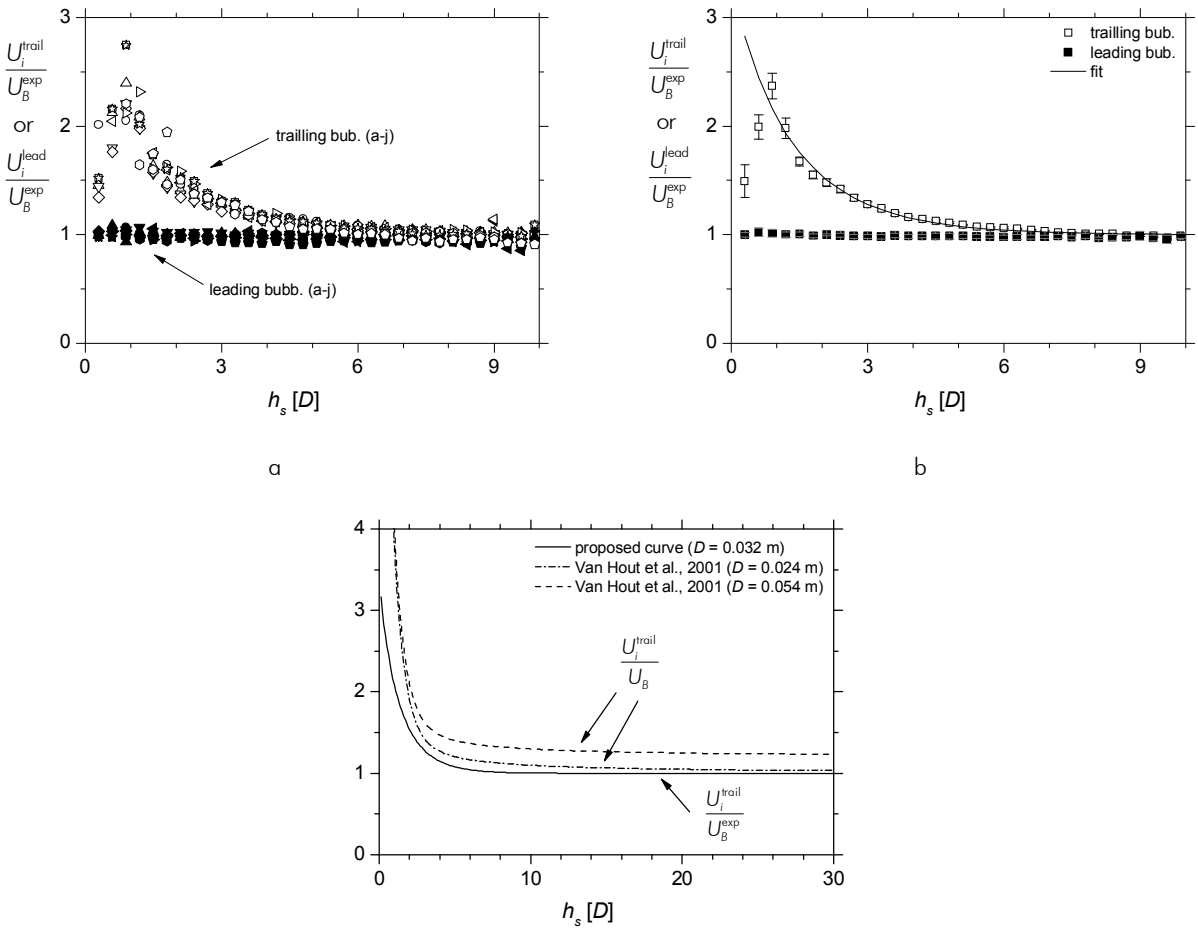

Figure 2.8 – (a) Bubble-to-bubble interaction curve for several experiments (0.032 m ID); (b) average bubble-to-bubble interaction curve and 95% confidence intervals (0.032 m ID), (c) comparison of the average bubble-to-bubble interaction curve with Van Hout's curves for 0.024 m and 0.054 m ID columns

They are defined considering the normalised velocities (U_i^{trail}/U_B^{exp} and U_i^{lead}/U_B^{exp}) in each slug length class, and computed as an interval ($\pm t\,S_X/\sqrt{n}$) around the average normalised velocity. Notice that there are different samples of normalised velocities for each slug length class considered. Moreover, S_x stands for the sample standard deviation, t refers to the t-student distribution and n is the number of class elements.

Figure 2.8b shows that the shorter the liquid slugs, the longer the error bands. This fact is obviously related to the higher standard deviation of the velocity samples as bubbles accelerate towards coalescence.

The acceleration of the trailing bubble towards the leading bubble occurs for liquid slugs shorter than 8-10D. A strong acceleration is observed for liquid slugs shorter than 3D in particular. Additionally, for very small liquid slug lengths ($h_s<1D$) a decrease in the trailing bubble velocity is observed. These observations are in agreement with the findings of Aladjem Talvy et al. (2000), Van Hout et al. (2001). Moreover, the decrease in the trailing bubble velocity for very short liquid slugs may be related to the dynamics in the main vortex of the bubble wake region, which extends to around 1-2D (Van Hout et al. (2002a), Sotiriadis and Thorpe (2005)).

An exponential fit of the trailing bubble velocity data is represented by the full line in the Figure 2.8b. The corresponding equation is:

$$\frac{U_i^{trail}}{U_B^{exp}} = 1 + 2.4e^{-0.8\left(\frac{h_{s,i-1}}{D}\right)^{0.9}} \qquad (2.14)$$

where U_i^{trail} refers to the velocity of the trailing bubble i flowing behind a liquid slug with length $h_{s,i\text{-}1}$. The bubble velocity is normalised by the experimental average undisturbed bubble velocity (U_B^{exp}). The trailing bubble slowdown for very short liquid slugs was, obviously, discarded in the fitting represented by Eq. (2.14). Nevertheless, this simplification has negligible effect in terms of simulation as it refers to instants on the verge of coalescence.

In Figure 2.8c, the bubble-to-bubble interaction curve obtained is compared with those proposed by Van Hout et al. (2001). Van Hout's curves are based on data obtained for 0.024 m and 0.054 m internal diameter columns. Despite this fact, and because the corresponding equations differ only on a single parameter (representing the undisturbed upward bubble velocity), a direct comparison between those curves and the proposed curve can be made. The analysis of the chart shows that, unlike the proposed bubble-to-bubble interaction curve, Van Hout's models still acknowledge some bubble interaction for liquid slugs longer than 8-10D. No evidence of this interaction has been found in the present experimental work (for a 0.032 m column).

2.6.4 Frequency distribution curves and average values of the main flow parameters

The influence of several flow parameters over the frequency distribution curves and corresponding averages is shown, in detail, in the following sections. Focus is put on parameters such as column vertical position and liquid and gas velocities. Two internal diameters are reported (0.032 m and 0.052 m). Table 2.2 compiles the operating conditions of all experiments reported in this section.

Table 2.2 – Superficial liquid and gas velocities used in several experiments and corresponding Reynolds numbers (based on U_G at ambient pressure and U_B^{exp})

			Reynolds number	
			liquid	wake
D [m]	U_L [m/s]	U_G [m/s]	Re_{U_M}	Re_{V_S}
0.032	0.044	0.084	4122	8526
0.032	0.098	0.085	5876	8378
0.032	0.151	0.088	7640	7875
0.032	0.194	0.085	8926	7568
0.032	0.102	0.088	6069	7582
0.032	0.102	0.158	8321	7443
0.032	0.102	0.205	9822	7596
0.032	0.102	0.260	11573	7707
0.052	0.047	0.106	7928	24226
0.052	0.074	0.105	9298	21806
0.052	0.101	0.105	10723	21920
0.052	0.145	0.105	12980	19716
0.052	0.101	0.106	10762	21881
0.052	0.101	0.160	13577	23852
0.052	0.101	0.211	16234	25831
0.052	0.101	0.259	18736	25691

2.6.4.1 0.032 m internal diameter

Flow development along the column

Two experiments with the same set of superficial liquid and gas velocities are compared in Figure 2.9 and Figure 2.10. Data acquisition occurred at 3.25 and 5.40 m from the base of the column, in a 0.032 m internal diameter column. The frequency distribution curves (and the corresponding log-normal fits) for bubble velocity, bubble length and liquid slug length are represented in Figure 2.9. The statistical parameters of the log-normal fits (average, mode and standard deviation) and additional flow stability parameters are plotted in Figure 2.10, against the

vertical coordinate of the column. More details on the calculation of the parameters of the log-normal fits can be found in Campos Guimarães and A. Sarsfield Cabral (1997).

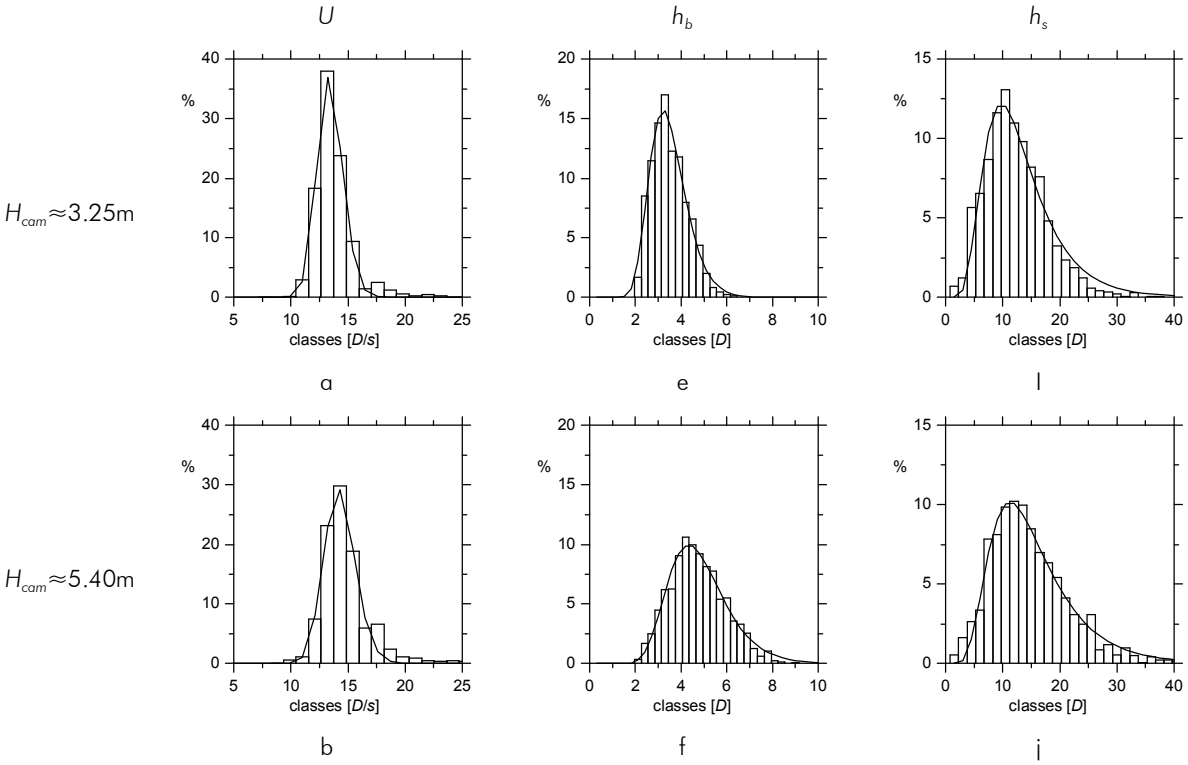

Figure 2.9 – Frequency distribution curves and log-normal fits at 3.25 m and 5.40 m from the base of the column, for experiments with U_L≈0.099 m/s and U_G≈0.085 m/s; column diameter: 0.032 m

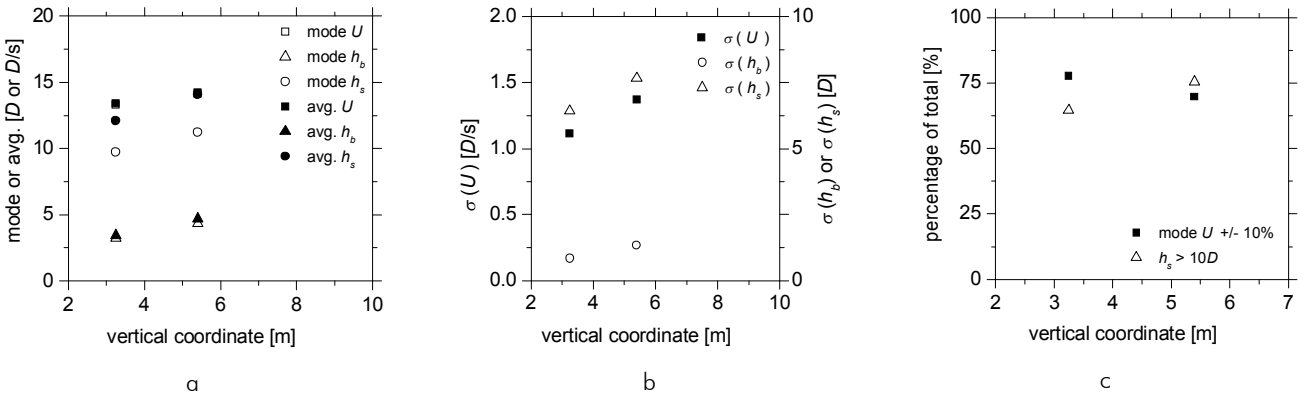

Figure 2.10 – Log-normal fit parameters (average, mode and standard deviation; a and b) and flow stability parameters (c) at 3.25 m and 5.40 m from the base of the column, for experiments with U_L≈0.099 m/s and U_G≈0.085 m/s; column diameter: 0.032 m

The analysis of the charts indicates that all depicted parameters increase along the column (the frequency distribution curves shift towards higher classes). Coalescence and expansion effects are accountable for the increase in the length of the liquid slugs and gas bubbles. As coalescence occurs along the column there is a decrease in the number of short liquid slugs and an increase in

the number of long bubbles. This is further strengthened by the expansion effect, for the bubble length in particular.

The slight increase in bubble velocity along the column requires a more detailed analysis. Although one would expect a decrease due to less frequent coalescences and less intense interactions, a second effect must be taken into consideration: the gas phase expansion. Indeed, the increase in bubble velocity due to the expansion of all bubbles flowing upstream (below) of each bubble overcomes the aforementioned decrease. Hence the overall slight increase of the average bubble velocity.

It is interesting to observe that the frequency distribution curves of all mentioned parameters become wider for higher vertical column position (a behaviour corroborated by the values of the standard deviation of the log-normal fits).

Two flow stability parameters were defined: the percentage of bubbles flowing after long slugs ($h_s > 10D$) and the percentage of bubbles whose velocity is within a 10% interval around the corresponding mode (most frequent value in a frequency distribution curve). The first parameter directly indicates the proportion of bubbles not undergoing coalescence (a direct indicator of flow stability) and the second is related to the dispersion of the bubble velocities around the corresponding mode (an indirect indicator of the bubble-to-bubble interaction). Figure 2.10c indicates that, at 5.4 m from the base of the column, 76% of the bubbles flow after slugs longer than 10*D* (whereas a figure of 64% was obtained at 3.25 m from base). This variation indicates an increase in the stability of the flow. The percentage of bubbles within a 10% interval around the bubble velocity mode is almost identical in the two column positions.

Superficial liquid and gas velocity (U_L and U_G)

Four experiments with increasing superficial liquid velocity are compared. The frequency distribution curves for the main flow parameters are plotted in Figure 2.11. The average, mode and standard deviation of the log-normal fits, and the flow stability parameters, are plotted against the superficial liquid velocity in Figure 2.12a-c. These charts confirm that, as expected (Eq. (2.1)), the average velocity of the bubbles increases with superficial liquid velocity (Figure 2.11a-d and Figure 2.12a). Moreover, the average length of the bubbles and the length of the liquid slugs decrease slightly with increasing superficial liquid velocity.

Due to flow continuity, the increase in the superficial liquid velocity, while keeping a constant superficial gas velocity, induces shorter bubbles and/or longer liquid slugs, at the column inlet. Shorter bubbles at inlet suggest a negative-slope trend, for the average bubble length, at the column top. Longer liquid slugs at inlet point towards a positive-slope trend for the average length of the liquid slugs at the column top, as well as a less frequent coalescence along the column.

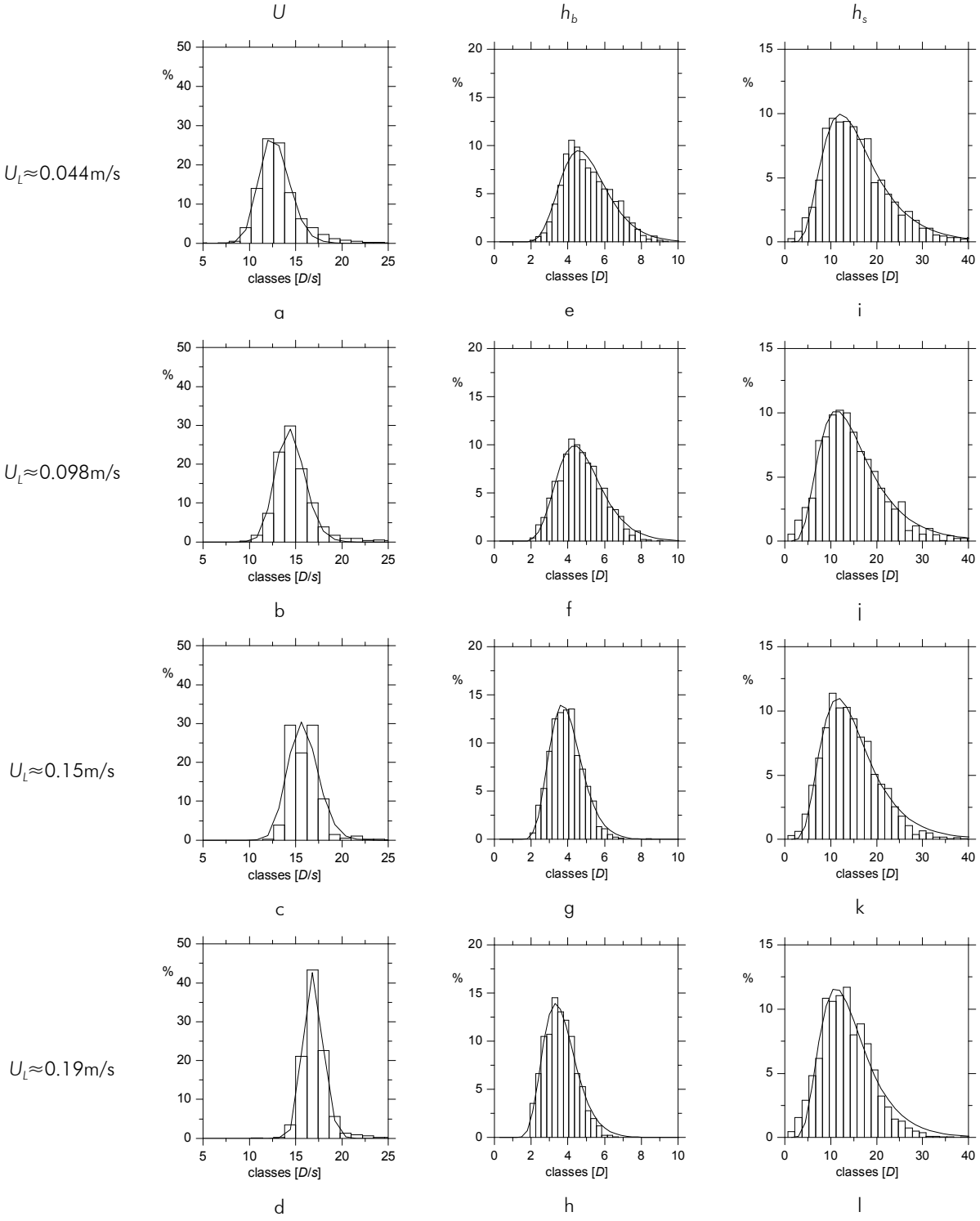

Figure 2.11 – Frequency distribution curves and log-normal fits for experiments with U_G≈0.085 m/s and U_L≈0.044, 0.098, 0.15 and 0.19 m/s; vertical coordinate: 5.4 m; column diameter: 0.032 m

According to the results, this latter consequence has a dominant effect. Indeed, the less frequent coalescence strengthens the inlet trend for the average length of the bubbles and inverts the inlet trend for the average length of the liquid slugs (intense coalescence induces longer

bubbles separated by longer liquid slugs). Thus, at the top of the column, both the average bubble length and liquid slug length decrease slightly for increasing superficial liquid velocity.

For all the mentioned parameters there is a decrease of the standard deviation for increasing superficial liquid velocity (Figure 2.11a-d, Figure 2.11e-h, Figure 2.11i-l; Figure 2.12b). This decrease together with the increasing percentage of bubbles within a 10% interval around the velocity mode (Figure 2.12c) indicates an increase of the flow stability for increasing superficial liquid velocity.

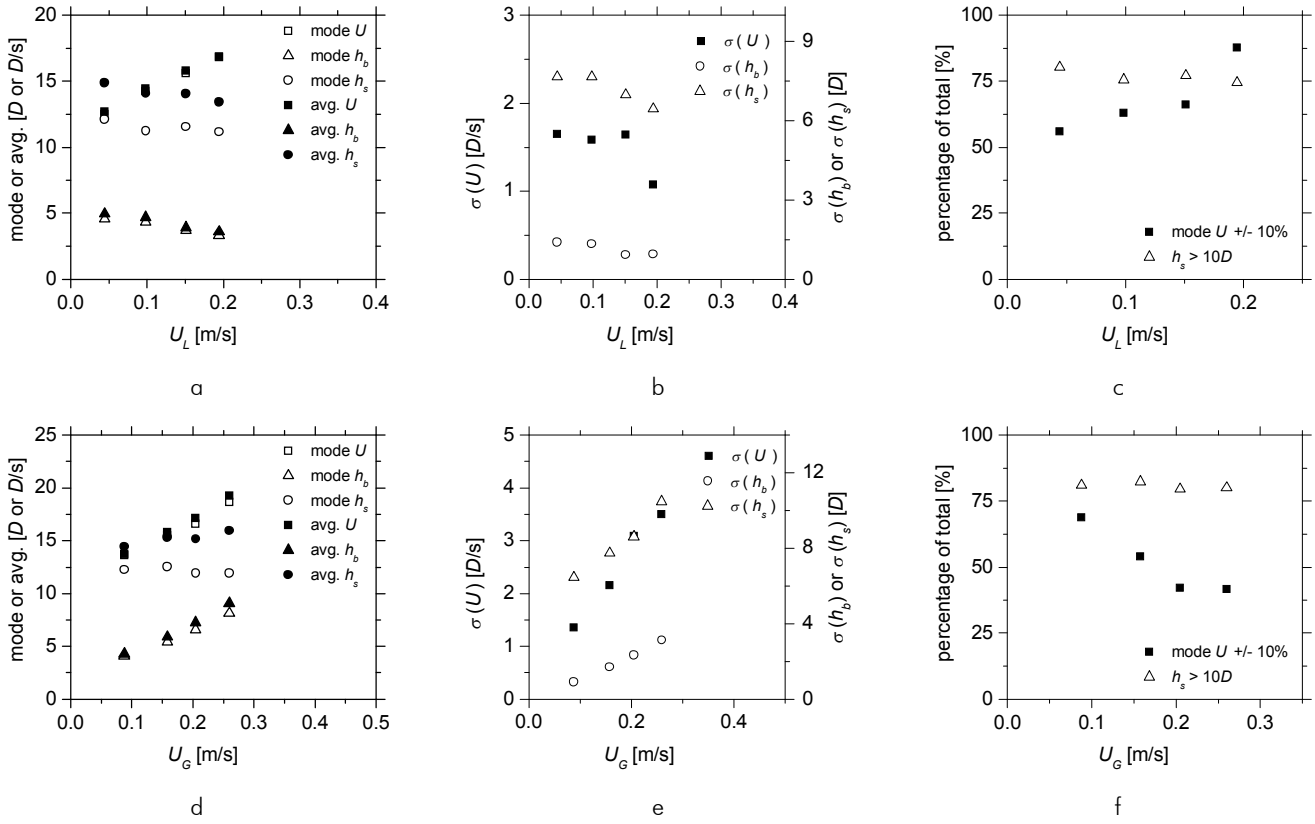

Figure 2.12 – Log-normal fit parameters (average, mode and standard deviation) and flow stability parameters for (a-c) experiments with $U_G \approx 0.085$ m/s and $U_L \approx 0.044$, 0.098, 0.15 and 0.19 m/s; (d-f) experiments with $U_L \approx 0.10$ m/s and $U_G \approx 0.088$, 0.16, 0.21 and 0.26 m/s; vertical coordinate: 5.4 m; column diameter: 0.032 m

Data from four experiments with increasing superficial gas velocity are also compared in this section. The average, mode and standard deviation of the log-normal fits (of the frequency distribution curves) and the flow stability parameters are plotted against the superficial gas velocity in Figure 2.12d-f. As shown in the charts, the average (and mode) of the velocity and length distributions increase with increasing superficial gas velocity (Figure 2.12d). The average length of liquid slugs increases slightly with increasing superficial gas velocity (Figure 2.12d), whereas the

corresponding mode has the opposite behaviour. These latter variations are coherent with the increasing asymmetry of the corresponding frequency distribution curves.

Due to flow continuity, the increase of the superficial gas velocity, while keeping the superficial liquid velocity constant, induces longer bubbles and/or shorter liquid slugs, at the column inlet. Longer bubbles at inlet suggest a positive-slope trend for the average length of the bubbles, at the column top. Shorter liquid slugs at inlet point towards a negative-slope trend, for the average length of the liquid slugs, at the column top, as well as a more frequent coalescence along the column (as bubbles enter the column at shorter distances). The coalescence rate effect is once again dominant in terms of the output distributions of bubble lengths and liquid slug lengths (since intense coalescence induces longer bubbles and longer liquid slugs). Indeed, these two flow parameters increase for increasing superficial gas velocity. Notice that the slight decrease in the liquid slug length mode, for increasing superficial gas velocity (Figure 2.12d), is a direct consequence of the increasing asymmetry of the corresponding frequency distribution curves.

The standard deviation of the frequency distribution curves escalates for increasing superficial gas velocity (Figure 2.12e). This variation together with the decreasing percentage of bubbles within a 10% interval around the bubble velocity mode (Figure 2.12f) indicates a less stabilized flow pattern for increasing superficial gas velocity.

2.6.4.2 0.052 m internal diameter

Superficial liquid and gas velocity (U_L and U_G)

Four experiments with increasing superficial liquid velocity in a 0.052 m column are compared. The average, mode and standard deviation of the log-normal fits (of the frequency distribution curves) and the flow stability parameters are plotted against the superficial liquid velocity in Figure 2.13a-c. As expected, the average (and mode) of the velocity distributions increases with increasing superficial liquid velocity (Figure 2.13a). Moreover, the average length of the bubbles and liquid slugs decreases slightly with increasing superficial liquid velocity (Figure 2.13a).

Following an approach similar to the one used for the narrower column, it is seen that, by flow continuity, the increasing superficial liquid velocity for constant gas velocity induces shorter bubbles and longer slugs at the column inlet, as well as a lower coalescence rate along the column. As for the narrower column, the effect over the coalescence rate is dominant, since the average length of bubbles and liquid slugs decrease slightly for increasing superficial liquid velocity.

The standard deviations of bubble velocity and liquid slug length decrease for increasing superficial liquid velocity (Figure 2.13b). This variation together with the increasing percentage of bubbles within a 10% interval around the velocity mode (Figure 2.13c) indicates an increase in flow stability for increasing superficial liquid velocity. Similar conclusions were drawn for the 0.032 m column.

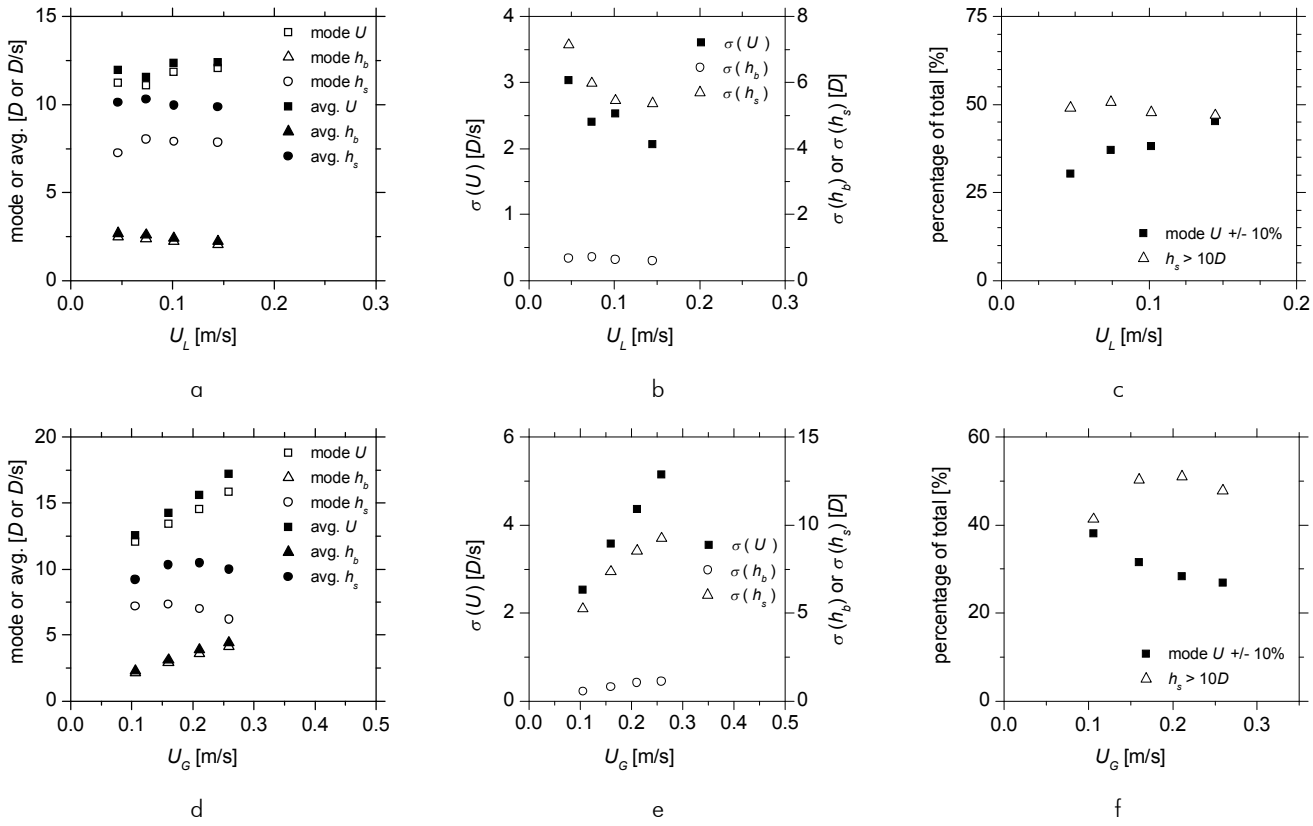

Figure 2.13 – Log-normal fit parameters (average, mode and standard deviation) and flow stability parameters for (a-c) experiments with $U_G \approx 0.10$ m/s and $U_L \approx 0.047$, 0.074, 0.10 and 0.15 m/s; (d-f) experiments with $U_L \approx 0.10$ m/s and $U_G \approx 0.11$, 0.16, 0.21 and 0.26 m/s; vertical coordinate: 5.4 m; column diameter: 0.052 m

Data from four experiments with increasing superficial gas velocity are also compared in this section. The frequency distribution curves for the main flow parameters are plotted in Figure 2.14. The average, mode and standard deviation of the log-normal fits and the flow stability parameters are plotted against the superficial gas velocity in Figure 2.13d-f. The average (and mode) of the velocity and length distributions increases for increasing superficial gas velocity (Figure 2.14a-d, Figure 2.14e-h and Figure 2.13d). The average length of liquid slugs does not have a well-defined behaviour (Figure 2.13d), whereas the corresponding mode slightly decreases. These latter variations are corroborated by the increasing asymmetry of the corresponding frequency distribution curves (Figure 2.14i-l).

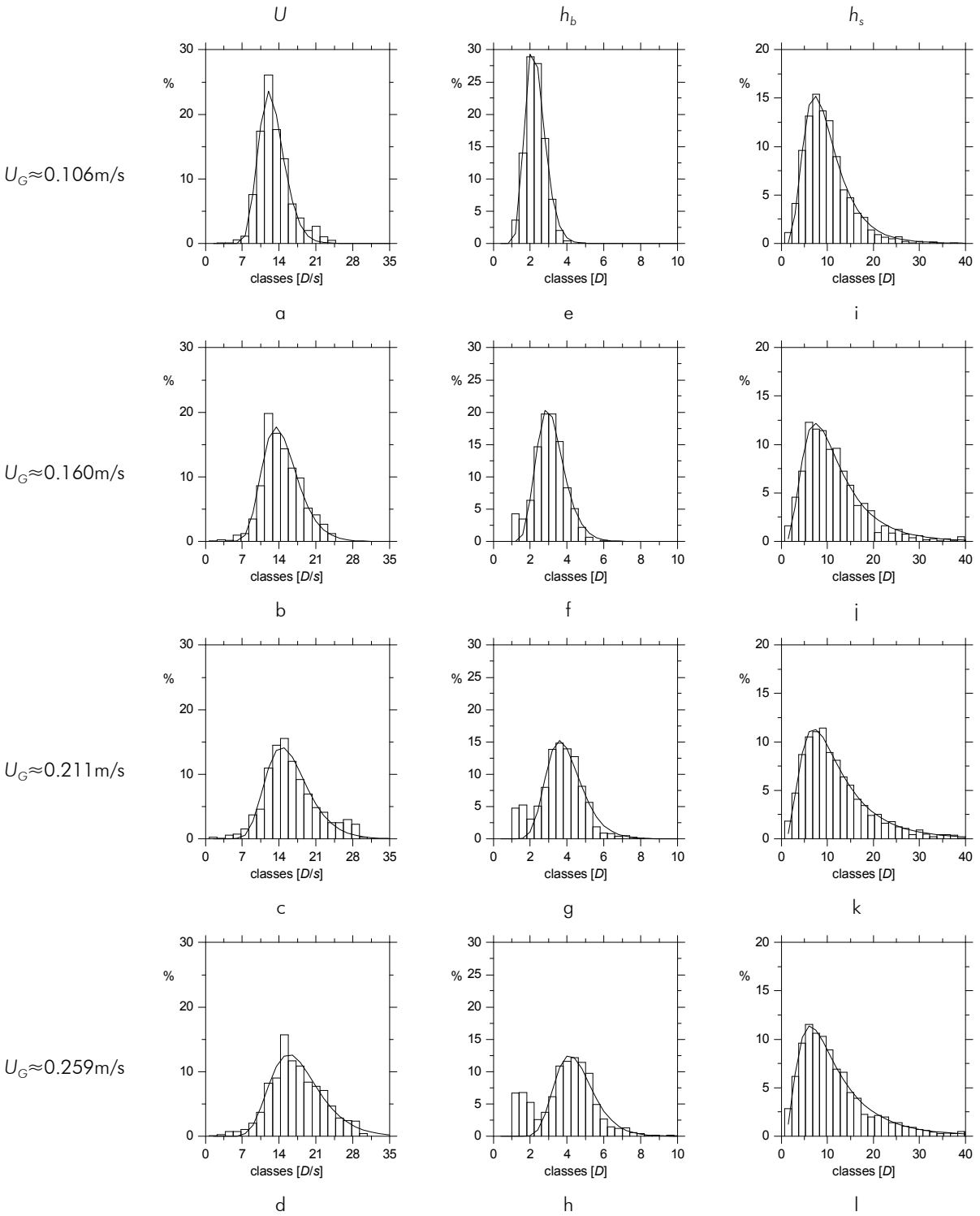

Figure 2.14 – Frequency distribution curves and log-normal fits for experiments with U_L≈0.10 m/s and U_G≈0.11, 0.16, 0.21 and 0.26 m/s; vertical coordinate: 5.4 m; column diameter: 0.052 m

As mentioned for the narrower column, the increasing superficial gas velocity for constant liquid velocity induces, by continuity, longer bubbles and shorter slugs at the column inlet, as well as higher coalescence rate along the column. In agreement with the conclusions drawn in the last section this behaviour points towards overall positive-slope trends at the column top for both the

average length of bubbles and of liquid slugs. However, in Figure 2.13d, an inconsistent variation can be observed in the average length of liquid slugs (in particular for the highest superficial gas velocity). This is the result of the competition between the effect of the length of the liquid slugs at the column inlet and the effect of coalescence along the column. For the reported experiment, this latter effect does not completely invert the initial trend.

It is interesting to note that a bimodal bubble length distribution seems to appear, mainly for the higher values of superficial gas velocity (Figure 2.14g and Figure 2.14h). Though very subtle, an identical behaviour has been observed for the narrower column. No phenomenological reasons can be given at this moment to account for these peculiar distributions.

The standard deviation of all frequency distribution curves escalates for increasing superficial gas velocity (Figure 2.13e). This variation, together with the decreasing percentage of bubbles within a 10% interval around the bubble velocity mode (Figure 2.13f), indicates a less stabilized flow pattern for increasing superficial gas velocity. Similar conclusions were drawn for the 0.032 m column.

A direct comparison between the above experimental results and other authors' findings (for instance Van Hout et al. (2001), Van Hout et al. (2002b)) is not possible due to differences in the column diameters and in the superficial gas and liquid velocities. An alternative approach is followed. The reported experimental results together with Van Hout's data will be used to support the development and validation of a new slug flow simulator, with wider ranges of validity/applicability.

2.6.5 Experimental values of C and drift velocity

In order to evaluate the parameter C and the drift velocity (C and U_∞ as in Eq. (2.1)) for the experiments reported in the previous sections, the experimental average upward bubble velocities (U_B^{exp}) are plotted against the average superficial velocity of the mixture (U_M). This representation is shown in Figure 2.15 for both column internal diameters (0.032 m and 0.052 m). These data are plotted together with the corresponding linear fit (for the 0.052 m column) and the theoretical predictions of U_B as given by Eq. (2.1), considering turbulent regime (C equal to 1.2). The values of U_M were corrected to the pressure at coordinate 5.4 m.

A very good agreement is obtained between theoretical predictions and experimental results for the narrower column (0.032 m). Two experiments (open points) are slightly apart from the theoretical predictions, an expected behaviour since they refer to transition (or quasi-transition) flow conditions in the main liquid (Re_{U_M} equal to 3890 and 5650, respectively, with U_M corrected for the pressure at 5.4 m).

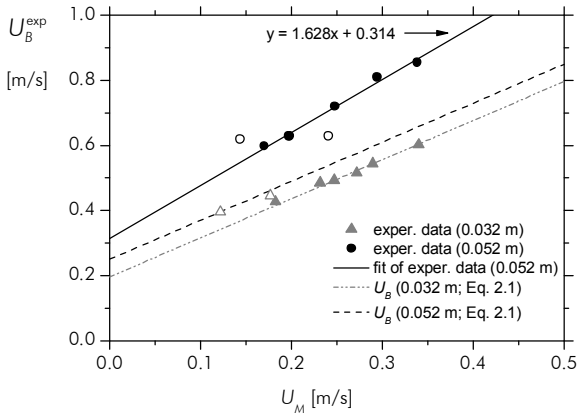

Figure 2.15 – Experimental average upward bubble velocity plotted against U_M, for column internal diameters of 0.032 m and 0.052 m; vertical coordinate: 5.4 m

The linear fit of the experimental data for the 0.052 m column did not take into consideration two experiments (open points) whose corresponding velocity values are, to some extent, apart from the trend. A very good correlation is achieved for the remaining data.

A poor agreement is observed between theoretical predictions and experimental results for the larger diameter column (0.052 m), a result already reported by other researchers (Van Hout et al. (2001), Van Hout et al. (2002b), among others). Both the experimental parameter C (1.628) and the experimental drift velocity U_∞ (0.314 m/s) are moderately higher than the theoretical predictions for turbulent regime (C=1.2 and U_∞=0.25 m/s; for a 0.052 m column). This discrepancy must be ascribed to two factors. First, the highly aerated liquid slugs (in particular for high superficial gas velocities) can result in an increase in the experimental drift velocity (Van Hout et al. (2002b)). Secondly, the level of turbulence in the liquid between bubbles (higher than for the narrower column, as confirmed by the Reynolds numbers in Table 2.2), generates instantaneous velocity profiles considerably different from the average ones. The trailing bubble nose always follows the higher instantaneous liquid velocity ahead of it, and so, there is a continuous acceleration and deceleration of the bubbles rising in the column even when no Taylor bubbles are ahead. This kinematic behaviour is in agreement with the instantaneous elongations and relaxations of the bubble shape, easily observed in the video frames. The high values of experimental parameter C are, therefore, consistent with this scenario.

2.7 Conclusions

An extensive experimental study on free bubbling gas-liquid vertical slug flow is reported. Data were acquired through a non-intrusive image analysis technique, based on the

straightforward analysis of sequences of image frames of the flow. The flow pattern in the wake of the bubbles and in the liquid was turbulent.

Parameters such as the column diameter, the column vertical coordinate, the superficial liquid and gas velocities and the velocity and length of the leading bubble were found not to influence the bubble-to-bubble interaction curve. A single correlation for the bubble-to-bubble interaction is proposed, relating the trailing bubble velocity to the length of the liquid slug ahead of the bubble. Bubble-to-bubble interaction was found to occur only for liquid slugs shorter than 8-10D.

As expected, the increasing superficial liquid velocity was shown to enhance the flow stability, for both column diameters. The superficial gas velocity produced the opposite effect. Considerable asymmetry has been observed for both column diameters in the distributions of the liquid slug lengths.

A good agreement was found between theoretical predictions for U_B and the experimental results obtained for the 0.032 m internal diameter column. For the 0.052 m internal diameter column, however, the theory under-predicted the experimental results considerably, a discrepancy also reported by other researchers (Van Hout et al. (2001), Van Hout et al. (2002b), among others).

The obtained bubble-to-bubble interaction curve, the frequency distribution curves of the main flow parameters and the corresponding average values are crucial data for the development and validation of a new slug flow simulator with wide ranges of validity/applicability.

2.8 Acknowledgments

The authors gratefully acknowledge the financial support of Fundação para Ciência e Tecnologia through project POCTI/EQU/33761/1999 and scholarship SFRH/BD/11105/2002. POCTI (FEDER) also supported this work via CEFT.

2.9 Appendix – Results of error analysis for main flow parameters

Every measurement is accomplished within the precision and bias limits of the equipment used in the experimental procedure. Considering that every measured quantity has an associated uncertainty, it is interesting to assess how these uncertainties propagate through the algebraic transformations required to compute every dependent variables. Following the *general uncertainty analysis approach*, a procedure has been implemented for parameters such as bubble velocity, bubble length, liquid slug length, gas and superficial liquid velocities and experimental upward bubble velocity, in order to calculate their relative uncertainties due to initial uncertainties in the

definition of, for instance, the positioning of the bubble boundaries. The results of this analysis are shown in Table 2.3.

Table 2.3 – Relative uncertainties of some flow parameters

	relative uncertainty [%]
U_i	5.0
$h_{b,i}$	2.5
$h_{s,i}$	7.0
U_L	6.3
U_G	7.5
U_B^{exp}	5.0

The results indicate that every slug cell parameter (bubble velocity, bubble length and liquid slug length), determined through the reported image analysis technique, is calculated with a relative uncertainty lower than 7.0 %. The experimental upward bubble velocity is assessed with a 5.0% uncertainty. Additionally, the superficial gas and liquid velocities are evaluated with relative uncertainties between 6.3 % and 7.5 %. These low relative uncertainties increase the level of confidence in the reported results.

The aforementioned results refer to the uncertainty of individual bubbles. Shorter intervals (in percentage) are found, however, if one assesses the intervals around the sample averages that contain, with a certain confidence level, the real average of each parameter (i.e. the confidence intervals: $\pm t\, S_X / \sqrt{n}$). To illustrate the aforesaid, the relative (half) confidence intervals around the trailing bubble velocity estimates of Figure 2.8b, are given, in Figure 2.16, together with the number of elements in each slug length class. This representation shows that, for liquid slugs longer than 4*D*, the half confidence interval extends no further than 1.1% from the corresponding average, which confirms the accurateness of the experimental technique and reported results.

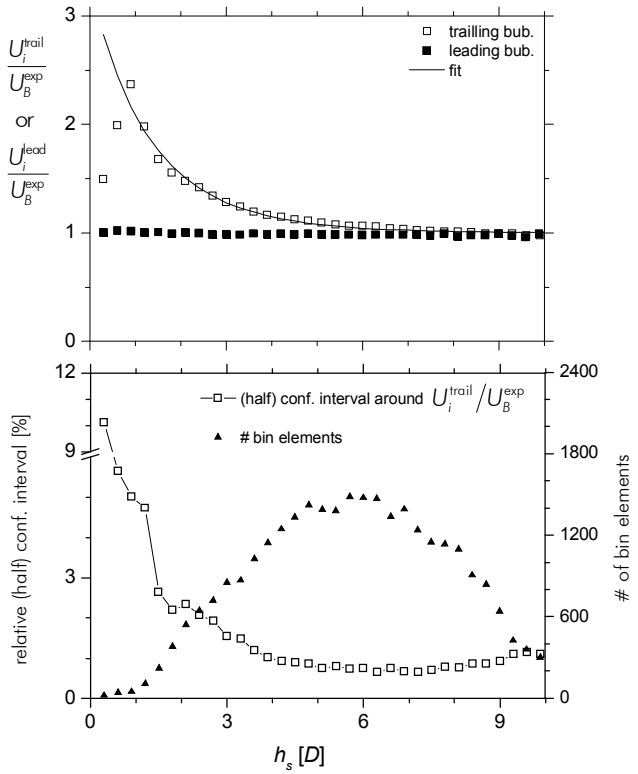

Figure 2.16 – Relative (half) confidence intervals for the estimates of U_i^{trail}/U_B^{exp} and number of elements in each slug length class (bin) plotted against h_s; confidence intervals computed as $\pm t\,S_X/\sqrt{n}$, for confidence level of 95%; 0.032 m ID

2.10 Notation

Roman symbols

a, b and *c*	dimensionless fit parameters	
C	empirical coefficient	
D	column internal diameter	[m]
g	acceleration of gravity	[m/s^2]
$h_{b,\,i}$	length of gas bubble *i*	[m]
$h_{cal.,\,m}$	height of the calibration element, in metres	[m]
$h_{cal.,\,px}$	height of the calibration element, in pixels	[pixel]
h_{im}	height of the field of view	[m]
h_s	length of liquid slug	[m]
$h_{s,\,i}$	length of liquid slug *i*	[m]
H_{cam}	vertical coordinate of the video camera (from the base of the column)	[m]
n	number of element in each class	[#]
S_x	sample standard deviation (for bubble velocity)	[m/s]
t	critical value (t-student distribution)	

t_i	time instant	[s]
t_{i+1}	time instant immediately after t_i	[s]
U_B	upward bubble velocity	[m/s]
U_B^{exp}	experimental average upward bubble velocity in undisturbed conditions	[m/s]
U_G	superficial gas velocity	[m/s]
U_i	upward velocity of bubble *i* (U_i^{trail} and U_i^{lead} for trailing and leading bubble, respectively)	[m/s]
U_∞	upward bubble velocity in a stagnant liquid (drift velocity)	[m/s]
U_L	superficial liquid velocity	[m/s]
U_M	superficial mixture velocity ($= U_L + U_L$)	[m/s]
V_S	liquid velocity relative to the bubble ($= U_B^{exp} - U_M$)	[m/s]
$z_{nose,\ i}$	vertical coordinate of the nose of bubble i, within each image frame	[pixel]
$z_{rear,\ i}$	vertical coordinate of the rear of bubble i, within each image frame	[pixel]

Greek symbols

σ	standard deviation of the distribution of bubble velocities	[m/s]
μ	liquid viscosity	[Pa s]
ρ	liquid density	[kg/m^3]

Dimensionless groups

Re_{U_M}	Reynolds number based on the mixture velocity ($= \rho U_M D/\mu$)
Re_{V_S}	Reynolds number based on the liquid velocity relative to the bubble ($= \rho V_S D/\mu$)

2.11 References

Aladjem Talvy, C., Shemer, L. and Barnea, D., 2000. On the interaction between two consecutive elongated bubbles in a vertical pipe. Int. J. Multiphas. Flow 26: 1905-1923.

Campos Guimarães, R. and A. Sarsfield Cabral, J. (1997). Estatística, McGraw-Hill de Portugal Limitada.

Collins, R., De Moraes, F. F., Davidson, J. F. and Harrison, D., 1978. The Motion of Large Gas Bubble Rising Through Liquid Flowing in a Tube. J. Fluid Mech. 28: 97-112.

Moissis, R. and Griffith, P., 1962. Entrance effects in a two-phase slug flow. J. Heat Transfer 84: 29-39.

Nicklin, D. J., Wilkes, J. O. and Davidson, J. F., 1962. Two-phase flow in vertical tubes. Transactions of the Institution of Chemical Engineers 40: 61-68.

Nogueira, S., Sousa, R. G., Pinto, A. M. F. R., Riethmuller, M. L. and Campos, B. L. M., 2003. Simultaneous PIV and pulsed shadow technique in slug flow: a solution for optical problems. Exp. Fluids 35: 598- 609.

Pinto, A. M. F. R. and Campos, J. B. L. M., 1996. Coalescence of two gas slugs rising in a vertical column of liquid. Chem. Eng. Sci. 51(1): 45-54.

Pinto, A. M. F. R., Pinheiro, M. N. C. and Campos, J. B. L. M., 1998. Coalescence of two gas slugs rising in a co-current flowing liquid in vertical tubes. Chem. Eng. Sci. 53(16): 2973-2983.

Sotiriadis, A. A. and Thorpe, R. B., 2005. Liquid re-circulation in turbulent vertical pipe flow behind a cylindrical bluff body and a ventilated cavity attached to a sparger. Chem. Eng. Sci. 60(4): 981-994.

The MathWorks, I. (2002). Help files of "MATLAB: the language of technical computing".

Van Hout, R., Barnea, D. and Shemer, L., 2001. Evolution of statistical parameters of gas-liquid slug flow along vertical pipes. Int. J. Multiphas. Flow 27(9): 1579-1602.

Van Hout, R., Barnea, D. and Shemer, L., 2002b. Translational velocities of elongated bubbles in continuous slug flow. Int. J. Multiphas. Flow 28(8): 1333-1350.

Van Hout, R., Gulitski, A., Barnea, D. and Shemer, L., 2002a. Experimental investigation of the velocity field induced by a Taylor bubble rising in stagnant water. Int. J. Multiphas. Flow 28(4): 579-596.

White, E. T. and Beardmore, R. H., 1962. The Velocity of Single Cylindrical Air Bubbles Through Liquids Contained in Vertical Tubes. Chem. Eng. Sci. 17: 351-361.

3 Hydrodynamics of gas-liquid slug flow along vertical pipes in turbulent regime – A simulation study[3]

3.1 Abstract

A thorough study on the simulation of gas-liquid vertical slug flow, based on air-water co-current experimental data (Sotto Mayor et al. (2006a)), is reported. The flow pattern in the near wake of bubbles and in the main liquid is turbulent. The slug flow simulator includes adequate computation of gas phase expansion along the column and the introduction, at the column inlet, of distributed gas flow rates and liquid slug lengths. A slug flow entrance-length of 50-70*D* was found for the ranges of superficial gas and liquid velocities studied (0.1-0.5 m/s). A general expression is proposed to predict the modes and standard deviations of bubble velocity, bubble length, and liquid slug length, as a function of several parameters (column vertical coordinate, superficial gas and liquid velocities and column diameter). Gas phase expansion was found to play a major role in the evolution of the velocity and length of bubbles along the column. The liquid slug length is shown to depend mostly on the coalescence effect.

[3] Based on the paper by T. Sotto Mayor, A.M.F.R. Pinto and J.B.L.M. Campos, submitted to Chemical Engineering Research & Design (CheRD)

3.2 Introduction

Several attempts have been made to simulate gas-liquid slug flow in vertical co-current columns operating in turbulent regime. The main purpose is to gather information on the evolution of bubble and liquid slug length distributions along the column. Their average and maximal values (in particular for slug length) as well as several other two-phase flow parameters are indispensable for many engineering calculations. Barnea and Taitel (1993) simulated gas-liquid slug flow in vertical columns operating in the turbulent regime. The model assumes a liquid slug length distribution at the column inlet (random or uniform distribution) and predicts its evolution along the column. The bubble velocity as a function of the liquid slug length ahead of the bubble (as well as the minimal stable liquid slug length) must be introduced as an input relation. The authors adopted the correlation format of Moissis and Griffith (1962), which was established for a short range of operation conditions (in terms of gas and liquid flow rates). Hasanein et al. (1996) implemented a similar strategy using, however, a different correlation between the bubble velocity and the length of the liquid slug ahead of it (based on air-kerosene experimental data). More recently, Van Hout et al. (2001), Van Hout et al. (2003), reported a study on gas-liquid slug flow along vertical and inclined pipes, respectively, in which some simulation results are reported (only for slug length parameter). However, these slug flow simulations were achieved without an exact implementation of the gas phase expansion during the upward movement of the bubbles, and considering constant volumetric gas flow rate at the column inlet (an unreal scenario due to the changing gas hold-up in the column). Moreover, the effects of the superficial gas and liquid velocities and column diameter over the flow parameters were not yet thoroughly analysed. Despite the published models/simulators and experimental data, some doubts still exist concerning the prevailing mechanism in the development of the slug flow pattern: do the inlet gas and liquid distributions determine the development of the slug flow pattern or, alternatively, does the overtaking mechanism by which bubbles coalesce along the column overcome the inlet distributions and determine the output of slug flow experiments? This issue, stressed by Fabre and Liné (1992), remains an open question and, therefore, requires some attention.

The main goal of this work is to formulate a robust predictive model and, through simulation, to produce information on developing slug flow patterns for a large range of operation conditions. The expansion of the gas phase during the rise of the bubbles and the gas flow rate distribution at the column inlet are implemented. The empirical correlation relating the velocity of a bubble and the length of the liquid slug ahead of it is given as input. This correlation was determined for a large range of operating conditions using an non-intrusive technique (see Sotto

Mayor et al. (2006a) for details). The output of the simulation is compared not only with the mentioned experimental results but also with the findings of others researchers.

3.3 Experimental work

A series of air-water co-current slug flow experiments were performed in 6.5 m long acrylic vertical columns with internal diameters of 0.032 m and 0.052 m. These experiments are thoroughly described in Sotto Mayor et al. (2006a) but a brief summary of the experimental approach is given here. The experimental data was collected using an image analysis technique (Sotto Mayor et al. (2006b)) at two vertical coordinates (3.25 m and 5.40 m from the base of the column) and for several superficial gas and liquid velocities (U_G and U_L up to 0.26 m/s and 0.20 m/s, respectively). The operating conditions were designed to have turbulent regime in the main liquid and in the near-wake bubble region. The experimental study served mainly to gather information on the flow pattern characteristics (i.e. bubble length, bubble velocity, liquid slug length) at a given vertical coordinate, and to establish the bubble-to-bubble interaction curve governing the approach and coalescence of consecutive bubbles. The first type of data is crucial for the validation of the simulation approach (section 3.5.2) whereas the second is required to implement the relative motion of bubbles inside the column, i.e. to simulate the development of the slug flow pattern (section 3.4.1.2). The following chapter describes the assumptions and approaches of the slug flow simulation.

3.4 Simulator characteristics

Two adjacent domains are considered in a slug flow column: the bubble formation domain, prior to the column itself, and the simulation domain, where slug flow pattern is expected. Bubble-to-bubble interaction and the expansion of the gas phase are considered only inside the simulation domain. This domain is defined by the input of the column internal diameter (ID) and height. A tank with a large cross-sectional area is located at the top of the column (where gas-liquid separation occurs) with a lateral exit (assuring an almost constant level of aerated liquid). The origin of the vertical coordinate matches the boundary between bubble formation and simulation domains.

3.4.1 Model assumptions and inputs

The main assumptions of the model for bubble shape, thickness of the annular liquid film and velocity of bubbles are described in the following sections.

3.4.1.1 Bubble shape and surrounding liquid film

The bubble shape is taken cylindrical. The thickness of the liquid flowing around the bubbles, δ, is calculated assuming a free-falling film. Following the approach of Brown (1965) for laminar regime in the film, one can use the following equation to compute the liquid film thickness, for continuous co-current gas-liquid flow:

$$\frac{\delta}{R_c} = \left\{ \frac{3\nu}{2g(R-\delta)} \left[(R_c - \delta)^2 U_B^{exp} - R_c^2 (U_G + U_L) \right] \right\}^{1/3} \tag{3.1}$$

where υ is the kinematic viscosity, R_c is the column internal radius, g is the acceleration of gravity, U_B^{exp} is the experimental upward bubble velocity in undisturbed conditions and U_G and U_L are the superficial gas and liquid velocities, respectively.

3.4.1.2 Bubble velocity as a function of the liquid slug length ahead of it – an input relation

Consider a train of Taylor bubbles flowing upwards in a vertical column, in slug flow pattern (as a set of consecutive slug unit cells, i.e. bubble plus the liquid slug below it). The velocity of a trailing bubble flowing in the column depends on the length of the liquid slug ahead of it. In the experimental study mentioned previously, Sotto Mayor et al. (2006a) found a single curve for this dependency, for the two diameters and column vertical coordinates tested (0.032 m and 0.052 m; 3.25 m and 5.40 m, respectively). The obtained average bubble-to-bubble interaction curve is shown in Figure 3.1a together with the best fit equation.

The form and parameters of the fit equation are shown below:

$$\frac{U_i^{trail}}{U_B^{exp}} = 1 + 2.4e^{-0.8\left(\frac{h_{s,i-1}}{D}\right)^{0.9}} \tag{3.2}$$

where U_i^{trail} refers to the velocity of a trailing bubble i flowing behind a liquid slug with length $h_{s,\,i-1}$ (bubbles and slugs numbered from top to bottom), and D stands for the column diameter. The trailing bubble velocity is normalised by the experimental upward bubble velocity in undisturbed conditions (U_B^{exp}).

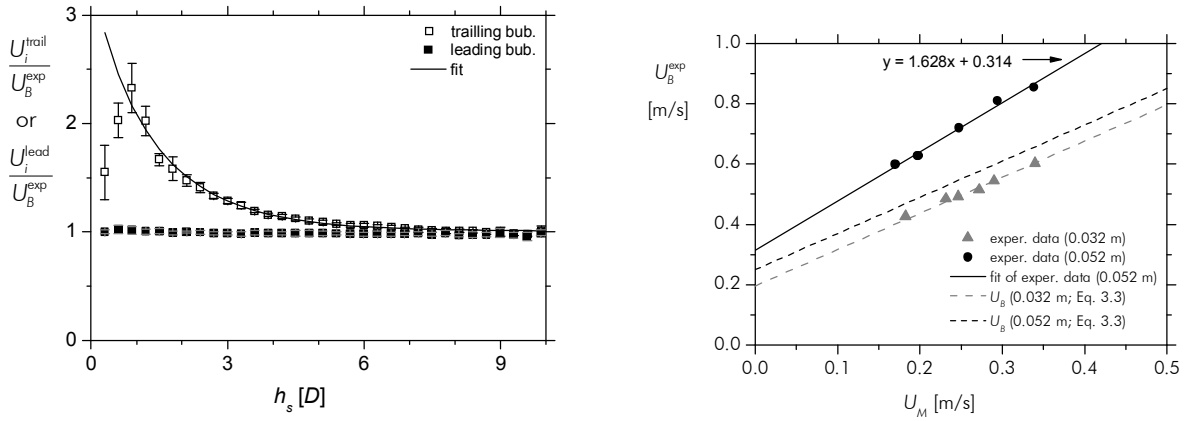

a b

Figure 3.1 – (a) Average bubble-to-bubble interaction curve with 95% confidence intervals and (b) experimental average upward bubble velocity plotted against U_M, after correction for vertical coordinate 5.4 m; internal diameter: 0.032 m and 0.052 m; data after Sotto Mayor et al. (2006a)

The estimates of U_B^{exp} obtained in the experimental study are plotted against the superficial mixture velocity ($U_M = U_L + U_G$) in Figure 3.1b, together with the predictions from Nicklin et al. (1962) for co-current flow in turbulent regime. The Nicklin correlation is of the form:

$$U_B = U_\infty + CU_M \tag{3.3}$$

where U_∞, the drift velocity, is the bubble rising velocity through a stagnant liquid and C an empirical parameter depending on the flow regime in the liquid. The drift velocity can be computed by $0.35\sqrt{gD}$ for inertial controlled regime (White and Beardmore (1962)) whereas parameter C is generally taken equal to 1.2 for turbulent regime in the liquid (Nicklin et al. (1962), Collins et al. (1978), Bendiksen (1984)).

For the narrower column reported in Sotto Mayor et al. (2006a) (0.032 m), a good agreement was obtained between the parameter U_B^{exp} and the estimates of U_B (Eq. (3.3)) based on values of C and U_∞ as in the literature (C=1.2 and U_∞=0.196 m/s). For the larger column (0.052 m), the values of U_B^{exp} were found higher than the estimates of U_B computed in the same way (Eq. (3.3) with C and U_∞ as in the literature). Therefore, the simulations for the larger column must be based on estimates of U_B^{exp} computed using the best fit values of C and U_∞ (1.628 and 0.314 m/s, respectively).

3.4.2 Slug flow conditions at inlet

The simulation algorithm considers two independent variable distributions at the column inlet: slug length and gas flow rate distributions. Several types of slug length distributions were

implemented (normal, uniform, constant and user-defined distributions). A normal distribution was implemented for the gas flow rate. Normal distributions were prepared using the Box Muller algorithm (Campos Guimarães and A. Sarsfield Cabral (1997)). The following sections provide information about the relations governing the inlet slug flow for constant and distributed gas flow rates.

3.4.2.1 Bubble length as a function of the slug length – constant gas flow rate

Consider Figure 3.2a, representing a train of Taylor bubbles flowing in the bubble formation domain (prior to the column inlet). In order to assure constant gas and liquid superficial velocities, a relationship must exist (at the referred coordinate) between the length of each bubble and the length of the liquid slug, in each unit cell. Notice in Figure 3.2a the presence of long liquid slugs flowing immediately after long bubbles.

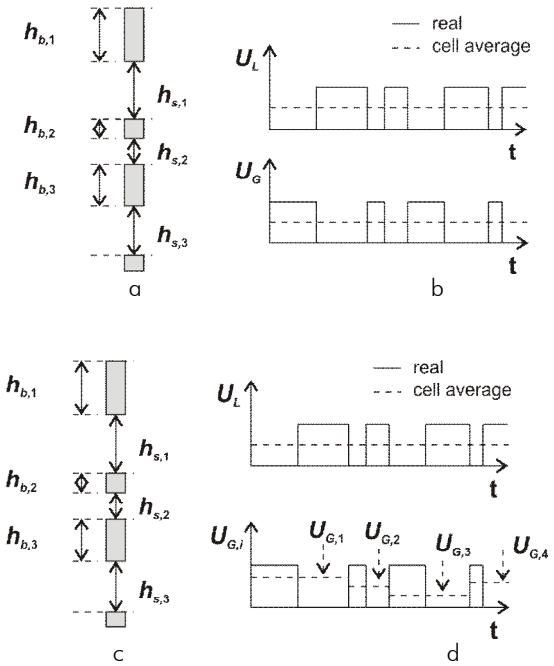

Figure 3.2 – Representation of gas liquid distributions, in the bubble formation domain, for (a-b) constant gas flow rate and (c-d) variable gas flow rate

Assuming a cylindrical bubble shape, one can write:

$$U_G S_c \Delta t_i = S_b h_{b,i} \tag{3.4}$$

where Δt_i refers to the time interval required for the entrance of a slug unit cell (bubble + slug), $h_{b,\,i}$ is the length of bubble i, and S_c and S_b stand for column and bubble cross-sectional area,

respectively. Considering that in the bubble formation domain no bubble-to-bubble interaction is acknowledged, bubbles move upwards in the column at their undisturbed velocity (given by U_B^{exp}). Therefore:

$$U_B^{exp}\Delta t_i = h_{b,i} + h_{s,i} \tag{3.5}$$

By combining the previous equations and rearranging, it follows:

$$h_{b,i} = \frac{h_{s,i}}{\frac{S_b U_B^{exp}}{S_c U_G} - 1} \tag{3.6}$$

Eq. (3.6), valid at the column inlet, relates the length of each bubble to the length of the liquid slug flowing bellow, for given superficial gas and liquid velocities (U_B^{exp} encloses the influence of U_L as in Eq. (3.3)). Thus, having prepared a slug length distribution and defined the superficial gas and liquid velocities, one can prepare the corresponding bubble length distribution by using Eq. (3.6) for all unit cells. Notice that the slug length distribution is the independent distribution, whereas the bubble length distribution is the dependent one.

3.4.2.2 Bubble length as a function of the slug length – variable gas flow rate

The turbulence at the column base, caused by the injection of the gas followed by bubble formation (intense bubble coalescence and break-up), and the constant alteration of the hydrostatic pressure in this region due to the changing gas hold-up in the column, advise acknowledgement of a variable gas flow rate at the column inlet. For this purpose a distributed gas flow rate (with a certain average and standard deviation) was implemented in the simulation code. Figure 3.2c depicts this issue. Notice in Figure 3.2d that each unit cell has a different gas superficial velocity in this new scenario.

At the column inlet, the relationship between the length of the bubbles and the length of the liquid slugs for each unit cell is now given by:

$$h_{b,i} = \frac{h_{s,i}}{\frac{S_b U_B^{exp}}{S_c U_{G,i}} - 1} \tag{3.7}$$

where $U_{G,i}$ is the superficial gas velocity associated to each unit cell (Figure 3.2d). Having defined a slug length distribution and a gas flow rate distribution (and defined U_L) one can thus prepare the

corresponding bubble length distribution, by using Eq. (3.7), for all unit cells. In this new situation two independent distributions exist: slug length distribution and gas flow rate distribution.

3.4.3 Simulation start-up

The simulation start-up is initiated by defining the superficial gas velocity, U_G^{inlet}, at the hydrostatic pressure at the column inlet. That parameter relates the volume of gas passing at the inlet coordinate with the time required for the entrance of *n* unit cells, and it can be determined by:

$$U_G^{inlet} = \frac{S_b \sum_{i=1}^{n} h_{b,i}}{S_c \sum_{i=1}^{n} \Delta t_i} \tag{3.8}$$

Notice that the Box Muller algorithm, used to prepare the gas flow rate distribution, requires the input of the arithmetic average of the distribution to be created, $U_G^{inlet}\big|_{\mu}$, as in the following equation:

$$U_G^{inlet}\Big|_{\mu} = \frac{\sum_{i=1}^{n} U_{G,i}}{n} = \frac{S_b \sum_{i=1}^{n} \frac{h_{b,i}}{\Delta t_i}}{S_c n} \tag{3.9}$$

Bearing in mind that Eqs. (3.8) and (3.9) define two different quantities, an iterative procedure had to be implemented to initiate the simulation. Figure 3.3 illustrates the strategy pursued. The iterative cycle converges when the parameter U_G^{inlet} (evaluated at the inlet through Eq. (3.8)) reaches the proposed value, introduced as input. Once the convergence is achieved the simulator holds two distributions (slug length and bubble length distributions, related by Eq. (3.7)) which assure the required average superficial liquid and gas velocities at the column inlet. However, the use of the superficial gas velocity at the inlet hydrostatic pressure is not a practical approach since the ambient pressure is usually taken as reference. In order to prepare the simulator to receive the average superficial gas velocity at ambient pressure as input, an outer iterative cycle was implemented. This external iterative cycle requires several slug flow simulations with differing values of U_G^{inlet} to be run iteratively, until the required average superficial gas velocity is achieved at the top of the column. Bisections' method was used within the mentioned iterative cycles.

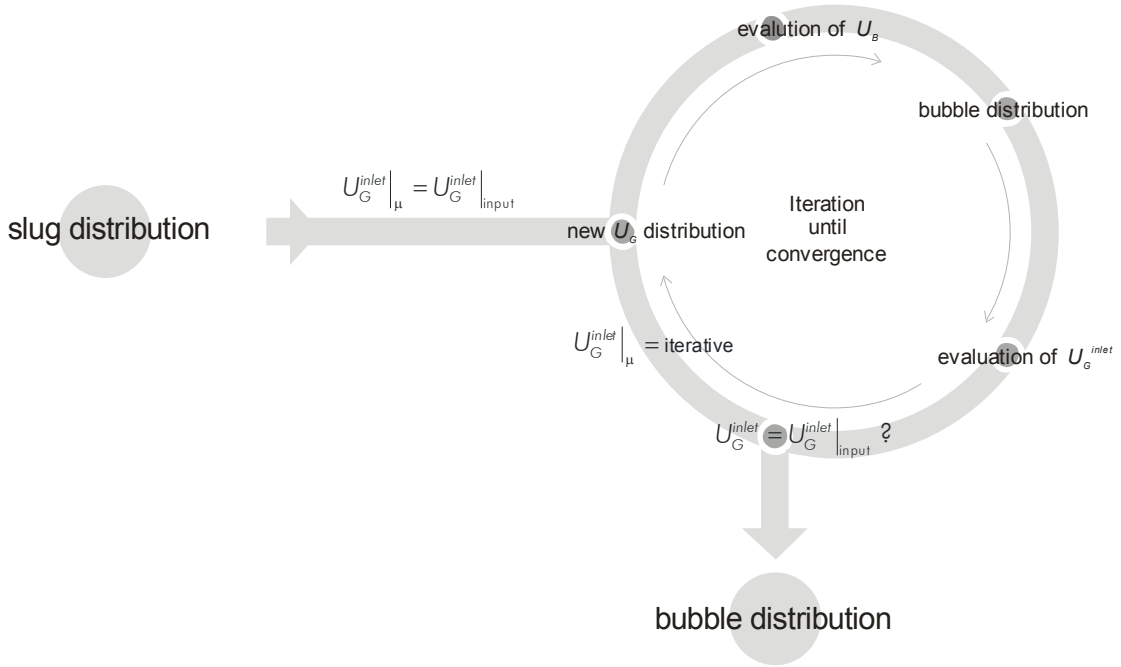

Figure 3.3 – Representation of the iterative approach of the simulation start-up

3.4.4 The displacement of the bubbles along the column

The displacement of bubbles along the column is implemented as the incremental movement of their boundaries (bubble nose and rear) between consecutive instants (t_i and t_{i+1}). The position of the rear of bubble i at instant t_{i+1}, $z_{rear,i}^{t_{i+1}}$, is computed by updating its position at t_i, $z_{rear,i}^{t_i}$, according to its velocity (U_i).

$$z_{rear,i}^{t_{i+1}} = z_{rear,i}^{t_i} + U_i\,(t_{i+1} - t_i) \tag{3.10}$$

Bubble velocity U_i has two contributions: one related to the length of the slug ahead of the bubble (given by Eq. (3.2)), and another related to the expansion of the gas bubbles flowing upstream (below) the bubble. This latter contribution is described in the following section. The update of the position of the bubble rear is achieved assuming a constant bubble velocity between consecutive time instants, an assumption whose accuracy increases for decreasing time increment. The position of the bubble nose is updated according to:

$$z_{nose,i}^{t_{i+1}} = z_{rear,i}^{t_{i+1}} + h_{b,i}^{t_{i+1}} \tag{3.11}$$

Taking the boundaries of two consecutive bubbles, the length of the liquid slug flowing in-between them is given by:

$$h_{s,i}^{t_{j+1}} = z_{rear,i}^{t_{j+1}} - z_{nose,i+1}^{t_{j+1}} \tag{3.12}$$

This strategy extends to all the bubbles flowing in the column.

3.4.5 Expansion of the gas phase along the column

As gas bubbles rise along a vertical column there is a decrease in the hydrostatic pressure acting on each bubble. According to the *ideal gas law* this decrease results in the expansion of the gas phase, i.e. an increase in the volume of each bubble. Notice that when the pressure drop in the liquid phase (at the wall and at the wake of the bubbles) is discarded, the hydrostatic gradient is the only pressure grading acting on the bubble.

It is reasonable to assume that, with an open tank at the column top, the bubble expansion occurs as a rise of the bubble nose region (reference frame attached to the bubble), since there is no volume, upstream (below) of each bubble, to accommodate the extra volume resulting from the bubble expansion. Thus, the bubble expansion induces the upward displacement of everything ahead of the bubble (liquid and gas).

In order to calculate the volume (or length) of bubbles at a given column position, the hydrostatic pressure acting on each bubble and the number of moles of air in each bubble must be known. This latter parameter can be assessed, for instance, at the entrance of the column (inlet position) where the hydrostatic pressure can easily be computed.

3.4.5.1 Evaluation of the amount of air in a bubble, at the column inlet

As bubbles enter the simulation domain (where expansion phenomena are acknowledged), different hydrostatic pressures act on each bubble depending on the gas hold-up in the column. Figure 3.4a depicts one of these instants. The hydrostatic liquid height above a bubble *i*, at the instant it enters the column, can be calculated taking only the amount of liquid inside the column at that instant:

$$H_{hyd,i} = z_{liq.} - \frac{S_b}{S_c}\sum_{k=1}^{i-1}\left(h_{b,k}\,\alpha_k\right) \tag{3.13}$$

where $H_{hyd,\,i}$ is the hydrostatic liquid height above the bubble *i* and α_k a parameter informing on the positioning of the bubbles relative to the tank base (z_T). This parameter is defined as follows:

$$\begin{cases} \text{bubbles totally inside the column} & \Rightarrow \ \alpha_k = 1 \\ \text{bubbles crossing the tank base} & \Rightarrow \ \alpha_k = (z_T - z_{rear,k}) / h_{b,k} \\ \text{bubbles totally inside the tank} & \Rightarrow \ \alpha_k = 0 \end{cases} \tag{3.14}$$

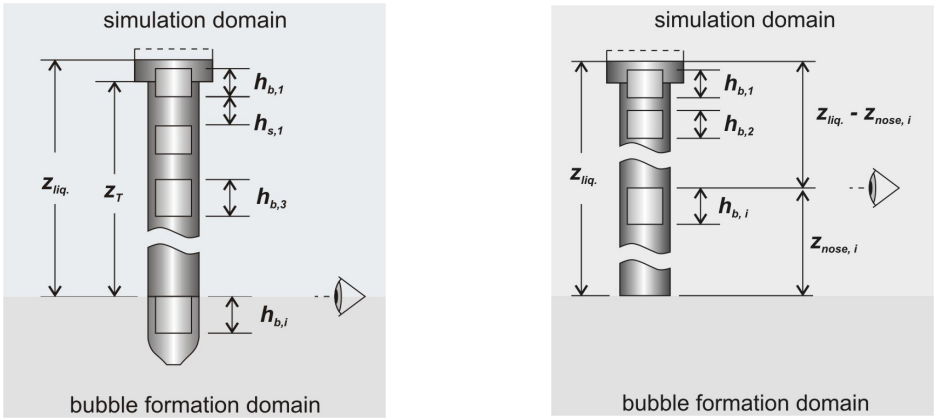

Figure 3.4 – Representation of the upward movement of a Taylor bubble (a) at inlet and (b) inside the column

The last parcel of the right hand side of Eq. (3.13) accounts for the decrease in $H_{hyd,\,i}$ (relative to the scenario of a column full of liquid), due to the presence of bubbles inside the column. The use of parameter α_k is related to the following. The tank cross-sectional area is considerably higher than the column's and, thus, it is reasonable to assume that the pressure at the base of the tank depends only on the height of liquid above that position ($z_{liq} - z_T$), regardless of the presence of a bubble entering the tank (or even totally inside the tank). However, the portion of a bubble still inside the column (i.e. below z_T) should not be neglected when computing the hydrostatic liquid height above the bubble at the column inlet ($H_{hyd,\,i}$). The volume of liquid inside the column is reduced by the presence of a bubble crossing the tank base (or totally inside the column) and, consequently, the pressure acting on the bubble at the column inlet is also reduced. Notice, for instance, that the presence of a bubble totally inside the tank does not alter the pressure acting at the column inlet and, in agreement with this, the summation in the previous equation does not depend on the length of such a bubble (since $\alpha_k = 0$).

Once defined $H_{hyd,\,i}$, the hydrostatic pressure acting on bubble *i* at the inlet coordinate can then be computed by:

$$P_{hyd,i} = \rho g H_{hyd,i} \tag{3.15}$$

where ρ is the density of the liquid and *g* is the acceleration of gravity. An algebraic transformation of the *ideal gas law* with further substitution of the pressure according to Eq. (3.15) gives origin to an expression that computes the number of moles of air in a bubble *i*, at the inlet coordinate:

$$n_i = \frac{h_{b,i} S_b \left(P_{atm} + \rho g H_{hyd,i} \right)}{RT} \tag{3.16}$$

where P_{atm} stands for ambient pressure, T refers to the temperature, R is the *ideal gas* constant and n_i is the number of moles of air in bubble i. As before, this strategy extends to all the bubbles entering the column. The computation of the previous parameter is a requirement for the implementation of the bubble expansion along the column. Note that bubbles having the same length might contain different number of moles of air, provided that the hydrostatic pressure acting on the bubbles is different by the time they enter the simulation domain. This fact is related to the requirement of a determined volumetric gas flow rate (distributed but nonetheless determined) at the inlet coordinate, at the expense of a changing mass flow rate.

3.4.5.2 Gas expansion – effect over the length of the bubble

Figure 3.4b illustrates an instant in the upward movement of bubbles inside the simulation domain. The hydrostatic pressure acting on bubble i is given by an expression similar to Eq. (3.13), with a correction to account for the positioning of the bubble ($z_{nose,\,i}$).

$$H_{hyd,i} = z_{liq.} - z_{nose,i} - \frac{S_b}{S_c} \sum_{k=1}^{i-1} \left(h_{b,k} \alpha_k \right) \tag{3.17}$$

If Eq. (3.16) is transformed to isolate $h_{b,\,i}$ and $H_{hyd,\,i}$ is further substituted according to Eq. (3.17), one obtains:

$$h_{b,i} = \frac{n_i RT}{S_b \left(P_{atm} + \rho g H_{hyd,i} \right)} \tag{3.18}$$

Knowing the positioning of a bubble i, Eq. (3.18) allows the computation of the length of a bubble i as a function of the hydrostatic pressure acting on it. This is not, however, a sequential calculation. The length of a bubble is a function of the vertical coordinate of the bubble nose (see Eq. (3.18)) whose computation, in turn, requires an estimate of the length of the bubbles (see Eq. (3.11)). This requires an iterative approach. Figure 3.5 illustrates this procedure.

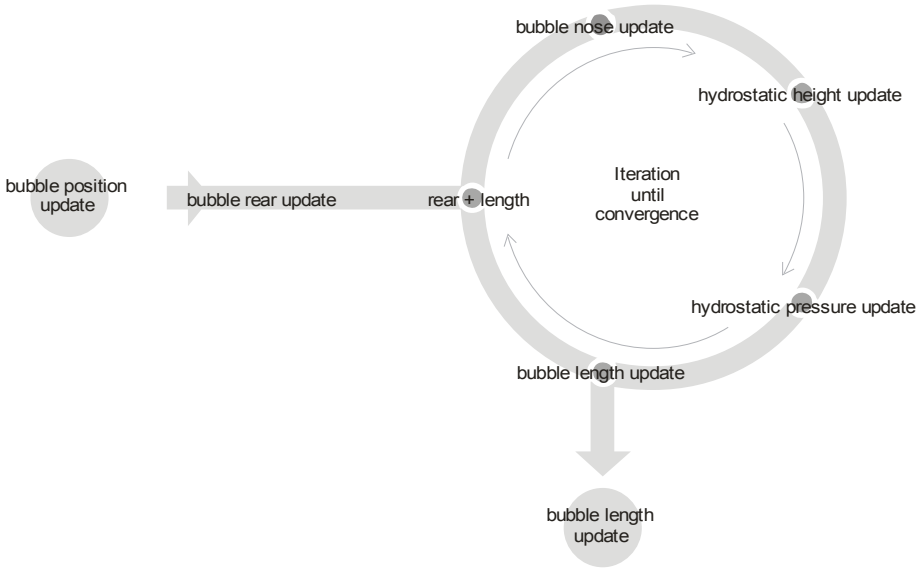

Figure 3.5 – Iterative procedure for the implementation of the upward bubble movement and consequent expansion

3.4.5.3 Gas expansion – effect over the velocity of the bubble

Consider two consecutive instants (t_i and t_{i+1}) in the movement of a train of bubbles inside the column. From instant t_i to t_{i+1}, all bubbles had their positions updated according to their upward velocity (section 3.4.4). The hydrostatic height above each bubble decreased from instant t_i to t_{i+1} and, therefore, all bubbles expanded accordingly (section 3.4.5.2). Consider a bubble i inside the column and the liquid flowing ahead of it. The expansion of the bubbles under bubble i induces a raise in the liquid and gas ahead of them, proportional to the sum of the individual expansions undergone by each bubble (Δh_1, ..., Δh_n), and given by:

$$\Delta z_{\text{expans.}}^{\text{ahead } i} = \frac{S_b}{S_c} \sum_{k=i+1}^{n} \Delta h_k \tag{3.19}$$

This "extra" upward displacement of liquid and gas can be seen as an increase in the liquid and gas superficial velocities. This increase can be calculated dividing $\Delta z_{\text{expans.}}^{\text{ahead } i}$ by the time increment between the two consecutive instants under focus ($t_{i+1} - t_i$), as in the following equation:

$$\Delta U_{\text{expans.}}^{\text{ahead } i} = \frac{\Delta z_{\text{expans.}}^{\text{ahead } i}}{t_{i+1} - t_i} = \frac{S_b}{S_c (t_{i+1} - t_i)} \sum_{k=i+1}^{n} \Delta h_k \tag{3.20}$$

where $\Delta U_{\text{expans.}}^{\text{ahead } i}$ is the increase in the flow velocity ahead of bubble i, due to the expansion of all bubbles flowing below it.

The upward velocity of gas bubbles flowing in a co-current liquid flow depends on the velocity profile of the liquid phase ahead. This dependence is usually introduced by parameter C (equal to the ratio between the maximum and average liquid velocity), whose value depends on the flow regime (or velocity profile) in the liquid. Thus, the overall velocity of a trailing bubble flowing in co-current flow is the result of two contributions: one related to the length of the liquid slug ahead of it (Eq. (3.2)), and another related to the "extra" upward displacement of the liquid and gas due to the gas phase expansion (Eq. (3.20)). The following equation allows the computation of the overall velocity of a trailing bubble *i*, in a train of bubbles flowing upwards:

$$U_i^{\text{trail}} = U_B^{\text{exp}}\left[1+2.4e^{-0.8\left(h_{s,i-1}/D\right)^{0.9}}\right]+\frac{C\,S_b}{S_c\left(t_{j+1}-t_j\right)}\sum_{k=i+1}^{n}\Delta h_k \qquad (3.21)$$

where U_B^{exp} must be computed by Eq. (3.3) after substitution of U_G by U_G^{inlet}. This substitution allows for the estimation of the undisturbed upward bubble velocity discarding the effect of the gas phase expansion along the column. Recall that this effect is computed by the last parcel of the right hand side of Eq. (3.21). In addition, the values of C and U_∞ required for the computation of U_B^{exp} are set as discussed in section 3.4.1.2. Finally, the estimates of U_i^{trail} given by Eq. (3.21) are used in Eq. (3.10) to update the position of bubble boundaries (implementing in that way the upward movement of bubbles).

3.5 Results and discussion

3.5.1 Grid tests

Several simulations were performed to determine the time increment and the initial number of bubbles needed to assure adequate representativity of the simulation results. These analyses were based on the bubble-to-bubble interaction curve and on the frequency distribution curves for bubble velocity, bubble length and liquid slug length. The simulation results were found to be adequately represented when simulations were based on a minimal number of 2500 bubbles and a time increment of 0.005 s.

3.5.2 Simulation results versus experimental data

In the following sections a comparison between experimental data and simulation results for three column diameters (0.052, 0.032 and 0.024 m) is shown. The experimental data for the

larger columns (0.052 and 0.032 m; 6.5 m long) are thoroughly described in Sotto Mayor et al. (2006a), whereas the data for the narrower column (0.024 m; 10 m long) are taken from Van Hout et al. (2001) and Van Hout et al. (2003). Normal distributions of slug length (h_s) and superficial gas velocity (U_G) are introduced at the inlet, for the three columns reported (distribution of h_s: $\mu \approx 5D$ and $\sigma \approx 2D$; distribution of U_G: $\sigma/\mu \approx 10\%$). The inlet distributions, however, are shown later not to determine the outlet results.

3.5.2.1 0.052 m internal diameter

Two flow conditions are compared in this section: one with superficial liquid and gas velocities equal to 0.074 m/s and 0.10 m/s (Figures 3.6a-c and 3.7a-b) and another with 0.10 m/s and 0.21 m/s, respectively (Figures 3.6d-f and 3.7c-d); ambient pressure is used as the reference throughout the whole chapter, unless told otherwise. Experimental values of C and drift velocity ($C=1.628$ and $U_\infty=0.314$ m/s, from Sotto Mayor et al. (2006a)) are used to estimate the experimental upward bubble velocity (U_B^{exp}). The focus is on results at 5.4 m from the base of the column (vertical column coordinate at which the experimental data were acquired).

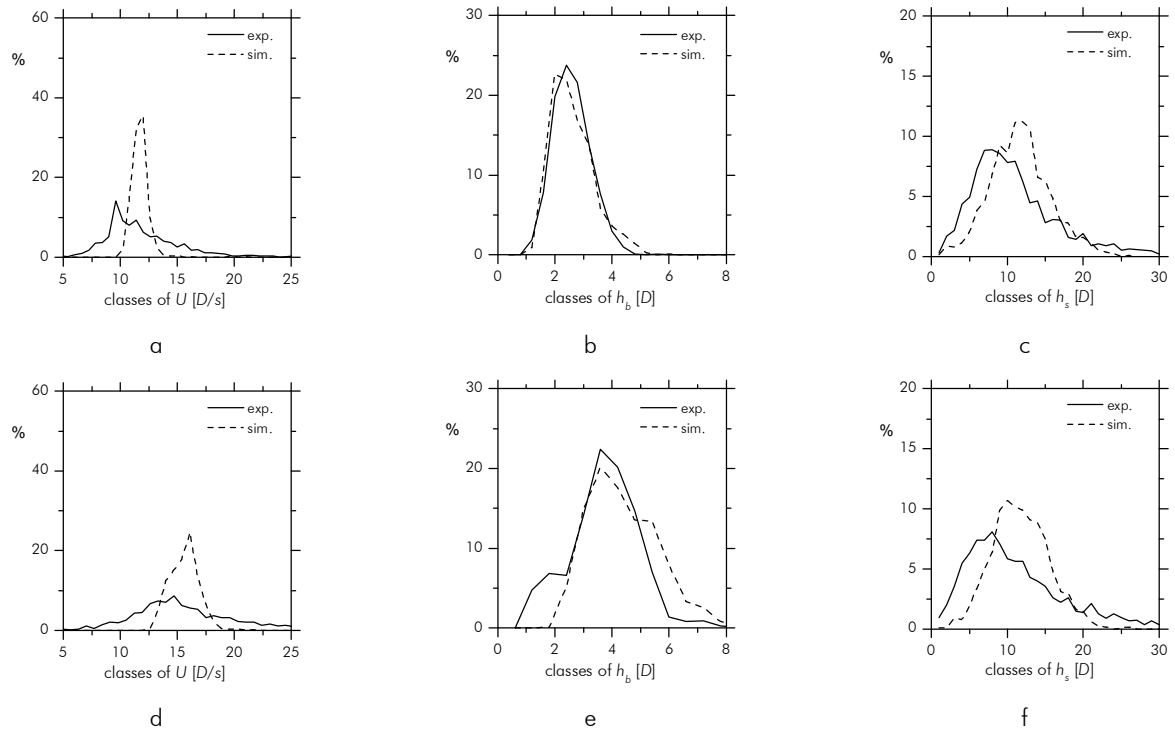

Figure 3.6 – Frequency distribution curves: (a) bubble velocity, (b) bubble length and (c) slug length, for an experiment/simulation with $U_L \approx 0.074$ m/s and $U_G \approx 0.10$ m/s; (d) bubble velocity, (e) bubble length and (f) slug length, for an experiment/simulation with $U_L \approx 0.10$ m/s and $U_G \approx 0.21$ m/s; 0.052 m ID; vertical coordinate: 5.4 m

The distributions of bubble velocity, resulting from the simulation of both flow conditions, have lower standard deviations than the corresponding experimental distributions (Figures 3.6a and 3.6d, in terms of the frequency distribution curves, or Figures 3.7b and 3.7d, directly from the standard deviation charts). The high standard deviations of the experimental distributions are related to the continuous acceleration and slowing down of bubbles rising in the column, in part due to the level of turbulence of the flow and to the aeration level of the slugs. More details on this issue can be found in Sotto Mayor et al. (2006a). Despite the discrepancy in the standard deviations, good agreement exists in terms of the average and mode of the velocity distributions (as can be seen in the charts of Figures 3.7a and 3.7c).

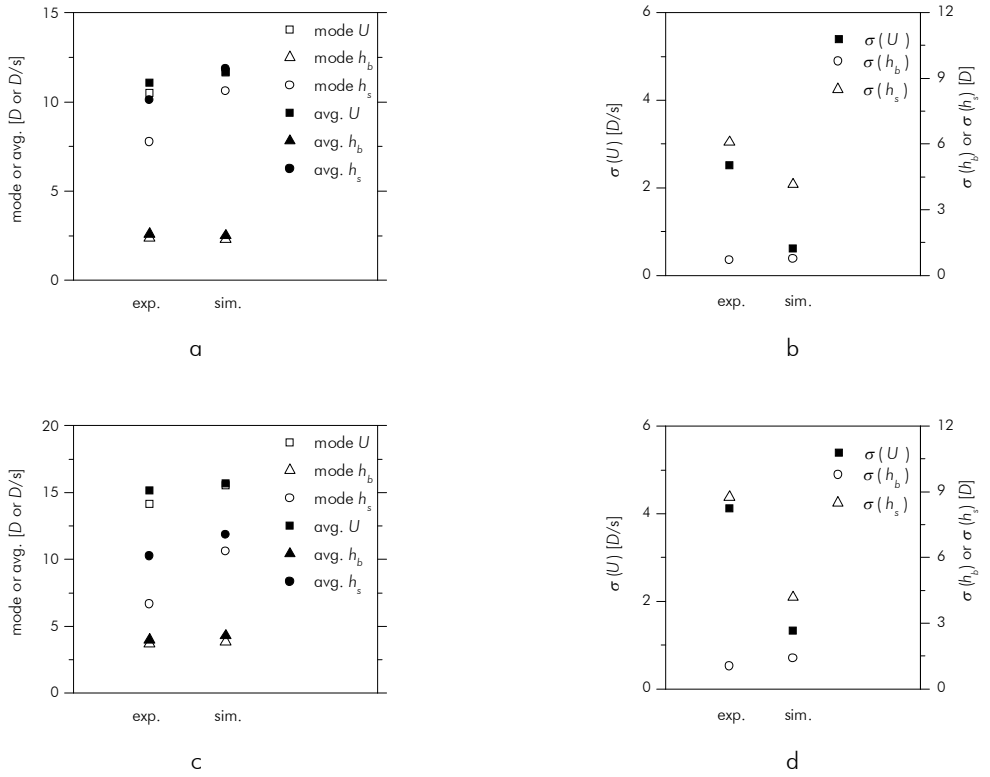

Figure 3.7 – Log-normal fit parameters: (a) average, mode and (b) standard deviation, for an experiment/simulation with $U_L \approx 0.074$ m/s and $U_G \approx 0.10$ m/s; (c) average, mode and (d) standard deviation, for an experiment/simulation with $U_L \approx 0.10$ m/s and $U_G \approx 0.21$ m/s; 0.052 m ID; vertical coordinate: 5.4 m

Excellent agreement is found between experimental data and simulation results regarding the distribution of bubble lengths, for both the flow conditions compared (Figures 3.6b and 3.6e). Quite reasonable agreement is obtained for the distribution of slug lengths (Figures 3.6c and 3.6f). The charts of Figures 3.7a and 3.7c, showing the corresponding log-normal fit parameters, corroborate these conclusions.

The experimental slug length frequency distribution curves show wider tails than the corresponding simulation curves (Figures 3.6c and 3.6f). This discrepancy may be partially related to the experimental methodology used. In fact, in order to calculate the length of liquid slugs, constant velocity was assumed for the preceding bubbles between the moment those bubbles cross a certain reference line and the moment the following bubbles do. Considering the high standard deviation of the experimental distributions of the bubble velocities (Figures 3.7b and 3.7d), this assumption, although unavoidable, may lead to a marginal increase in the occurrence of extreme slug length values (either short or long).

3.5.2.2 0.032 m internal diameter

Following an approach similar to that used for the larger column (0.052 m), two different flow conditions are compared here: one with a lower gas flow rate ($U_L \approx 0.10$ m/s and $U_G \approx 0.088$ m/s) and another with a higher gas flow rate ($U_L \approx 0.10$ m/s and $U_G \approx 0.26$ m/s). Experimental values of C and drift velocity, for the 0.032 m internal diameter column, are estimated according to the literature ($C=1.2$ and $U_\infty = 0.196$ m/s; see section 3.4.1.2).

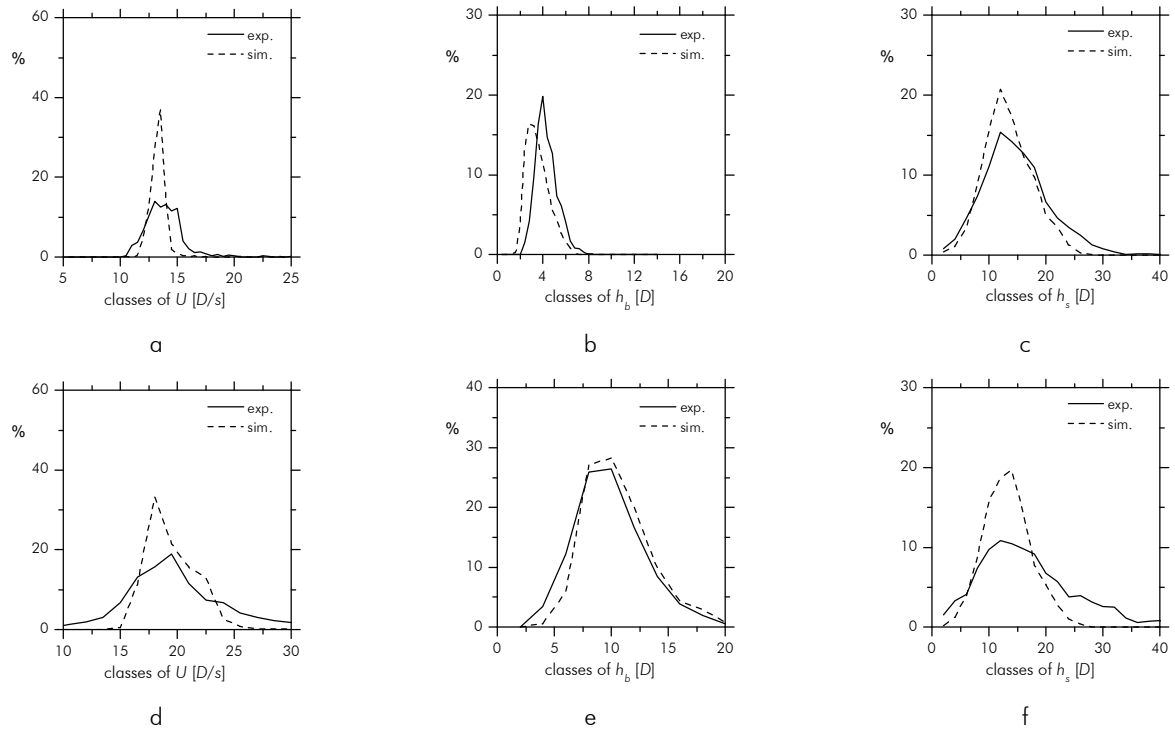

Figure 3.8 – Frequency distribution curves: (a) bubble velocity, (b) bubble length and (c) slug length, for an experiment/simulation with $U_L \approx 0.10$ m/s and $U_G \approx 0.088$ m/s; (d) bubble velocity, (e) bubble length and (f) slug length, for an experiment/simulation with $U_L \approx 0.10$ m/s and $U_G \approx 0.26$ m/s; 0.032 m ID; vertical coordinate: 5.4 m

There is a very good agreement between experimental data and simulation results regarding the average and mode of the bubble velocity distributions (Figures 3.9a and 3.9c), for both flow conditions. As for the larger column, however, different standard deviations are obtained (Figures 3.9b and 3.9d). The bubble length distributions from the simulations of both flow rate conditions represent the corresponding experimental data (Figures 3.8b and 3.8e) reasonably well.

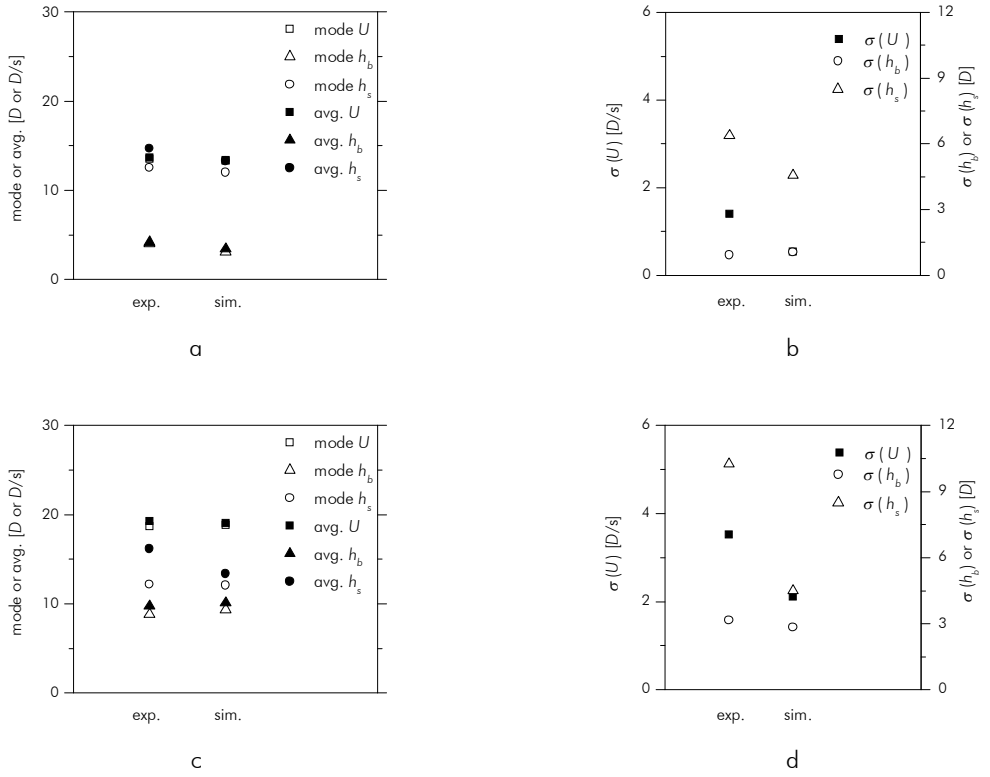

Figure 3.9 – Log-normal fit parameters: (a) average, mode and (b) standard deviation, for an experiment/simulation with $U_L \approx 0.10$ m/s and $U_G \approx 0.088$ m/s; (c) average, mode and (d) standard deviation, for an experiment/simulation with $U_L \approx 0.10$ m/s and $U_G \approx 0.26$ m/s; 0.032 m ID; vertical coordinate: 5.4 m

There is a slight underestimation, though, for the lower flow rate condition. The slug length distributions from the simulations of both flow conditions are in good agreement with the experimental data. Slightly wider tails in the experimental frequency distribution curves occur, however, particularly for the higher flow rate condition (Figure 3.8f). Similar behaviour has been observed for the larger column. Nevertheless, very similar modes are obtained (Figures 3.9a and 3.9c).

3.5.2.3 0.024 m internal diameter

In order to extend the validity ranges of the proposed simulator, the experimental results regarding a 0.024 m internal diameter column reported by Van Hout et al. (2001) were compared

to simulation results. The flow in a 10 m long column was simulated considering two reported conditions: one with $U_L \approx 0.01$ m/s and $U_G \approx 0.41$ m/s (Figure 3.10a-b) and another with $U_L \approx 0.10$ m/s and $U_G \approx 0.63$ m/s (Figure 3.10c-d). Experimental values of C and drift velocity are considered well-predicted by expressions in the literature ($C=1.2$ and $U_\infty=0.17$ m/s, following White and Beardmore (1962)), an assumption corroborated by the author's findings (translational bubble velocities obtained approaching the upward bubble velocity as defined by Nicklin, Eq. (3.3), near the top of the column). Focus is put on the data acquired at 6.88 m from the base of the column.

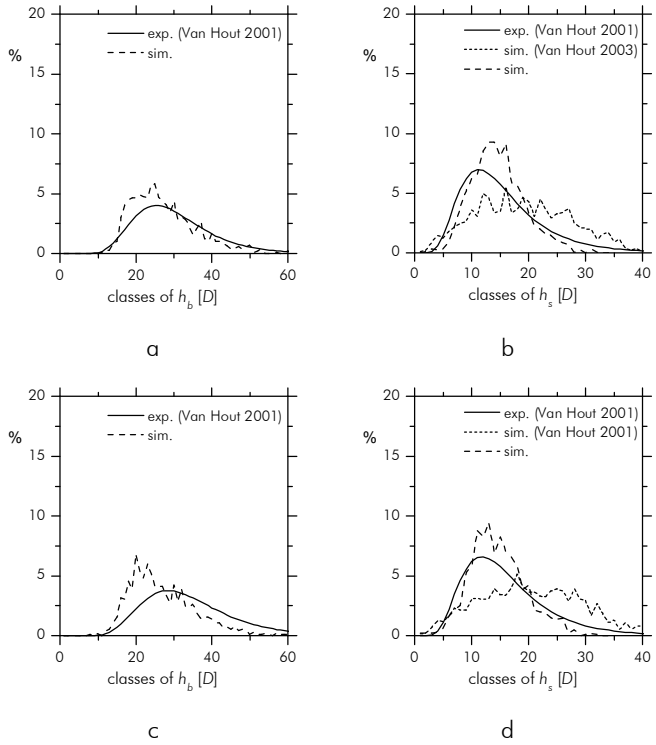

Figure 3.10 – Frequency distribution curves of (a) bubble length and (b) slug length, for an experiment/simulation with $U_L \approx 0.01$ m/s and $U_G \approx 0.41$ m/s; (c) bubble length and (d) slug length, for an experiment/simulation with $U_L \approx 0.10$ m/s, $U_G \approx 0.63$ m/s; 0.024 m ID, vertical coordinate: 6.88 m

A very reasonable agreement between experimental data and simulation results is obtained, for both flow rate conditions, regarding the frequency distribution curves for bubble length (Figures 3.10a and 3.10c). Moreover, a very good agreement is obtained for the slug length variable (Figures 3.10b and 3.10d). Indeed, very similar modes are obtained from the distribution curves for this variable, for both flow rate conditions. In Figures 3.10b and 3.10d, the simulated frequency distribution curves from Van Hout et al. (2001), Van Hout et al. (2003) for the slug length variable are also shown (curves drawn directly from the charts of the mentioned publications). No simulation curves are given, unfortunately, regarding the frequency distribution for bubble length. Nevertheless, from the analysis of the frequency distribution curves for slug

length, it can be concluded that a better representation of the reported experimental data is obtained by using the simulator described in the present work.

3.5.3 On the influence of the inlet slug length distribution

Three simulations with different inlet slug length distributions are compared in order to assess the extent of the influence of this parameter over the outlet results. Normal distributions with increasing inlet average lengths (2*D*, 5*D* and 8*D*) and similar standard deviations (1*D*, 2*D* and 2*D*, respectively) are used. All average slug lengths are shorter than 10*D* in order to assure that most bubbles entering the column are within the interaction range (up to 8-10*D*) regarding the preceding bubbles (see Figure 3.1a or Sotto Mayor et al. (2006a)). A lower standard deviation is used for the slug distribution centred on 2*D* in order to avoid the unreal scenario of negative slug length values. Even so, for a normal distribution, only 95% of the values are within an interval of two standard deviations from the average. Therefore, the 2.5% of the values of the distribution that theoretically fall on the negative side of the axis are transformed into the corresponding symmetric values. No major difference exists between the resulting distribution and the theoretical normal distribution. All inlet parameters other than slug length and bubble length are similar for the three simulations being compared (slug and bubble length are related by Eq. (3.7) at inlet). Long columns (6.5 m) with an internal diameter of 0.032 m are considered. Figures 3.11a and 3.11c show the frequency distribution curves for the inlet liquid slug length and bubble length, respectively, whereas Figures 3.11b and 3.11d show the corresponding curves at 5.4 m from the base of the column.

From an analysis of the charts it is clear that, despite the inlet differences, similar frequency distribution curves are obtained at 5.4 m from the base of the column, for both slug length and bubble length (Figures 3.11b and 3.11d). In order to further analyse the influence of the inlet distributions along the column, focus was put on the evolution of those distributions as the bubbles move upwards. For this purpose, the above simulations were compared once again, at several observation points along the column (a point every 0.6 m). Log-normal curves were afterwards fitted to the slug and bubble length frequency distribution curves obtained at each observation point. In Figure 3.12, the maximal relative differences of the average and mode of the log-normal local fits are plotted against the vertical coordinate of the column. It can be seen in chart (a) that the maximal relative difference between the log-normal fit parameters for the three simulations decreases along the column. Indeed, despite the differences in the inlet distributions, similar frequency distribution curves are obtained for vertical column positions above 65*D*, when $U_L \approx 0.10$ m/s and $U_G \approx 0.26$ m/s (conditions reported in chart (a); accepting a maximal difference of 10%).

This value defines the extent of the entrance length of the slug flow (for the U_L and U_G mentioned). By extending the aforementioned approach to a set of increasing superficial gas and liquid velocities (0.10, 0.23, 0.36 and 0.50 m/s) the chart of Figure 3.12b is obtained, showing the variation of the entrance length with these parameters. A linear surface (both in U_L and in U_G), was fitted to the data and it is shown also in the chart. From this chart it can be concluded that for the given U_L and U_G range the entrance length ranges from 50*D* to 70*D*. Additionally, within this range this parameter increases slightly with superficial gas velocity while it decreases with superficial liquid velocity. This behaviour is in agreement with the variation of the gas hold-up in the column. A similar entrance-length range was obtained for the 0.052 m internal diameter column. Notice that the vertical column position used extensively as reference in the previous sections is far above the mentioned entrance-length range (5.4 m equals 169*D* for the narrower column and 104*D* for the larger one). A figure of 60*D* is given by Van Hout et al. (2003) for the homonymous parameter (based on the analysis of the coalescence rate along the column).

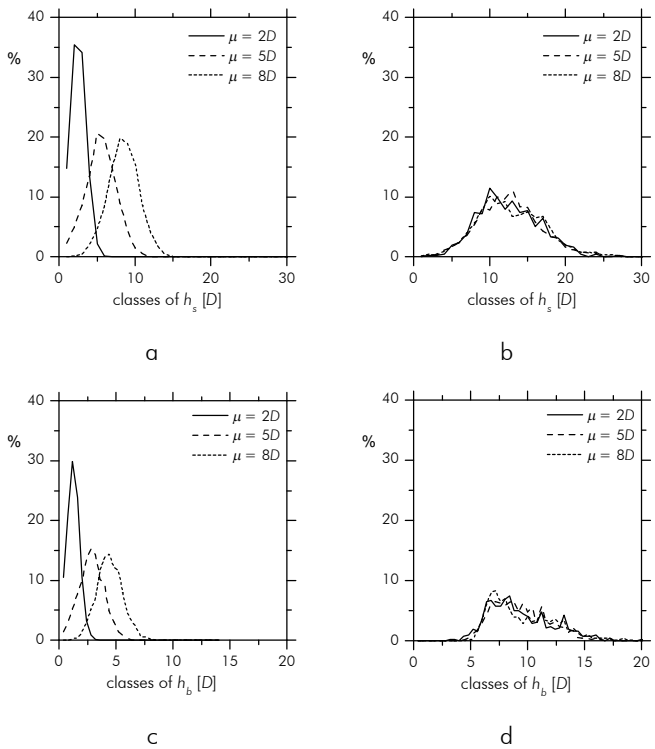

Figure 3.11 – Frequency distribution curves of (a) slug length at inlet, (b) slug length at outlet, (c) bubble length at inlet and (d) bubble length at outlet, for simulations with different inlet average slug length (2D, 5D and 8D); $U_L \approx 0.10$ m/s, $U_G \approx 0.26$ m/s; 0.032 m ID, vertical coordinate: 5.4 m

Figure 3.13 gives information on the dependence of the coalescence curve on the inlet slug length distributions (for a given flow condition). The coalescence curve is given as the

percentage of coalescence along the column (compared to the total number of coalescences occurring in the 6.5 m long column).

Most coalescence occurs in the entrance length of the slug flow (50-70*D*), in particular for the simulations with the smaller inlet average slug lengths (about 90% and 80% of the total coalescences occur under 70*D*, for inlet averages equal to 2*D* and 5*D*, respectively). Moreover, the coalescence curve broadens for increasing inlet average slug length (Figure 3.13a). Additionally, the mode and median of the curves (corresponding to the position of maximal and 50% of total coalescences) shift upwards as the inlet average slug length increases (Figure 3.13b).

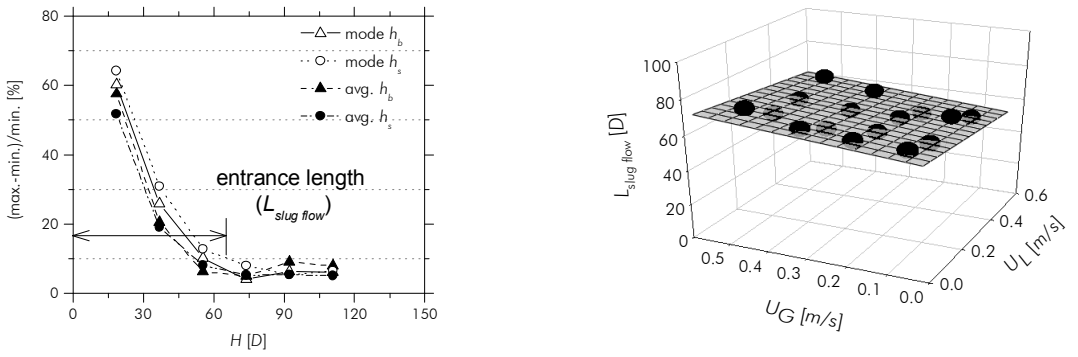

a b

Figure 3.12 – (a) Maximal relative difference of the mode and average of log-normal fits, along the column, for simulations with increasing average inlet slug lengths (2i, 5*D* and 8*D*), $U_L \approx 0.10$ m/s and $U_G \approx 0.26$ m/s; (b) entrance length of slug flow for simulations with U_L and U_G equal to 0.10, 0.23, 0.36 and 0.50 m/s; 0.032 m ID

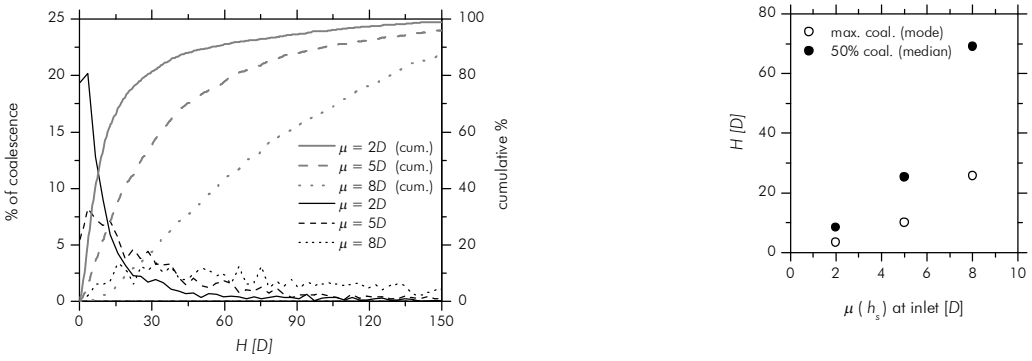

a b

Figure 3.13 – (a) Coalescence events along the column (intervals of 0.1 m) for slug length distributions with increasing average and (b) vertical position of maximal and 50% of the total coalescences (mode and median of the curves, respectively); 0.032 m ID; $U_L \approx 0.10$ m/s, $U_G \approx 0.26$ m/s

The results discussed in this section show that the stabilized slug flow pattern depends more on the overtaking mechanism (which determines the bubble coalescence) than it does on the type

of bubble injector/nozzle (which changes the inlet distributions). Barnea and Taitel (1993) arrived at similar conclusions, although they were using a different overtaking model and discarding the gas phase expansion.

3.5.4 Values of the main flow parameters

Several simulations with increasing superficial gas and liquid velocities (0.10, 0.23, 0.36 and 0.50 m/s) and three column diameters (0.024, 0.032 and 0.052 m) are compared in order to study the influence of these parameters over the distributions of bubble velocity, bubble length and liquid slug length, along the column (6.5 m long). Normal distributions of slug length (μ=5D, σ=2D) are acknowledged at the inlet of the column. The column diameter is used for normalisation purposes. Log-normal distributions were fitted to the curves obtained. Nonlinear estimation was implemented in order to fit the modes and standard deviations (for U, h_b and h_s) computed by the log-normal fits. The general form of the equation is:

$$z = a(H)^2 + bH + c(U_L)^2 + dU_L + e(U_G)^2 + fU_G + gD^2 + hD + iHU_L + \\ + jHU_G + kHD + lU_LU_G + mU_LD + nU_GD + o \quad (3.22)$$

where quadratic, linear and crossed terms in H_i, the vertical coordinate, U_L, U_G and D are acknowledged. Considering that not all parameters in the above equation are required to adequately represent some of the results obtained, relevant coefficients were determined (for a 95% confidence level) to each case. Non-significant coefficients were excluded from the fits. Standard errors for each coefficient were also calculated. The coefficient estimates and corresponding standard errors obtained are shown in Tables 3.1 and 3.2.

For an easier understanding of the results, 3-D representations of the data are shown for two particular cases: at the column top (H≈5.3 m) and along the column for increasing U_G.

Table 3.1 – Coefficients (estimate and standard error) and residuals (SSE: sum of squares of error; SSE/n_{dat}: average sum of squares of error) of the surface fits in Figures 3.14 and 3.15, focussing modes; equation form: $z = a(H_i)^2 + bH_i + c(U_L)^2 + dU_L + e(U_G)^2 + fU_G + gD^2 + hD + iH_iU_L + jH_iU_G + kH_iD + lU_LU_G + mU_LD + nU_GD + o$

	mode (U)		mode (h_b)		mode (h_s)	
	estimate	stand. error	estimate	stand. error	estimate	stand. error
a	1.24×10^{-3}	2.98×10^{-4}	-1.69×10^{-3}	2.70×10^{-4}	-5.32×10^{-3}	1.54×10^{-4}
b	-1.22×10^{-2}	2.46×10^{-3}	2.40×10^{-2}	1.93×10^{-3}	3.75×10^{-2}	1.12×10^{-3}
c	...	...	6.10×10^{-1}	3.09×10^{-2}	-7.32×10^{-2}	1.75×10^{-2}
d	7.03×10^{-1}	1.74×10^{-2}	-4.04×10^{-1}	2.44×10^{-2}	5.92×10^{-2}	1.25×10^{-2}
e	8.01×10^{-2}	3.41×10^{-2}	-1.08×10^{-1}	3.09×10^{-2}	-1.87×10^{-2}	3.44×10^{-3}
f	5.64×10^{-1}	2.69×10^{-2}	6.81×10^{-1}	2.44×10^{-2}	...	...
g	$4.93 \times 10^{+2}$	$8.32 \times 10^{+0}$	$-1.13 \times 10^{+2}$	$7.54 \times 10^{+0}$	...	...
h	$-3.33 \times 10^{+1}$	6.71×10^{-1}	$8.17 \times 10^{+0}$	6.01×10^{-1}	$5.10 \times 10^{+0}$	7.88×10^{-2}
i	1.01×10^{-2}	2.68×10^{-3}	-3.98×10^{-2}	2.43×10^{-3}	...	...
j	3.41×10^{-2}	2.68×10^{-3}	6.27×10^{-2}	2.43×10^{-3}	...	...
k	1.38×10^{-1}	3.39×10^{-2}	...	...	7.51×10^{-1}	1.75×10^{-2}
l	-8.10×10^{-2}	2.75×10^{-2}	-8.72×10^{-1}	2.49×10^{-2}	...	...
m	$1.73 \times 10^{+1}$	3.48×10^{-1}	$3.42 \times 10^{+0}$	3.15×10^{-1}	-4.85×10^{-1}	1.79×10^{-1}
n	$1.26 \times 10^{+1}$	3.48×10^{-1}	$-2.76 \times 10^{+0}$	3.15×10^{-1}	...	...
o	7.29×10^{-1}	1.42×10^{-2}	-1.31×10^{-1}	1.26×10^{-2}	2.11×10^{-2}	3.39×10^{-3}
SSE [m^2 or m^2/s^2]	6.69×10^{-2}		5.50×10^{-2}		1.80×10^{-2}	
$SSE/n_{dat.}$ [m^2 or m^2/s^2]	1.55×10^{-4}		1.27×10^{-4}		4.16×10^{-5}	
r^2	0.998		0.985		0.996	

Table 3.2 – Coefficients (estimate and standard error) and residuals (SSE: sum of squares of error; SSE/n_{dat}: average sum of squares of error) of the surface fits in Figures 3.14 and 3.15, focussing σ; equation form: $z = a(H_i)^2 + bH_i + c(U_L)^2 + dU_L + e(U_G)^2 + fU_G + gD^2 + hD + iH_iU_L + jH_iU_G + kH_iD + lU_LU_G + mU_LD + nU_GD + o$

	σ (U)		σ (h_b)		σ (h_s)	
	estimate	stand. error	estimate	stand. error	estimate	stand. error
a	2.26×10^{-3}	1.15×10^{-4}	...	...	-2.51×10^{-3}	1.67×10^{-4}
b	-1.40×10^{-2}	9.03×10^{-4}	5.99×10^{-3}	6.52×10^{-4}	1.43×10^{-2}	1.22×10^{-3}
c	...	...	2.24×10^{-1}	1.30×10^{-2}	...	...
d	...	...	-1.64×10^{-1}	1.02×10^{-2}	...	...
e	6.62×10^{-2}	7.90×10^{-3}	...	...	...	...
f	...	...	2.37×10^{-1}	6.64×10^{-3}	...	...
g	$2.98 \times 10^{+1}$	$3.21 \times 10^{+0}$	$-4.10 \times 10^{+1}$	$3.17 \times 10^{+0}$	...	...
h	$-2.11 \times 10^{+0}$	2.55×10^{-1}	$3.07 \times 10^{+0}$	2.56×10^{-1}	$2.38 \times 10^{+0}$	6.73×10^{-2}
i	-5.74×10^{-3}	4.76×10^{-4}	-1.17×10^{-2}	1.02×10^{-3}	...	...
j	3.61×10^{-2}	9.85×10^{-4}	1.85×10^{-2}	1.02×10^{-3}	...	...
k	-4.86×10^{-2}	1.31×10^{-2}	-3.52×10^{-2}	1.29×10^{-2}	3.36×10^{-1}	1.90×10^{-2}
l	...	...	-3.04×10^{-1}	1.05×10^{-2}	2.57×10^{-2}	6.64×10^{-3}
m	...	...	$1.44 \times 10^{+0}$	1.33×10^{-1}	...	...
n	$2.12 \times 10^{+0}$	1.17×10^{-1}	$-1.26 \times 10^{+0}$	1.33×10^{-1}	-4.81×10^{-1}	7.83×10^{-2}
o	5.91×10^{-2}	4.80×10^{-3}	-4.36×10^{-2}	5.37×10^{-3}	8.08×10^{-3}	2.68×10^{-3}
SSE [m^2 or m^2/s^2]	1.01×10^{-2}		9.75×10^{-3}		2.14×10^{-2}	
$SSE/n_{dat.}$ [m^2 or m^2/s^2]	2.33×10^{-5}		2.26×10^{-5}		4.95×10^{-5}	
r^2	0.983		0.978		0.974	

3.5.4.1 Results at the column top

The mode, standard deviation and corresponding ratio (from the log-normal fits) for bubble velocity, bubble length and liquid slug length are plotted against increasing values of U_L and U_G (Figure 3.14), for the 0.032 m ID column. Focus is put on the frequency distribution curves obtained at 5.3 m from the column base. The corresponding 3-D surfaces (computed by Eq. (3.22) with $H \approx 5.3$ m) are also shown in the charts.

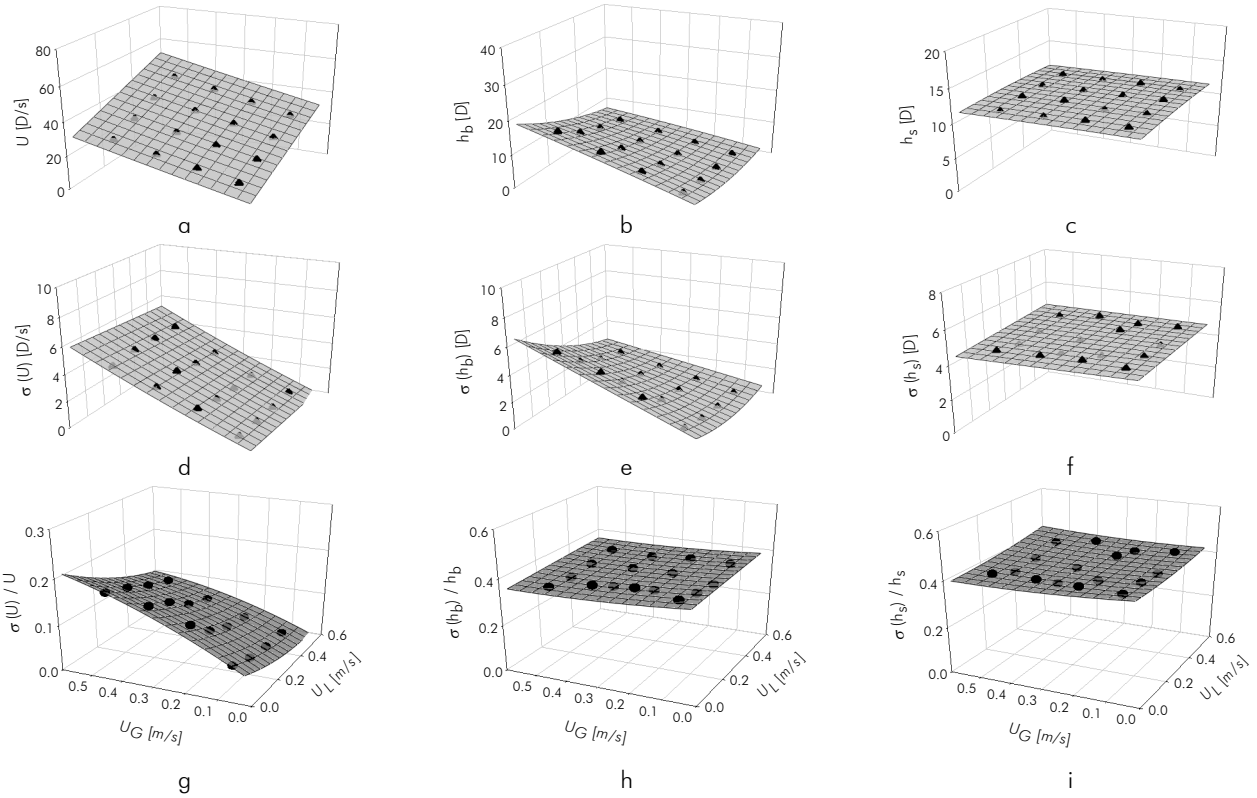

Figure 3.14 – Mode (a-c), standard deviation (d-f) and corresponding ratio (g-i) of log-normal fits; (a), (d) and (g) bubble velocity; (b), (e) and (h) bubble length; (c), (f) and (i) liquid slug length; simulations with U_L and U_G equal to 0.10, 0.23, 0.36 and 0.50 m/s; 0.032 m ID; vertical coordinate: 5.3 m

As expected, the most probable (mode) bubble velocity increases with superficial gas and liquid velocities. Moreover, the variation is linear on U_L and almost linear on U_G (in Eq. (3.22), $c=0$ and e is very small, as shown in Table 3.1). An excellent agreement exists between the surface fit and the simulation results for the three column diameters ($r^2=0.998$). Additionally, the corresponding standard deviation increases with U_G and slightly decreases with U_L. Moreover, this parameter reaches no more than 18% of the corresponding modes (Figure 3.14g). This low percentage confirms that the scattering of the bubble velocity values is low and that these are reasonably centred on the corresponding mode value (as seen in section 3.5.2).

The bubble length mode and corresponding standard deviation increase with U_G whereas they decrease with U_L (Figures 3.14b and 3.14e). This behaviour, a direct consequence of flow

continuity and coalescence along the column, is analysed in detail in Sotto Mayor et al. (2006a). This somewhat proportional variation results in a quasi-constant ratio between the mode and standard deviation of bubble length variable (30-40%; see Figure 3.14h).

Similar slug length modes (10-13D) are obtained for the ranges of superficial gas and liquid velocities studied (0.10-0.50 m/s). These results indicate that this parameter is almost independent of U_L or U_G. However, a linear dependence on column diameter exists (corresponding coefficient equal to 5.10, in Table 3.1). As for the bubble velocity parameter, there is very good agreement between the surface fit and the modes of slug length, for the three column diameters (r^2=0.996). The standard deviation/mode ratio for the slug length parameter is approximately 35-45% for the ranges of U_L and U_G studied.

Finally, both mode and standard deviation surfaces become flatter for increasing column diameters. This behaviour is related to the normalisation procedure. Nevertheless, similar σ/mode ratios are obtained for the three column diameters studied.

3.5.4.2 Results along the column

The mode and standard deviation of the main flow parameters are plotted against H and U_G (Figure 3.15), for U_L=0.23 m/s and D=0.032 m. The corresponding 3-D surfaces (computed by Eq. (3.22)) are also shown in the charts.

The most probable (mode) bubble velocity value slightly increases along the column (Figure 3.15a). Although one would expect a decrease for higher column vertical coordinates (due to less frequent coalescences), the gas phase expansion camouflages and overtakes the effect of the decreasing coalescence. As confirmation of this, the increase in bubble velocity along the column is slightly more pronounced for higher superficial gas velocities. There is excellent agreement between the surface fits and the simulation results for this parameter for the three column diameters. The standard deviation values reach no more than 18% of the corresponding modes.

The bubble length mode and corresponding standard deviation increase along the column and with increasing U_G. The variation of the most probable value is the result of the coalescence along the column (recall that coalescence increases the bubble length) and of the flow continuity effects, by which an increasing superficial gas velocity favours the formation of longer bubbles. The corresponding standard deviation reaches 30-45% of the corresponding mode, for the ranges of U_G and H studied.

The most probable slug length increases along the column due to the coalescence phenomena. No change is perceived in this parameter for increasing U_G (surface of Figure 3.15c

approximately parallel to U_G axis). There is a weak dependence on column diameter, however (mode of h_s slightly decreases for increasing D). Nevertheless, the most probable slug length value varies in the range 10-13D at H≈5.3 m (6-8D, at H≈0.6 m), for the three column diameters studied. A similar behaviour is found for the standard deviation of the slug length parameter leading, therefore, to a reasonably steady σ/mode ratio (35-50%).

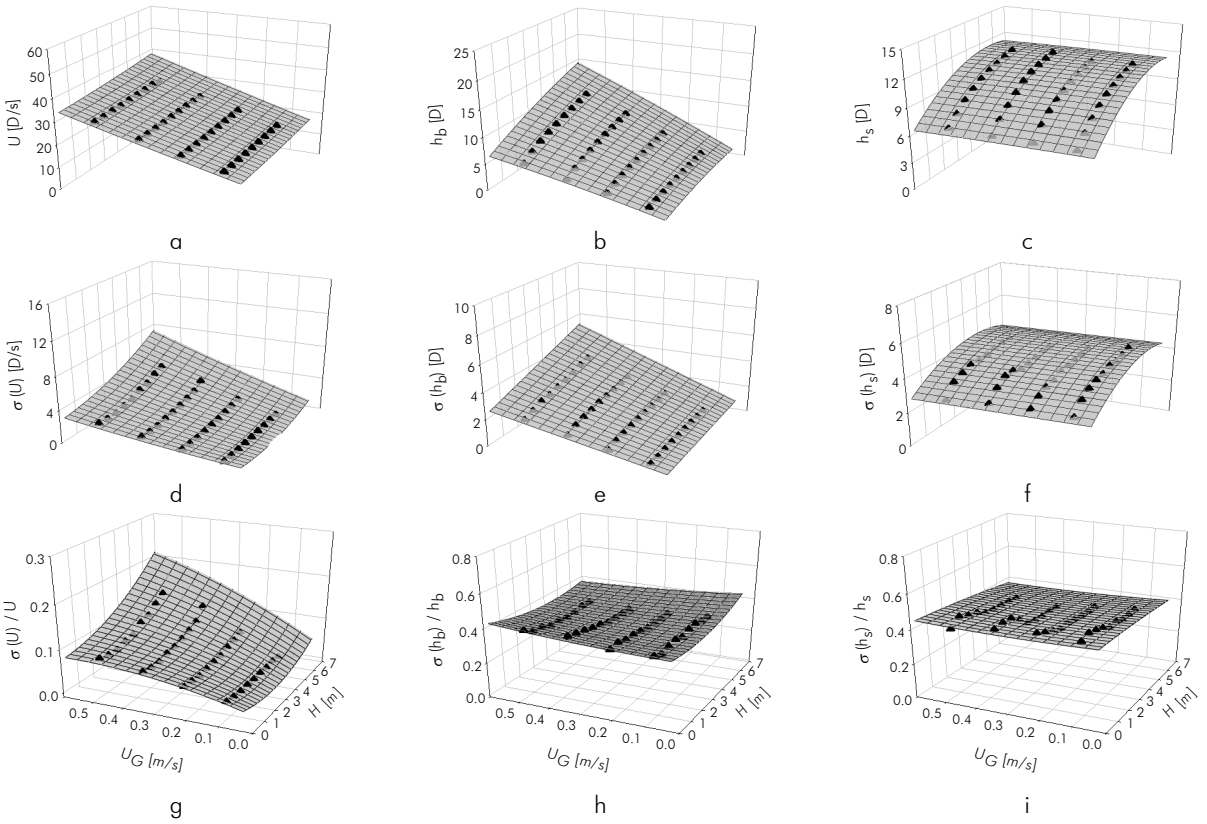

Figure 3.15 – Mode (a-c), standard deviation (d-f) and corresponding ratio (g-i) of log-normal fits along the column; (a), (d) and (g) bubble velocity; (b), (e) and (h) bubble length; (c), (f) and (i) liquid slug length; simulations with U_L≈0.23 m/s and U_G ≈0.10, 0.23, 0.36 and 0.50 m/s; 0.032 m ID

3.6 Conclusions

A detailed simulation study on gas-liquid vertical slug flow is reported. The slug flow simulation is grounded on the bubble-to-bubble empirical correlation drawn from the experimental data reported in Sotto Mayor et al. (2006a). The flow pattern in the near-wake bubble region and in the main liquid is turbulent, for the ranges of parameters studied.

Proper implementation of the gas phase expansion along the column (considering effect over bubble length and velocity) is proposed. Distributed gas flow rates and liquid slug lengths are acknowledged at the column inlet. Simulation data are validated for three column diameters (0.052, 0.032 and 0.024 m).

The inlet slug length distribution was shown not to influence the slug flow pattern for distances above 50-70*D* (from the base of the column). This defines the extent of the entrance length of slug flow for the ranges of superficial gas and liquid velocities studied (0.10-0.50 m/s).

General expressions are proposed (with a set of fit coefficients) to compute the mode and standard deviation (of log-normal fits) for bubble velocity, bubble length, and liquid slug length, as a function of H, the vertical coordinate, U_L, U_G and D. These expressions are shown to adequately represent the simulation data for the ranges of parameters studied.

Bubble velocity is shown to increase with U_L, U_G and H. The evolution of U along the column confirms the dominant influence of the gas phase expansion over the overall variation of this parameter. Bubble length is shown to increase with U_G and H, a natural outcome of the coalescence effect and of the gas expansion. The liquid slug length increases along the column, and is almost independent of U_L and U_G. Liquid slug length modes between 10D and 13D are obtained at the column top ($H \approx 5.3$ m), for the ranges of U_L, U_G and D studied. This parameter is shown to mostly depend on the coalescence effect along the column.

Reasonably similar σ/mode ratios are obtained for the three column diameters studied.

3.7 Notation

Roman symbols

C	empirical coefficient	
D	column internal diameter	[m]
g	acceleration of gravity	[m/s^2]
$h_{b,\,i}$	length of gas bubble i	[m]
$h_{s,\,i}$	length of liquid slug i	[m]
H	vertical coordinate along the column	[m]
$H_{hyd,\,i}$	hydrostatic liquid height above bubble i	[m]
$L_{slug\ flow}$	entrance length of slug flow	[m]
n	number of slug unit cells	[#]
$n_{dat.}$	number of data used in the non-linear estimation	[#]
n_i	number of moles of air in bubble i	[mol]
P_{atm}	ambient pressure	[Pa]
$P_{hyd,\,i}$	hydrostatic pressure acting on bubble i	[Pa]
r^2	coefficient of determination of fits (=[*SST*-*SSE*]/*SST*)	
R	universal gas constant	[J/(K mol)]
R_c	column internal radius	[m]
S_b	bubble cross-section area	[m^2]

S_c	column cross-section area	[m^2]
SSE	sum of squares of error (sum of squares of residuals)	[m^2] or [m^2/s^2]
$SSE/\ n_{dat.}$	average sum of squares of error	[m^2] or [m^2/s^2]
SST	total sum of squares (sum of squares about the mean)	[m^2] or [m^2/s^2]
t	time	[s]
t_i, t_{i+1}	consecutive time instants	[s]
T	temperature	[K]
U	upward velocity of bubble (U_i^{trail} and U_i^{lead} for the i^{th} trailing and leading bubbles, respectively)	[m/s]
U_B	upward bubble velocity (according to Nicklin's equation)	[m/s]
U_B^{exp}	experimental upward bubble velocity	[m/s]
U_G	superficial gas velocity	[m/s]
$U_{G,\,i}$	superficial gas velocity of slug unit i	[m/s]
U_G^{inlet}	superficial gas velocity, at column inlet	[m/s]
$U_G^{inlet}\big\vert_{\mu}$	arithmetic average of superficial gas velocity, at column inlet	[m/s]
U_∞	upward bubble velocity in a stagnant liquid (drift velocity)	[m/s]
U_L	superficial liquid velocity	[m/s]
z	parameter to be fit by nonlinear estimation	[m] or [m/s]
$z_{liq.}$	liquid free-surface coordinate	[m]
$z_{nose,\,i}$	vertical coordinate of bubble nose (bubble i)	[m]
$z_{rear,\,i}$	vertical coordinate of bubble rear (bubble i)	[m]
z_T	vertical coordinate of the tank base	[m]

Greek symbols

α_i	parameter informing on the bubble positioning relative to the tank base (z_T)	
δ	film thickness	[m]
Δh_i	increase of bubble length due to expansion (bubble i)	[m]
Δt_i	time interval for complete entrance of slug unit i	[s]
$\Delta U_{expans.}^{ahead\ i}$	increase in flow velocity, ahead bubble i, due to expansion of bubbles below	[m/s]
$\Delta z_{expans.}^{ahead\ i}$	raise in liquid and gas, ahead bubble i, due to expansion of bubbles below	[m]
μ	average (mean)	
ρ	density of liquid	[kg/m^3]
σ	standard deviation	
υ	liquid kinematic viscosity	[m^2/s]

3.8 Acknowledgments

The authors gratefully acknowledge the financial support of Fundação para Ciência e a Tecnologia through project POCTI/EQU/33761/1999 and scholarship SFRH/BD/11105/2002. POCTI (FEDER) also support this work via CEFT.

3.9 References

Barnea, D. and Taitel, Y., 1993. A model for slug length distribution in gas-liquid slug flow. Int. J. Multiphas. Flow 19(5): 829-838.

Bendiksen, K. H., 1984. An experimental investigation on the motion of long bubbles in inclined tubes. Int. J. Multiphas. Flow 10(4): 467-483.

Brown, R. A. S., 1965. The mechanics of large gas bubbles in tubes. I - Bubble velocities in stagnant liquids. 43: 217-223.

Campos Guimarães, R. and A. Sarsfield Cabral, J. (1997). Estatística, McGraw-Hill de Portugal Limitada.

Collins, R., De Moraes, F. F., Davidson, J. F. and Harrison, D., 1978. The Motion of Large Gas Bubble Rising Through Liquid Flowing in a Tube. J. Fluid Mech. 28: 97-112.

Fabre, J. and Liné, A., 1992. Modeling of two-phase slug flow. Ann. Rev. Fluid Mech. 24: 21-46.

Hasanein, H. A., Tudose, G. T., Wong, S., Malik, M., Esaki, S. and Kawaji, M., 1996. Slug flow experiments and computer simulation of slug length distribution in vertical pipes. AIChE Symposium Series 92(310): 211-219.

Moissis, R. and Griffith, P., 1962. Entrance effects in a two-phase slug flow. J. Heat Transfer 84: 29-39.

Nicklin, D. J., Wilkes, J. O. and Davidson, J. F., 1962. Two-phase flow in vertical tubes. Transactions of the Institution of Chemical Engineers 40: 61-68.

Sotto Mayor, T., Ferreira, V., Pinto, A. M. F. R. and Campos, J. B. L. M., 2006a. Hydrodynamics of gas-liquid slug flow along vertical pipes in turbulent regime. An experimental study. Submitted to International Journal of Heat and Fluid Flow.

Sotto Mayor, T., Pinto, A. M. F. R. and Campos, J. B. L. M., 2006b. An image analysis technique for the study of gas-liquid slug flow along vertical pipes - Associated uncertainty. In revision in Flow Measurement and Instrumentation.

Van Hout, R., Barnea, D. and Shemer, L., 2001. Evolution of statistical parameters of gas-liquid slug flow along vertical pipes. Int. J. Multiphas. Flow 27(9): 1579-1602.

Van Hout, R., Shemer, L. and Barnea, D., 2003. Evolution of hydrodynamic and statistical parameters of gas-liquid slug flow along inclined pipes. Chem. Eng. Sci. 58(1): 115-133.

White, E. T. and Beardmore, R. H., 1962. The velocity of single cylindrical air bubbles through liquids contained in vertical tubes. Chem. Eng. Sci. 17: 351-361.

4 Hydrodynamics of gas-liquid slug flow along vertical pipes in laminar regime – Experimental and simulation study[4]

4.1 Abstract

An experimental and simulation study on free bubbling vertical slug flow in laminar regime was developed. A non-intrusive image analysis technique and a developed simulation code (SFS – Slug Flow Simulator) were used for the purpose. A single correlation was obtained for the prediction of the bubble velocity as a function of the length of the liquid slug ahead of the bubble. Strong bubble interaction was found for liquid slugs shorter than 2*D*, with weak and decreasing interaction persisting for longer liquid slugs. Coalescence, though sparse, was found to occur along the whole column length (6.5 m). These observations differ from the findings regarding turbulent regime (bubble interaction for liquid slugs shorter than 8-10*D* and coalescence mainly in the lower part of the column). A slug flow entrance length of 70-100*D* was obtained for inlet slug length distributions centred on 2-4*D*, for the ranges of superficial gas and liquid velocities studied (0.05-0.20 m/s). More contrasting inlet slug length distributions (for instance centred on 2*D* and 5*D*) were found not to evolve to a single flow pattern within the 6.5 m length of the column. General expressions were proposed to predict the evolution of the mode and standard deviation of bubble velocity, bubble length and liquid slug length distributions as a function of the vertical column coordinate and superficial gas and liquid velocities. Bubble coalescence was found to govern the evolution of the liquid slug length along the column. Gas expansion and bubble coalescence were found to play important roles in the evolution of bubble length and velocity.

[4] Based on the paper by T. Sotto Mayor, A.M.F.R. Pinto and J.B.L.M. Campos, submitted to Industry & Engineering Chemistry Research (IECR)

4.2 Introduction

When gas and liquid flow in a pipe they assume various configurations/flow patterns. These depend on fluid properties, pipe diameters, geometry and superficial gas and liquid velocities. Bubbly, slug, churn and annular flow are examples of patterns which occur for increasing ratios of gas/liquid flow rates.

Slug flow is a complex and intermittent two-phase flow pattern which can be found in several industrial applications (Fabre and Liné (1992)) such as air-lifts, nuclear and chemical reactors, geothermal power plants, membrane and crystallization processes, hydrocarbon production and transportation and also in natural volcanic phenomena (such as at Stromboli volcano (James et al. (2004))).

In slug flow regime, bullet-shaped bubbles (known as Taylor bubbles) occupy most of the pipe cross-sectional area and flow separated by more or less aerated liquid plugs (termed slugs). The liquid flows around the Taylor bubble in a thin annular film, whose thickness stabilises when the shear and gravitational forces reach equilibrium (originating a free-falling film). The annular film expansion at the rear of the bubbles creates a relatively confined flow (the bubble wake), with forms varying from a closed well-defined region to an open random-like recirculation (laminar and turbulent wakes, respectively). The nature of the bubble wake determines the column length below the bubble (in a moving reference frame) required for full recovery of the undisturbed velocity profile in the liquid, after bubble passage. The interaction of consecutive bubbles, a consequence of the evolving velocity profiles in the near-wake liquid region, controls the eventual merging of bubbles (coalescence).

Several studies on the motion of Taylor bubbles in stagnant or moving liquids are reported in the literature (Dumitrescu (1943), Davies and Taylor (1950), Nicklin et al. (1962), White and Beardmore (1962), Collins et al. (1978), Fernandes et al. (1983), Mao and Dukler (1989) and Wallis (1969) are some early examples). They set the basis for the early understanding and modelling of slug flow pattern. From an isolated bubble to a train of bubbles, several studies have since been reported covering different aspects of the flow pattern. For instance, studies based on Particle Image Velocimetry (PIV) have provided detailed descriptions of the flow characteristics in the vicinity of Taylor bubbles. Van Hout et al. (2002) studied the velocity field induced by a Taylor bubble rising in stagnant water; Bugg and Saad (2002) reported results for a stagnant viscous fluid (0.084 Pa s); Nogueira et al. (2006b), Nogueira et al. (2006a) mention studies on the flow around Taylor bubbles for a wide range of liquid viscosities (0.001-1.5 Pa s) and for stagnant and flowing conditions; Sousa et al. (2005), Sousa et al. (2006) report studies on Non-Newtonian

liquids or, in a different diameter scale, Thulasidas et al. (1997) studied the flow patterns in the liquid slugs inside capillaries. Other interesting contributions can be mentioned while addressing slug flow in small-scale diameters: Thulasidas et al. (1999), Vandu et al. (2005), van Baten and Krishna (2004) and Kreutzer et al. (2001), Kreutzer et al. (2005).

The unsteadiness and complexity of slug flow pattern makes the development of simulation methodologies for the prediction of characteristics difficult. However, these are essential for the design, optimization and operation of applications incorporating such flow pattern.

Slug flow in turbulent regime has received much attention from the research community. Several experimental and simulation studies on continuous co-current turbulent slug flow are reported (for instance Barnea and Taitel (1993), Pinto et al. (2001), Sotto Mayor et al. (2006a), Sotto Mayor et al. (2006b), Van Hout et al. (2001)). Considering mostly air-water mixtures, probably because of easy availability and handling, they provided valuable insight into the principles of continuous turbulent slug flow and have enabled the development of robust flow simulation codes.

Many industrial applications encompass slug flow in viscous or non-Newtonian fluids (e.g. air-lift reactors, hydrocarbon production and transportation, depolarization in membrane separation processes), and yet no information is found in the literature regarding continuous co-current slug flow in laminar regime. Since this is a frequent scenario in these fluids/applications there is a clear need for information on this topic. This investigation proposes to extend experimental and simulation studies to continuous laminar flow conditions. The resulting comparison of laminar and turbulent experimental/simulation data is a further incentive for the work reported here.

4.3 Experimental set-up

The experimental apparatus is shown schematically in Figure 4.1. Experiments were performed in an acrylic vertical pipe 6.5 m long with an internal diameter of 0.032 m. An 85% (w/w) aqueous glycerol solution ($\mu \approx 0.114$ Pa s and $\rho \approx 1165$ kg/m^3) was used as flowing medium at superficial velocities up to 0.21 m/s. The liquid flow rate was measured at the outlet of the tank before and after each experiment. The liquid temperature was monitored continuously during the experiments by thermocouples placed inside the tank and at the column inlet. Temperature differences between the top and the base of the column were constantly smaller than 0.5 ºC. The viscosity of the glycerol solution was measured at the experiments temperature in a Brookfield rotating viscometer. Air from a pressure line was introduced laterally at the base of the column

through a 0.003 m internal diameter injector. The air flow rate was measured by calibrated rotameters at superficial velocities up to 0.38 m/s (at 1 bar and 20°C).

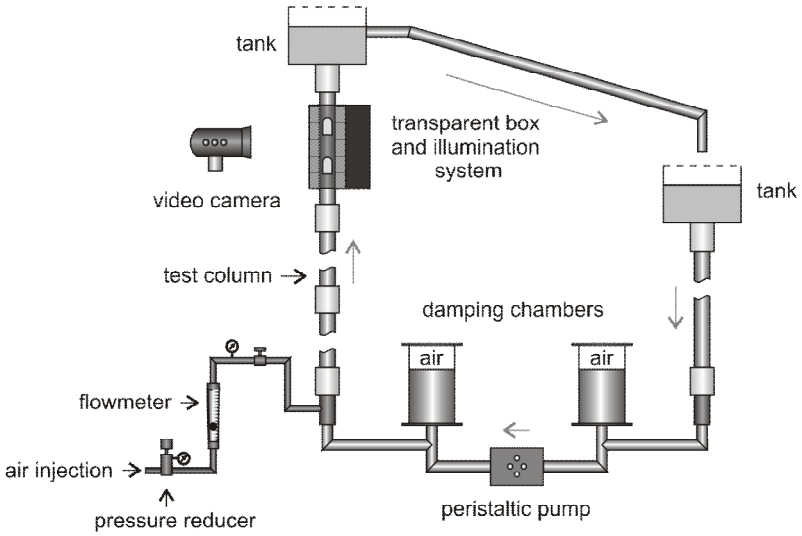

Figure 4.1 – Schematic representation of the experimental set-up

Images of the flow pattern 3.25 m above the base of the column were recorded using a Canon digital video camcorder (model XM1) operating at a frequency of 25 Hz (exposure times varying from 1/4000s to 1/8000s). Image distortion was minimized by the use of a rectangular transparent acrylic box (filled with the liquid medium) surrounding the column test-section. Images of up to 0.47 m of column were captured in the camera field of view.

Uniform illumination over the whole test section was achieved by means of the illumination system illustrated in Figure 4.2a.

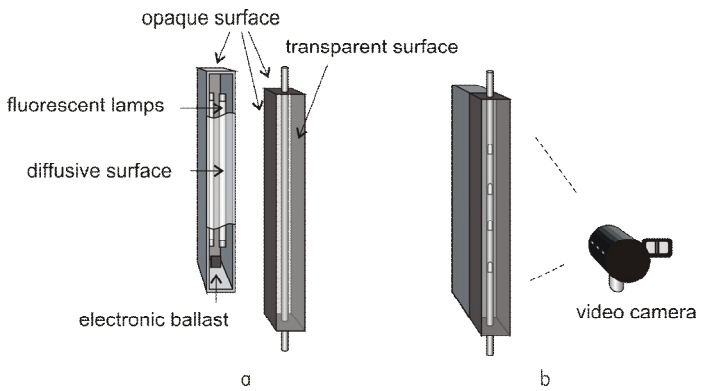

Figure 4.2 – Schematic representation of the illumination system

Two fluorescent lamps, equipped with an electronic ballast to avoid light scintillation problems (boosting scintillation frequencies to kHz range), were mounted inside an opaque box

with a diffusive surface in front of the lamps for greater light uniformity. The illumination kit was placed in contact with the transparent acrylic box as illustrated in Figure 4.2b.

4.4 Video processing

Each video frame was scrutinized by a set of custom-made image analysis routines for the purpose of bubble tracking. These routines (built in MATLAB (The MathWorks (2002))) implement image loading, conversion, enhancement, filtering and erosion steps. A threshold length of 0.5*D* is considered in order to distinguish between Taylor bubbles and small bubbles in the liquid slugs. The thresholding procedure allows to spot the position of the Taylor bubble nose and to obtain a rough estimate of the position of the Taylor bubble rear (the oscillations of the bubble wake and the aeration level of liquid slugs makes bubble rear tracking difficult). The estimate of the position of the bubble rear is further improved by tracking the lowest pixel of the central area of each bubble (the lighter region). This strategy assures a more accurate estimation of the bubble rear boundary and provides, thus, more reliable bubble length and slug length data.

The image processing comprises two different types of approaches: *moving-point data analysis* which aims at the definition of the bubble-to-bubble interaction correlation (velocity-wise), and *fixed-point data analysis* focussing on the flow pattern at a fixed vertical coordinate. The former allows the establishment of an empirical bubble-to-bubble interaction curve for velocity, governing the approach and coalescence of consecutive bubbles, and the latter enables the gathering of information on bubble characteristics (length, velocity, distance and bubble frequency) at a given vertical coordinate. These two types of data are crucial inputs for the simulation of slug flow pattern. The following section describes in detail the data obtained.

4.5 Experimental data

Several experimental conditions were studied. Superficial gas and liquid velocities (U_G and U_L, respectively) were chosen to fulfil the requirement of laminar regime in the main liquid between bubbles, in the near-wake bubble region and in the annular film around bubbles. All operating conditions except condition f comply with this requirement (according to the corresponding Reynolds numbers in Table 4.1). The Reynolds number based on V_S (liquid velocity as seen by the bubble) for condition f indicates transitional regime in the near-wake bubble region. More details on the calculation of these Reynolds numbers and corresponding critical values can be found in section 4.8.

Moving-point and fixed-point data analysis (Sotto Mayor et al. (2006a)) were performed on all video recordings of the flow in order to draw as much information as possible from slug flow pattern in laminar regime. The data resulting from these approaches are described in detail below.

Table 4.1 – Superficial liquid and gas velocities and Reynolds numbers in main liquid, in the near-wake region and in the liquid film, for several experiments

				Reynolds number		
		$(T_{amb.}, P_{amb.})$	$(T_{amb.}, P_{acq.})$	liquid	wake	Film
Condition	U_L [m/s]	U_G [m/s]	U_G [m/s]	Re_{U_M}	Re_{V_S}	Re_{u_δ}
a	0.020	0.060	0.046	22	75	11
b	0.035	0.060	0.046	26	78	11
c	0.104	0.060	0.046	49	94	11
d	0.205	0.117	0.089	96	144	13
e	0.205	0.187	0.141	113	156	12
f	0.205	0.379	0.288	161	202	13
g	0.211	0.110	0.083	96	144	13
h	0.211	0.187	0.142	115	162	13

4.5.1 Moving-point data analysis

Several thousand frames (up to 4000) containing more than one Taylor bubble were analysed with moving-point data analysis. Focus was put on the variation of the trailing bubble velocity according to the length of the liquid slug flowing ahead. In Figure 4.3a, the velocities of the leading and trailing bubbles are plotted against the liquid slug length for all operating conditions shown in Table 4.1. The bubble velocities are normalised by the experimental average upward bubble velocity in undisturbed conditions, U_B^{exp} (whose computation is described later), and the liquid slug length is normalized by the column internal diameter.

An analysis of Figure 4.3a shows that the acceleration of the trailing bubble towards the leading one occurs for all operating conditions, mainly for liquid slugs shorter than 2D. A very strong acceleration is observed particularly for liquid slugs shorter than 1D, where the trailing bubble travels up to twice as fast as the leading bubble. The strong increase of the ratio U_i^{trail}/U_B^{exp} for short liquid slugs indicates (approximately) the length of the bubble wake. From the shape of the bubble-to-bubble interaction curves, one can conclude that the length of the bubble wake is approximately 1D for all experimental conditions studied (a figure of 0.4D is reported for stagnant conditions in a PIV study by Nogueira et al. (2006b); also using PIV for stagnant conditions, Bugg and Saad (2002) report that, at 0.77D below the bubble, the liquid velocity at the column axis is about 10% of the bubble velocity, a figure that provides a rough estimate of the length of the

bubble wake). This parameter seems to be independent of the superficial gas and liquid velocities (in the ranges studied). However, there is still some interaction between consecutive bubbles, for liquid slugs longer than 3*D*, since the trailing bubble travels slightly faster than the leading bubble (about 5%, 3.5% and 1% faster for $h_s \approx 3D$, 5*D* and 10*D*, respectively). This indicates that the full recovery of the undisturbed laminar profile in the liquid occurs very slowly (requiring up to 10-12*D*, in a moving reference frame).

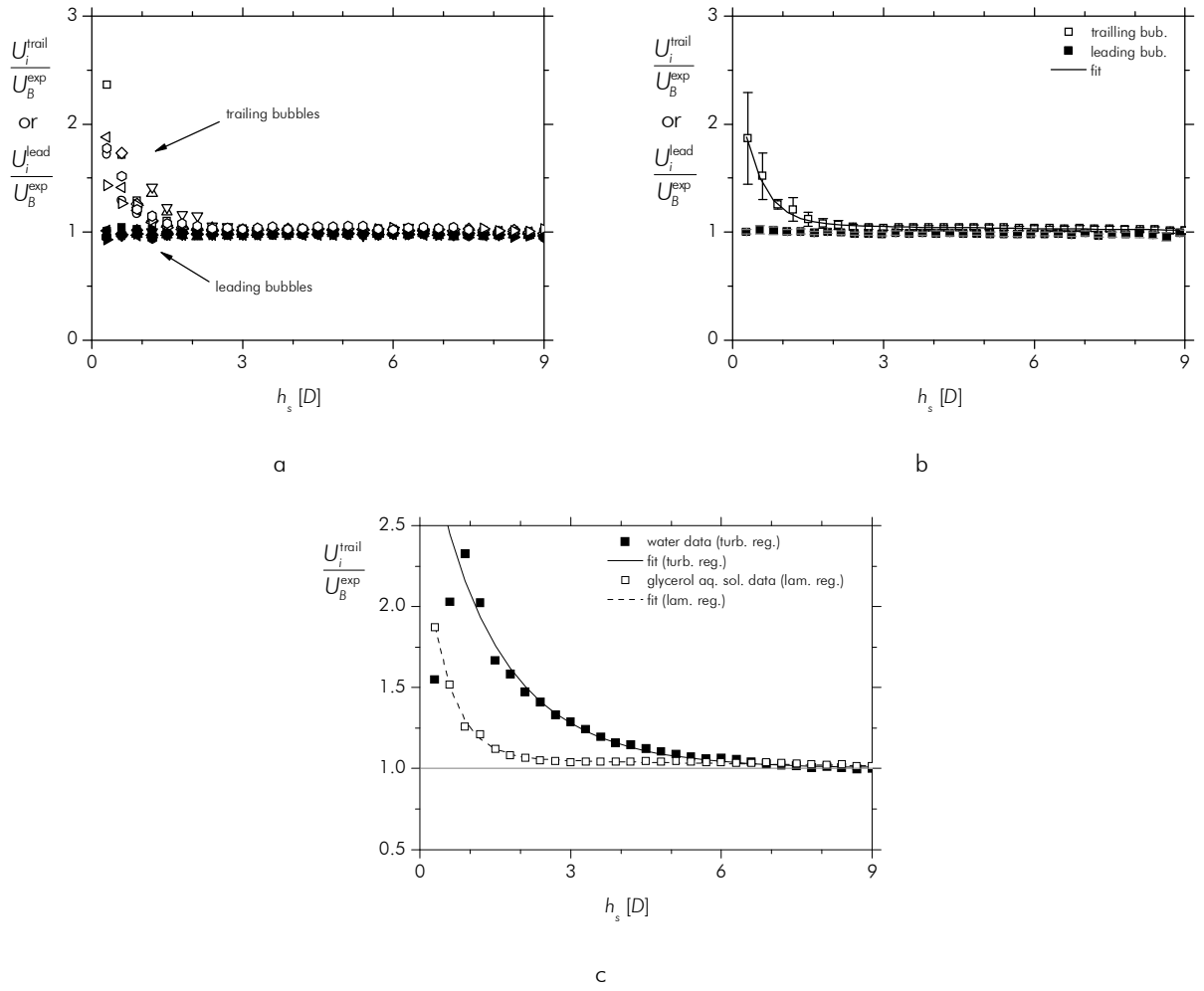

Figure 4.3 – (a) Bubble-to-bubble interaction curves for operating conditions a-h of Table 4.1; (b) average bubble-to-bubble interaction curve with 95% confidence intervals; (c) bubble-to-bubble interaction curve for turbulent regime (water, after Sotto Mayor et al. (2006a)) and laminar regime (glycerol aqueous solution, present data)

By averaging the normalised velocities shown in Figure 4.3a, for each slug length class (0.3*D* wide), the smoother bubble-to-bubble interaction curve shown in Figure 4.3b is obtained. Error bands corresponding to a 95% confidence level are represented for the trailing bubble velocity. The shorter the liquid slug the longer the error bands, behaviour which is related to the higher standard deviation of the velocity samples as bubbles approach coalescence. The

increasing trailing bubble velocity for decreasing liquid slug length has been fitted by an empirical exponential equation of the form:

$$\frac{U_i^{\text{trail}}}{U_B^{\text{exp}}} = -3.85 + 0.82e^{-\left(\frac{h_{s,i-1}-0.3}{0.48}\right)} + 4.91e^{-\left(\frac{h_{s,i-1}-0.3}{1002.48}\right)} \quad (4.1)$$

where U_i^{trail} refers to the velocity of the trailing bubble *i* flowing behind a liquid slug with length $h_{s,i-1}$ (in column diameters; bubbles and slugs numbered from top to bottom). The first exponential term fits the strong acceleration of the trailing bubble in the vicinity of the leading bubble (near its wake), whereas the second exponential term fits the slow acceleration of the trailing bubble for longer liquid slugs (where the velocity profile in the liquid gradually evolves to the laminar profile). Note, however, that Eq. (4.1) is used to predict the bubble relative displacement, only for liquid slugs up to 12*D*. For longer liquid slugs, no bubble-to-bubble interaction is observed and, thus, the ratio $U_i^{\text{trail}}/U_B^{\text{exp}}$ is set to unity.

Sotto Mayor et al. (2006a) reported a study on co-current slug flow in turbulent regime (using water as flowing medium). The present bubble-to-bubble experimental data (for laminar regime) are plotted together with the homonymous data of Sotto Mayor et al. (for turbulent regime) in Figure 4.3c.

The bubble-to-bubble interaction curves for laminar and turbulent regimes differ considerably. The acceleration of the trailing bubble for turbulent regime occurs for liquid slugs shorter than 8-10*D*. Moreover, no evidence of bubble interaction has been found for longer liquid slugs. These two different interaction curves originate, consequently, different degrees of coalescence. Indeed, according to these curves there is a lot more frequent coalescence (mostly) in the lower part of the column in turbulent regime than in laminar regime. This happens because bubbles flowing separated by a given h_s require a considerably smaller portion of column to coalesce when flowing in turbulent regime, than they do when flowing in laminar regime (trailing bubbles catch up more slowly in laminar regime, mainly if flowing more than 2*D* apart).

4.5.2 Fixed-point data analysis

Fixed-point data analysis covered between 1000 and 2300 bubbles. The minimum number of bubbles to have converged statistics (1000) was determined by comparing smaller subsets of data. The superficial gas and liquid velocities (in Table 4.1) were chosen to allow direct analysis of the influence of those parameters over the characteristics of the slug flow pattern. Thus, conditions a-c feature increasing U_L for constant U_G whilst conditions d-f feature increasing U_G for constant U_L. Snapshots of the flow patterns for those operating conditions are shown in Figure 4.4. Different

ranges of superficial velocities are discerned in the operating conditions. Conditions a-c, regarding low superficial mixture velocities (0.08 m/s < U_M < 0.16 m/s), show bubble rear axisymmetry and non-aerated liquid slugs. On the contrary, conditions d-f, concerning higher superficial mixture velocities (0.32 m/s < U_M < 0.58 m/s), show bubble rear asymmetry and oscillation, as well as increasingly aerated liquid slugs. Recall that condition f (in Table 4.1) concerns already transitional regime in the near-wake bubble region (Re_{V_S} =202; critical values according to Pinto et al. (1998)). The influence of several parameters on the flow pattern characteristics is analysed quantitatively below.

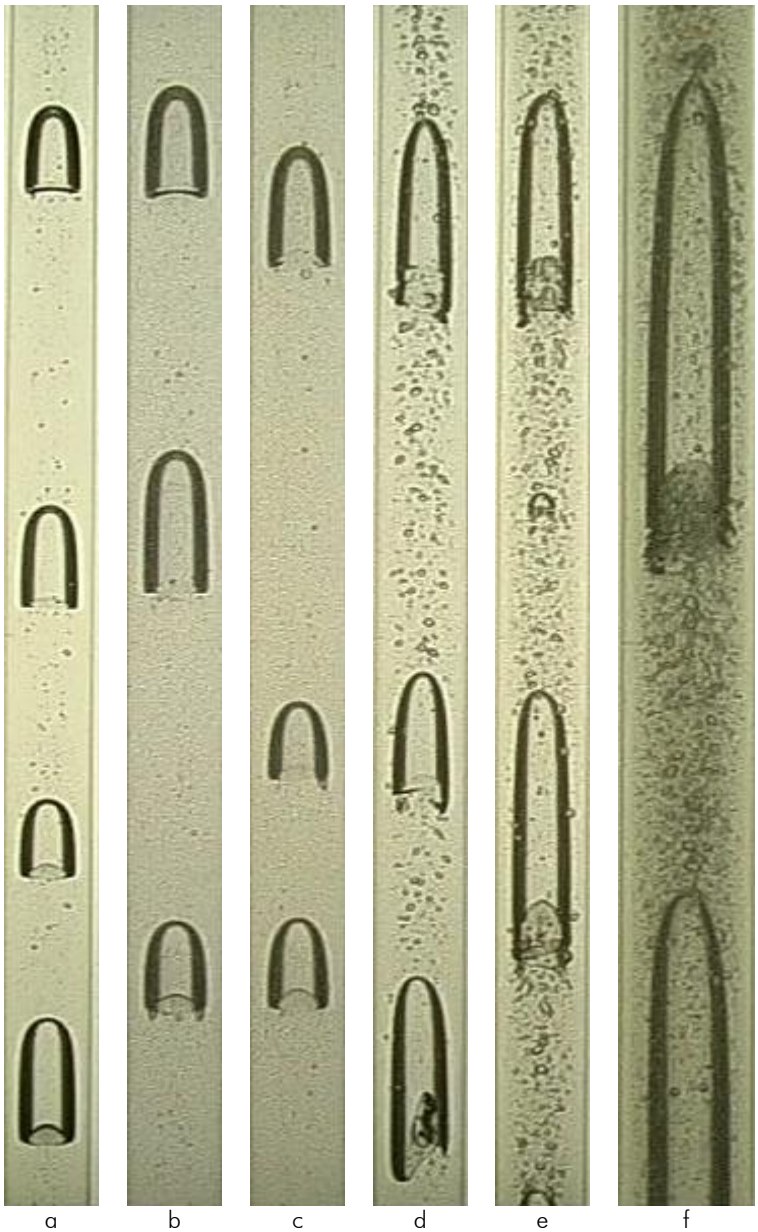

Figure 4.4 – Snapshots of flow pattern for different superficial liquid and gas velocities (for operating conditions see Table 4.1)

4.5.2.1 Superficial liquid velocity (U_L)

In this section, three experiments with increasing superficial liquid velocity are compared (for constant superficial gas velocity). The frequency distribution curves for the main flow parameters are plotted in Figure 4.5. The average, mode and standard deviation of the log-normal fits are plotted against the superficial liquid velocity in Figure 4.6. The log-normal fitting procedure aims at simplifying the comparison between different frequency distribution curves. Similar approaches are followed for all distribution curves shown in this chapter.

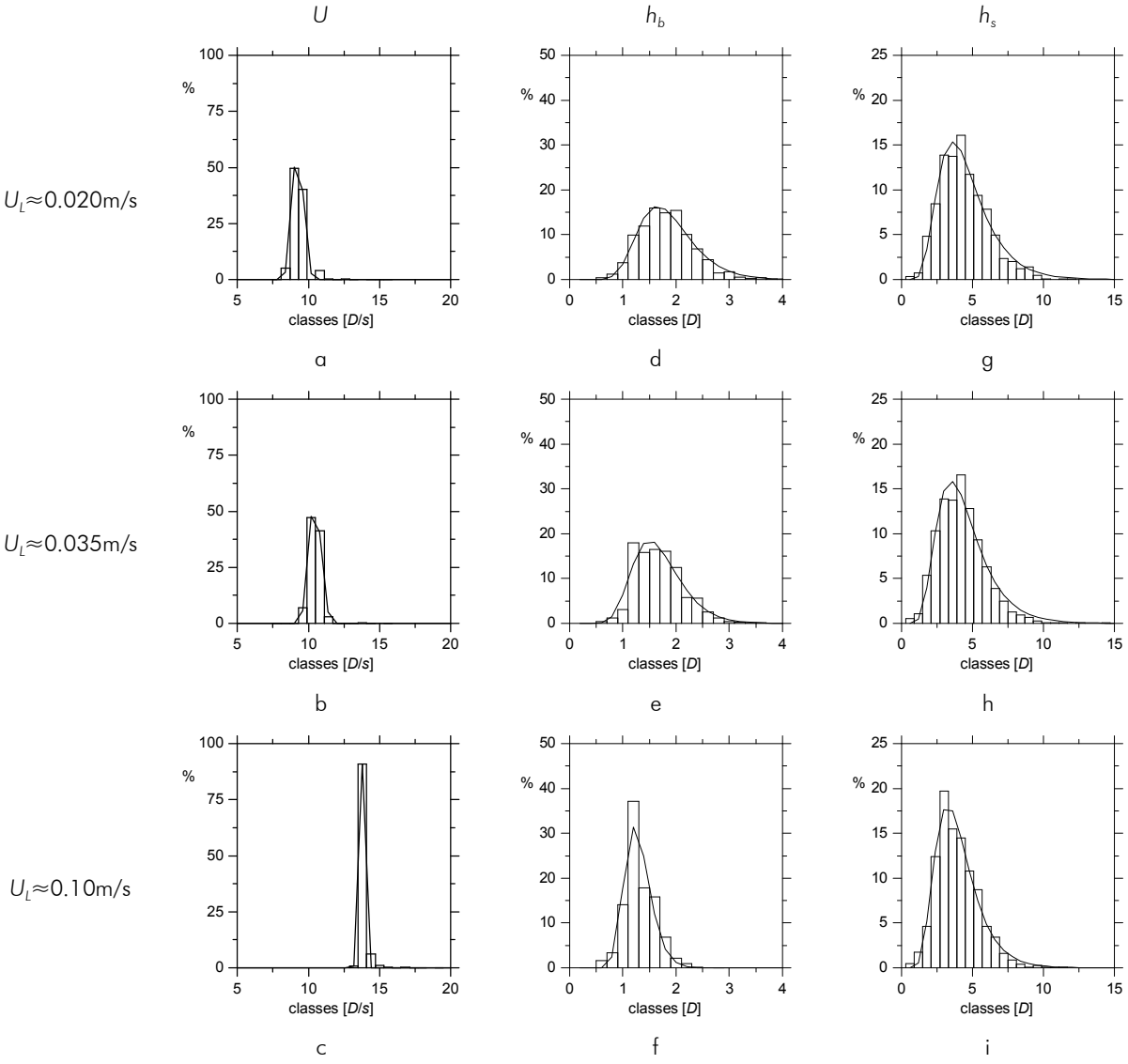

Figure 4.5 – Frequency distribution curves and log-normal fits for experiments with U_L≈0.020, 0.035 and 0.10 m/s; U_G≈0.060 m/s; vertical coordinate: 3.25 m

The most probable (mode) and average values of the distribution of bubble velocities increase with superficial liquid velocity (Figure 4.5a-c and Figure 4.6a). Both the modes and

averages of the distributions of bubble length (h_b) and of liquid slug length (h_s) decrease with increasing U_L (Figure 4.5d-f, Figure 4.5g-i and Figure 4.6a).

The variations in the bubble length and liquid slug length with U_L are the result of the competition between two effects: the inlet slope effect and the coalescence effect. These are discussed in detail below. On the one hand, as U_L increases (for constant U_G) longer slugs and shorter bubbles are formed at the inlet of the column (an experimental observation explained by flow continuity). Thus, if the chart of Figure 4.6a was focusing on the data at the column inlet, one would observe an increase in h_s (longer slugs) and a decrease in h_b (shorter bubbles), for increasing U_L. Said differently, one would have an inlet positive-slope trend for h_s and an inlet negative-slope trend for h_b, respectively. On the other hand, the fact that, for increasing U_L, the bubbles enter the column at higher distances (the inlet positive-slope trend for h_s) implies that there is a decrease in the number of coalescences along the column. This leads, in turn, to a decrease in both h_b and h_s. There is thus a competition between the inlet slope effect and the coalescence effect. The coalescence effect is dominant in the variation of h_b and h_s with U_L. Indeed, the smaller number of coalescences strengthens the inlet (negative-slope) trend of h_b and inverts the inlet (positive-slope) trend of h_s. As a result, at 3.25 m from the base of the column both variables decrease slightly with increasing superficial liquid velocity.

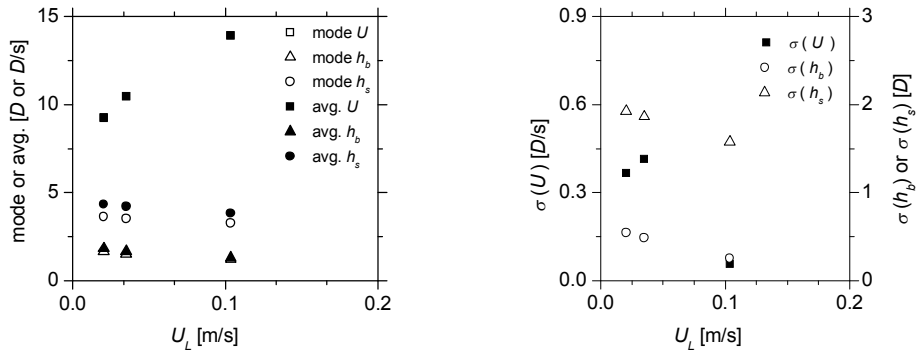

Figure 4.6 – Log-normal fit parameters: (a) average and mode, and (b) standard deviation for experiments with U_L≈0.020, 0.035 and 0.10 m/s; U_G≈0.060 m/s; vertical coordinate: 3.25 m

The standard deviation of all mentioned parameters decreases with increasing superficial liquid velocity (Figure 4.5a-c, Figure 4.5d-f, Figure 4.5g-i; Figure 4.6b). A slight deviation from this trend exists for the operating condition b (regarding the standard deviation of bubble velocity, Figure 4.6b). However, the relative contiguity of U_L values for operating conditions a and b (0.020 and 0.035 m/s; see Table 4.1) and the very low standard deviation of bubble velocity when compared to the corresponding average (<4%) diminish the relevance of the aforementioned deviation. The variation of the standard deviation of h_b and h_s indicates a more stabilised flow

pattern for increasing U_L. Similar findings are reported for studies in turbulent regime (Sotto Mayor et al. (2006a)).

4.5.2.2 Superficial gas velocity (U_G)

Data from three experiments with increasing superficial gas velocity (and constant superficial liquid velocity) are compared in this section. The frequency distribution curves for the main flow parameters are plotted in Figure 4.7. The average, mode and standard deviation of the log-normal fits are plotted against the superficial gas velocity in Figure 4.8.

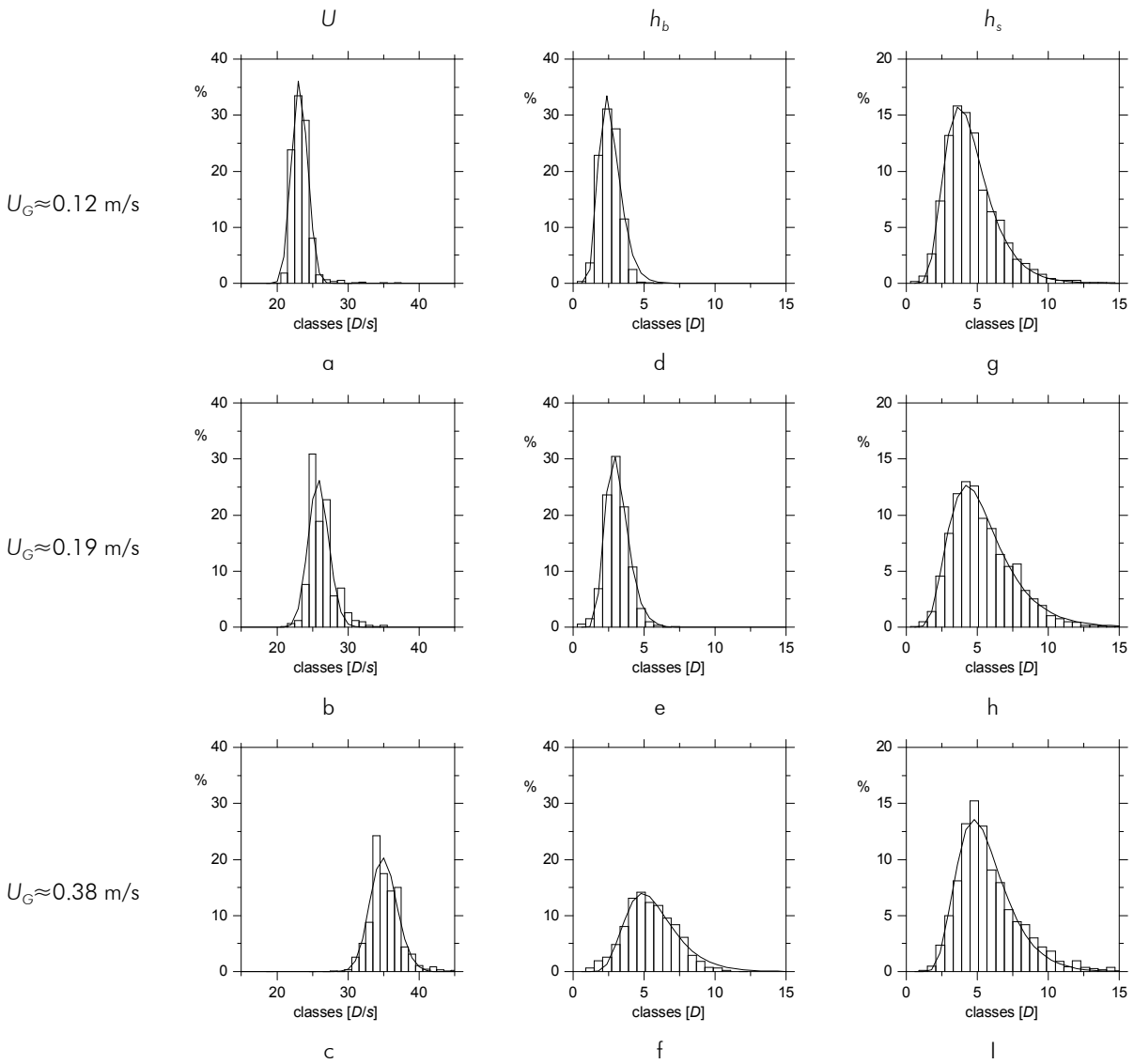

Figure 4.7 – Frequency distribution curves and log-normal fits for experiments with U_L≈0.21 m/s and U_G≈0.12, 0.19 and 0.38 m/s; vertical coordinate: 3.25 m

The average and the most probable values of the distributions of all parameters (U, h_b and h_s) increase with increasing superficial gas velocity (Figure 4.7a-c, Figure 4.7d-f, Figure 4.7g-i and Figure 4.8a).

The variation of the bubble length with U_G is the result of the strengthening of the inlet positive-slope trend by the coalescence effect along the column. Recall that increasing U_G while maintaining U_L induces longer bubbles and shorter liquid slugs, which in turn favours coalescence (and therefore both effects point towards the growth of bubble length with U_G). To the contrary, the variation of the liquid slug length with U_G results from the competition of the aforementioned effects (inlet trend and coalescence). As before, the coalescence effect is dominant since h_s increases with U_G (the inlet negative-slope trend is overcome by the more frequent coalescence events, increasing h_b and h_s).

The standard deviations of bubble velocity and bubble length escalate for increasing U_G (Figure 4.8b). The standard deviation of the slug length does not have a clear dependence, however (Figure 4.8b). The increasing standard deviation implies a less stabilized flow pattern for increasing superficial gas velocity. This conclusion is corroborated by the snapshots of the flow pattern shown in Figure 4.4 (in particular for the operating condition f). Similar findings are reported for turbulent regime (Sotto Mayor et al. (2006a)).

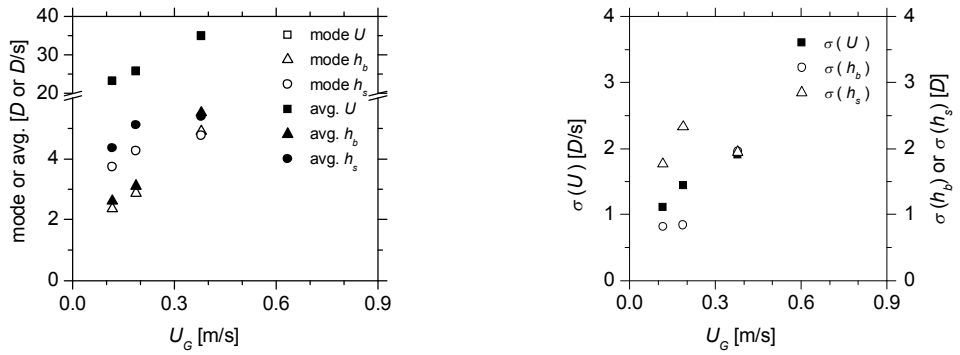

a b

Figure 4.8 – Log-normal fit parameters: (a) average and mode, and (b) standard deviation for experiments with $U_L \approx 0.21$ m/s and $U_G \approx 0.12$, 0.19 and 0.38 m/s; vertical coordinate: 3.25 m

4.5.2.3 Experimental values of C and drift velocity

The experimental average bubble velocity in undisturbed conditions (U_B^{exp}) is also assessed through fixed-point data analysis. For the purpose of assuring undisturbed bubble velocity only bubbles flowing behind liquid slugs longer than 5D are considered. However, a slight bubble-to-bubble interaction still exists in these conditions (see section 4.5.1). The establishment of 5D as the minimum liquid slug length for the computation of U_B^{exp} results from a balance between

representativity and accurateness. Indeed, computing U_B^{exp} values based only on bubbles flowing behind longer liquid slugs would jeopardize the representativity of the estimates as they would be based on a relatively small sample of bubbles. Besides, according to the bubble-to-bubble interaction fit (Eq. (4.1)), a given trailing bubble flows less than 3.5% faster than its leading bubble, provided that the liquid slug between them is longer than 5*D*. Thus, although the values of U_B^{exp} obtained in these conditions are slightly overestimated, the increasing representativity of the estimates (based on 500-1200 bubbles) clearly makes up for the eventual drawback in accuracy.

In order to estimate parameter C and the drift velocity (U_∞) for the experiments reported in the previous sections, the experimental average bubble velocity (U_B^{exp}) is plotted against the average superficial velocity of the mixture ($U_M=U_L+U_G$; see Figure 4.9). The values of U_M were corrected to the pressure at coordinate 3.25 m (see Table 4.1). The linear fit of the experimental data and correlation-based predictions of U_B are also shown in this figure. The predictions of U_B are computed following Nicklin et al. (1962):

$$U_B = U_\infty + C(U_L + U_G) \tag{4.2}$$

with C=2 and $U_\infty = 0.181$ m/s. The value of C for laminar regime was obtained theoretically by Collins et al. (1978) and experimentally for instance by Nicklin et al. (1962). The value of U_∞ used in the computation of U_B was estimated following White and Beardmore (1962) considering column diameter and liquid properties.

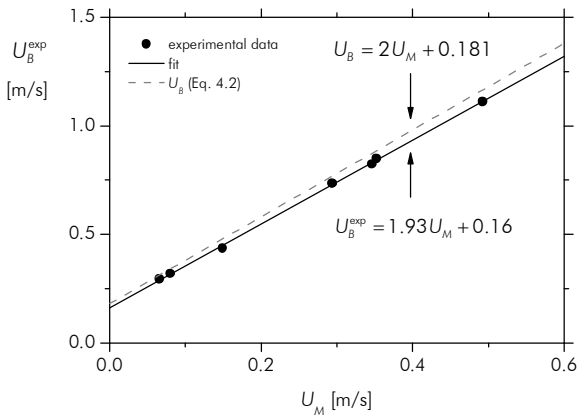

Figure 4.9 – Undisturbed average upward bubble velocity plotted against U_M; vertical coordinate: 3.25 m

A very good agreement was obtained between predictions and experimental results. The experimental value of C obtained (1.93) differs less than 3.5% from the theoretical value (2) and is within the range reported by Nicklin et al. (1962) (1.80-1.95). The experimental drift velocity

(0.16) is 12% lower than that following White and Beardmore (1962) (0.181 m/s). Notice that although the aerated level of the liquid slugs for condition f is fairly considerable (Figure 4.4f), the observed value of U_B^{exp} is still consistent with the correlation-based predictions.

The agreement between experimental results and correlation-based predictions indicates that the latter can be used as input for simulations of slug flow pattern in laminar regime. This is of significant importance as it widens the range of applicability of the simulation code (in terms of column diameter, liquid properties, etc.). Moreover, the aforementioned agreement further confirms the irrelevance of the accuracy concession in the computation of U_B^{exp}.

4.6 Slug flow simulation

A slug flow simulator (SFS) was used in the present study. The following section addresses the main assumptions of the simulator.

4.6.1 Simulator assumptions, approaches and output

In the simulator, a given number of randomly distributed liquid slugs (and Taylor bubbles) is assumed to enter the column at its base. The bubble length distribution is created using two independent normal distributions (prepared using Box Muller algorithm (Campos Guimarães and A. Sarsfield Cabral (1997))): the liquid slug length distribution and the superficial gas velocity distribution. The liquid slug length distribution allows to "introduce" in the simulation the influence of the gas injection system (in terms of the length of the gas bubbles and liquid slugs formed). The superficial gas velocity distribution is an attempt to include in the simulation the effect of the changing hydrostatic pressure at the column inlet, due to the variable gas hold-up inside the column.

The elements of the bubble length distribution ($h_{b,i}$) are calculated based on the mentioned distributions of the liquid slug length and superficial gas velocity, using the following equation, for each slug unit cell (i.e. slug + bubble):

$$h_{b,i} = \frac{h_{s,i}}{\frac{S_b U_B^{exp}}{S_c U_{G,i}} - 1} \tag{4.3}$$

where i refers to the index of the slug unit cell, and S_b and S_c stand for the bubble and the column cross-sectional area, respectively. The estimate of S_b is computed based on the liquid film thickness determined following Brown (1965) for free-falling conditions. The variables $h_{s,i}$ and $U_{G.i}$ refer to

the i^{th} elements of the slug length and the superficial gas velocity distributions, respectively. Eq. (4.3) was obtained by combining the following equations, at the inlet coordinate: $U_{G,i}S_c\Delta t_i = S_b h_{b,i}$ and $U_B^{exp}\Delta t_i = h_{b,i} + h_{s,i}$, where Δt_i is the time interval required for the entrance in the column of a slug unit cell. Figure 4.10 represents a set of slug unit cells, prepared as described above (note the distributed bubble lengths, slug lengths and superficial gas velocities and the constant superficial liquid velocity). As shown in Figure 4.10, the bubble shape is considered cylindrical in the simulation. Although this assumption does not alter the way slug flow pattern evolves along the column, a correction has been implemented on the length of the bubbles (considering spherical bubble noses, under the condition of equal bubble volume) in other to determine more realistic estimates of bubble length. The estimate of U_B^{exp} in Eq. (4.3) is retrieved using Eq. (4.2). The relation (4.3) serves to assure a given average U_L and U_G at the column inlet (inputs to the simulator). With the distributions of bubble length and liquid slug length at the column inlet, it is then possible to simulate the process of evolution of these distributions along the column.

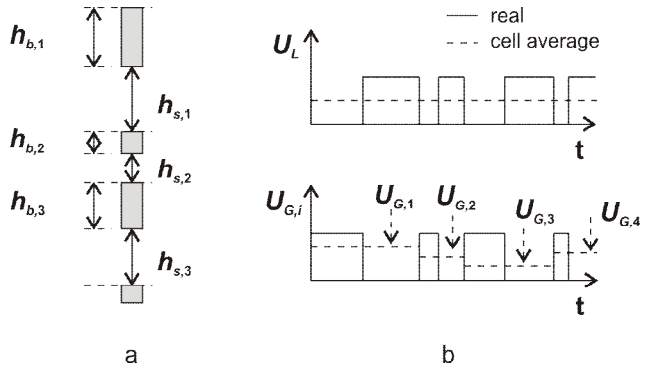

Figure 4.10 – (a) Representation of a train of slug unit cells (bubble + slug) and (b) superficial gas and liquid velocities for each slug unit cell

The displacement of bubbles along the column is implemented as the incremental movement of their boundaries (nose and rear), between consecutive instants, according to their velocities. The velocity of a given bubble *i* is computed, at each instant, as the result of the bubble-to-bubble interaction (given by Eq. (4.1)) and of the expansion of all bubbles flowing below. Bubble expansion (taken as a rise of the nose boundary) is implemented iteratively for each bubble, after updating its position, according to the hydrostatic pressure gradient along the column. The hydrostatic pressure inside the column, at a given vertical coordinate, is computed taking only the liquid inside the column (i.e. without the Taylor bubbles). This is a reasonable approach when discarding pressure losses in the liquid phase. A simulation time increment of 0.005 s is used based on grid testing (comparison of similar simulations with decreasing time increments).

The main outputs of the simulator are the coalescence rate along the column and the distributions of bubble velocity, bubble length and liquid slug length at any vertical column position. Furthermore, it is possible to determine the local/global gas hold-up values and the positioning of every bubble and liquid slug inside the column, for any time instant during the simulation.

4.6.2 Validation of the Simulation

Two issues are dealt with in this section: the applicability of the correlation-based estimates of parameters C and U_∞ for simulation purposes, and the comparison between experimental results and simulation data.

4.6.2.1 Parameters C and U_∞ – experimental versus correlation-based estimates

Two similar simulations of the operating condition d (Table 4.1) are compared in this section. All parameters of the simulations except C and U_∞ are similar. One simulation is based on the experimental values of these parameters (1.932 and 0.161 m/s, respectively) whilst another is based on the correlation predictions (2 and 0.181 m/s, respectively; see section 4.5.2.3). The frequency distribution curves of bubble velocity, bubble length and liquid slug length, obtained at 3.25 m from the base of the column, are shown in Figure 4.11. The average, mode and standard deviation of the corresponding log-normal fits, are shown in Figure 4.12.

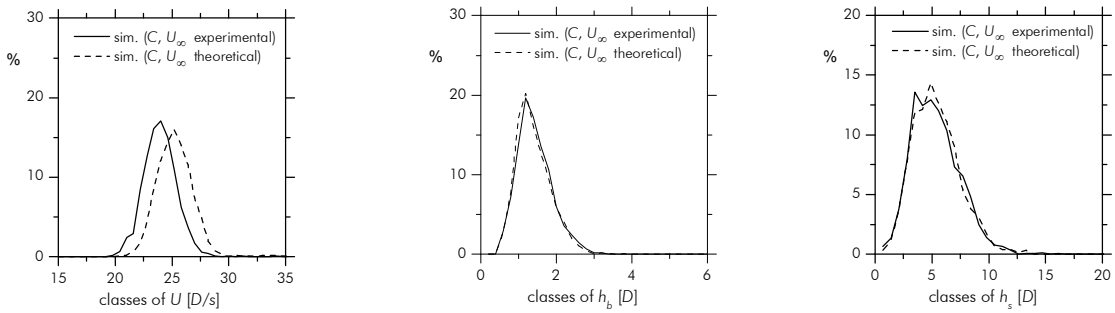

Figure 4.11 – Frequency distribution curves of (a) bubble velocity, (b) bubble length and (c) slug length, for simulations with experimental and predicted values of C and U_∞ (1.932, 0.161 m/s and 2, 0.181 m/s, respectively); $U_L \approx 0.20$ m/s, $U_G \approx 0.12$ m/s

The analysis of the charts shows that the output of both simulations is very similar. Both the frequency distribution curves (Figure 4.11) and the log-normal fit parameters (Figure 4.12) of bubble length and liquid slug length show considerable resemblance. Indeed, the main difference

in the outputs concerns the frequency distribution curves of bubble velocity (and, accordingly, the corresponding log-normal fit parameters). The simulation based on the correlation predictions of C and U_∞ shows a bubble distribution whose velocities slightly exceed the ones observed for the simulation based on the experimental parameters (the modes of the corresponding log-normal fit differ by about 6%). However, both frequency distribution curves are similar in shape (similar standard deviation). Therefore, no relevant bias is introduced in the simulations by using the correlation predictions of C and U_∞ instead of the observed experimental estimates. As already mentioned, this fact widens the range of applicability of the proposed simulator.

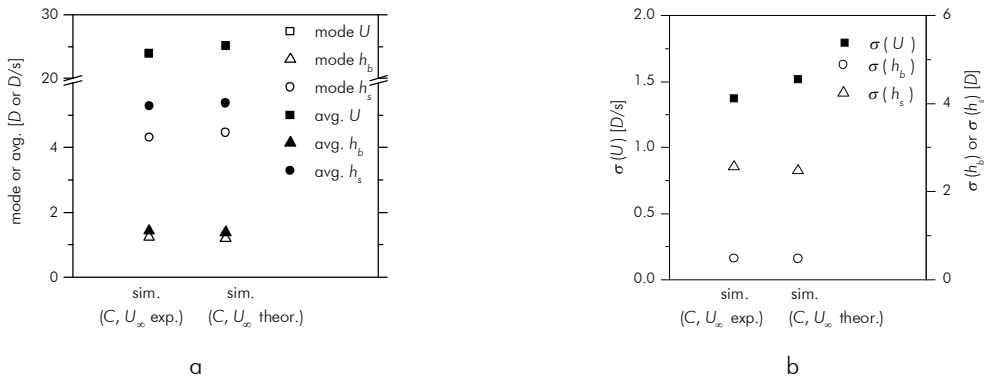

Figure 4.12 – Log-normal fit parameters (a) average, mode and (b) standard deviation, for simulations with experimental and predicted values of C and U_∞ (1.932, 0.161 m/s and 2, 0.181 m/s, respectively); $U_L \approx 0.20$ m/s, $U_G \approx 0.12$ m/s

4.6.2.2 Experimental data versus simulation results

A comparison between experimental data and simulation results, for operating conditions a and e, is shown in this section. The comparison only focuses on two operating conditions (out of eight possible) for the sake of simplicity of the analysis. Similar conclusions can be drawn for the other operating conditions. Normally distributed slug lengths are introduced at the inlet (average and standard deviation equal to 3D and 1D, respectively). Distributed superficial gas velocities are also considered (with standard deviation equal to 10% of the corresponding average). The focus is on the results at 3.25 m from the base of the column (vertical coordinate of acquisition). Notice that the characteristics of the inlet slug length distribution are shown later not to affect the results at the mentioned coordinate (see section 4.6.4).

The frequency distribution curves resulting from the simulation of both flow conditions indicate that simulation slightly overestimates the bubble velocity (Figures 4.13a and 4.13d; the modes of the corresponding log-normal fits differ about 10%). This minor discrepancy is partially related to the use of the correlation-based estimates of C and U_∞ instead of the experimental

values obtained. The simulation results for both flow conditions show some degree of underestimation for bubble length parameter (Figures 4.13b and 4.13e). This discrepancy is small for operating condition *a* (≈10%) and moderate for operating condition *e* (≈30%). Nevertheless, these deviations should be understood in a context of small absolute values. A very good agreement exists, however, between experimental data and simulation results for slug length variable (Figures 4.13c and 4.13f). Accordingly, the log-normal fits of the corresponding frequency distribution curves have very similar modes and standard deviations (Figure 4.14).

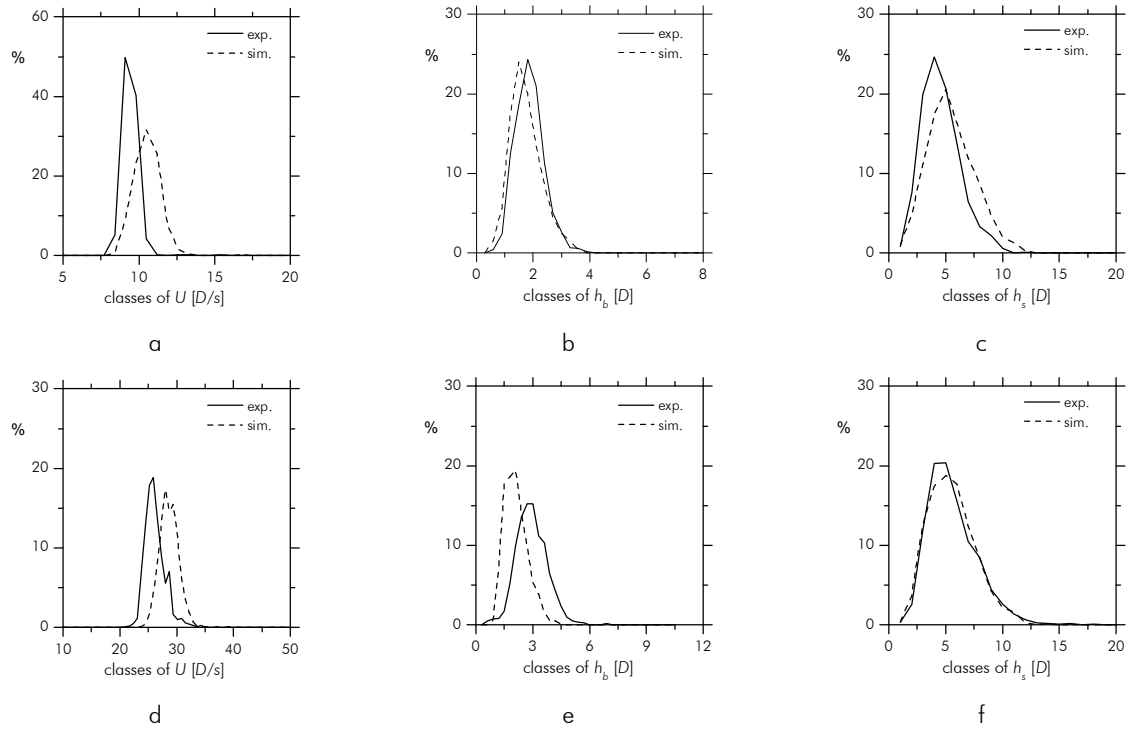

Figure 4.13 – Frequency distribution curves: (a) bubble velocity, (b) bubble length and (c) slug length, for an experiment/simulation with U_L≈0.020 m/s and U_G≈0.060 m/s; (d) bubble velocity, (e) bubble length and (f) slug length, for an experiment/simulation with U_L≈0.20 m/s and U_G≈0.19 m/s; vertical coordinate: 3.25 m

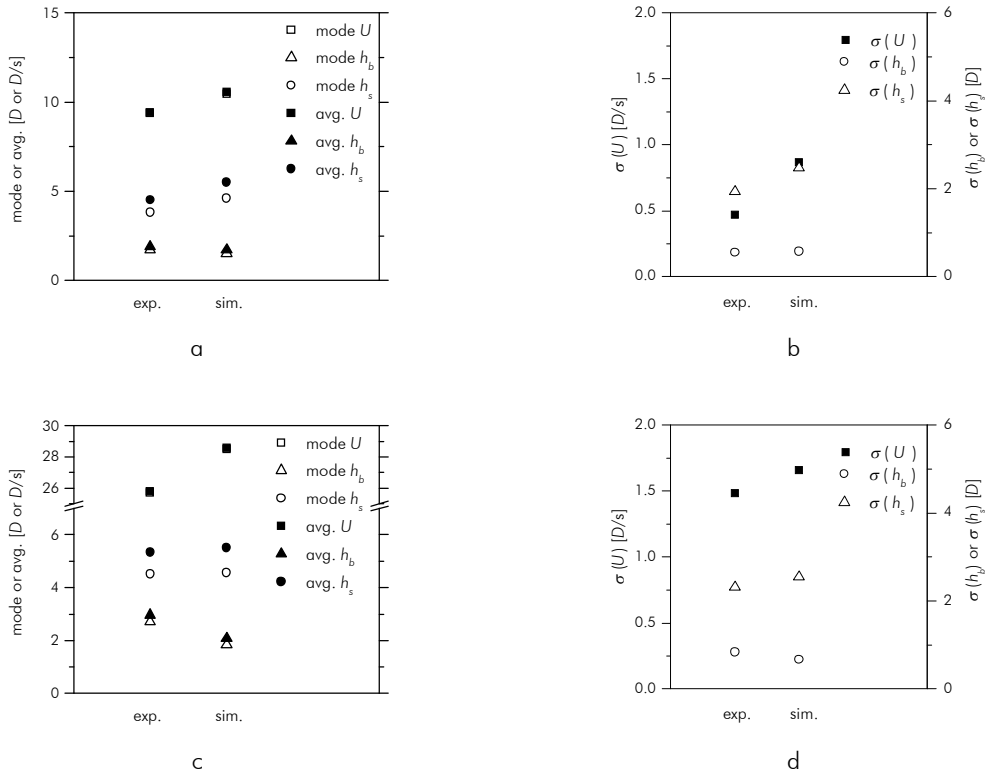

Figure 4.14 – Log-normal fit parameters: (a) average, mode and (b) standard deviation, for an experiment/simulation with $U_L \approx 0.020$ m/s and $U_G \approx 0.060$ m/s; (c) average, mode and (d) standard deviation, for an experiment/simulation with $U_L \approx 0.20$ m/s and $U_G \approx 0.19$ m/s; vertical coordinate: 3.25 m

4.6.3 The coalescence events along the column

The coalescence occurring along a column, for simulations based on different bubble-to-bubble interaction correlations, is discussed in this section. The correlation (4.1) and that proposed by Sotto Mayor et al. (2006a) for turbulent regime (both shown in Figure 4.3c) are used for simulations with U_L and U_G equal to 0.10 m/s. Similar inlet slug length distributions are used for both simulations (centred on 3*D*). The dispersion of coalescence events along the column for both simulations is shown in Figure 4.15

Coalescence occurs mostly in the lower part of the column for turbulent regime. As is evident in the corresponding cumulative curve, about 75% of all coalescence events occur in the first 30*D* of the column. To the contrary, the simulation based on correlation (4.1) shows a wider coalescence curve, covering the whole column length. Indeed, for the corresponding simulation, the first 30*D* of the column encompass only 30% of all coalescence events. These results show that the coalescence of bubbles in laminar slug flow must be considered as omnipresent along the whole length of the column. The evolution of the slug flow pattern is, thus, always affected by this phenomenon. These conclusions refer to the length of column used in this study.

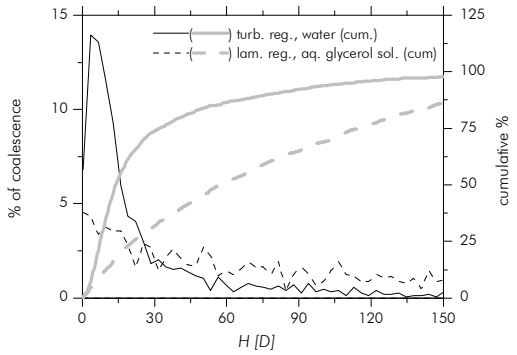

Figure 4.15 – Coalescence events along the column (steps of 0.1 m) for simulations for turbulent regime (water, after Sotto Mayor et al. (2006b) and laminar regime (glycerol aqueous solution); inlet slug length distributions centred on 3*D*; U_L and U_G equal to 0.1 m/s

4.6.4 The entrance length of slug flow

The gas injection system (nozzle) influences the way gas bubbles are formed in the liquid medium and affects, consequently, the length of the bubbles and liquid slugs. Thus, it determines the characteristics of the distributions of bubble length and liquid slug length obtained at the inlet of the column (changing, for instance, the mode, the median or the standard deviation of the distribution). However, the differences in the inlet distributions tend to dissipate along the column due to coalescence. Moreover, the length of column along which the influence of the different inlet distributions (the entrance effects) can be observed is usually known as the entrance length of slug flow. This concept is grounded on the idea that the slug flow evolves to a single slug flow pattern, regardless of the initial characteristics of the flow (in terms of bubble and slug distributions, for instance). However, although this idea is very compelling there are practical limitations to its applicability, namely in terms of the column length. Indeed, two very contrasting bubble length (and slug length) distributions, evolving in a column in slug flow regime, might never reach the "final" slug flow pattern due to the finite nature of the column. Thus, it is more useful to estimate a range of inlet distributions (for instance in terms of slug length) that do evolve to a single slug flow pattern for a given finite column length. This is a very interesting approach for practical applications.

Slug flow in a 6.5 m long (0.032 m internal diameter) column was simulated. Several simulations with different inlet slug length normal distributions were compared. Focus was put on the evolution along the column (in steps of 0.6 m) of the average and the most probable values of the bubble length and slug length distributions. Log-normal distributions were fitted to the slug and bubble length frequency distribution curves obtained along the column, to allow for a straightforward comparison. As a first approach, the evolution of inlet slug length distributions

centred on 2*D*, 3*D*, 4*D* and 5*D* was monitored (standard deviation equal to 0.5*D*, 1*D*, 1*D*, and 1*D*, respectively; no attempt was made to address inlet slug length distributions centred on values lower than 2*D* because the corresponding bubbles would be too short to be considered as Taylor bubbles, a scenario that would be outside the scope of the present work. Nevertheless, such small bubbles would undergo intense coalescence due to the short liquid slugs between them (see the interaction curve in Figure 4.3), which would result in slug length distributions similar to those considered above, at a vertical coordinate not far from the column base). The resulting maximum relative differences of the average and mode of the log-normal local fits are plotted against the vertical coordinate of the column in Figure 4.16a. This chart shows that even at the last observation point (185*D* or 5.9 m from the base of the column) the maximum relative difference between the aforementioned simulations exceeds 10%. The column is not long enough to allow full attenuation of the inlet differences. Or, alternatively, the inlet simulations are too contrasting so as to allow the definition of the entrance length of the slug flow, for a 6.5 m long column.

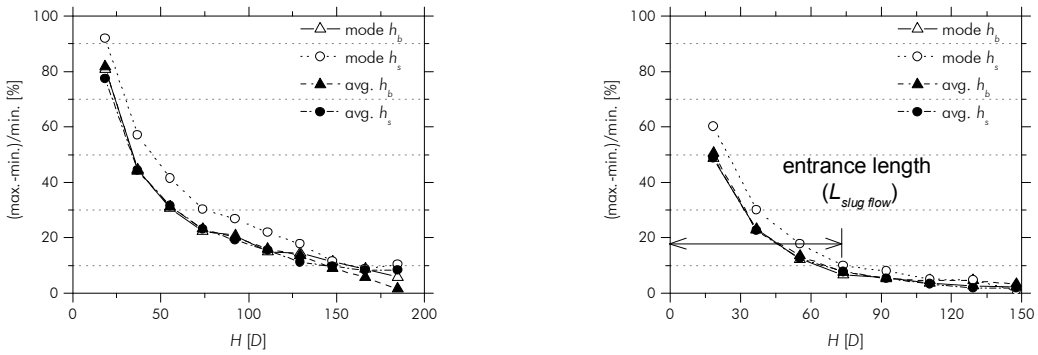

Figure 4.16 – Maximum relative difference of the mode and average of log-normal fits, along the column, for simulations with increasing average inlet slug lengths: (a) 2*D*, 3*D*, 4*D* and 5*D*; (b) 2*D*, 3*D* and 4*D*; $U_L \approx 0.20$ m/s and $U_G \approx 0.20$ m/s

A second approach was attempted regarding simulations with inlet slug length distributions centred instead on 2*D*, 3*D* and 4*D*. The results of this comparison are shown in Figure 4.16b. Unlike the first scenario, strong attenuation of the inlet differences occurs within the length of the column. It is thus possible to define the entrance length of slug flow for such a column and such inlet differences (and, obviously, such operating conditions). A figure of 75*D* (2.4 m) is obtained for $U_G = U_L = 0.20$ m/s (accepting a maximal difference of 10%). Spanning the aforementioned approach for a set of increasing superficial gas and liquid velocities (0.05, 0.10, 0.15 and 0.20 m/s) one obtains the chart of Figure 4.17a, showing the variation of the entrance length with these parameters (for 10% maximum relative difference). The entrance length ranges from 70*D* to 100*D*,

for U_G and U_L in the range mentioned above. However, if one is less demanding in terms of the maximum relative difference (accepting for instance 12% instead of the 10%) much smaller entrance lengths are obtained (as shown in Figure 4.17b). Nevertheless, this approach shows that the inlet slug length distributions must be centred on 2-4*D* to assure reduced entrance effects in the simulation results, from the acquisition coordinate upward (3.25 m or 101.5*D* from the base of the column). Notice that a study on turbulent slug flow (Sotto Mayor et al. (2006b)) revealed an entrance length ranging from 50*D* to 70*D* for convergence of inlet slug length distributions centred on 2*D*, 5*D* and 8*D* (for similar column length). Thus, in turbulent slug flow, much more contrasting inlet slug length distributions converge within the same column length, due to the more frequent coalescence (as shown in section 4.5.1).

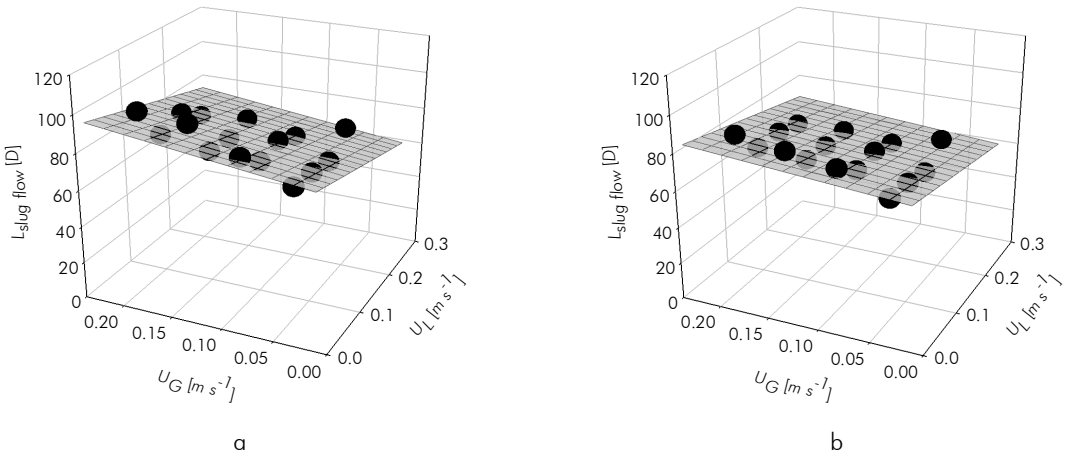

Figure 4.17 – Entrance length of slug flow for simulations with U_L and U_G equal to 0.05, 0.1, 0.15, and 0.20 m/s; average inlet slug lengths equal to 2*D*, 3*D* and 4*D*; maximum relative difference of (a) 10% and (b) 12%

4.6.5 Simulation study

An extensive simulation study was developed in order to expound the influence of U_G and U_L on the evolution of 3 variables along the column: bubble velocity (U), bubble length (h_b) and liquid slug length (h_s). For that purpose, several simulations with increasing U_G and U_L (0.05, 0.10, 0.15 and 0.20 m/s) were compared systematically (16 simulations). Normal distributions of slug length (average and standard deviation equal to 3*D* and 1*D*, respectively) are acknowledged at the inlet of the column for all simulations. Distributed superficial gas velocities are also considered (standard deviations equal to 10% of the corresponding averages). The evolution of the resulting distributions of U, h_b and h_s was monitored along the column, in steps of 0.6 m (10 vertical coordinates). Log-normal distributions were fitted to each frequency distribution curve obtained in order to simplify the comparison of different curves. This originates two parameters (mode and

standard deviation) per curve. This procedure finally results in a considerable amount of data (3 variables x 2 statistical parameters x 16 simulations x 10 vertical coordinates). However, data can be sorted into 6 different groups: 3 regarding modes (of U, h_b and h_s) and 3 regarding the corresponding standard deviations. Nonlinear estimation was implemented within each group of data in order to expound its dependence on U_L, U_G and H (vertical coordinate along the column). The general form of the fitting equation is:

$$z = a(H)^2 + bH + c(U_L)^2 + dU_L + e(U_G)^2 + fU_G + gHU_L + hHU_G + iU_LU_G + j \qquad (4.4)$$

where quadratic, linear and crossed terms in H, U_L and U_G are acknowledged. For each group of data, relevant fit coefficients were determined (for a 95% confidence level). Non-significant coefficients were excluded from the fits. Standard errors for each coefficient were also calculated. The coefficient estimates and corresponding standard errors obtained are shown in Tables 4.2 and 4.3.

3-D representations of the variation of U, h_b and h_s (modes and standard deviations) with H, U_L and U_G are shown in the following sections. Focus is put on the variation along the column for increasing U_G and at column outlet.

Table 4.2 – Coefficients (estimate and standard error) and residuals (*SSE*: sum of squares of error; $SSE/n_{dat.}$: average sum of squares of error) of the surface fits of Figures 4.18 and 4.19, focussing modes; equation form: $z = a(H)^2 + bH + c(U_L)^2 + dU_L + e(U_G)^2 + fU_G + gHU_L + hHU_G + iU_LU_G + j$; z in SI units

	mode (U)		mode (h_b)		mode (h_s)	
	estimate	stand. error	estimate	stand. error	estimate	stand. error
a	9.42×10^{-4}	7.80×10^{-5}	8.60×10^{-4}	5.30×10^{-5}	-3.77×10^{-4}	8.00×10^{-5}
b	-7.01×10^{-3}	5.83×10^{-4}	...	...	9.87×10^{-3}	5.98×10^{-4}
c	...	...	8.16×10^{-1}	8.80×10^{-2}	-3.57×10^{-1}	8.13×10^{-2}
d	$2.05 \times 10^{+0}$	3.54×10^{-3}	-1.12×10^{-1}	2.50×10^{-2}	8.05×10^{-2}	2.18×10^{-2}
e	...	...	...	...	...	...
f	$1.33 \times 10^{+0}$	7.66×10^{-3}	3.92×10^{-1}	1.18×10^{-2}	...	...
g	...	...	-3.51×10^{-2}	2.12×10^{-3}	7.73×10^{-3}	2.14×10^{-3}
h	1.03×10^{-1}	2.09×10^{-3}	6.03×10^{-2}	2.12×10^{-3}	...	...
i	...	...	$-1.59 \times 10^{+0}$	7.04×10^{-2}	...	...
j	1.97×10^{-1}	1.29×10^{-3}	8.99×10^{-3}	1.86×10^{-3}	1.06×10^{-1}	1.60×10^{-3}
SSE [m^2 or m^2/s^2]	9.83×10^{-4}		1.17×10^{-3}		1.02×10^{-3}	
$SSE/n_{dat.}$ [m^2 or m^2/s^2]	6.15×10^{-6}		7.33×10^{-6}		6.36×10^{-6}	
r^2	1.000		0.992		0.970	

Table 4.3 – Coefficients (estimate and standard error) and residuals (*SSE*: sum of squares of error; $SSE/n_{dat.}$: average sum of squares of error) of the surface fits of Figures 4.18 and 4.19, focussing σ; equation form: $z = a(H)^2 + bH + c(U_L)^2 + dU_L + e(U_G)^2 + fU_G + gHU_L + hHU_G + iU_LU_G + j$; z in SI units

	$\sigma(U)$		$\sigma(h_h)$		$\sigma(h_s)$	
	estimate	stand. error	estimate	stand. error	estimate	stand. error
a	5.97×10^{-4}	7.30×10^{-5}	7.22×10^{-4}	5.00×10^{-5}	1.08×10^{-3}	1.66×10^{-4}
b	-3.78×10^{-3}	5.03×10^{-4}	-2.59×10^{-3}	4.08×10^{-4}	1.03×10^{-2}	1.13×10^{-3}
c	...	...	3.59×10^{-1}	5.07×10^{-2}	...	...
d	8.46×10^{-2}	8.10×10^{-3}	-5.37×10^{-2}	1.45×10^{-2}	...	...
e	1.98×10^{-1}	6.84×10^{-2}	...	...	...	...
f	1.63×10^{-1}	1.50×10^{-2}	1.45×10^{-1}	7.04×10^{-3}	...	...
g	-1.55×10^{-2}	1.87×10^{-3}	-1.26×10^{-2}	1.34×10^{-3}	...	...
h	4.20×10^{-2}	1.87×10^{-3}	2.91×10^{-2}	1.34×10^{-3}	-6.83×10^{-3}	2.05×10^{-3}
i	-4.03×10^{-1}	5.47×10^{-2}	-6.34×10^{-1}	4.05×10^{-2}	...	...
j	...	...	4.56×10^{-3}	1.33×10^{-3}	3.77×10^{-2}	1.56×10^{-3}
SSE [m^2 or m^2/s^2]	9.18×10^{-4}		3.88×10^{-4}		4.41×10^{-3}	
$SSE/n_{dat.}$ [m^2 or m^2/s^2]	5.74×10^{-6}		2.42×10^{-6}		2.76×10^{-5}	
r^2	0.983		0.986		0.966	

4.6.5.1 Results along the column

The mode and standard deviation of the main flow parameters are plotted against *H* and U_G (Figure 4.18) for constant U_L (equal to 0.10 m/s). The corresponding 3-D surfaces (computed by Eq. (4.4)) are also shown in the charts.

The most probable value (mode) of liquid slug length has an almost steady increase along the column (Figure 4.18c) and shows no dependence on U_G. The evolution of this parameter with *H* is mainly related to the coalescence of bubbles along the column (expansion effects have little influence over the evolution of h_s; the fact that h_s shows almost no dependence on U_G corroborates this observation). Moreover, the steady variation rate of this parameter along the column confirms that the coalescence of bubbles occurs along the whole column (as already mentioned in section 4.6.3). As a consequence, both short liquid slugs (between coalescing bubbles) and increasingly longer slugs (since h_s increases with *H*) coexist in the column. To further confirm this, the standard deviation of h_s increases strongly along the column. Indeed, the corresponding standard deviation/mode ratio increases from 35-40% near the base, to 70-95%, at the top of the column (Figure 4.18i). A reasonably constant standard deviation/mode ratio (35-50%) was reported by Sotto Mayor et al. (2006b), for a study on turbulent regime. Additionally, in that study the liquid slug length evolved almost asymptotically along the column to about 11-12*D* at the top. No similar evolution of slug length parameter was found in the present study (laminar regime). The liquid slug length does not stabilise before the column outlet and, therefore, no asymptotical value is reached within the 6.5 m length of the column (Figure 4.18c). This is related to the fact that bubble coalescence occurs anywhere along the whole vertical coordinate of the column. For

turbulent regime in the liquid, the coalescence occurs mainly in the lower part of the column (Sotto Mayor et al. (2006b)).

The most probable value and the standard deviation of bubble length increase along the column and with U_G (Figures 4.18b and 4.18e). Coalescence and expansion effects can account for the variation of the most probable value along *H,* whilst flow continuity justifies its variation with U_G. Recall that due to flow continuity, increasing U_G for constant U_L favours the formation of longer bubbles. The standard deviation of this parameter ranges between 27% and 43% of the corresponding mode, for the ranges of U_G and *H* studied (Figure 4.18h). A quite similar range is reported for turbulent regime (30-45%; Sotto Mayor et al. (2006b)).

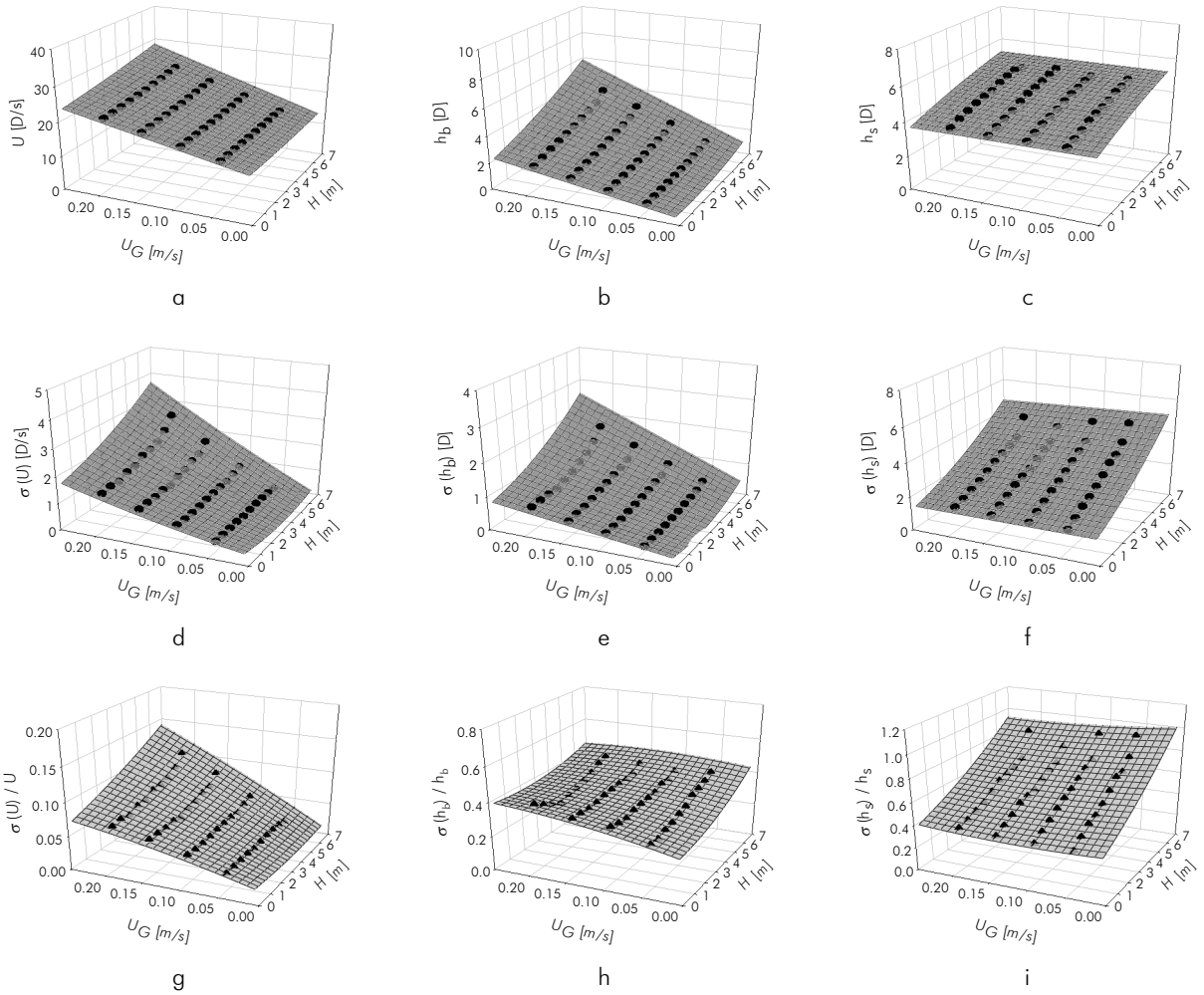

Figure 4.18 – Mode (a-c), standard deviation (d-f) and corresponding ratio (g-i) of log-normal fits along the column; (a), (d) and (g) bubble velocity; (b), (e) and (h) bubble length; (c), (f) and (i) liquid slug length; simulations with $U_L \approx 0.10$ m/s and $U_G \approx 0.05$, 0.10, 0.15 and 0.20 m/s

Both the most probable value and the standard deviation of bubble velocity parameter increase with *H* and U_G (Figures 4.18a and 4.18d). Additionally, although not very evident in the charts, their variation rates with *H* are slightly more pronounced for higher superficial gas velocity

(i.e. for higher gas hold-up). This indicates that the gas phase expansion plays an important role in the evolution of these parameters along the column. However as was already mentioned, the coalescence of bubbles also has a relevant influence in the evolution of bubble velocity along the column. The standard deviation of this parameter reaches no more than 12% of the corresponding mode (Figure 4.18g), for the ranges of U_G and U_L studied. As for the bubble length variable, this value is quite similar to that reported for turbulent regime (18%; Sotto Mayor et al. (2006b)).

4.6.5.2 Results at column outlet

The mode and standard deviation of the main flow parameters are plotted against increasing values of U_L and U_G in Figures 4.19a to 4.19f. The charts focus on the frequency distribution curves obtained at 5.9 m from the base of the column.

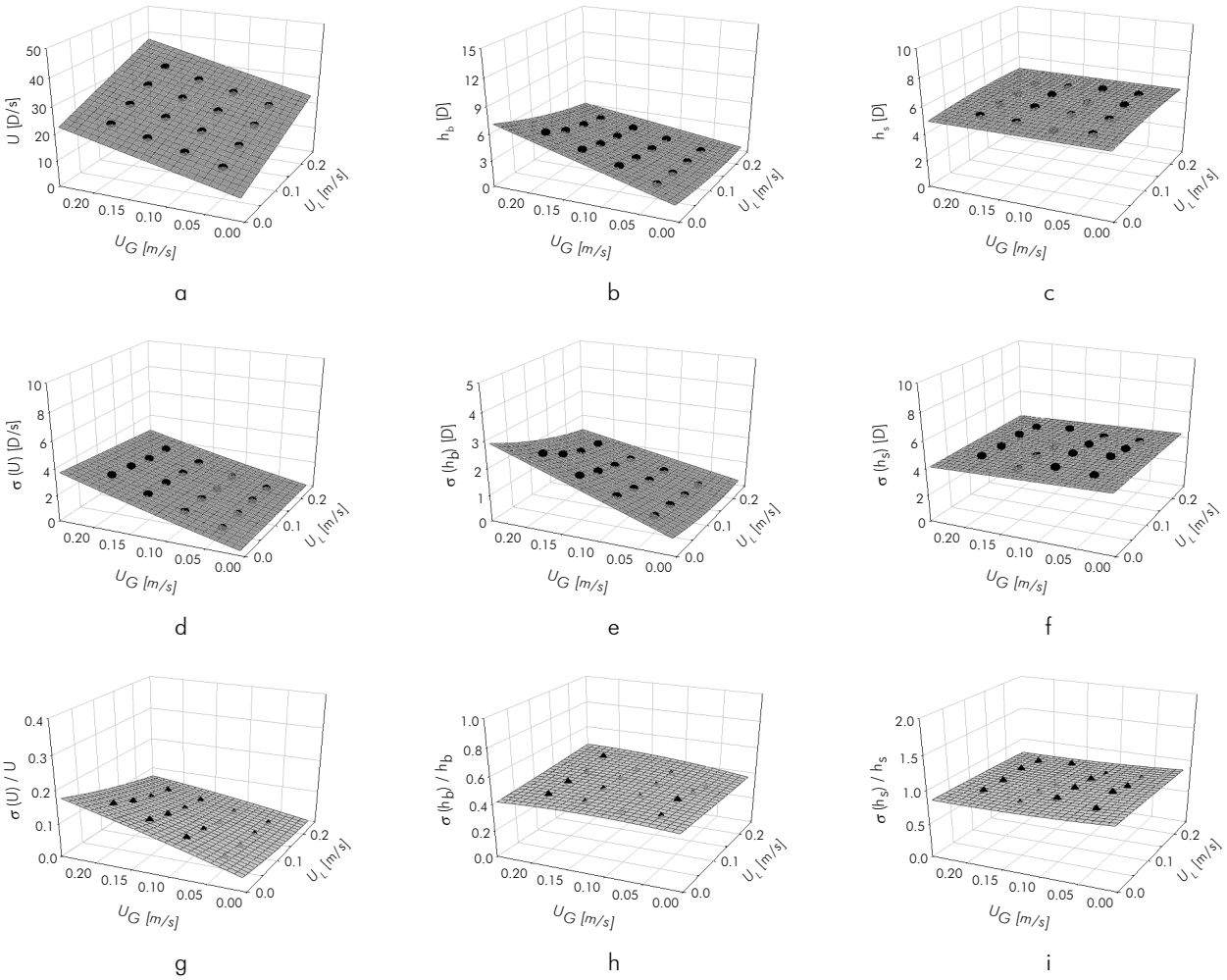

Figure 4.19 – Mode (a-c), standard deviation (d-f) and corresponding ratio (g-i) of log-normal fits; (a), (d) and (g) bubble velocity; (b), (e) and (h) bubble length; (c), (f) and (i) liquid slug length; simulations with U_L and U_G equal to 0.05, 0.10, 0.15 and 0.20 m/s; vertical coordinate: 5.9 m

The most probable bubble velocity increases linearly with both superficial gas and liquid velocities (Figure 4.19a). The corresponding standard deviation escalates with increasing U_G and decreasing U_L (Figure 4.19d). The standard deviation/mode ratio is smaller than 14% for the ranges of U_L and U_G studied (Figure 4.19g). Despite the wider ranges of U_L and U_G studied (0.10-0.50 m/s), Sotto Mayor et al. (2006b) report a quite similar figure (18%), for turbulent regime.

The most probable bubble length and corresponding standard deviation augment with increasing U_G and decreasing U_L (Figures 4.19b and 4.19e). Flow continuity accounts for these contrasting variations. Approximately constant standard deviation/mode ratios are obtained (circa 40%; Figure 4.19h) for the ranges of U_L and U_G studied. Similar ratios (30-40%) are reported for turbulent regime (Sotto Mayor et al. (2006b)).

Similar slug length modes and standard deviations are obtained at the column outlet, for the ranges of superficial velocities studied (Figures 4.19c and 4.19f). Those parameters show, therefore, weak dependence on U_L and U_G. The standard deviations are substantial, however, when compared to the corresponding modes (circa 70-95% as shown in Figure 4.19i). Lower standard deviation/mode ratios are reported for turbulent regime (35-45%; Sotto Mayor et al. (2006b)). This is obviously related to the different coalescence curves in both regimes (very scarce coalescence in the upper part of the column for turbulent regime, as opposed to coalescence along the whole column for laminar regime; see section 4.6.3 for more details).

4.7 Conclusions

An experimental and simulation study on free bubbling vertical slug flow is reported. A non-intrusive image analysis technique and a slug flow simulator (SFS) were used.

A single correlation for the bubble-to-bubble interaction is proposed, relating the trailing bubble velocity to the length of the liquid slug ahead of the bubble. Strong bubble interaction was found for liquid slugs shorter than 2D. However, some interaction (though weak) was found for longer liquid slugs (up to 10-12D of column). The shape of the bubble-to-bubble interaction curve showed that bubbles flowing more than 2D apart require a long portion of column to coalesce. This differs from the findings for turbulent regime. In turbulent conditions, bubble interaction occurs for liquid slugs shorter than 8-10D and bubbles flowing within this range are bound to coalesce in a short portion of column.

Flow stability was shown to increase with increasing superficial liquid velocity and with decreasing superficial gas velocity. Good agreement was obtained between experimental undisturbed bubble velocities and correlation-based predictions for laminar regime.

Slug flow simulation was developed based on the bubble-to-bubble interaction correlation obtained. Simulation results showed that bubble coalescence, although not very frequent, occurs at any point along the length of the column (in turbulent regime coalescence occurs mainly in the lower part of the column). Inlet slug length distributions centred on 2-4*D* were found to evolve to similar slug flow patterns within the 6.5 m of the column. An entrance length of 70-100*D* was found for these inlet distributions, for the ranges of superficial gas and liquid velocities studied (0.05-0.2 m/s).

General expressions are proposed to compute the variation of the mode and standard deviation (of log-normal fits) for bubble velocity, bubble length, and liquid slug length, as a function of the vertical coordinate (H) and superficial gas and liquid velocities (U_G, U_L, respectively). These expressions adequately represent the simulation data for the ranges of parameters studied.

Bubble velocity is shown to increase with U_L, U_G and H. Its evolution along the column is mainly the result of the gas phase expansion. Bubble length is shown to increase with U_G and H, as a result of coalescence, gas expansion and flow continuity. The liquid slug length increases along the column and is almost independent of U_G (and, therefore, U_L). Coalescence is shown to be the main effect governing the evolution of this parameter. Unlike in turbulent slug flow (Sotto Mayor et al. (2006b)), no stabilization of h_s occurs within the column length studied (6.5 m).

The outlet standard deviation/mode ratios for bubble velocity, bubble length and liquid slug length are smaller than 14%, about 40% and in the range 70-95%, respectively, for the ranges of superficial gas and liquid velocities studied.

4.8 Appendix – Calculation of Reynolds numbers (in the liquid, in the wake and in the annular film)

All Reynolds numbers are computed after correction of U_G for the experimental/ambient temperature and pressure at the acquisition coordinate (at 3.25 m from the column base).

The Reynolds number in liquid is based on the superficial mixture velocity ($U_M=U_L + U_G$) in a fixed reference frame. Thus, it can be obtained using the following equation:

$$Re_{U_M} = \frac{\rho U_M D}{\mu} \tag{4.5}$$

It is generally assumed that laminar regime in the liquid is obtained for Re_{U_M} smaller than 2100.

The Reynolds number in the near-wake bubble region is based on the downward liquid velocity as seen by the bubble ($V_S = U_B^{exp} - U_L - U_G$), thus, in a moving reference frame. It can be obtained using:

$$Re_{V_S} = \frac{\rho V_S D}{\mu} \tag{4.6}$$

Laminar regime in the near-wake bubble region is obtained for Re_{V_S} smaller than 175 (Pinto et al. (1998)).

The Reynolds number in the annular film is based on the downward liquid velocity in the film around the bubble, in a fixed reference frame, u_δ. The computation of u_δ requires some considerations. In a moving reference frame (attached to the bubble), flow continuity requires consistency between the liquid flow rate in the column cross-sectional area (ahead of a bubble), and the homonymous parameter in the annular cross-sectional area between the bubble interface and the pipe wall. This balance can be expressed by the following equation:

$$\pi R_c^2 V_S = \pi \left[R_c^2 - (R_c - \delta)^2 \right] v_\delta \tag{4.7}$$

where v_δ is computed by:

$$v_\delta = U_B^{exp} + u_\delta \tag{4.8}$$

and πR_c^2 and $\pi \left[R_c^2 - (R_c - \delta)^2 \right]$ are the column and annular film cross-sectional area, respectively. By solving Eq. (4.7) for v_δ one obtains the liquid velocity in the annular film around the bubble, in a moving reference frame (attached to the bubble).

$$v_\delta = \frac{R_c^2 V_S}{\delta(2R_c - \delta)} \tag{4.9}$$

Using Eq. (4.8) one can transform the previous expression to compute the liquid velocity in the annular film, in a fixed reference frame:

$$u_\delta = \frac{R_c^2 \left[U_B^{exp} - (U_L + U_G) \right]}{\delta(2R_c - \delta)} - U_B^{exp} \tag{4.10}$$

The Reynolds number in the annular film can thus be obtained using an expression similar to Eq. (4.5) but using the film thickness (δ) instead of the column diameter (D).

$$Re_{u_\delta} = \frac{\rho u_\delta \delta}{\mu} \tag{4.11}$$

The end of laminar regime in the annular film occurs for Re_{u_δ} in the range 250-400 (Fulford (1964)).

4.9 Notation

Roman symbols

C	empirical coefficient	
D	column internal diameter	[m]
h_b	length of gas bubble	[m]
h_s	length of liquid slug	[m]
H	vertical coordinate along the column	[m]
$L_{slug\ flow}$	entrance length of slug flow	[m]
i	index of bubble / slug	
$n_{dat.}$	number of data used in the nonlinear estimation	[#]
$P_{acq.}$	pressure at the acquisition coordinate	[Pa]
$P_{amb.}$	ambient pressure	[Pa]
r^2	coefficient of determination of fits (=[*SST*-*SSE*]/*SST*)	
R_c	column internal radius	[m]
S_b	bubble cross-sectional area	[m^2]
S_c	column cross-sectional area	[m^2]
SSE	sum of squares of error (sum of squares of residuals)	[m^2] or [m^2/s^2]
$SSE/n_{dat.}$	average sum of squares of error	[m^2] or [m^2/s^2]
SST	total sum of squares (sum of squares about the mean)	[m^2] or [m^2/s^2]
$T_{amb.}$	ambient temperature	[K]
u_δ	liquid velocity in the annular film in a fixed reference frame	[m/s]
U	upward velocity of bubble (U_i^{trail} and U_i^{lead} for the i^{th} trailing and leading bubbles)	[m/s]
U_B	upward bubble velocity (according to Nicklin's equation)	[m/s]
U_B^{exp}	experimental average upward bubble velocity in undisturbed conditions	[m/s]
U_G	superficial gas velocity	[m/s]
U_∞	upward bubble velocity in a stagnant liquid (drift velocity)	[m/s]
U_L	superficial liquid velocity	[m/s]

U_M	superficial mixture velocity (= U_L + U_L)	[m/s]
v_δ	liquid velocity in the annular film in a moving reference frame	[m/s]
V_S	liquid velocity relative to the bubble ($=U_B^{exp} - U_M$)	[m/s]
z	parameter to be fit by nonlinear estimation	[m] or [m/s]
$z_{nose,\,i}$	vertical coordinate of the nose of bubble i, within each image frame	[pixel]
$z_{rear,\,i}$	vertical coordinate of the rear of bubble i, within each image frame	[pixel]

Greek symbols

δ	liquid film thickness	[m]
Δt_i	time interval for complete entrance of slug unit *i*	[s]
σ	standard deviation (of bubble length or bubble velocity)	[m] or [m/s]
μ	liquid viscosity	[Pa s]
ρ	liquid density	[kg/m^3]

Dimensionless groups

Re_{v_δ}	Reynolds number based on the liquid velocity in the annular film in a fixed reference frame ($=\rho v_\delta \delta/\mu$)
Re_{U_M}	Reynolds number based on the mixture velocity ($=\rho U_M D/\mu$)
Re_{V_S}	Reynolds number based on the liquid velocity relative to the bubble ($=\rho V_S D/\mu$)

4.10 Acknowledgments

The authors gratefully acknowledge the financial support of Fundação para Ciência e Tecnologia through project POCTI/EQU/33761/1999 and scholarship SFRH/BD/11105/2002. POCTI (FEDER) also supported this work via CEFT.

4.11 References

Barnea, D. and Taitel, Y., 1993. A model for slug length distribution in gas-liquid slug flow. Int. J. Multiphas. Flow 19(5): 829-838.

Brown, R. A. S., 1965. The mechanics of large gas bubbles in tubes. I - Bubble velocities in stagnant liquids. CJChE 43: 217-223.

Bugg, J. D. and Saad, G. A., 2002. The velocity field around a Taylor bubble rising in a stagnant viscous fluid: numerical and experimental results. Int. J. Multiphas. Flow 28: 791-803.

Campos Guimarães, R. and A. Sarsfield Cabral, J. (1997). Estatística, McGraw-Hill de Portugal Limitada.

Collins, R., De Moraes, F. F., Davidson, J. F. and Harrison, D., 1978. The Motion of Large Gas Bubble Rising Through Liquid Flowing in a Tube. J. Fluid Mech. 28: 97-112.

Davies, R. M. and Taylor, G. I., 1950. The mechanics of large Bubbles rising through extended liquids and through liquids in tubes. Proc. R. Soc. Lond. A 200: 375-392.

Dumitrescu, D. T., 1943. Stromung an Einer Luftblase im Senkrechten Rohr. Z. Angeus. Math. Mec. 23: 139-149.

Fabre, J. and Liné, A., 1992. Modeling of two-phase slug flow. Ann. Rev. Fluid Mech. 24: 21-46.

Fernandes, R. C., Semiat, R. and Dukler, A. E., 1983. Hydrodynamic model for gas-liquid slug flow in vertical tubes. AIChE J. 29(6): 981-989.

Fulford, G. D., 1964. The flow of liquids in thin films. Adv. Chem. Eng. 5: 151-236.

James, M. R., Lane, S. J., Chouet, B. and Gilbert, J. S., 2004. Pressure changes associated with the ascent and bursting of gas slugs in liquid-filled vertical and inclined conduits. J. Volcanol. Geoth. Res. 129(1-3): 61.

Kreutzer, M. T., Du, P., Heiszwolf, J. J., Kapteijn, F. and Moulijn, J. A., 2001. Mass transfer characteristics of three-phase monolith reactors. Chem. Eng. Sci. 56(21-22): 6015-6023.

Kreutzer, M. T., Eijnden, M. G. v. d., Kapteijn, F., Moulijn, J. A. and Heiszwolf, J. J., 2005. The pressure drop experiment to determine slug lengths in multiphase monoliths. Catalysis Today 105(3-4): 667-672.

Mao, Z. S. and Dukler, A. E., 1989. An experimental study of gas-liquid slug flow. Experiments in Fluids (Historical Archive) 8(3 - 4): 169.

Nicklin, D. J., Wilkes, J. O. and Davidson, J. F., 1962. Two-phase flow in vertical tubes. Transactions of the Institution of Chemical Engineers 40: 61-68.

Nogueira, S., Riethmuller, M. L., Campos, B. L. M. and Pinto, A. M. F. R., 2006a. Flow in the nose region and annular film around a Taylor bubble rising through vertical columns of stagnant and flowing Newtonian liquids. Chem. Eng. Sci. 61: 845-857.

Nogueira, S., Riethmuller, M. L., Campos, B. L. M. and Pinto, A. M. F. R., 2006b. Flow patterns in the wake of a Taylor bubble rising through vertical columns of stagnant and flowing Newtonian liquids: an experimental study. Chem. Eng. Sci. 61 (doi: 10.1016/j.ces.2006.08.002): 7199-7212.

Pinto, A. M. F. R., Coelho Pinheiro, M. N. and Campos, J. B. L. M., 2001. On the interaction of Taylor bubbles rising in two-phase co-current slug flow in vertical columns: Turbulent wakes. Exp. Fluids 31(6): 643-652.

Pinto, A. M. F. R., Pinheiro, M. N. C. and Campos, J. B. L. M., 1998. Coalescence of two gas slugs rising in a co-current flowing liquid in vertical tubes. Chem. Eng. Sci. 53(16): 2973-2983.

Sotto Mayor, T., Ferreira, V., Pinto, A. M. F. R. and Campos, J. B. L. M., 2006a. Hydrodynamics of gas-liquid slug flow along vertical pipes in turbulent regime. An experimental study. Submitted to International Journal of Heat and Fluid Flow.

Sotto Mayor, T., Pinto, A. M. F. R. and Campos, J. B. L. M., 2006b. Hydrodynamics of gas-liquid slug flow along vertical pipes in turbulent regime. A simulation study. Submitted to Chemical Engineering Research and Design.

Sousa, R. G., Riethmuller, M. L., Campos, B. L. M. and Pinto, A. M. F. R., 2005. Flow around individual Taylor bubbles rising in stagnant CMC solutions: PIV measurements. Chem. Eng. Sci. 60: 1859-1873.

Sousa, R. G., Riethmuller, M. L., Campos, B. L. M. and Pinto, A. M. F. R., 2006. Flow around individual Taylor bubbles rising in stagnant polyacrylamide (PAA) solutions. Journal of Non-Newtonian Fluid Mechanics 135: 16-31.

The MathWorks, I. (2002). Help files of "MATLAB: the language of technical computing".

Thulasidas, T. C., Abraham, M. A. and Cerro, R. L., 1997. Flow patterns in liquid slugs during bubble-train flow inside capillaries. Chem. Eng. Sci. 52(17): 2947-2962.

Thulasidas, T. C., Abraham, M. A. and Cerro, R. L., 1999. Dispersion during bubble-train flow in capillaries. Chem. Eng. Sci. 54(1): 61-76.

van Baten, J. M. and Krishna, R., 2004. CFD simulations of mass transfer from Taylor bubbles rising in circular capillaries. Chem. Eng. Sci. 59: 2535-2545.

Van Hout, R., Barnea, D. and Shemer, L., 2001. Evolution of statistical parameters of gas-liquid slug flow along vertical pipes. Int. J. Multiphas. Flow 27(9): 1579-1602.

Van Hout, R., Gulitski, A., Barnea, D. and Shemer, L., 2002. Experimental investigation of the velocity field induced by a Taylor bubble rising in stagnant water. Int. J. Multiphas. Flow 28(4): 579-596.

Vandu, C. O., Liu, H. and Krishna, R., 2005. Mass transfer from Taylor bubbles rising in single capillaries. Chem. Eng. Sci. 60: 6430-6437.

Wallis, G. B. (1969). One dimensional two-phase flow. New York, McGraw Hill Book Co.

White, E. T. and Beardmore, R. H., 1962. The velocity of single cylindrical air bubbles through liquids contained in vertical tubes. Chem. Eng. Sci. 17: 351-361.

5 Vertical slug flow in laminar regime in the liquid and turbulent regime in the bubble wake – Comparison with fully turbulent and fully laminar regimes[5]

5.1 Abstract

An experimental and simulation study on free bubbling vertical slug flow in laminar regime in the main liquid and turbulent regime in the near-wake bubble region is reported. A non-intrusive image analysis technique and a previously developed slug flow simulator (SFS) were used. Two aqueous glycerol solutions (0.012-0.013 Pa s and 0.022 Pa s) were studied. A single bubble-to-bubble interaction curve was obtained. Strong interaction was found for bubbles flowing less than 3-4*D* apart, with slight interaction persisting for longer distances. The shape of the interaction curve bridges those for fully turbulent and fully laminar regimes. The experimental average bubble velocity in undisturbed conditions was shown not to follow the correlation-based predictions for laminar regime in the liquid. Alternative fitting coefficients are proposed. An entrance length of 50-80*D* (or 90-170*D*) was obtained for normal inlet slug length distributions centred on 2-5*D* (or 2-6*D*), for superficial gas and liquid velocities up to 0.40 m/s and 0.30 m/s, respectively. More contrasting inlet slug length distributions were found not to converge within the length of the column (6.5 m). An overall comparison between the three regimes is presented.

[5] Based on the paper by T. Sotto Mayor, A.M.F.R. Pinto and J.B.L.M. Campos, submitted to AIChE Journal

5.2 Introduction

Gas and liquid flowing through a pipe display several temporal and spatial characteristics/distributions that are often referred to as flow patterns. Examples of patterns occurring for increasing ratios of gas/liquid flow rates are bubbly, slug, churn and annular flows. This paper concerns slug flow pattern, in particular vertical slug flow. Among the several industrial applications encompassing slug flow there are (Fabre and Liné (1992)): hydrocarbon production and transportation, geothermal power plants and air-lifts, nuclear and chemical reactors. Furthermore, natural volcanic phenomena [e.g. Stromboli volcano (James et al. (2004))] can also be mentioned.

Intermittent, random and irregular are adjectives often applied while describing slug flow. It addresses the flow of large (Taylor) bubbles separated by liquid plugs/slugs with more or less aerated nature. These large bubbles fill almost completely the pipe cross-sectional area and force the liquid phase to flow around them in a thin annular film. The thickness of this film decreases until a balance between gravitational and shear forces is found. At the rear of the bubbles, the expansion of the annular film creates a more or less confined region known as the bubble wake. From closed well-defined recirculation (laminar wake) to open chaotic-like eddies (turbulent wake), several scenarios can occur depending on gas and liquid flow rates, fluid properties and column diameter.

The passage of a Taylor bubble disrupts the velocity profile in the flowing liquid. The length of column (reference attached to the bubble), after bubble passage, required for full recovery of the previously existent velocity profile is controlled by the nature and characteristics of the bubble wake region. Moreover, the dynamics in this region and on the liquid below determine the eventual interaction between consecutive bubbles which lead ultimately to coalescence.

The research on slug flow dates back to the early 1940s with the works of Dumitrescu (1943) and Davies and Taylor (1950) regarding the motion of single Taylor bubbles in stagnant liquid, later spanned to flowing liquid conditions by Nicklin et al. (1962). But other works such as those of White and Beardmore (1962), Collins et al. (1978), Fernandes et al. (1983), Mao and Dukler (1989) and Fabre and Liné (1992) should also be highlighted for their contributions for the understanding of fundamentals of slug flow pattern.

The successful design, optimization and operation of industrial applications incorporating slug flow pattern depends on the capacity to adequately simulate and predict flow characteristics for any given operating conditions. To that end, it is crucial to gather experimental data for all flow regimes and to develop ever more accurate models and simulators of slug flow.

Several experimental and simulation studies for continuous co-current turbulent slug flow can be found in the literature. For instance the works of Barnea and Taitel (1993), Pinto et al. (2001), Van Hout et al. (2001), Van Hout et al. (2003) and Sotto Mayor et al. (2006a), Sotto Mayor et al. (2006c) provide an interesting insight into the hydrodynamics of slug flow in turbulent regime. More recently, Sotto Mayor et al. (2006b) reported an experimental and simulation study regarding laminar flow conditions, which extended the information on the topic for flow conditions often occurring in industrial applications, namely those implying the use of viscous fluids. The ranges of Reynolds numbers covered in that study are, however, relatively narrow (up to 160 in the main liquid and 200 in the near-wake bubble region). In addition, as gas/liquid flow rate increases (and/or liquid viscosity decreases) a complex mix scenario occurs, for which laminar regime in the main liquid and turbulent regime in the near-wake bubble region, are expected. Besides causing difficulties in accurately predicting bubble velocities (as stressed by Pinto et al. (2005)), the mentioned scenario was, to the best of our knowledge, only (briefly) reported in the study of Pinto et al. (2001) and, therefore, very few information exists regarding the extent of the interaction between consecutive bubbles, frequency of coalescence along the column, flow characteristics, etc.. There is thus a clear need for input on this topic.

This investigation proposes to extend the experimental and simulation studies from the fully turbulent (Sotto Mayor et al. (2006a), Sotto Mayor et al. (2006c)) and fully laminar (Sotto Mayor et al. (2006b)) regimes to the mentioned mix scenario, so as to provide information on the flow characteristics of that scenario and to allow an overall comparison of the hydrodynamics of the three regimes/scenarios. Such approach aims favouring a comprehensive understanding of the continuous co-current slug flow pattern.

5.3 Experimental set-up

The experimental apparatus of Sotto Mayor et al. (2006a), Sotto Mayor et al. (2006b) was used in the present study (see Figure 5.1). Experiments were performed in an acrylic vertical pipe 6.5 m long with internal diameter of 0.032 m. Two different aqueous glycerol solutions were utilised as flowing mediums (61-62 wt%, $\mu\approx$0.012-0.013 Pa s, $\rho\approx$1113-1114 kg/m^3 and 69 wt%, $\mu\approx$0.022 Pa s, $\rho\approx$1131 kg/m^3). The study covered superficial liquid velocities up to 0.29 m/s. The liquid temperature was monitored continuously during the experiments by thermocouples placed inside the tank and at the column inlet. The temperatures at these two locations differed less than 0.5 °C for every experiment performed. A Brookfield rotating viscometer was used to measure the viscosity of the aqueous glycerol solutions at the experimental temperatures. A 0.003 m internal diameter injector was employed to feed air from a pressured line

to the column. The air flow rate was measured by calibrated rotameters at superficial velocities up to 0.37 m/s (at 1 bar and 20°C). A Canon digital video camcorder operating at 25 Hz (exposure times: 1/4000s-1/8000s) was chosen to capture images of the flow pattern at 3.25 m from the base of the column (acquisition coordinate). Image distortion was minimized by the use of a rectangular transparent acrylic box (filled with the liquid medium) surrounding the column test-section. Images of 0.29-0.47 m of column were captured in the camera field of view.

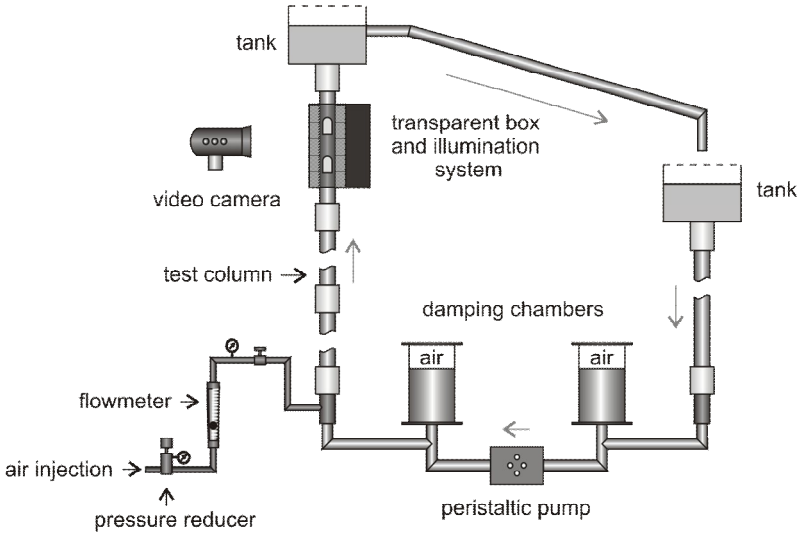

Figure 5.1 – Schematic representation of the experimental facility

5.4 Video processing

Each video was decomposed in a set of sequential frames to be analysed by image analysis routines (Sotto Mayor et al. (2006d)). The goal was to track bubbles in each frame in order to gather information about their characteristics and relative motion. A series of operations (e.g. filtering, enhancement, erosion) was implemented over each frame, and a threshold length of 0.5*D* was used in order to distinguish between Taylor bubbles and small bubbles in the liquid slugs. The bubble nose boundaries were retrieved in this way and the bubble rear boundaries (difficult to track due to the oscillations of the bubble wake and the aeration level of liquid slugs) were obtained by tracking the lowest pixel of the central area of each bubble (the lighter region). This latter strategy enables a more accurate estimation of the positioning of the bubble rear boundaries which results, ultimately, in more reliable bubble length and slug length data.

Two different approaches (Sotto Mayor et al. (2006a)) were pursued while processing the bubble data: moving-point data analysis and fixed-point data analysis. Moving-point data analysis allows the establishing of an empirical bubble-to-bubble interaction curve (informing on the variation of the trailing bubble velocity with the distance between bubbles) which regulates the coalescence of consecutive bubbles. Fixed-point data analysis focuses on the bubble

characteristics (length, velocity, distance) at a given vertical coordinate. The first approach provides an empirical relation crucial for the simulation of the slug flow pattern (the bubble-to-bubble interaction curve) whereas the second informs on the flow characteristics (distribution of parameters) and also provides a frame for the validation of the simulation code. The following section describes the data obtained.

5.5 Experimental data

Two different aqueous glycerol aqueous solutions were studied for superficial liquid and gas velocities (U_L and U_G) in the ranges 0.038-0.29 m/s and 0.11-0.37 m/s, respectively. Throughout the whole chapter and unless told otherwise, the values of U_G are given after correction for ambient conditions (pressure-wise and temperature-wise). The superficial velocities and the solution compositions were designed to have laminar regime in the main liquid between bubbles and turbulent regime in the near-wake bubble region (see Figure 5.2 for details.). The flow regime in the main liquid is assessed through the values of the Reynolds number based on the superficial mixture velocity ($U_M = U_L + U_G$). Laminar regime in the main liquid is assumed for $Re_{U_M} < 2100$. The flow regime in the near-wake bubble region is assessed computing the Reynolds number based on the liquid velocity as seen by the bubble ($V_S = U_B^{exp} - U_L - U_G$, where U_B^{exp} stands for the experimental average upward bubble velocity in undisturbed conditions). Following the work of Pinto et al. (1998), the regime in the near-wake bubble region is assumed turbulent for $Re_{V_S} > 525$. The properties of the solutions, the superficial velocities and the relevant Reynolds numbers are given in Table 5.1, for each experiment performed. The following sections describe the outcome of the flow analysis performed following the mentioned moving-point and fixed-point approaches.

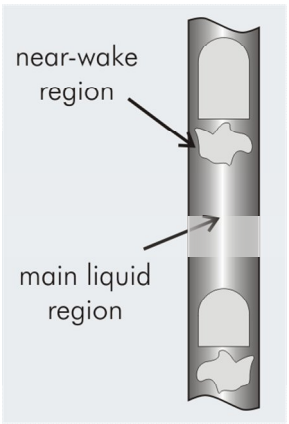

Figure 5.2 – Flow regions in the definition of the Reynolds number (in the near-wake and in the main liquid)

Table 5.1 – Physical properties of the aqueous glycerol solutions, superficial liquid and gas velocities and Reynolds numbers in the main liquid and in the near-wake region for several experiments (Reynolds numbers based on U_B^{exp} and U_G corrected for the pressure at the acquisition location)

							Reynolds number	
					($T_{amb.}$, $P_{amb.}$)	($T_{amb.}$, $P_{acq.}$)	liquid	wake
	m/m [weight %]	μ x 10^3 [Pa s]	ρ [kg/m^3]	U_L [m/s]	U_G [m/s]	U_G [m/s]	Re_{U_M}	Re_{V_S}
a	62.1	12.7	1114	0.038	0.115	0.088	355	842
b	"	12.7	1114	0.038	0.183	0.141	502	937
c	60.8	11.6	1113	0.103	0.184	0.141	749	1021
d	"	11.6	1113	0.199	0.184	0.141	1045	1053
e	"	11.6	1113	0.195	0.368	0.283	1470	1290
f	69.4	22.0	1131	0.103	0.185	0.142	402	569
g	"	22.0	1131	0.196	0.114	0.087	465	581
h	"	22.0	1131	0.196	0.181	0.139	550	606
i	"	22.0	1131	0.196	0.368	0.282	786	714
j	"	22.0	1131	0.292	0.185	0.142	714	638

5.5.1 Moving-point data analysis

Moving-point data analysis was performed, for each experiment, over a considerable number of frames (2000-8000), each containing more than one Taylor bubble. This procedure allowed gathering a vast amount of data on the relative motion of consecutive bubbles (in terms of bubble velocity and distance). By focusing on the variation of the trailing bubble velocity with the length of the liquid slug flowing ahead, information on coalescence events was compiled. In Figure 5.3a, the velocities of the leading and trailing bubbles are plotted against the liquid slug length for most operating conditions shown in Table 5.1. Condition *e* was not considered in the representation since the stronger lens magnification used while capturing the corresponding video, a requirement due to the higher agitation of the flow (see Reynolds numbers in Table 5.1 and snapshots of Figure 5.4), resulted in a reduced number of frames containing more than one Taylor bubble. For the purpose of generalization, bubble velocities are normalised by the experimental average upward bubble velocity in undisturbed conditions, U_B^{exp}, and the liquid slug length is normalised by the column internal diameter, *D*.

The velocities of the trailing bubbles increase for decreasing liquid slug lengths, for all operating conditions studied. Moreover, the trailing bubble acceleration is more pronounced for liquid slugs shorter than 3*D*. In addition, this behaviour appears to be independent of the superficial liquid and gas velocities and of the solution properties (for the ranges studied). For this reason, a single bubble-to-bubble interaction curve was established by averaging the normalised

trailing bubble velocities of Figure 5.3a, for each slug length class (0.3*D* wide). Figure 5.3b shows the resulting smoother curve together with the best-fit (empirical) equation:

$$\frac{U_i^{trail}}{U_B^{exp}} = 1 + 0.916e^{-\left(\frac{h_{s,i-1}-0.811}{0.775}\right)} + 0.02e^{-\left(\frac{h_{s,i-1}-0.811}{14.574}\right)} \quad (5.1)$$

where U_i^{trail} refers to the velocity of the trailing bubble *i* flowing behind a liquid slug with normalised length $h_{s,i-1}$ (bubbles and slugs numbered from top to bottom).

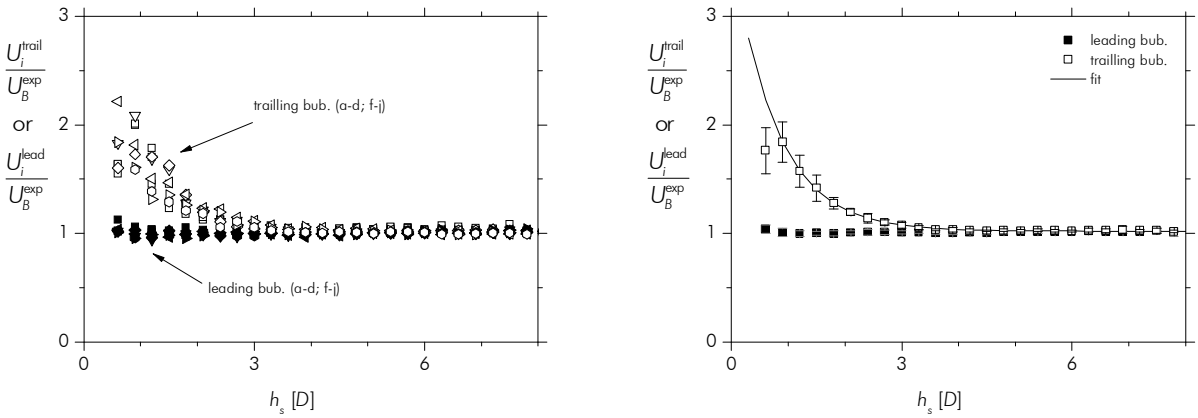

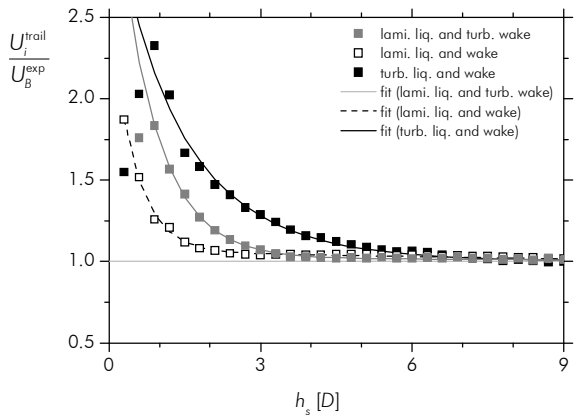

Figure 5.3 – (a) Bubble-to-bubble interaction curve for several experiments; (b) average bubble-to-bubble interaction curve with 95% confidence intervals; (c) bubble-to-bubble interaction curve for turbulent regime in liquid and wake (after Sotto Mayor et al. (2006a)), laminar regime in liquid and wake (after Sotto Mayor et al. (2006b)) and laminar regime in liquid and turbulent regime in wake (present data)

A close analysis of the average interaction curve (Eq. (5.1)) indicates 3–4*D* as the threshold slug length range for strong bubble-to-bubble interaction (in this range, the trailing bubbles rise between 7% and 3% faster than an undisturbed bubble). In addition, a slight bubble-to-bubble

interaction persists for liquid slugs longer than 4*D* (for $h_s \approx 5D$, 7*D* and 10*D* the trailing bubbles ride about 1.9%, 1.3% and 1% faster than undisturbed bubbles).

Sotto Mayor et al. (2006a) and Sotto Mayor et al. (2006b) report studies on turbulent and laminar regime (both in the main liquid and in the near-wake bubble region), whose main findings regarding the bubble-to-bubble interaction are compared with the present data (laminar regime in the main liquid and turbulent regime in the near-wake region) in Figure 5.3c. The curves for the three scenarios are very different. The interaction curve for turbulent regime (Sotto Mayor et al. (2006a)) indicates bubble interaction for liquid slugs shorter than 8-10*D*. In laminar regime (Sotto Mayor et al. (2006b)), bubble interaction occurs mainly for liquid slugs shorter than 2*D*, with some interaction persisting for longer distances (at $h_s \approx 10D$, trailing bubbles still ride about 1% faster than undisturbed bubbles). The present data show a bubble-to-bubble interaction behaviour somewhat in the middle of the two aforementioned scenarios (interaction mainly for liquid slugs shorter than 3-4*D* and slight interaction for longer liquid slugs). In addition and quite like the turbulent scenario (Sotto Mayor et al. (2006a)), a slight decrease in the velocity of the trailing bubble can be observed for very short liquid slugs ($h_s < 1D$). This behaviour may be related to the dynamics in the main vortex of the bubble wake region, which extends to about 1-2*D* (Van Hout et al. (2002a), Sotiriadis and Thorpe (2005)).

The differences in the bubble-to-bubble interaction curves of the three scenarios indicate different degrees of coalescence, for a given column length. Experiments in turbulent regime are associated with the higher number of coalescences, in particular in the lower section of the column (above which most bubbles flow too apart to allow for bubble coalescence in the remaining column length). In opposition, experiments in laminar regime feature less coalescences, although spread along the whole column length (bubbles flowing more than 2*D* apart require a long portion of column to coalesce). Experiments in the mix scenario (laminar regime in the main liquid and turbulent regime in the near-wake region) bridge the previous two outcomes. More details on the coalescence occurrence for these three scenarios can be found in section 5.6.3, focussing simulation results.

5.5.2 Fixed-point data analysis

Between 1400 and 2000 bubbles were scrutinised by fixed-point data analysis, for each operating condition. The idea was to compile a vast amount of data on bubble characteristics (length, velocity and distance) at a given vertical coordinate (3.25 m from the base of the column) in order to allow the characterisation of the flow pattern at that location. Besides assuring laminar regime in the main liquid and turbulent regime in the near-wake bubble region, U_L and U_G were

chosen to allow a straightforward analysis of the influence of those parameters over the flow pattern characteristics (see Table 5.1). For that purpose, conditions b-d, regarding the less viscous solution (0.012-0.013 Pa s), feature increasing U_L for constant U_G whereas conditions g-i, regarding the more viscous solution (0.022 Pa s), feature increasing U_G for constant U_L. Notice in Figure 5.4 the high aeration level of the liquid slugs, in particular for the experiments with the less viscous solution (conditions a-e). The influence of some parameters over the flow pattern characteristics is discussed in the following sections.

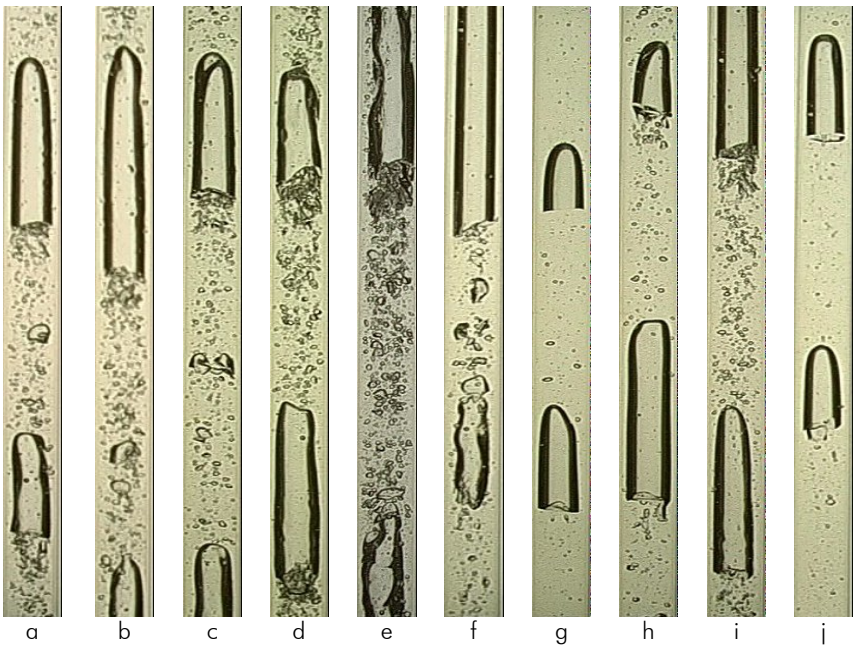

Figure 5.4 – Snapshots of the flow pattern for different superficial liquid and gas velocities (operating conditions as in Table 5.1)

5.5.2.1 Superficial liquid velocity (U_L)

Three experiments with increasing U_L and similar U_G are compared in this section. Conditions b-d (Table 5.1), regarding the less viscous solution, are addressed. The comparison focuses on the frequency distribution curves of the main bubble characteristics (velocity, length and distance) and on the corresponding log-normal fit parameters (average, mode and the standard deviation). These data are shown in Figure 5.5 and Figure 5.6, respectively.

As expected, the most probable (mode) and average values of the bubble velocity distributions increase with U_L (Figure 5.5a-c and Figure 5.6a). The modes and averages of the distributions of bubble length (h_b) and liquid slug length (h_s) decrease with increasing U_L (Figure 5.5d-f, Figure 5.5g-i and Figure 5.6a). These latter variations must be ascribed to the less frequent coalescence occurring for increasing U_L. Notice that by flow continuity an increase in U_L (for constant U_G) favours the formation of shorter bubbles and longer liquid slugs. This means for

instance that, from conditions b to d (Table 5.1), one must expect an inlet positive-slope trend for h_s (when h_s is plotted against U_L). In addition, this inlet trend in h_s implies a decrease in the number of coalescences occurring along a given column length (when bubbles enter the column at higher distances they are bound to coalesce less). However, a decrease in coalescence brings about a decrease in the average bubble length and liquid slug length. There is thus a competition between two effects: the inlet slope effect (which implies a decrease in h_b and an increase in h_s) and the coalescence effect (which implies a decrease in both variables).

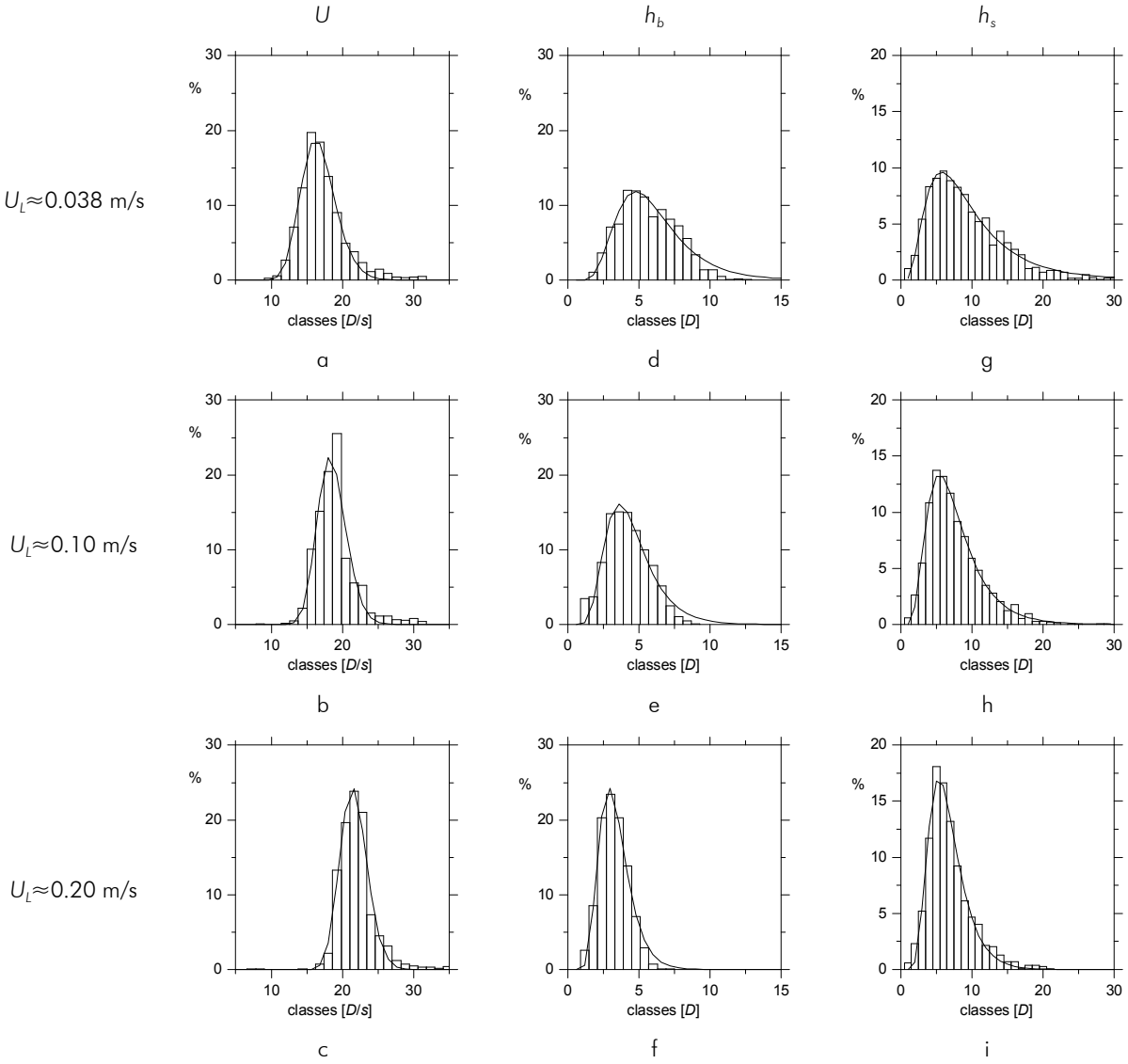

Figure 5.5 – Frequency distribution curves and log-normal fits for experiments with U_L≈0.038, 0.10 and 0.20 m/s; U_G≈0.18 m/s; aqueous glycerol solution: 61-62 wt% (μ≈0.012-0.013 Pa s); vertical coordinate: 3.25 m

The charts of Figure 5.5 and Figure 5.6 indicate that the coalescence effect is dominant in the variation of h_b and h_s with U_L. Indeed, at 3.25 m from the base of the column, both variables decrease slightly with increasing U_L. Notice that similar predominance of the coalescence effect

over the inlet slope effect has been reported for studies regarding turbulent (Sotto Mayor et al. (2006a)) and laminar (Sotto Mayor et al. (2006b)) scenarios.

The standard deviation of the log-normal fits of U, h_b and h_s decrease with increasing U_L (Figure 5.5a-c, Figure 5.5d-f, Figure 5.5g-i; Figure 5.6b). This variation indicates that flow pattern stabilises for increasing U_L. Similar observations are reported for fully turbulent (Sotto Mayor et al. (2006a)) and fully laminar (Sotto Mayor et al. (2006b)) scenarios.

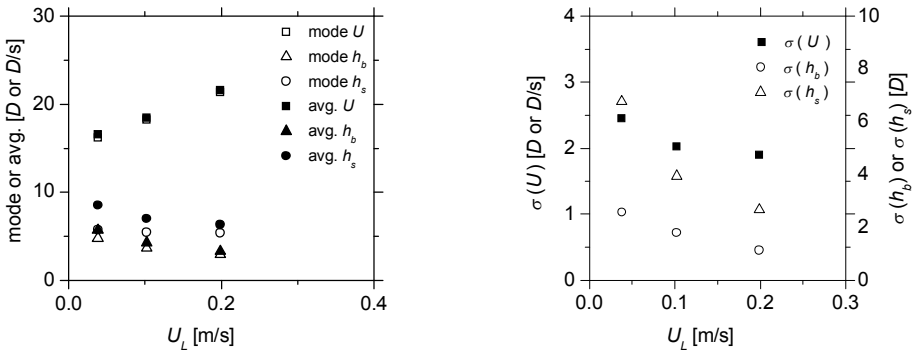

a b

Figure 5.6 – Log-normal fit parameters: (a) average and mode, and (b) standard deviation for experiments with $U_L \approx 0.038$, 0.10 and 0.20 m/s; $U_G \approx 0.18$ m/s; aqueous glycerol solution: 61-62 wt% ($\mu \approx 0.012$-0.013 Pa s); vertical coordinate: 3.25 m

5.5.2.2 Superficial gas velocity (U_G)

This section addresses conditions g-i of Table 5.1, i.e. experiments with increasing U_G for constant U_L, regarding the more viscous solution. The comparison focuses, as before, on the frequency distribution curves of the main bubble characteristics (Figure 5.7) and the corresponding log-normal fit parameters (Figure 5.8).

The mode and average values of the distributions of bubble velocity and bubble length increase for increasing U_G (Figure 5.8a). In addition, the homonymous parameters for the liquid slug length show almost no variation with U_G. Notice that the variations of h_b and h_s with U_G are, as discussed previously for increasing U_L, the result of two competing effects: the inlet slope effect and the coalescence effect. Recall that the inlet slope effect (consequence of flow continuity) implies that longer bubbles and shorter slugs result from increasing U_G while maintaining U_L. However, because shorter slugs indicate an escalation in the coalescence occurrence (bubbles entering the column at shorter distances are bound to coalesce more, for a given column length) an increase in both h_b and h_s is to be expected due to the more frequent coalescence. There are, thus, two different effects to be considered (inlet trend and coalescence). While both effects point towards an increase of h_b with U_G, the overall variation of h_s is the result of the competition

between both effects. The fact that the average liquid slug length appears to be independent of U_G (Figure 5.8) is an indicator that the influence of these opposing effects over the variation of this parameter is similar (hence both effects compensate).

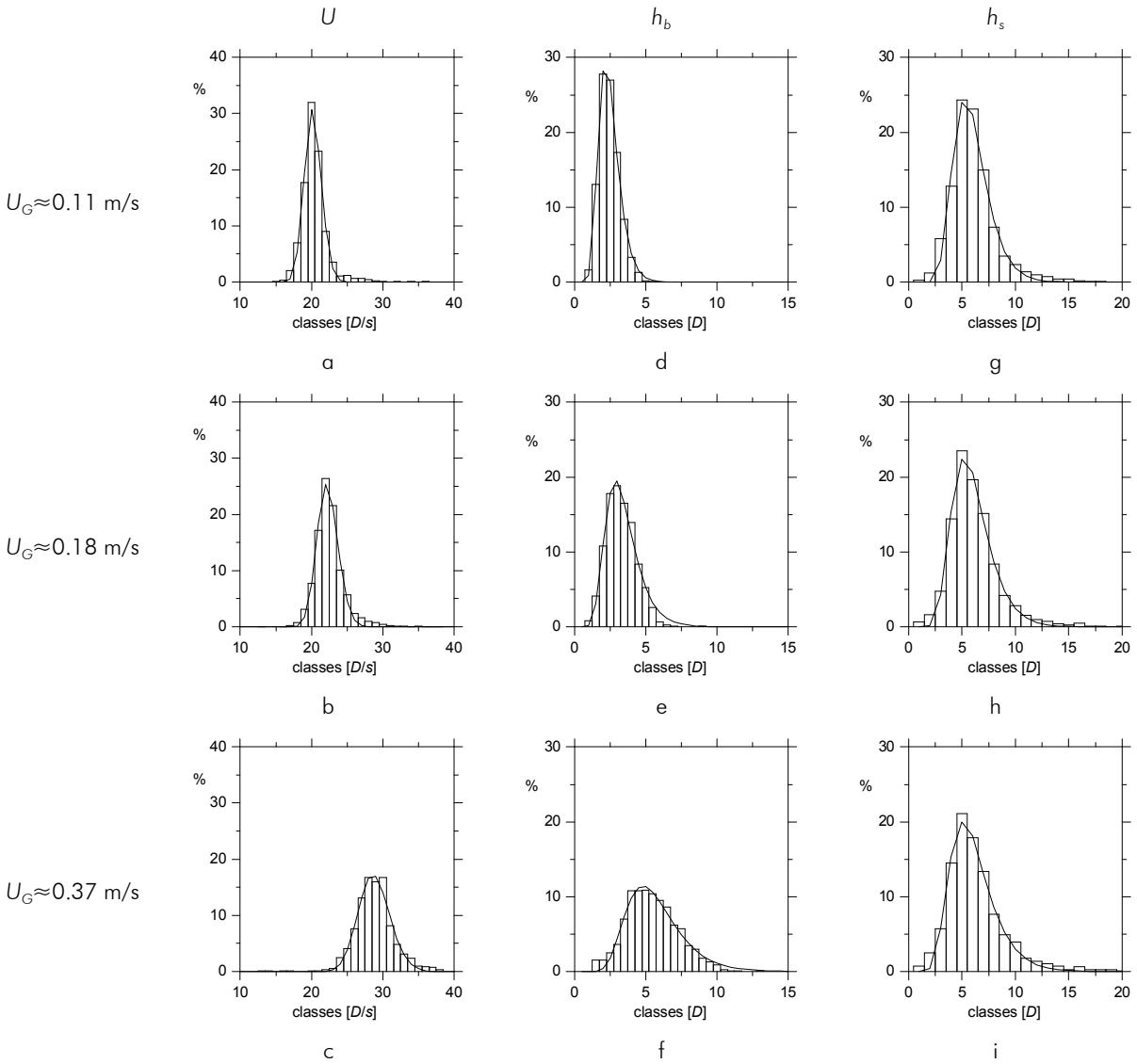

Figure 5.7 – Frequency distribution curves and log-normal fits for experiments with U_L≈0.20 m/s and U_G≈0.11, 0.18 and 0.37 m/s; aqueous glycerol solution: 69 wt% (μ≈0.022 Pa s); vertical coordinate: 3.25 m

The standard deviation of the log-normal fits of all parameters escalates with increasing U_G (Figure 5.8b). All frequency distribution curves become, thus, wider for increasing U_G, which indicates a less stabilised flow pattern. The snapshots of the flow pattern (Figure 5.4g-i) corroborate this observation. Similar observations are reported for fully turbulent (Sotto Mayor et al. (2006a)) and fully laminar (Sotto Mayor et al. (2006b)) scenarios.

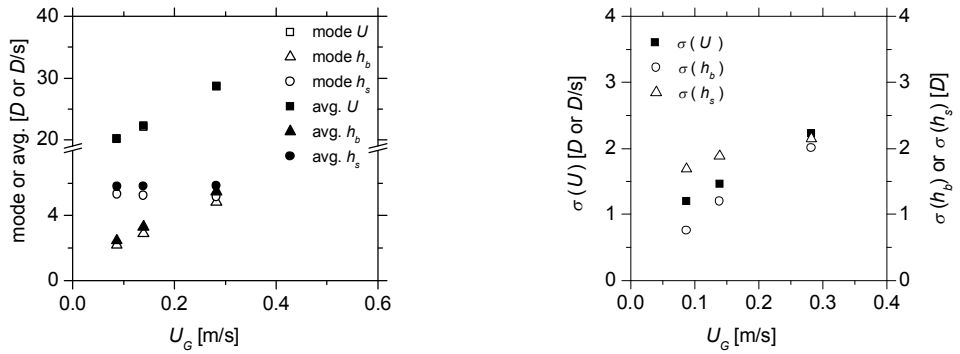

a b

Figure 5.8 – Log-normal fit parameters: (a) average and mode, and (b) standard deviation for experiments with U_L≈0.20 m/s and U_G≈0.11, 0.18 and 0.37 m/s; aqueous glycerol solution: 69 wt% (μ≈0.022 Pa s); vertical coordinate: 3.25 m

5.5.2.3 Viscosity of the solution (μ)

Three sets of experimental conditions can be compared in order to assess the influence of the solution viscosity over the main bubble characteristics. Conditions c and f, d and h and, finally, e and i, have similar values of U_L and U_G in order to allow their direct comparison (see Table 5.1). The frequency distribution curves of U, h_b and h_s regarding the last pair of conditions (e and i) are shown in Figure 5.9. As perceived in the figure, all distribution curves are quite similar for both aqueous glycerol solutions. Notice that similar conclusions would be drawn if focussing on the remaining pairs of conditions (c and f, d and h). This indicates that for the ranges of U_L and U_G studied, the main bubble characteristics do not depend on the viscosity of the solution.

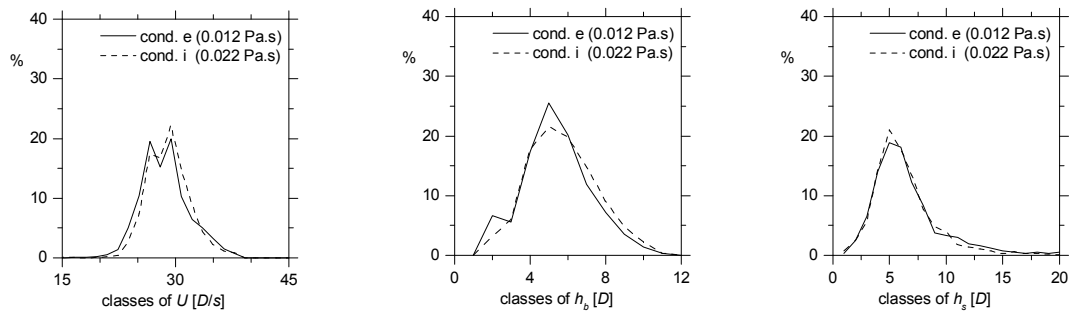

a b c

Figure 5.9 – Frequency distribution curves of: (a) bubble velocity, (b) bubble length and (c) slug length, for experiments with different aqueous glycerol solutions; U_L≈0.20 m/s and U_G≈0.37 m/s (conditions e and i)

5.5.3 Experimental values of C and drift velocity

The experimental average bubble velocity in undisturbed conditions (U_B^{exp}) is a parameter of significant importance for the characterization, modelling and simulation of slug flow pattern. Its

computation must be achieved considering velocity data based on undisturbed bubbles, i.e. bubbles whose velocity is not affected by the eventual proximity of preceding bubbles. Valuable information has been drawn from the moving-point data analysis (section 5.5.1) regarding the dependence of the trailing bubble velocity on the length of the liquid slug between bubbles. As discussed in section 5.5.1, a trailing bubble flowing after a 7*D* long liquid slug rises about 1.3% faster than an undisturbed bubble (see Eq. (5.1)). Despite the resulting slight overestimation in the computation of U_B^{exp}, 7*D* was used as threshold slug length for undisturbed conditions. The choice for this value resulted from a balance between representativity and accuracy of the U_B^{exp} estimates. The minimum 7*D* slug length requirement resulted in U_B^{exp} estimates based on ensembles of 300-800 bubbles for each experimental condition, figures assuring that the increased representativity clearly makes up for the slight drawback in accuracy.

In Figure 5.10, the estimates of U_B^{exp} are plotted against the average superficial velocity of the mixture (U_M) after correction for the pressure at the acquisition coordinate. A linear fit of the data and correlation-based predictions of U_B for laminar and turbulent regime in the main liquid are also shown in the figure. Recall that U_B can be computed following Nicklin et al. (1962) as:

$$U_B = U_\infty + C(U_L + U_G) \tag{5.2}$$

where U_∞, the drift velocity, is calculated as $0.35\sqrt{gD}$ (following Wallis (1969)) and C is an empirical parameter depending on the flow regime in the main liquid. Parameter C, usually taken equal to the ratio between the maximum liquid velocity (at the axis) and the average liquid velocity, ranges from 1.2 for turbulent regime (Nicklin et al. (1962), Collins et al. (1978), Sotto Mayor et al. (2006a)) to approximately 2 for laminar regime (a parabolic velocity profile; Nicklin et al. (1962), Collins et al. (1978), Sotto Mayor et al. (2006b)).

Despite the Reynolds numbers in Table 5.1 suggesting laminar regime in main liquid, the representation of U_B^{exp} versus U_M (Figure 5.10) does not follow the correlation-based predictions for laminar regime. The experimental C obtained (1.34, equal to the slope of the linear fit) is considerably smaller than the typical C for laminar regime (2), and, thus, the values of U_B^{exp} are smaller than predicted. This can be ascribed to the following. Given that the flow regime in the near-wake bubble region is turbulent (see section 5.5), the velocity profiles in the liquid emerging from this region are relatively flat. Further, the length of column required for the full development of a laminar velocity profile (starting from a flat profile) is a function of the corresponding Reynolds number. The constant of proportionality is variously quoted as 0.028 (experimental, Govier and Aziz (1972)) and 0.06 (theoretical, White (1999)). For the experiments reported here ($355 < Re_{U_M} < 1470$; Table 5.1), one obtains column lengths (for full development of the profile) of

about 10-40*D* or 20-90*D*, respectively. Judging by the frequency distribution curves of Figure 5.5g-i and Figure 5.7g-i, most of the Taylor bubbles upon which the computation of U_B^{exp} was based, rose behind liquid slugs much shorter than these ranges. Therefore, it is reasonable to assume that the velocity profiles ahead of these bubbles were not fully developed and, consequently, the bubble velocities (and hence U_B^{exp}) were lower than those for a fully developed laminar profile. From a different perspective, it is plausible that the liquid slugs in co-current continuous slug flow (with turbulent wakes) are, most of time, not long enough to allow the full development of the laminar velocity profile in the liquid between bubbles. Instead, the average velocity profile in the liquid lies somewhere in between the turbulent and the laminar regime profiles. As a consequence, the estimates of U_B^{exp} (and of *C*) are smaller than predicted. This reasoning is in agreement with the findings of Pinto et al. (2001). Note, however, that when the flow regime in the near-wake bubble region is laminar (as in the study of Sotto Mayor et al. (2006b)), the velocity profiles in the liquid emerging from the wakes are less flat (than for the turbulent-wake scenario discussed here) and, thus, the length of column required for the full re-establishment of a laminar profile in the liquid is considerably shorter. As a consequence, the estimates of U_B^{exp} and *C*, for co-current continuous operation (with laminar wakes), follow the correlations in the literature (i.e. $C \approx 1.93$ as in Sotto Mayor et al. (2006b)).

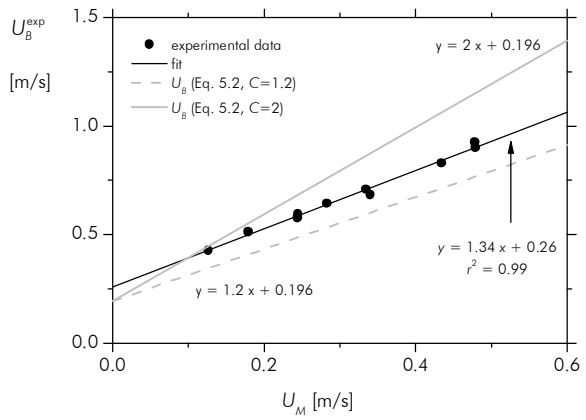

Figure 5.10 – Experimental average upward bubble velocity in undisturbed conditions plotted against U_M; aqueous glycerol solutions 61-62 wt% (0.012-0.013 Pa s) and 69 wt% (0.022 Pa s); U_M corrected for pressure at vertical coordinate 3.25 m

The experimental drift velocity obtained (0.26 m/s) is about 30% higher than the correlation-based predictions (0.196 m/s; Wallis (1969)). This discrepancy must be ascribed to the level of aeration of the liquid slugs. The trailing bubbles can catch up some of the slower small bubbles dispersed in the liquid slugs and merge/coalesce with them. This results ultimately in the

increase of the drift velocity. An interesting study by Van Hout et al. (2002b) on this issue provides support for this reasoning.

The experimental values of C and U_∞ obtained were used in the slug flow simulator to estimate the experimental average upward bubble velocity in undisturbed conditions, for any given superficial mixture velocity.

5.6 Slug flow simulation

A slug flow simulation code (SFS; Sotto Mayor et al. (2006c), Sotto Mayor et al. (2006e)) was used in the simulation study. The main assumptions of the simulation approach are discussed in this section.

In the simulation, a given number of non-aerated liquid slugs and Taylor bubbles are assumed to enter the column at its base. The liquid slug lengths ($h_{s,i}$), normally distributed around a given average, constitute one of the independent distributions. The other is the distribution of the superficial gas velocities ($U_{G,i}$), with a different value for each slug unit cell (i.e. slug + bubble). These distributions, defined using the Box Muller algorithm (Campos Guimarães and A. Sarsfield Cabral (1997)), are then used to prepare the distribution of bubble lengths (the dependent distribution). The closure law for this calculation is:

$$h_{b,i} = \frac{h_{s,i}}{\frac{S_b U_B^{\exp}}{S_c U_{G,i}} - 1} \tag{5.3}$$

where S_b and S_c are the bubble and the column cross-sectional area, respectively. The estimate of S_b is computed assuming a cylindrical bubble shape and a liquid film thickness determined following Brown (1965) for free-falling conditions. Eq. (5.3) was obtained by combining the following equations, at the column inlet:

$$U_{G,i} S_c \Delta t_i = S_b h_{b,i} \tag{5.4}$$

and

$$U_B^{\exp} \Delta t_i = h_{b,i} + h_{s,i} \tag{5.5}$$

where Δt_i is the time interval required for the entrance in the column of the slug unit cell and $h_{b,i}$ is length of bubble i. The estimates of $U_B^{\exp}$ (computed by Eq. (5.2) with experimental values of C and

U_∞) are used in Eq. (5.5) since, at the column inlet, bubbles are assumed to rise at their undisturbed velocity.

The relation (5.3) assures that the distributions of slug length and bubble length introduced in the column produce at the inlet coordinate a given average U_L and U_G (both inputs to the simulator). Moreover, there is a twofold advantage in the use of distributed variables at the onset of the simulation: the slug length distribution introduces the influence of the gas injection system (i.e. the effect over the length of the bubbles and liquid slugs entering the column) whereas the superficial gas velocity distribution allows to address the effect of the changing hydrostatic pressure at the column inlet, due to the variable gas hold-up inside the column.

The evolution of the bubble and slug length distributions along the column is implemented by finite increments of the bubble nose and rear positioning, according to each bubble velocity. At every instant, the velocity of a bubble *i* is computed as the result of the bubble-to-bubble interaction (Eq. (5.1)) and of the expansion of all bubbles flowing below. Bubble expansion is implemented as the "extra" rise of the bubble nose due to the decreased pressure acting on it, at every new position. The pressure gradient along the column is predicted discarding the pressure losses in the liquid phase (at the wall and at the wake of the bubbles), which reduces to compute the hydrostatic pressure gradient.

Grid testing (i.e. comparison of similar simulations with decreasing time increments) showed that the adequate time increment is 0.005 s. A similar approach produced 2500 as the minimum number of Taylor bubbles to have converged statistics.

The main outputs of the simulator are the coalescence rate along the column and the distributions of bubble velocity, bubble length and liquid slug length at any vertical column position.

The cylindrical bubble shape assumption used within the simulator is refined, after the completion of each simulation, by updating the obtained bubble length data considering spherical bubble noses (under the condition of equal bubble volume). Although the bubble shape assumption does not alter the way the simulator predicts the evolution of the slug flow pattern along the column, this correction produces more realistic estimates of the bubble length parameter.

5.6.1 Experimental data versus simulation results

Experimental and simulation results for two operating conditions (e and f in Table 5.1) are compared in this section for the purpose of validation of the simulation code (for the regimes in question). Similar conclusions can be drawn for the remaining operating conditions. Simulations

are based on normal inlet distributions of slug length (average: 5*D*, standard deviation: 1.5*D*) and U_G (standard deviation equal to 10% of the corresponding average). Focus is put on the results at the acquisition coordinate (3.25 m from the base of the column). Notice that the characteristics of the inlet slug length distribution are shown later not to affect the results at this coordinate.

The experimental results for both operating conditions are generally well predicted by simulation (Figure 5.11 and Figure 5.12). The agreement between the experimental and simulated frequency distribution curves of bubble velocity and bubble length is notorious (for both operating conditions). For the slug length variable (Figure 5.11c and 5.11f), a less perfect agreement was obtained between the experimental and simulated frequency distribution curves (and the corresponding log-normal fit parameters). Nevertheless, the shape of the curves is fairly similar.

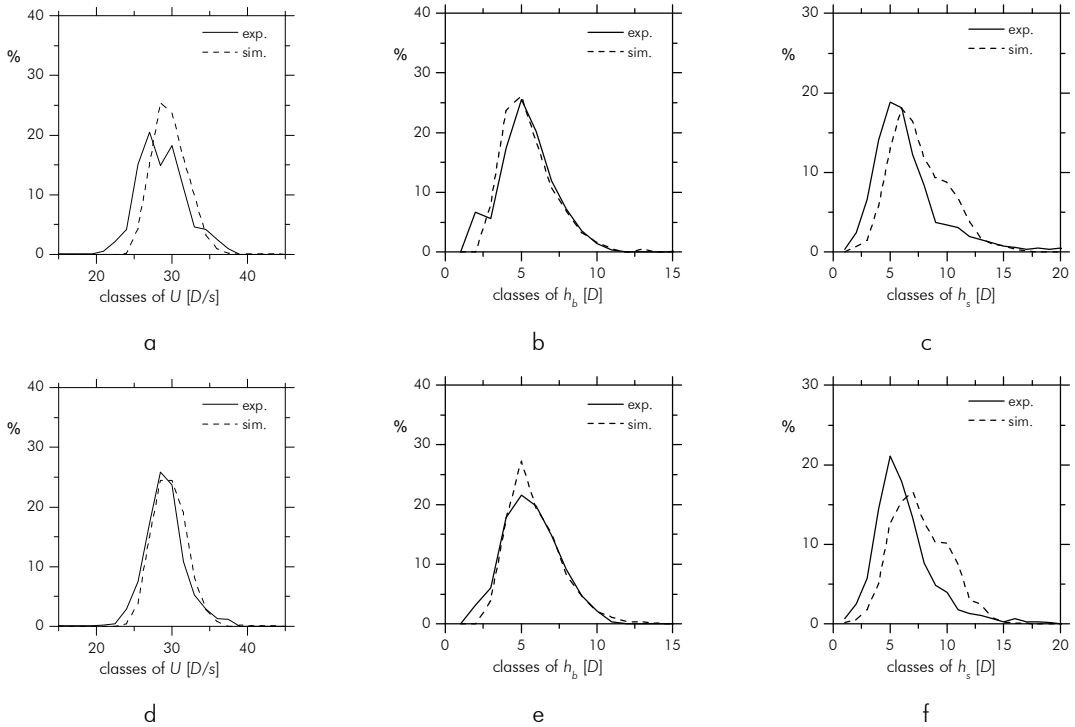

Figure 5.11 – Frequency distribution curves: (a) bubble velocity, (b) bubble length and (c) slug length, for an experiment/simulation with $U_L \approx 0.20$ m/s and $U_G \approx 0.37$ m/s, aqueous glycerol solution 61 wt% (0.012 Pa s); (d) bubble velocity, (e) bubble length and (f) slug length, for an experiment/simulation with $U_L \approx 0.20$ m/s and $U_G \approx 0.37$ m/s, aqueous glycerol solution 69 wt% (0.022 Pa s); vertical coordinate: 3.25 m

The results described in this section indicate that the SFS tool (equipped with the correlations (5.1) and (5.2)) can be used to predict successfully the results of slug flow experiments, for laminar regime in the main liquid and turbulent regime in the near-wake bubble region. Furthermore, these results show that the assumption of non-aerated liquid slugs does not prevent a good matching between experimental and simulation data (for the ranges of U_L and U_G studied and provided that correlation (5.2) is based on the experimental estimates of C and U_∞).

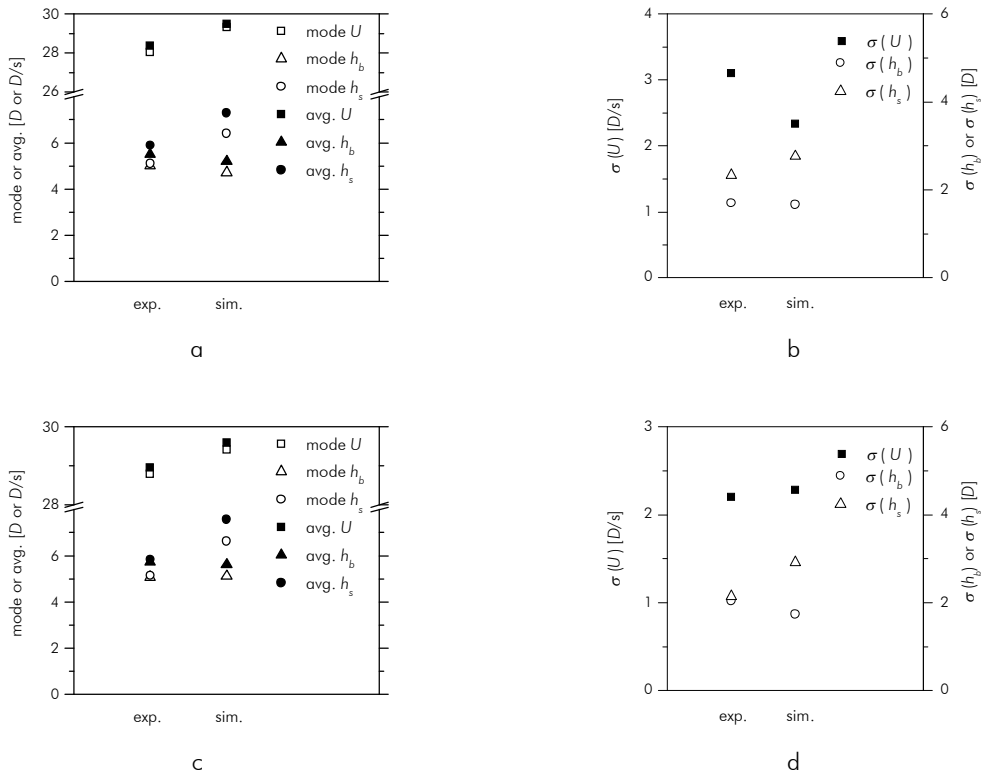

Figure 5.12 – Log-normal fit parameters: (a) average, mode and (b) standard deviation, for an experiment/simulation with $U_L \approx 0$. 20 m/s and $U_G \approx 0.37$ m/s, aqueous glycerol solution 61 wt% (0.012 Pa s); (c) average, mode and (d) standard deviation, for an experiment/simulation with $U_L \approx 0.20$ m/s and $U_G \approx 0.37$ m/s, aqueous glycerol solution 69 wt% (0.022 Pa s); vertical coordinate: 3.25 m

5.6.2 The entrance length of slug flow

The entrance length of slug flow refers to the column length above which the initial differences of the distributions introduced at the column inlet become negligible (i.e. whose relative differences become percentage-wise smaller than a given value). This parameter is highly relevant for practical applications of slug flow since it informs, for instance, on the extent of the influence of the gas injection nozzle (which influences the characteristics of the inlet distributions). Conversely, it informs on the range of inlet distributions that converge to similar flow patterns within a given column length.

The simulations used for the computation of the entrance length of slug flow were based on a 6.5 m long column (0.032 m internal diameter) and a hypothetical liquid solution based on the average properties (66 wt%, $\mu \approx 0.017$ Pa s) of the aqueous glycerol solutions used in the experiments.

The flow characteristics of simulations with different inlet slug length distributions were monitored along the column (in steps of 0.6 m). A fitting procedure was implemented (Log-normal)

over every parameter distribution to allow for an easy comparison/assessment. The focus was put on the average and most probable value (mode) of the bubble length and slug length distributions.

Simulations with inlet normal slug length distributions centred on 2*D*, 4*D* and 5*D* (standard deviations equal to 0.5*D*, 1*D*, and 1.5*D*, respectively) were monitored and compared along the column. In Figure 5.13, the maximal relative differences of the average and mode of the log-normal local fits (of h_b and h_s) are plotted against the vertical coordinate of the column, for a given set of superficial gas and liquid velocities ($U_L \approx 0.1$ m/s and $U_G \approx 0.4$ m/s). A figure of about 70*D* (2.24 m) is obtained for the entrance length of the slug flow (Figure 5.13), for these operating conditions and accepting a maximum relative difference of 10% for all parameters. Spanning the aforementioned approach for a set of increasing superficial liquid and gas velocities ($U_L \approx 0.10$, 0.17, 0.23 and 0.30 m/s, and $U_G \approx 0.10$, 0.20, 0.30 and 0.40 m/s) one obtains the chart of Figure 5.14a, showing the extent of the entrance length of slug flow for the given ranges of U_L and U_G. Notice that these ranges were chosen to address the experimental operating conditions (see Table 5.1) and to produce laminar regime in the main liquid between bubbles and turbulent regime in the near-wake bubble region. For the chosen ranges of U_L and U_G, the entrance length of slug flow ranges from about 50*D* to 80*D* (Figure 5.14a). This indicates, for instance, that any simulation result based on inlet slug length distributions centred on 2-5*D*, has reduced entrance effects at any vertical coordinate above 80*D*. Recall that this was the case for the simulations used in section 5.6.1 for the validation of the SFS tool (vertical coordinate in question: 3.25 m≈100*D*, and inlet slug length distribution centred on 5*D*).

More contrasting inlet slug length distributions (i.e. centred on 2-6*D*) were also found to converge within the 6.5 m of the column (again accepting a maximum relative difference of 10%). However, the obtained entrance length of slug flow is, as expected, much higher (90-170*D*, for the ranges of U_L and U_G studied). The corresponding results are shown in Figure 5.14b. For even more contrasting inlet distributions no full convergence of the flow patterns occurs within the length of the column.

Similar studies for fully laminar regime (Sotto Mayor et al. (2006b)) have shown that only less contrasting inlet slug length distributions converge to a single flow pattern, for the same column length (entrance length in the range 70-100*D*, for inlet slug length distributions centred on 2-4*D*). However, when considering turbulent regime, far more contrasting inlet distributions converge. Sotto Mayor et al. (2006a) report entrance lengths in the range 50-70*D* for convergence of inlet slug length distributions centred on 2-8*D*. These differences are a direct consequence of the different coalescence occurrence for the three regimes/scenarios (laminar, turbulent and the mix scenario, the present study). The higher the coalescence occurrence, the wider the converging range of inlet differences, for a given column length.

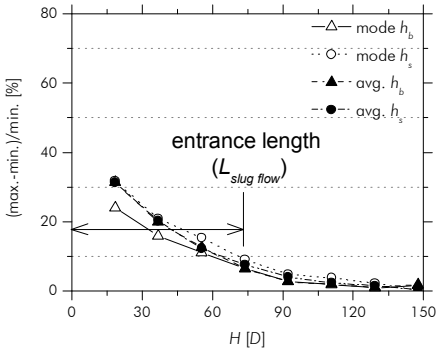

Figure 5.13 – Maximal relative difference of the mode and average of log-normal fits along the column, for simulations with inlet normal slug lengths distributions centred on 2*D*, 4*D* and 5*D*; U_L≈0.10 m/s and U_G≈0.40 m/s

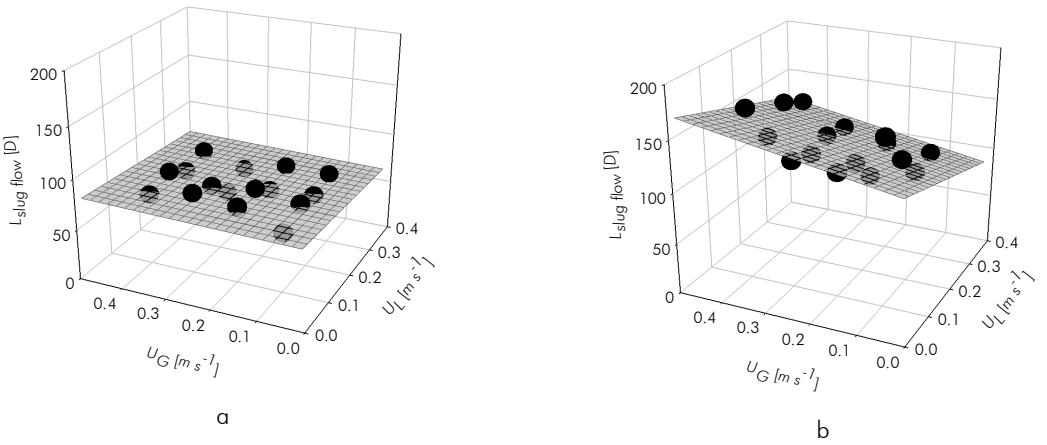

Figure 5.14 – Entrance length of slug flow for simulations with U_L≈0.10, 0.17, 0.23 and 0.30 m/s, and U_G≈0.10, 0.20, 0.30 and 0.40 m/s; maximal relative difference accepted: 10%; inlet normal slug length distributions centred on: (a) 2*D*, 4*D* and 5*D*, and (b) 2*D*, 4*D*, 5*D* and 6*D*

5.6.3 The coalescence events along the column

Two approaches are pursued in this section in order to study the influence of the bubble-to-bubble interaction curves and of the inlet slug length distribution over the coalescence occurrence along the column. The former implies using different bubble-to-bubble interaction curves, i.e. correlation (5.1) and those proposed by Sotto Mayor et al. (2006a), Sotto Mayor et al. (2006b) for fully turbulent and fully laminar regimes, and similar normal inlet slug length distributions (centred on 4*D*), the result of which is shown in Figure 5.15a. The latter implies using different inlet slug length distributions (centred on 3*D*, 4*D* and 5*D*) and a single bubble-to-bubble interaction curve, i.e. correlation (5.1). The result of this second approach is shown in Figure 5.15b.

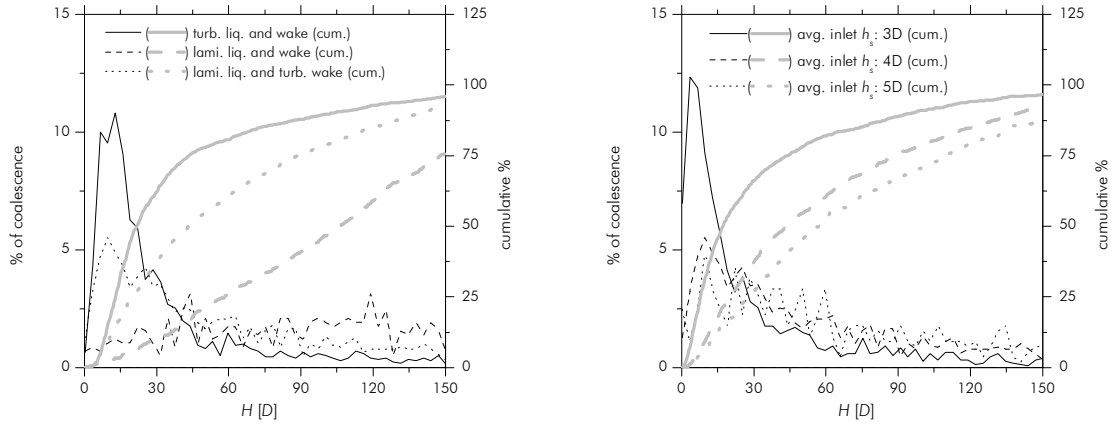

Figure 5.15 – Coalescence events along the column (steps of 0.1 m) for simulations with U_L and U_G equal to 0.1 m/s; (a) turbulent regime in liquid and wake (after Sotto Mayor et al. (2006c)), laminar regime in liquid and wake (after Sotto Mayor et al. (2006b)) and laminar regime in liquid and turbulent regime in wake (present data); normal inlet slug length distributions: N(4*D*, 1*D*); (b) laminar regime in liquid and turbulent regime in wake; normal inlet slug length distributions: N(3*D*, 1*D*), N(4*D*, 1*D*) and N(5*D*, 1.5*D*)

The interaction curve regarding the mix scenario (laminar regime in the main liquid and turbulent regime in the near-wake region) produces, as expected, coalescence curves somewhere in between those obtained for fully turbulent and fully laminar regimes. This is the natural outcome of the corresponding shapes of the interaction curves (Figure 5.3c). The mix scenario coalescence curve indicates some predominance of coalescence in the lower part of the column, less evident than for turbulent regime and greater than for laminar regime (Figure 5.15a). However, the second approach discussed in this section (mix scenario interaction curve and different inlet slug length distributions) confirms that the positional predominance of the coalescence along the column depends on the characteristics of the inlet slug length distribution. For the inlet distribution centred on the shorter slugs (3*D*), there are clearly more coalescences in the lower part of the column, whereas for inlet distributions centred on increasingly longer slugs (4*D* and 5*D*), the resulting coalescence curve widens and spreads more and more along the column (Figure 5.15b). Notice that both the validation of the SFS tool (section 5.6.1)) and the extensive simulation study discussed in the following sections are based on inlet slug length distributions centred on 5*D* (implying thus coalescence along the whole column). Nevertheless, despite the relation between the shape of the coalescence curve and the characteristics of the inlet slug length distribution, quite similar flow characteristics are obtained 50-80*D* above the base of the column, for inlet slug length distributions centred on 2-5*D* (as discussed in section 5.6.2). These conclusions refer to the length of column used in this study.

5.6.4 Simulation study

The SFS tool was used extensively in order to study the influence of U_G and U_L on the evolution of slug flow characteristics along the column. Three variables are focused in particular: bubble velocity (U), bubble length (h_b) and liquid slug length (h_s). Several simulations with increasing U_G (0.10, 0.20, 0.30 and 0.40 m/s) and U_L (0.10, 0.17, 0.23 and 0.30 m/s) were prepared and systematically compared. Each simulation was based on inlet normal slug length distributions centred on $5D$ (with standard deviation equal to $1.5D$) and distributed U_G (standard deviations as 10% of the corresponding averages). The evolution of the distributions of those variables (U, h_b and h_s) along the column was monitored in steps of 0.6 m. For the sake of simplicity, log-normal distributions were fitted to each frequency distribution curve obtained, which produced two parameters per curve (mode and standard deviation). This procedure resulted in 6 different groups of data: 3 regarding modes (of U, h_b and h_s) and 3 regarding the corresponding standard deviations. For the purpose of generalization, nonlinear estimation was implemented within each group of data. This procedure addressed three parameters: U_L, U_G and H, the vertical coordinate along the column. The general form of the fitting equation is:

$$z = a(H)^2 + bH + c(U_L)^2 + dU_L + e(U_G)^2 + fU_G + gHU_L + hHU_G + iU_LU_G + j \qquad (5.6)$$

where quadratic, linear and crossed terms in H, U_L and U_G are acknowledged. For each group of data, relevant fit coefficients were determined (for a 95% confidence level). The coefficient estimates obtained as well as the corresponding standard errors are shown in Table 5.2 (for modes) and Table 5.3 (for standard deviations). These coefficients allow predicting the characteristics of the frequency distribution curves of any of the main flow parameters (U, h_b and h_s) for a given set of operating conditions and vertical coordinate (U_L, U_G and H).

The following sections show 3-D representations of the variation of U, h_b and h_s (in terms of the modes and standard deviations of the corresponding frequency distribution curves) with H, U_L and U_G. Their values along the column and at the column outlet are focused.

Table 5.2 – Coefficients (estimate and standard error) and residuals (SSE: sum of squares of error; SSE/$n_{dat.}$: average sum of squares of error) of the surface fits of Figures 5.16 and 5.18, focussing modes; equation form: $z = a(H)^2 + bH + c(U_L)^2 + dU_L + e(U_G)^2 + fU_G + gHU_L + hHU_G + iU_LU_G + j$; z in SI units

	mode (U)		mode (h_b)		mode (h_s)	
	estimate	stand. error	estimate	stand. error	estimate	stand. error
a	1.63×10^{-3}	1.27×10^{-4}	9.10×10^{-4}	8.10×10^{-5}	-6.39×10^{-4}	9.30×10^{-5}
b	-9.05×10^{-3}	1.08×10^{-3}	...	...	1.20×10^{-2}	7.25×10^{-4}
c	...	...	6.51×10^{-1}	6.99×10^{-2}	...	...
d	$1.35 \times 10^{+0}$	1.36×10^{-2}	-1.56×10^{-1}	3.07×10^{-2}	3.72×10^{-2}	9.93×10^{-3}
e	9.90×10^{-2}	3.22×10^{-2}	...	...	...	...
f	9.32×10^{-1}	1.89×10^{-2}	4.87×10^{-1}	9.62×10^{-3}	3.83×10^{-2}	6.09×10^{-3}
g	6.45×10^{-3}	2.57×10^{-3}	-2.76×10^{-2}	2.23×10^{-3}	4.99×10^{-3}	1.88×10^{-3}
h	5.39×10^{-2}	1.70×10^{-3}	4.81×10^{-2}	1.54×10^{-3}	...	...
i	-1.49×10^{-1}	3.90×10^{-2}	$-1.14 \times 10^{+0}$	3.85×10^{-2}	-1.66×10^{-1}	2.86×10^{-2}
j	2.71×10^{-1}	3.72×10^{-3}	9.86×10^{-3}	3.47×10^{-3}	1.64×10^{-1}	2.23×10^{-3}
SSE [m^2 or m^2/s^2]	2.48×10^{-3}		2.46×10^{-3}		1.36×10^{-3}	
SSE/$n_{dat.}$ [m^2 or m^2/s^2]	1.55×10^{-5}		1.54×10^{-5}		8.50×10^{-6}	
r^2	0.999		0.995		0.965	

Table 5.3 – Coefficients (estimate and standard error) and residuals (*SSE*: sum of squares of error; *SSE*/$n_{dat.}$: average sum of squares of error) of the surface fits of Figures 5.16 and 5.18, focussing σ; equation form: $z = a(H)^2 + bH + c(U_L)^2 + dU_L + e(U_G)^2 + fU_G + gHU_L + hHU_G + iU_LU_G + j$; z in SI units

	$\sigma(U)$		$\sigma(h_b)$		$\sigma(h_s)$	
	estimate	stand. error	estimate	stand. error	estimate	stand. error
a	1.55×10^{-3}	1.15×10^{-4}	6.20×10^{-4}	6.30×10^{-5}	...	...
b	-1.29×10^{-2}	8.82×10^{-4}	-1.16×10^{-3}	5.37×10^{-4}	1.07×10^{-2}	4.01×10^{-4}
c	...	...	2.62×10^{-1}	3.53×10^{-2}	2.90×10^{-2}	9.30×10^{-3}
d	...	...	-7.81×10^{-2}	1.56×10^{-2}	...	...
e	...	...	...	...	-7.84×10^{-2}	2.78×10^{-2}
f	7.99×10^{-2}	5.62×10^{-3}	1.92×10^{-1}	4.97×10^{-3}	4.74×10^{-2}	1.49×10^{-2}
g	-7.33×10^{-3}	1.08×10^{-3}	-8.61×10^{-3}	1.28×10^{-3}	...	...
h	4.79×10^{-2}	1.53×10^{-3}	1.40×10^{-2}	8.45×10^{-4}	-4.26×10^{-3}	1.46×10^{-3}
i	...	...	-4.08×10^{-1}	1.94×10^{-2}	...	...
j	1.91×10^{-2}	1.77×10^{-3}	4.34×10^{-3}	2.07×10^{-3}	4.69×10^{-2}	2.07×10^{-3}
SSE [m^2 or m^2/s^2]	2.09×10^{-3}		6.22×10^{-4}		1.90×10^{-3}	
SSE/$n_{dat.}$ [m^2 or m^2/s^2]	1.31×10^{-5}		3.89×10^{-6}		1.19×10^{-5}	
r^2	0.987		0.991		0.958	

5.6.4.1 Results along the column

The mode and the standard deviation of the main flow parameters are plotted against H and U_G (Figure 5.16) for constant U_L (equal to 0.17 m/s). The 3-D surfaces computed by Eq. (5.6) are also shown in the charts.

The most probable value (mode) of bubble velocity increases with H as well as U_G (Figure 5.16a). Its variation with H is the result of both the gas expansion and the coalescence of bubbles, whereas its variation with U_G is the result of the increasing gas flow rates (see Eq. (5.2)). The standard deviation of this parameter reaches no more than 16% of the corresponding mode (Figure 5.16g), for the ranges of U_L and U_G studied.

The most probable value of bubble length increases with H and U_G (Figure 5.16b). As for the bubble velocity variable, its variation along the column is related to the gas expansion and the coalescence effect. Its variation with the superficial gas velocity derives from flow continuity (longer bubbles result from increasing U_G, for constant U_L). The standard deviation of h_b shows a similar behaviour, which results ultimately in a relatively constant standard deviation/mode ratio (32-42%).

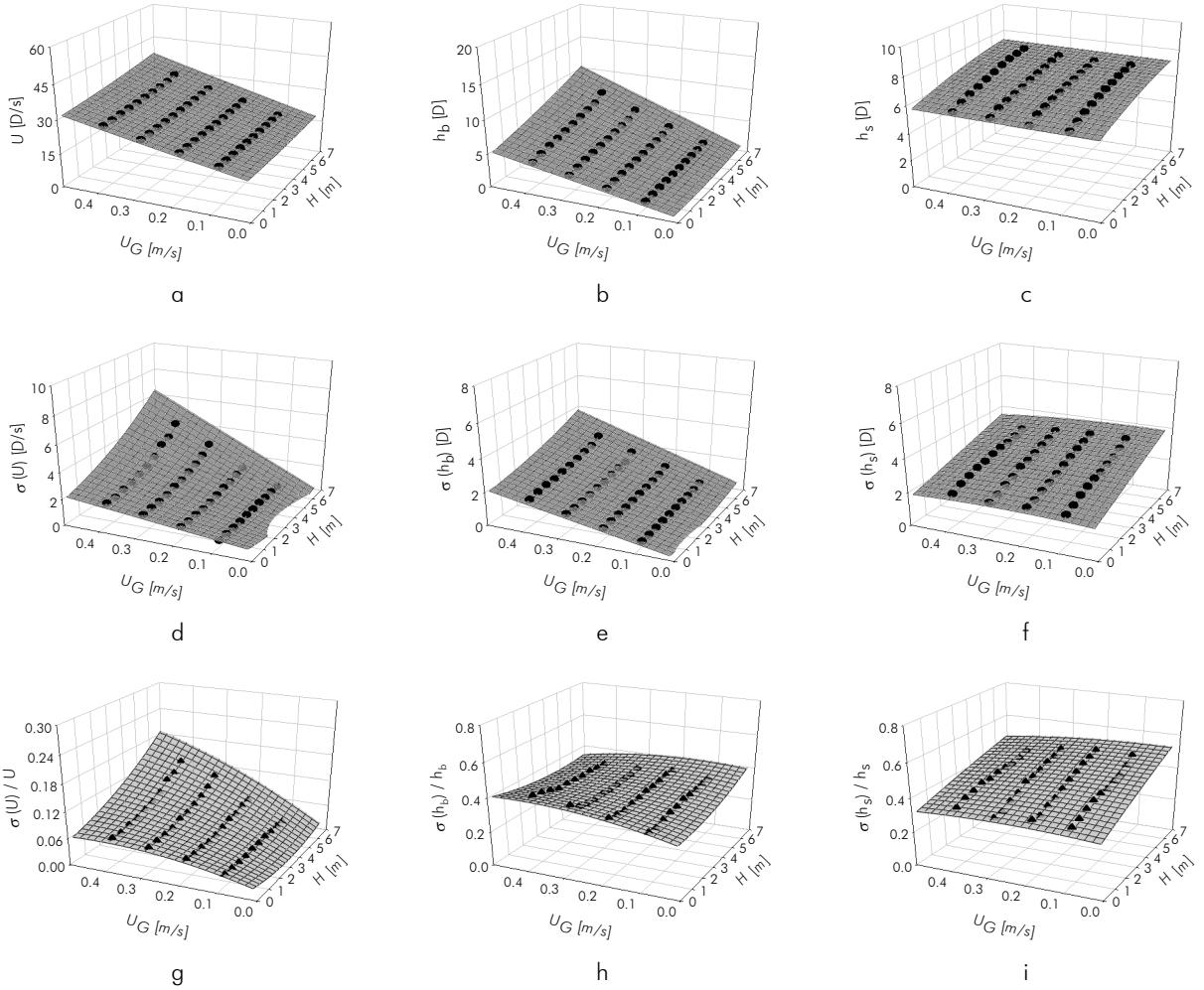

Figure 5.16 – Mode (a-c), standard deviation (d-f) and corresponding ratio (g-i) of log-normal fits along the column; (a), (d) and (g) bubble velocity; (b), (e) and (h) bubble length; (c), (f) and (i) liquid slug length; simulations with $U_L \approx 0.17$ m/s and $U_G \approx 0.10$, 0.20, 0.30 and 0.40 m/s

The mode of liquid slug length increases along the column but shows no dependence on U_G. The latter indicates that gas expansion is not relevant in the evolution of this parameter. Its variation with H is basically the result of bubble coalescence. Moreover, the reasonably steady variation rate of this parameter along the column confirms that bubble coalescence spans the whole column length. The fact that the standard deviation/mode ratio of this parameter increases from 30-35% near the base of the column, to 45-55% at its top, corroborates the aforesaid. Indeed, the high standard deviation of h_s at the column top is due to the coexistence of long (h_s

escalates with *H*) and short liquid slugs (between coalescing bubbles) at that location, which confirms ultimately the occurrence of coalescence.

The present data is compared with the findings for fully turbulent (Sotto Mayor et al. (2006c)) and fully laminar (Sotto Mayor et al. (2006b)) scenarios, in Figure 5.17 (for U_G and U_L equal to 0.1 m/s).

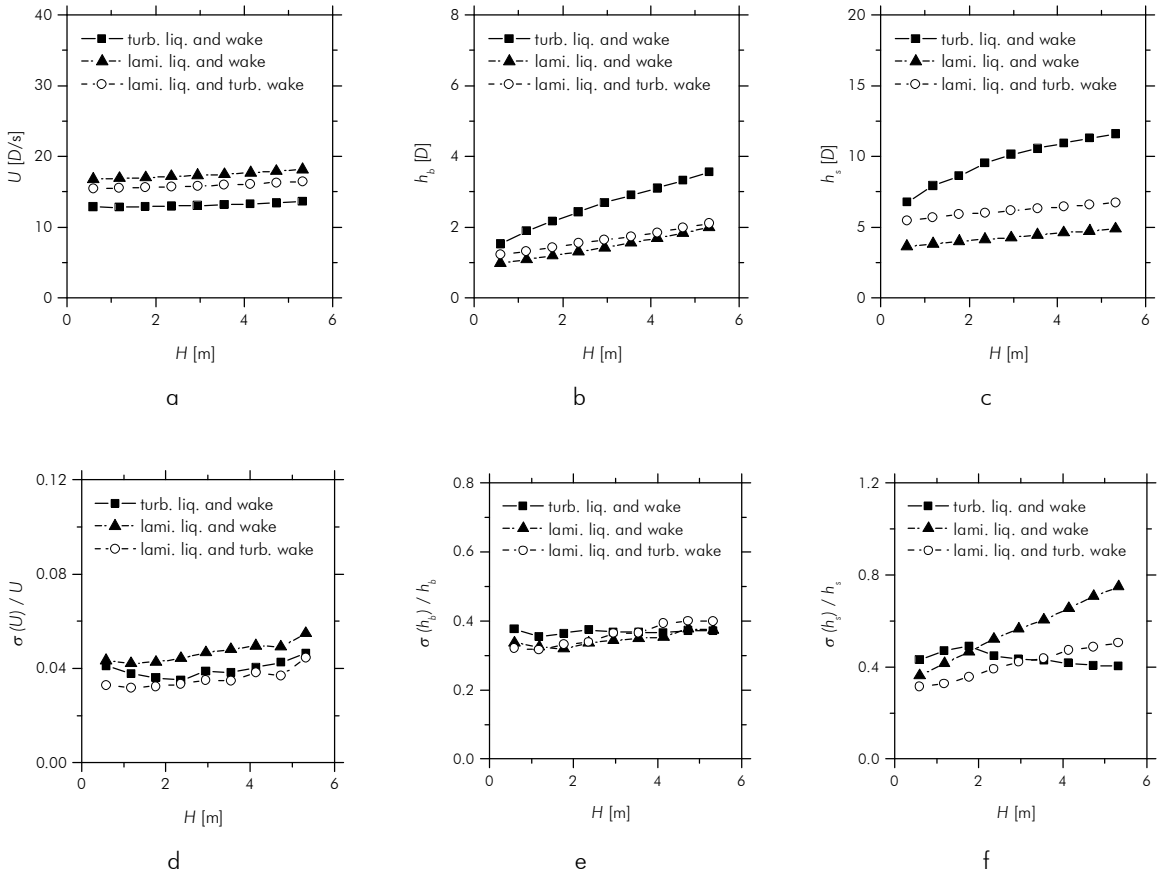

Figure 5.17 – Mode (a-c) and standard deviation/mode ratio (d-f) of log-normal fits along the column for simulations for turbulent regime in liquid and wake (after Sotto Mayor et al. (2006c)), laminar regime in liquid and wake (after Sotto Mayor et al. (2006b)) and laminar regime in liquid and turbulent regime in wake (present data); (a) and (d) bubble velocity; (b) and (e) bubble length; (c) and (f) liquid slug length; $U_L \approx 0.10$ m/s and $U_G \approx 0.10$ m/s

The present data (mix scenario) shows an evolution along the column (regarding the modes of the main flow parameters) somewhere in between the results for fully turbulent and fully laminar regimes/scenarios. Furthermore, the results for the mix scenario are closer to those for fully laminar regime than to those for fully turbulent, in particular for bubble velocity and bubble length variables (Figure 5.17a and b). In addition, the evolution along the column of h_s, for fully turbulent regime, is clearly different from that for fully laminar and mix scenarios. While h_s escalates along the column at fairly steady rates for both mix and fully laminar scenarios, different variation rates

can be observed for fully turbulent regime (higher variation near the base and lower variation near the top). These differences are obviously related to the different coalescence curves for the three scenarios (section 5.6.3). Recall that the fully turbulent regime implies frequent coalescence in the lower portion of the column (hence the high variation rate of h_s in that zone), whereas both fully laminar and the mix scenarios (in particular for inlet slug length distributions centred on 5*D*) feature coalescence along the whole column length. In agreement with this, the standard deviation/mode ratio escalates along the column for both fully laminar and mix scenarios while, for fully turbulent conditions, a decrease can be observed, in the upper portion of the column, due to a decrease in coalescence (Figure 5.17f).

The standard deviation/mode ratio for h_b is reasonably similar for the three scenarios (Figure 5.17e) and varies between 27% and 45%, for the ranges of U_L and U_G studied. The homonymous ratio for U is also similar for the three scenarios.

5.6.4.2 Results at column outlet

The mode and standard deviation of the main flow parameters are plotted against increasing values of U_L and U_G in Figures 5.18a to 5.18f, for vertical coordinate 5.9 m. As before, the 3-D surfaces computed by Eq. (5.6), with $H \approx 5.9$ m, are also shown in the charts.

The most probable bubble velocity increases linearly with U_L and almost linearly with U_G (Figure 5.18a). The corresponding standard deviation escalates with increasing U_G and decreasing U_L. The variation of the standard deviation with U_G and U_L is related to the gas phase expansion and flow continuity (longer bubbles resulting from increasing U_G undergo higher expansion than shorter bubbles since the expansion rate is a function of bubble length). The standard deviation/mode ratio is smaller than 16% for the ranges of U_L and U_G studied (Figure 5.18g).

The most probable bubble length increases with increasing U_G and decreasing U_L (Figure 5.18b). These variations can be ascribed to flow continuity. The variation of the corresponding standard deviation is somewhat similar, resulting in a quasi-constant standard deviation/mode ratio (34-41%; Figure 5.18h).

The mode and the standard deviation of slug length show almost no dependence on U_G or U_L (Figures 5.18c and 5.18f). For the ranges of U_G or U_L studied, figures of about 7*D* and 3.5*D* are obtained, respectively. This results in relatively constant standard deviations/mode ratios between 45% and 55%.

As for the data along the column, the findings for fully turbulent and fully laminar scenarios (Sotto Mayor et al. (2006c) and Sotto Mayor et al. (2006b), respectively) are compared with the present data (mix scenario) in Figure 5.19. The comparisons focus data for increasing U_G and

constant U_L (0.1 m/s) at 5.3 m from the base of the column (H≈5.3 m). Furthermore, they focus slightly different ranges of U_G for each scenario, although with some overlapping. Notice for instance the narrow range of U_G studied for fully laminar regime when compared to that for fully turbulent. The width of these ranges is obviously related the scenario one aims to obtain/study.

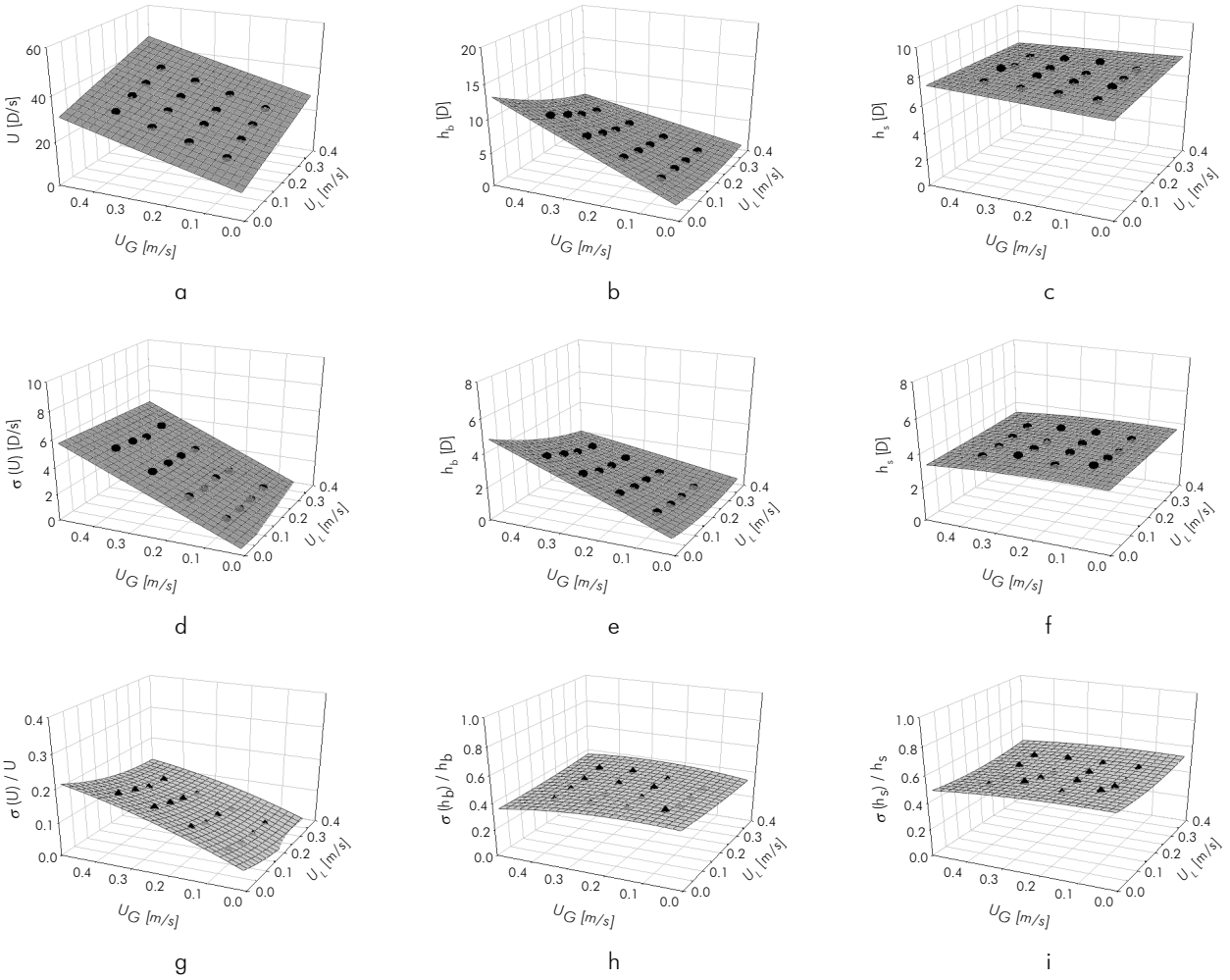

Figure 5.18 – Mode (a-c), standard deviation (d-f) and corresponding ratio (g-i) of log-normal fits; (a), (d) and (g) bubble velocity; (b), (e) and (h) bubble length; (c), (f) and (i) liquid slug length; simulations with U_L≈0.10, 0.17, 0.23 and 0.30 m/s, U_G≈0.10, 0.20, 0.30 and 0.40 m/s; vertical coordinate: 5.9 m

By analysing the range of U_G common to the three scenarios (0.1-0.2 m/s) one concludes that the bubble velocity is higher for the fully laminar regime and lower for the fully turbulent (Figure 5.19a). This derives from the experimental values of parameter C (Eq. (5.2)) obtained for each scenario (1.93, 1.34 and 1.2 for laminar, mix and turbulent, respectively). In addition, longer bubbles are obtained for the fully turbulent regime whereas quite similar lengths are obtained for both the fully laminar and the mix scenarios (Figure 5.19b). This is due to the more frequent coalescence for fully turbulent regime, and the higher expansion rate of the resulting longer bubbles. The more frequent coalescence for the fully turbulent scenario also accounts for the

longer liquid slugs reaching the top of the column (when compared to those for the other scenarios; Figure 5.19c).

The standard deviation/mode ratio of U and h_b is quite similar for the three scenarios, when U_G overlapping exists (Figures 5.19d and 5.19e). The homonymous ratio for h_s is higher for the fully laminar regime and lower for the fully turbulent regime. This in agreement with the corresponding coalescence curves (Figure 5.15b).

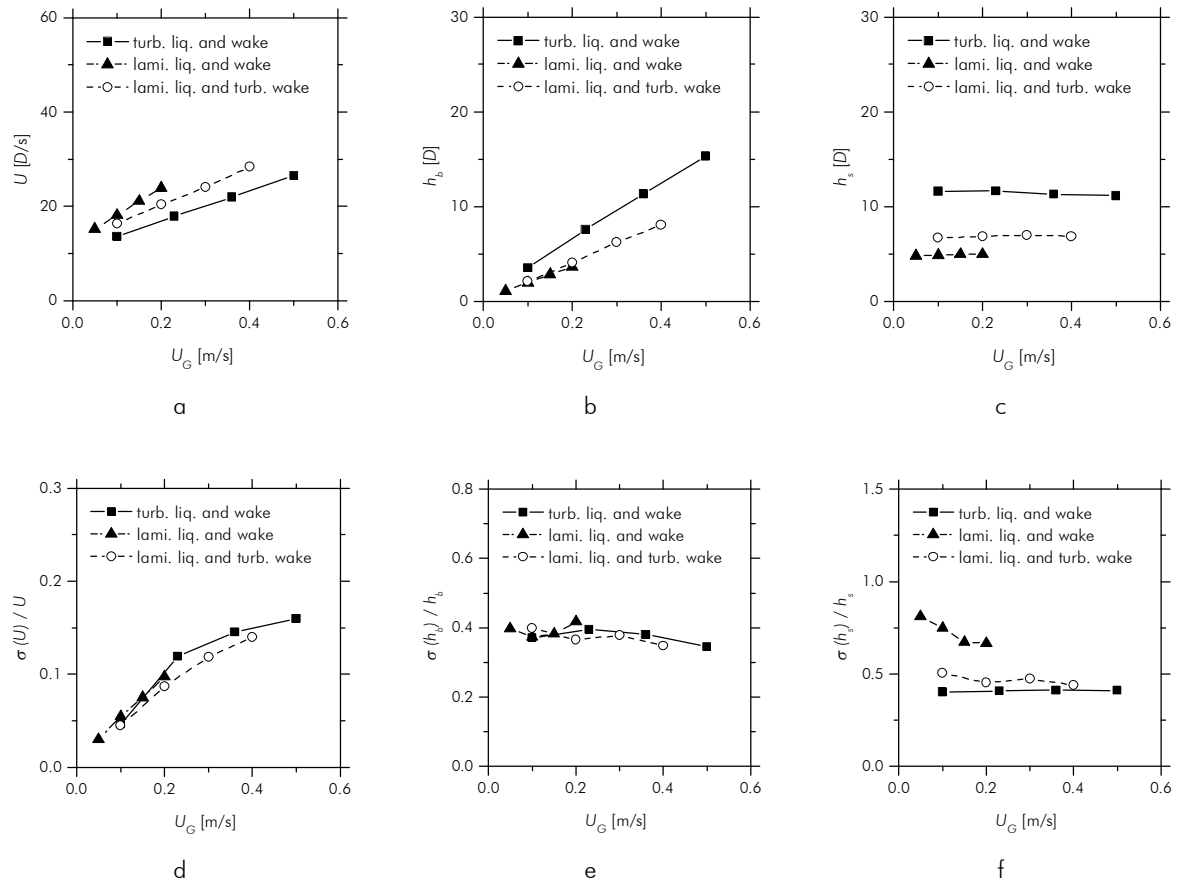

Figure 5.19 – Mode (a-c) and standard deviation/mode ratio (d-f) of log-normal fits for simulations for turbulent regime in liquid and wake (after Sotto Mayor et al. (2006c)), laminar regime in liquid and wake (after Sotto Mayor et al. (2006b)) and laminar regime in liquid and turbulent regime in wake (present data); (a) and (d) bubble velocity; (b) and (e) bubble length; (c) and (f) liquid slug length; $U_L \approx 0.10$ m/s, vertical coordinate: 5.3 m

5.7 Conclusions

An experimental and simulation study on free bubbling vertical slug flow is reported. Operating conditions leading to laminar regime in the main liquid and turbulent regime in the near-wake bubble region are addressed. The study was conducted using a non-intrusive image analysis technique (Sotto Mayor et al. (2006c)) and a slug flow simulator (SFS; Sotto Mayor et al. (2006e)).

A correlation for the interaction between consecutive bubbles is proposed. It relates the velocity of the trailing bubble with the length of the liquid slug ahead of the bubble. Strong interaction was found between bubbles flowing less than 3-4*D* apart, with slight and decreasing interaction persisting for longer distances. The shape of the bubble-to-bubble interaction curve for the present scenario bridges those for the fully turbulent and fully laminar regimes. For fully turbulent regime, bubble interaction occurs for liquid slugs shorter than 8-10*D* while, for fully laminar regime, strong bubble interaction occurs mainly for liquid slugs shorter than 2*D* (although with some interaction persisting for longer distances).

The flow characterization disclosed an increase in flow stability with increasing superficial liquid velocity and with decreasing superficial gas velocity. Liquid viscosity was found not to affect the flow pattern characteristics, for the ranges of viscosity studied (0.012-0.022 Pa s). The experimental average bubble velocity in undisturbed conditions was shown not to follow the correlation-based predictions for laminar regime in the main liquid. Thus, the experimental values of C and U_∞ obtained were used to estimate that parameter for any given superficial mixture velocity.

An extensive simulation study was developed based on the obtained bubble-to-bubble interaction curve and the estimates of the undisturbed bubble velocity. As for the fully turbulent and the fully laminar regimes, different inlet slug length distributions were found to evolve to similar flow patterns (i.e. to converge) within the length of the column. However, the degree of contrast of the inlet slug length distributions that converge, within a given column length, is different for the three scenarios. For the mix scenario, normal inlet slug length distributions centred on 2-5*D* were found to converge within the first 50-80*D* of the column (entrance length of the slug flow), for the ranges of U_L and U_G studied (0.1-0.3 m/s and 0.1-0.4 m/s, respectively). This range of attenuable inlet differences is narrower than that for fully turbulent regime (2-8*D*) and wider than that for fully laminar regime (2-4*D*). Coalescence was found to occur along the whole column length for the chosen inlet slug length distributions (centred on 5*D*).

An effort was made to propose general expressions for the computation of the mode and standard deviation (of log-normal fits) for bubble velocity, bubble length and liquid slug length. These are a function of the superficial gas and liquid velocities (U_G, U_L, respectively) and of the vertical coordinate (H). Very good agreement was found between these general expressions and the simulation data obtained.

Bubble velocity increases with U_L, U_G and H. Coalescence and mainly gas expansion account for its variation with H. Bubble length increases with U_G and H and decreases with U_L. These variations result from flow continuity, coalescence and gas expansion effects. Slug length

increases along the column and shows almost no dependence on U_G and U_L. The evolution of this parameter is mainly controlled by coalescence.

For similar operating conditions (U_G, U_L and H), bubble velocity in the mix scenario is lower than for fully laminar regime and higher than for fully turbulent. Bubble length is higher for fully turbulent regime and similar for the mix and laminar scenarios. The liquid slug length is higher for fully turbulent regime and lower for fully laminar.

The standard deviation/mode ratios for bubble velocity and bubble length are reasonably similar for the three scenarios. The homonymous parameter for liquid slug length is clearly higher for fully laminar conditions.

The reported study provides detailed information on slug flow pattern characteristics in the mix scenario, and a comparison of the obtained results with those for fully turbulent and fully laminar regimes. It is, thus, an attempt to favour a holistic understanding of slug flow features and governing rules.

5.8 Notation

Roman symbols

C	empirical coefficient	
D	column internal diameter	[m]
h_b	length of gas bubble	[m]
h_s	length of liquid slug	[m]
H	vertical coordinate along the column	[m]
$L_{slug\ flow}$	entrance length of slug flow	[m]
i	index of bubble / slug	
$n_{dat.}$	number of data used in the nonlinear estimation	[#]
$P_{acq.}$	pressure at the acquisition coordinate	[Pa]
$P_{amb.}$	ambient pressure	[Pa]
r^2	coefficient of determination of fits (=[*SST*-*SSE*]/*SST*)	
R_c	column internal radius	[m]
SSE	sum of squares of error (sum of squares of residuals)	[m^2] or [m^2/s^2]
$SSE/\ n_{dat.}$	average sum of squares of error	[m^2] or [m^2/s^2]
SST	total sum of squares (sum of squares about the mean)	[m^2] or [m^2/s^2]
$T_{amb.}$	ambient temperature	[K]
U	upward bubble velocity (U_B^{exp} and U_i^{lead} for trailing and leading bubble i, respectively)	[m/s]
U_B	upward bubble velocity (according to Nicklin's equation)	[m/s]
U_B^{exp}	experimental average upward bubble velocity in undisturbed conditions	[m/s]

U_G	superficial gas velocity	[m/s]
U_∞	upward bubble velocity in a stagnant liquid (drift velocity)	[m/s]
U_L	superficial liquid velocity	[m/s]
U_M	superficial mixture velocity (= $U_L + U_L$)	[m/s]
V_S	liquid velocity relative to the bubble ($= U_B^{exp} - U_M$)	[m/s]
z	parameter to be fit by nonlinear estimation	[m] or [m/s]

Greek symbols

σ	standard deviation (of bubble length or bubble velocity)	[m] or [m/s]
μ	liquid viscosity	[Pa s]
ρ	liquid density	[kg/m^3]

Dimensionless groups

Re_{U_M}	Reynolds number based on the mixture velocity ($= \rho U_M D/\mu$)
Re_{V_S}	Reynolds number based on the liquid velocity relative to the bubble ($= \rho V_S D/\mu$)

5.9 Acknowledgments

The authors gratefully acknowledge the financial support of Fundação para Ciência e Tecnologia through project POCTI/EQU/33761/1999 and scholarship SFRH/BD/11105/2002. POCTI (FEDER) also supported this work via CEFT.

5.10 References

Barnea, D. and Taitel, Y., 1993. A model for slug length distribution in gas-liquid slug flow. Int. J. Multiphas. Flow 19(5): 829-838.

Brown, R. A. S., 1965. The mechanics of large gas bubbles in tubes. I - Bubble velocities in stagnant liquids. Canadian Journal of Chemical Engineering 43: 217-223.

Campos Guimarães, R. and A. Sarsfield Cabral, J. (1997). Estatística, McGraw-Hill de Portugal Limitada.

Collins, R., De Moraes, F. F., Davidson, J. F. and Harrison, D., 1978. The Motion of Large Gas Bubble Rising Through Liquid Flowing in a Tube. J. Fluid Mech. 28: 97-112.

Davies, R. M. and Taylor, G. I., 1950. The mechanics of large Bubbles rising through extended liquids and through liquids in tubes. Proc. R. Soc. Lond. A 200: 375-392.

Dumitrescu, D. T., 1943. Stromung an Einer Luftblase im Senkrechten Rohr. Z. Angeus. Math. Mec. 23: 139-149.

Fabre, J. and Liné, A., 1992. Modeling of two-phase slug flow. Ann. Rev. Fluid Mech. 24: 21-46.

Fernandes, R. C., Semiat, R. and Dukler, A. E., 1983. Hydrodynamic model for gas-liquid slug flow in vertical tubes. AIChE J. 29(6): 981-989.

Govier, W. and Aziz, K. (1972). The flow of complex mixtures in pipes. New York, USA, Van Nostrand Reinhold Edition.

James, M. R., Lane, S. J., Chouet, B. and Gilbert, J. S., 2004. Pressure changes associated with the ascent and bursting of gas slugs in liquid-filled vertical and inclined conduits. J. Volcanol. Geoth. Res. 129(1-3): 61.

Mao, Z.-S. and Dukler, A. E., 1989. An experimental study of gas-liquid slug flow. Experiments in Fluids (Historical Archive) 8(3 - 4): 169.

Nicklin, D. J., Wilkes, J. O. and Davidson, J. F., 1962. Two-phase flow in vertical tubes. Transactions of the Institution of Chemical Engineers 40: 61-68.

Pinto, A. M. F. R., Coelho Pinheiro, M. N. and Campos, J. B. L. M., 2001. On the interaction of Taylor bubbles rising in two-phase co-current slug flow in vertical columns: Turbulent wakes. Exp. Fluids 31(6): 643-652.

Pinto, A. M. F. R., Coelho Pinheiro, M. N., Nogueira, S., Ferreira, V. and Campos, J. B. L. M., 2005. Experimental study of the transition in the velocity of individual Taylor bubbles in vertical upward co-current liquid flow. Chem. Eng. Res. Des. 83(A9): 1103-1110.

Pinto, A. M. F. R., Pinheiro, M. N. C. and Campos, J. B. L. M., 1998. Coalescence of two gas slugs rising in a co-current flowing liquid in vertical tubes. Chem. Eng. Sci. 53(16): 2973-2983.

Sotiriadis, A. A. and Thorpe, R. B., 2005. Liquid re-circulation in turbulent vertical pipe flow behind a cylindrical bluff body and a ventilated cavity attached to a sparger. Chem. Eng. Sci. 60(4): 981-994.

Sotto Mayor, T., Ferreira, V., Pinto, A. M. F. R. and Campos, J. B. L. M., 2006a. Hydrodynamics of gas-liquid slug flow along vertical pipes in turbulent regime. An experimental study. Submitted to International Journal of Heat and Fluid Flow.

Sotto Mayor, T., Pinto, A. M. F. R. and Campos, J. B. L. M., 2006b. Hydrodynamics of gas-liquid slug flow along vertical pipes in laminar regime - Experimental and simulation study. Submitted to Industrial & Engineering Chemistry Research.

Sotto Mayor, T., Pinto, A. M. F. R. and Campos, J. B. L. M., 2006c. Hydrodynamics of gas-liquid slug flow along vertical pipes in turbulent regime. A simulation study. Submitted to Chemical Engineering Research and Design.

Sotto Mayor, T., Pinto, A. M. F. R. and Campos, J. B. L. M., 2006d. An image analysis technique for the study of gas-liquid slug flow along vertical pipes - Associated uncertainty. In revision in Flow Measurement and Instrumentation.

Sotto Mayor, T., Pinto, A. M. F. R. and Campos, J. B. L. M., 2006e. Slug Flow Simulation - a tool for the teaching and learning of two-phase slug flow regime in vertical columns. Accepted for publication in International Journal of Engineering Education.

Van Hout, R., Barnea, D. and Shemer, L., 2001. Evolution of statistical parameters of gas-liquid slug flow along vertical pipes. Int. J. Multiphas. Flow 27(9): 1579-1602.

Van Hout, R., Barnea, D. and Shemer, L., 2002b. Translational velocities of elongated bubbles in continuous slug flow. International Journal of Multiphase Flow 28(8): 1333-1350.

Van Hout, R., Gulitski, A., Barnea, D. and Shemer, L., 2002a. Experimental investigation of the velocity field induced by a Taylor bubble rising in stagnant water. International Journal of Multiphase Flow 28(4): 579-596.

Van Hout, R., Shemer, L. and Barnea, D., 2003. Evolution of hydrodynamic and statistical parameters of gas-liquid slug flow along inclined pipes. Chem. Eng. Sci. 58(1): 115-133.

Wallis, G. B. (1969). One dimensional two-phase flow. New York, McGraw Hill Book Co.

White, E. T. and Beardmore, R. H., 1962. The Velocity of Single Cylindrical Air Bubbles Through Liquids Contained in Vertical Tubes. Chem. Eng. Sci. 17: 351-361.

White, F. M. (1999). Fluid mechanics, McGraw-Hill International Editions.

6 Conclusions and suggestions for future work

The following sections summarize the main conclusions of this research and provide some suggestions for future work.

6.1 Conclusions

The present thesis describes an experimental and numerical investigation on co-current continuous slug flow in vertical columns. The study aimed at providing information on the characteristics and governing correlations of such flow pattern, for all possible flow regimes/scenarios.

The experimental study of co-current continuous slug flow was enabled by the development of a non-intrusive technique, based on the automatic analysis of videos of the flow. An image analysis code was developed for the purpose of sequentially and easily extracting information on the length, velocity and distance of the Taylor bubbles in each video frame. These data allowed the characterization of the flow pattern, for each experimental condition studied.

The numerical investigation was enabled by the development of a slug flow simulator (SFS) based on several correlations for bubble motion and interaction, drawn from the experimental study. The simulation code addresses several features of the slug flow pattern, including the gas phase expansion along the column. Such features, hitherto not totally accomplished for continuous operation, allowed a thorough study of the influence of this phenomenon on the evolution of several flow parameters. Of particular relevance is the finding that the gas expansion rate is not constant during a slug flow experiment (time-wise), but rather oscillatory and dependent on the configuration of the column outlet system.

The experimental (and numerical) study addressed operating conditions leading to the three scenarios possible in slug flow: the fully turbulent and the fully laminar scenarios (in the main liquid and in the near-wake bubble region) and the mix scenario (laminar regime in the main liquid

and turbulent regime in the near-wake bubble region). For each scenario, different but unique bubble-to-bubble interaction correlations were obtained. The corresponding interaction curves show that strong interaction occurs for liquid slugs shorter than 8-10*D*, 3-4*D* and 2*D*, for the fully turbulent, the mix and the fully laminar scenarios, respectively. Consequently, the occurrence of coalescence along the column is different for the three scenarios. The fully turbulent scenario is associated with a higher number of coalescences (concentrated at the lower part of the column) whereas the fully laminar scenario is associated with the lower number of coalescences (spread along the whole column length). The mix scenario bridges the previous two outcomes.

The experimental average bubble velocity in undisturbed conditions (U_B^{exp}) was found to follow the correlation-based predictions in the literature (Nicklin et al., 1962), for both the fully turbulent and the fully laminar scenarios. This indicates that, for these scenarios, the velocity profiles in the liquid ahead of undisturbed trailing bubbles were approximately fully developed. This seems not to be the case for the mix scenario, where the estimates of U_B^{exp} obtained are considerably lower than expected. It is probable that for the mix scenario the liquid slugs in co-current continuous slug flow are, most of time, not long enough to allow the full development of the laminar velocity profile in the liquid between bubbles (starting from a relatively flat profile at the turbulent wake region).

The proposed slug flow simulator (SFS) was shown to very reasonably predict the frequency distribution curves of bubble velocity, bubble length and liquid slug length (and corresponding average and most probable values), for all operating conditions and flow regimes/scenarios studied. The SFS tool thus emerged as a valuable asset for the simulation of vertical slug flow.

A simulation study was developed on the evolution of different inlet distributions (or flow patterns) along the column. The study showed that, due to coalescence, most of these different inlet distributions tend to evolve to similar flow patterns above a given column length. This allowed determination of the entrance length of slug flow, i.e. the column length required for convergence of different inlet distributions, and also the establishment of the range of converging inlet differences. This information is relevant for practical applications of slug flow since it informs, for instance, on the extent of the influence of the gas injection nozzle. Entrance lengths of 50-70*D*, 50-80*D* and 70-100*D* were found for the fully turbulent, the mix and the fully laminar scenarios, respectively (for convergence of inlet slug length distributions centred on 2-8*D*, 2-5*D* and 2-4*D*, respectively). These results are in agreement with the number of coalescences occurring for each scenario (higher coalescence allows for lower entrance lengths and convergence of more contrasting inlet distributions).

Extensive simulation studies were developed for each of the three scenarios in order to expound the influence of parameters such as the superficial gas and liquid velocities (U_G and U_L,

respectively) on the evolution of bubble velocity, bubble length and liquid slug length along the column. General expressions are given for the prediction of the mode and standard deviation of the distributions of bubble velocity, bubble length and liquid slug length, given U_G, U_L, D (column diameter) and H (vertical coordinate along the column).

The study reported here is an attempt to describe slug flow features and characteristics so as to provide for a deeper understanding of its governing rules and relevant parameters.

6.2 Suggestions for future work

The experimental study on slug flow for the mix scenario (laminar regime in the main liquid and turbulent regime in the near-wake bubble region) has shown that the experimental average bubble velocity in undisturbed conditions does not follow the correlation-based predictions in the literature (Nicklin et al., 1962). As mentioned previously, a possible explanation is that, in continuous co-current operation, the liquid slugs may not be long enough to allow for the full development of the laminar velocity profile. Still, it would be interesting to assess the veracity of this explanation. For that purpose, the velocity profiles in the liquid ahead of trailing bubbles would have to be measured. Such a task could be accomplished using Particle Image Velocimetry, for instance.

The experimental technique proposed in this work was used for the study of co-current continuous slug flow for water and acqueous glycerol solutions (Newtonion liquids). However, without any adaptation, the same technique could be used for the study of slug flow in other liquids, such as non-Newtonian ones. This would contribute to deepen the knowledge of slug flow pattern, with liquids also of great interest for industrial applications. Furthermore, the resulting experimental data could be used to equip the SFS tool with correlations for simulating successfully slug flow pattern for those liquids.

The SFS tool developed in this thesis considers only non-aerated liquid slugs. Although the simulation results obtained for all flow regimes do not seem to be significantly affected by this simplification (judging by the agreement between simulation results and experimental data), it could still be interesting to refine the algorithm in order to accommodate different levels of slug aeration. These could be retrieved using models in literature or determined by an experimental technique to be developed. From the simulation point of view, the problem of the expansion of the small bubbles in the liquid slug would have to be tackled, which would add to an even more realistic simulation of the slug flow pattern.

A On the gas expansion and gas hold-up in vertical slugging columns – a simulation study[6]

A.1 Abstract

A study on the gas phase expansion and gas hold-up occurring in free bubbling vertical slug flow is reported. A slug flow simulator (SFS) supported by air-water experimental data was used for this purpose. The study was accomplished by implementing in the simulator the gas phase expansion along the column. Effects over bubble lengths and bubble velocities were considered. The flow in 6.5 m and 20 m long columns with internal diameter of 0.032 m was simulated. Expansion of gas phase along the column is shown to slightly decrease the occurrence of bubble coalescence. Liquid free-surface oscillations (due to bubble burst events and continuous inlet of liquid and gas in the column) were found to affect the expansion of the gas phase, especially for high gas flow rates. The gas phase expansion for different outlet column configurations was studied. The use of a high and large cross-sectional tank (to dampen free-surface oscillations) is shown not to assure a permanent expansion rate of the gas phase. Simulations with and without gas expansion along the column were compared for the computation of average flow parameters. Approximate approaches (with constant U_G, corrected for the mid-column pressure) were found suitable for the prediction of the average slug length and gas hold-up. Those approaches are, however, inadequate for the computation of the average bubble length and velocity along the vertical coordinate of the column.

[6] Based on the paper by T. Sotto Mayor, A.M.F.R. Pinto and J.B.L.M. Campos, accepted for publication in Chemical Engineering Processing (CEP)

A.2 Introduction

Gas-liquid mixtures flow in pipes in different flow patterns which depend on flow rates, fluid properties, pipe diameter, inclination and configuration. Slug flow is one of these flow patterns and can be characterized by the flowing of long bubbles (known as Taylor bubbles) occupying most of column cross-sectional area, separated by more or less aerated liquid plugs (termed slugs). It is a complex, irregular and intermittent phenomenon that can be found in several engineering applications (various types of reactors, membrane processes or extraction and transportation of hydrocarbons, just to mention a few) and even in natural phenomena (e.g. volcanic events).

Much of the primary modelling of slug flow was based on the early works of Dumitrescu (1943), Davies and Taylor (1950) and Nicklin et al. (1962). They set the bases for the first understanding of two-phase slug flow pattern. Several works followed focussing different aspects of such flow pattern (e.g. White and Beardmore (1962), Collins et al. (1978), Fabre and Liné (1992)).

The numerical simulation of two-phase vertical slug flow pattern has been attempted by several researchers (e.g. Barnea and Taitel (1993), Hasanein et al. (1996), Van Hout et al. (2001)). It serves as a tool for the study of the influence of several phenomena over the development of the flow, as well as an outcome predictor for any process/application in which this flow occurs. The usual approach requires the input of bubble-to-bubble interaction correlations relating the trailing bubble velocity to the length of the liquid slug ahead of the bubble. Different interaction correlations have been proposed (e.g. Hasanein et al. (1996), Van Hout et al. (2001), Sotto Mayor et al. (2006a)) depending, for instance, on experimental conditions, fluid properties, flow regimes, etc.. The simulation of slug flow pattern is often achieved, however, without accurate implementation of the gas phase expansion along the column (in terms of effect over bubble length and over bubble velocity). Two workarounds to address this problem are often implemented. The simplest one involves performing the flow simulation based on gas related parameters given at ambient pressure (e.g. Barnea and Taitel (1993), Hasanein et al. (1996)). A more elaborate approach involves correcting those parameters for the pressure at the middle of the column (e.g. Coelho Pinheiro et al. (2000)). These are, nevertheless, approximate approaches which comprise limitations that should be considered while elaborating on data obtained in that way. In addition, there can be operating conditions whose simulation may not produce reasonable results when using such approximate approaches (for instance regarding the simulation of the flow in long columns). There is thus a need for input in this area.

Two-phase flows are known to play a relevant role in volcanic events. Slug flow is believed, for instance, to be responsible for Strombolian eruptions at basaltic volcanoes (Seyfried and Freundt (2000)). There are also reports associating bubble coalescence and rise to both tremor and eruption seismic signals (e.g. Chouet et al. (2003)). In addition, bubble formation, ascent and burst at the surface are often related to strong pressure oscillations during volcanic events (James et al. (2004)). But these issues are also relevant for Industry in terms of the structural integrity of facilities (for instance in hydrocarbon and natural gas extraction plants). Thus, the implementation of the gas phase expansion in a slug flow simulator can be an asset to promote a deeper understanding of the flow dynamics at the source of those phenomena.

The main goal of this work is to provide information on the influence of the gas phase expansion over the evolution of the slug flow pattern in vertical columns. An algorithm for implementation of gas phase expansion along the column is proposed and subjects like the column outlet configuration and its influence on the gas expansion rate, the pressure and bubble velocity oscillations and the gas hold-up inside the column are addressed.

A.3 Experimental work

A series of air-water co-current slug flow experiments (Sotto Mayor et al. (2006a)) were performed in a 6.5 m long acrylic vertical column (0.032 m internal diameter). An image analysis technique (Sotto Mayor et al. (2006b)) was used to collect data on the flow pattern characteristics, at two vertical coordinates (3.25 m and 5.40 m from the base of the column) and for several superficial gas and liquid velocities (U_G and U_L up to 0.26 m/s and 0.20 m/s, respectively). The operating conditions were designed to have turbulent regime in the main liquid and in the near-wake bubble region. Two types of approaches were pursued while scrutinizing the flow frames: the *moving-point data analysis* and the *fixed-point data analysis*. The former allowed the establishment of an empirical bubble-to-bubble interaction curve for velocity, governing the approach and coalescence of consecutive bubbles, and the latter allowed to gather information on bubble characteristics (length, velocity, distance) at a given vertical coordinate.

Similar bubble-to-bubble interaction curves (velocity-wise) were obtained at the two vertical coordinates tested, for all the superficial gas and liquid velocities studied. The obtained average bubble-to-bubble interaction curve is shown in Figure A.1a, together with the best fit equation. The form and parameters of this equation are shown below:

$$\frac{U_i^{\text{trail}}}{U_B^{\text{exp}}} = 1 + 2.4e^{-0.8\left(\frac{h_{s,i-1}}{D}\right)^{0.9}} \tag{A.1}$$

where D is the column internal diameter (ID), U_i^{trail} refers to the velocity of the trailing bubble i, flowing behind a liquid slug with length $h_{s,\,i-1}$ and U_B^{exp} is the experimental average upward bubble velocity in undisturbed conditions. The estimates of U_B^{exp} are plotted against the superficial mixture velocity ($U_M = U_L + U_G$) in Figure A.1b, together with the Nicklin et al. (1962) predictions for co-current flow in turbulent regime. The Nicklin correlation is of the form:

$$U_B = U_\infty + CU_M \tag{A.2}$$

where U_∞ is the drift velocity and C an empirical parameter related to the velocity profile in the liquid. The drift velocity in a 0.032 m ID column equals 0.196 m/s (inertia-controlled regime; White and Beardmore (1962)) whereas parameter C equals 1.2 for turbulent regime in the liquid (Nicklin et al. (1962)). The agreement between the experimental estimates of U_B^{exp} and the Nicklin predictions (Eq. (A.2)) is evident.

Besides the relations (A.1) and (A.2), crucial inputs for the simulation of the slug flow pattern, the experimental study allowed to collect a vast amount of data on the flow characteristics at the two vertical coordinates tested. These data provided the means for the validation of the simulation results (section A.5.1). The following chapter describes the assumptions and approaches of the slug flow simulator.

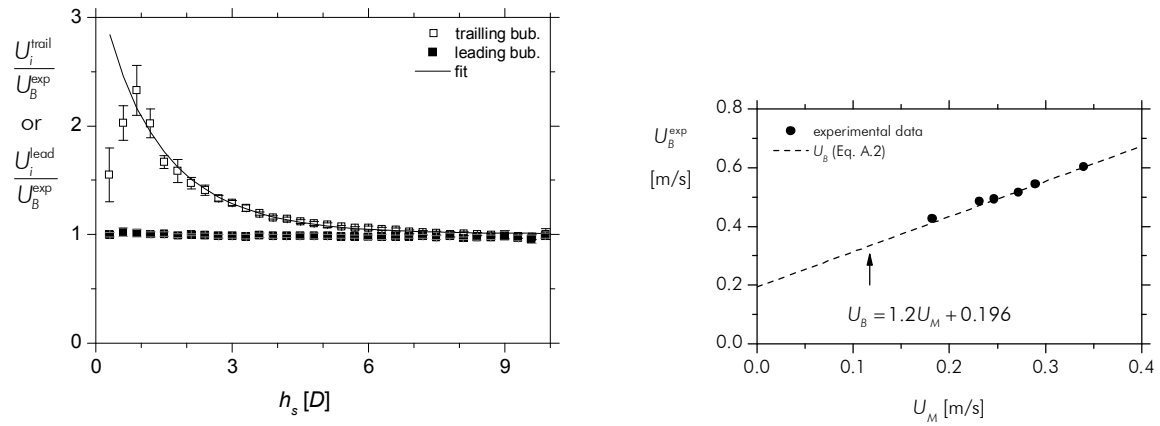

a b

Figure A.1 – (a) Average bubble-to-bubble interaction curve with 95% confidence intervals (vertical coordinates: 3.25 m and 5.4 m) and (b) experimental average upward bubble velocity plotted against U_M after correction for vertical coordinate 5.4 m; internal diameter: 0.032 m; data after Sotto Mayor et al. (2006a)

A.4 Slug flow Simulator

The following sections describe the main assumptions of the slug flow simulator.

A.4.1 Onset of the simulation

A given number of randomly distributed liquid slugs (and Taylor bubbles) is assumed to enter the column at its base. These distributed variables "introduce" in the simulation the effect of the gas injection system (in terms of the length of the gas bubbles and liquid slugs formed). The slug length (normal) distribution is prepared using Box Muller algorithm (Campos Guimarães and A. Sarsfield Cabral (1997)) and the bubble length distribution is prepared as a dependent distribution (i.e. a function of the slug length distribution). Assuming a cylindrical bubble shape, one can write:

$$U_G S_c \Delta t_i = S_b h_{b,i} \tag{A.3}$$

where Δt_i is the time interval required for the entrance in the column of a unit cell (i.e. bubble + slug), $h_{b,i}$ is length of bubble i and S_b and S_c stand for the bubble and the column cross-sectional area, respectively. The estimate of S_b is computed based on the liquid film thickness determined following Brown (1965) for free-falling conditions. At the column inlet, bubbles are assumed to rise at their undisturbed velocity, $U_B^{\exp}$, and thus:

$$U_B^{\exp} \Delta t_i = h_{b,i} + h_{s,i} \tag{A.4}$$

By combining the previous equations and rearranging one obtains:

$$h_{b,i} = \frac{h_{s,i}}{\frac{S_b U_B^{\exp}}{S_c U_G} - 1} \tag{A.5}$$

The previous equation establishes the relation between the elements of the liquid slug distribution and the elements of the bubble length distribution that assure, at the column inlet, a given U_G and U_L (inputs to the simulation). The use of Eq. (A.5) for each unit cell allows thus to prepare the bubble length distribution as a function of the liquid slug length distribution. With the distributions of bubble length and liquid slug length at the column inlet, it is then possible to simulate the process of evolution of these distributions along the column.

A.4.2 Bubble motion along the column

The displacement of bubbles along the column is implemented as the incremental movement of their boundaries (bubble nose and rear). The position of the i^{th} bubble rear, at instant t_{j+1}, $z_{rear,i}^{t_{j+1}}$, is computed by updating its position at t_j, $z_{rear,i}^{t_j}$, according to its velocity (U_i).

$$z_{rear,i}^{t_{j+1}} = z_{rear,i}^{t_j} + U_i (t_{j+1} - t_j) \tag{A.6}$$

The velocity of the bubble i (U_i) has two contributions: one related to the length of the liquid slug ahead of it (Eq. (A.1)), and another related to the expansion of the gas bubbles flowing below. This latter contribution will be described in detail in the following section. The position of the bubble nose is updated using:

$$z_{nose,i}^{t_{j+1}} = z_{rear,i}^{t_{j+1}} + h_{b,i}^{t_{j+1}} \tag{A.7}$$

Taking the boundaries of two consecutive bubbles, the length of the liquid slug flowing between them is given by:

$$h_{s,i}^{t_{j+1}} = z_{rear,i}^{t_{j+1}} - z_{nose,i+1}^{t_{j+1}} \tag{A.8}$$

Eqs. (A.6)-(A.8) are used for all bubbles flowing in the column, at every time increment.

A.4.3 Expansion of the gas phase along the column

As gas bubbles move upwards in the column, the pressure acting on each bubble decreases and, consequently, bubbles expand. Discarding the pressure drops in the liquid phase (at the wall and at the wake of the bubbles) the pressure along the column can be predicted taking only the hydrostatic pressure gradient. If one holds, then, the hydrostatic pressure at a given vertical coordinate, one can estimate the volume (or length) of a bubble, at that location, by using the *ideal gas law*. However, that computation requires an a priori knowledge of the number of moles of air in each bubble. This parameter can be assessed, for instance, at the base of the column (inlet position) where the hydrostatic pressure can easily be computed.

A.4.3.1 Evaluation of the amount of air in a bubble

Consider Figure A.2a representing the instant a bubble *i* enters the simulation domain. The fact that some bubbles are already inside the column, means the pressure acting on the bubble at the inlet, is smaller than it would be if the column was full of liquid. Furthermore, given that the axial pressure gradients along the (free-falling) liquid films are negligible and that the pressure recovery at the rear of the bubbles (when the liquid films slow down) is proportional to the amount of liquid in the films, one can compute the hydrostatic liquid height above a bubble *i* ($H_{hyd,\,i}$) taking only the liquid inside the column (as if the Taylor bubbles were removed from the column). Thus, for the scenario depicted in Figure A.2a, one can write:

$$H_{hyd,,i} = z_{liq.} - \frac{S_b}{S_c}\sum_{k=1}^{i-1} h_{b,k} \tag{A.9}$$

where $z_{liq.}$ refers to the coordinate of the liquid free-surface.

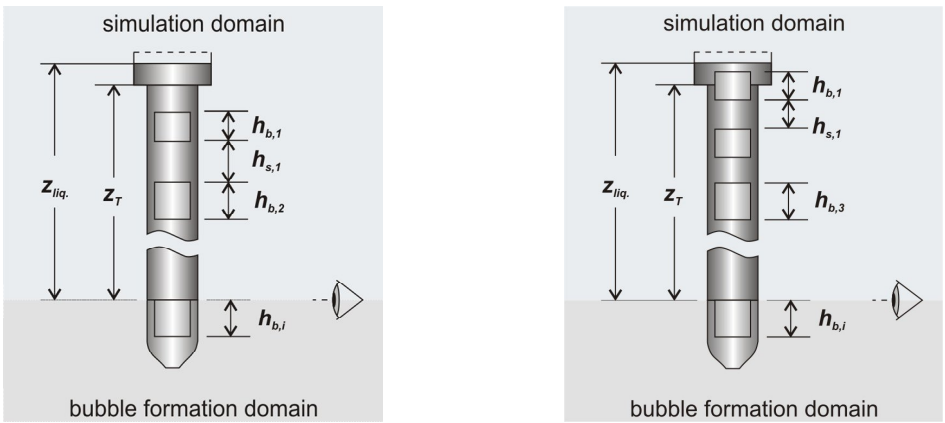

Figure A.2 – Representation of the upward movement of a Taylor bubble at column inlet with (a) bubbles only inside the column and (b) bubbles entering the tank

Let us consider now the slightly more complex scenario of computing $H_{hyd,\,i}$ when one bubble is crossing the base of a tank (z_T) placed at the top of the column. This scenario is depicted in Figure A.2b. Given that the tank cross-sectional area is considerably higher than the column's, it is reasonable to assume that the pressure at the base of the tank depends only on the height of liquid above that position ($z_{liq} - z_T$), regardless of the presence of a bubble entering the tank (or even totally inside the tank). However, the portion of a bubble still inside the column (i.e. below z_T) should not be neglected when computing the hydrostatic liquid height above the bubble at the column inlet ($H_{hyd,\,i}$). The volume of liquid inside the column is reduced by the presence of a bubble crossing the tank base (or totally inside the column) and, consequently, the pressure acting on the

bubble at the column inlet is also reduced. Thus, one must consider a new parameter, α_k, informing on the positioning of the bubbles relative to the tank base. It should be defined as follows:

$$\begin{cases} \text{bubbles totally inside the column} & \Rightarrow \ \alpha_k = 1 \\ \text{bubbles crossing the tank base} & \Rightarrow \ \alpha_k = (z_T - z_{rear,k}) / h_{b,k} \\ \text{bubbles totally inside the tank} & \Rightarrow \ \alpha_k = 0 \end{cases} \tag{A.10}$$

A more general form of Eq. (A.9) can, then, be written:

$$H_{hyd,i} = z_{liq.} - \frac{S_b}{S_c} \sum_{k=1}^{i-1} \left(h_{b,k} \, \alpha_k \right) \tag{A.11}$$

which allows the computation of the hydrostatic liquid height above a bubble *i*, at the column inlet, in all possible scenarios (bubbles only inside the column, bubbles crossing the tank base, bubbles inside the column and inside the tank). For instance, the presence of a bubble totally inside the tank does not alter the pressure acting at the column inlet and, in agreement with this, the summation in the previous equation does not depend on the length of such a bubble (since α_k=0).

Having defined the hydrostatic liquid height above a bubble *i* at the inlet coordinate, the corresponding hydrostatic pressure can be computed as:

$$P_{hyd,i} = \rho \, g H_{hyd,i} \tag{A.12}$$

where ρ is the density of the liquid and *g* the acceleration of gravity. An algebraic transformation of the *ideal gas law* with further substitution of the pressure according to Eq. (A.12) yields an expression that computes the amount of air in a bubble *i*, at the inlet coordinate:

$$n_i = \frac{h_{b,i} \, S_b \left(P_{atm} + \rho \, g H_{hyd,i} \right)}{RT} \tag{A.13}$$

where P_{atm} stands for ambient pressure, *T* refers to the temperature, *R* is the *ideal gas* constant and n_i is the number of moles of air in bubble *i*. Eq. (A.13) Should be used for all bubbles entering the column in order to gather information on the number of moles of air in each bubble. This information is needed to predict the bubble length as bubbles move along the column. The following section addresses this issue.

A.4.3.2 Effect over the length of the bubble

Figure A.3 illustrates an instant in the upward movement of bubbles inside the simulation domain. The hydrostatic liquid height above bubble *i* is given by an expression similar to Eq. (A.11) with a correction to account for the positioning of the bubble ($z_{nose,\,i}$).

$$H_{hyd,i} = z_{liq.} - z_{nose,i} - \frac{S_b}{S_c}\sum_{k=1}^{i-1}\left(h_{b,k}\,\alpha_k\right) \tag{A.14}$$

Taking Eq. (A.13) and transforming it to isolate $h_{b,\,i}$, one obtains:

$$h_{b,i} = \frac{n_i\,RT}{S_b\left(P_{atm} + \rho\,g\,H_{hyd,i}\right)} \tag{A.15}$$

where $H_{hyd,\,i}$ is now given by Eq. (A.14). Knowing the positioning of a bubble *i*, Eq. (A.15) allows the computation of its length as a function of the hydrostatic pressure acting on it. This is not, however, a sequential calculation. The length of a bubble is a function of the vertical coordinate of the bubble nose (see Eq. (A.15)) whose computation, in turn, requires an estimate of the length of the bubbles (see Eq. (A.7)). This requires thus an iterative approach. After using Eq. (A.6) to update the positioning of every bubble rear, the "new" lengths of the bubbles are determined by iterating Eqs. (A.7), (A.14), (A.15), (A.7), … until convergence is attained.

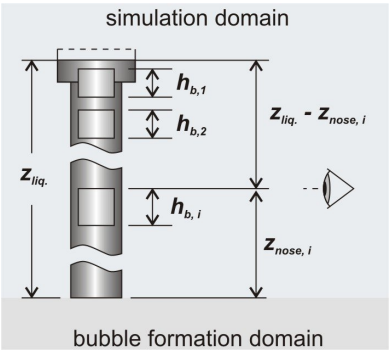

Figure A.3 – Representation of the upward movement of a Taylor bubble inside the column

A.4.3.3 Effect over the velocity of the bubble

The bubble expansion is seen as a rise of the bubble nose region (reference frame attached to the bubble). Therefore, bubble expansion results in the upward displacement of everything ahead of the bubble (liquid and gas) by an amount proportional to the expansion of the bubble. Consider Figure A.4, representing the position of several bubbles, flowing upwards in a

column, at instant t_j. Consider that, at instant t_{j+1} all bubbles had their positions updated according to their velocity (see Eq. (A.6)). The hydrostatic height above each bubble decreased from instant t_j to t_{j+1} and, therefore, all bubbles expanded accordingly (as described in the previous section).

Consider bubble *i*, in white in Figure A.4, and the liquid flowing ahead of it (zone A). The expansion of the bubbles under bubble *i* induces a raise in the liquid and gas ahead of them, proportional to the sum of the individual expansions undergone by each bubble (Δh_1, ..., Δh_n), and given by:

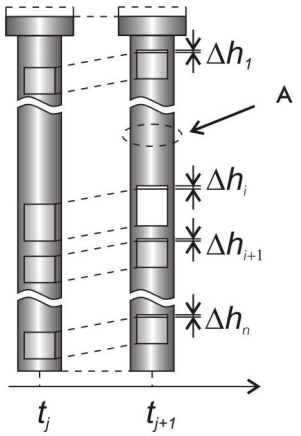

Figure A.4 – Two consecutive moments in the upward movement of bubbles

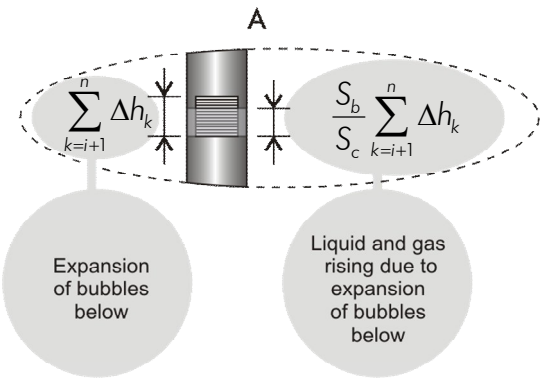

Figure A.5 – Liquid and gas rise ahead bubble *i* due to the expansion of bubbles below it (zone A in Figure A.4)

$$\Delta z_{\text{expans.}}^{\text{ahead } i} = \frac{S_b}{S_c} \sum_{k=i+1}^{n} \Delta h_k \qquad \text{(A.16)}$$

This "extra" upward displacement of liquid and gas (Figure A.5) can be seen as an increase in the superficial liquid and gas velocities. This increase can be calculated dividing $\Delta z_{\text{expans.}}^{\text{ahead } i}$ by the time increment between the two consecutive instants under focus ($t_{j+1} - t_j$), as in the following equation:

$$\Delta U_{\text{expans.}}^{\text{ahead } i} = \frac{\Delta z_{\text{expans.}}^{\text{ahead } i}}{t_{i+1} - t_i} = \frac{S_b}{(t_{i+1} - t_i) S_c} \sum_{k=i+1}^{n} \Delta h_k \tag{A.17}$$

where $\Delta U_{\text{expans.}}^{\text{ahead } i}$ is the increase in the flow velocity ahead of bubble *i*, due to the expansion of all bubbles flowing below it.

The upward velocity of gas bubbles flowing in a co-current liquid flow depends on the velocity profile in the liquid phase. This dependence is usually introduced by parameter *C* (equal to the ratio between the maximum and average liquid velocity), whose value depends on the flow regime (or velocity profile) in the liquid. Thus, the overall velocity of a bubble flowing in co-current flow is the result of two contributions: one related to the length of the liquid slug ahead of it (Eq. (A.1)), and another related to the "extra" upward displacement of the liquid and gas due to the gas phase expansion (Eq. (A.17)). The following equation allows the computation of the overall velocity of the bubble *i*, in a train of bubbles flowing upwards:

$$U_i = U_B^{\exp} \left[1 + 2.4 e^{-0.8 \left(\frac{h_{s,i-1}}{D} \right)^{0.9}} \right] + \frac{C S_b}{(t_{i+1} - t_i) S_c} \sum_{k=i+1}^{n} \Delta h_k \tag{A.18}$$

where the experimental average upward bubble velocity is computed by a transformed version of Nicklin's equation:

$$U_B^{\exp} = U_\infty + C(U_L + U_G^{inlet}) \tag{A.19}$$

where U_G^{inlet}, the superficial gas velocity at the inlet coordinate, is used instead of U_G in order to estimate the undisturbed upward bubble velocity discarding the effect of the gas phase expansion along the column. Recall that this effect is computed by the last parcel of the right hand side of Eq. (A.18). Correlation-based values of U_∞ and *C* (0.196 m/s and 1.2, respectively) were used in the simulations. The overall bubble velocity, given by Eq. (A.18), is used in Eq. (A.6) to update the position of bubble boundaries, implementing thus the bubble displacement.

A.5 Simulation results

Three major topics are addressed in this section: the validation/benchmarking of the simulator, the gas expansion along the column and the gas hold-up in the column.

A.5.1 Simulation validation/benchmarking

In this section, a brief comparison between experimental data and simulation results is shown, concerning two column internal diameters: 0.032 and 0.024 m. The experimental data for the larger column is thoroughly described in Sotto Mayor et al. (2006a) while the data for the narrower column are taken from Van Hout et al. (2001), Van Hout et al. (2003). The simulation results were obtained introducing at the inlet of the columns normally distributed slug lengths ($\mu \approx 5D$ and $\sigma \approx 2D$). The characteristics of the inlet distributions were found, however, not to determine the flow pattern obtained at the column outlet (see section A.5.2).

Two different flow conditions ($U_L \approx 0.10$ m/s and $U_G \approx 0.088$ m/s; $U_L \approx 0.10$ m/s and $U_G \approx 0.26$ m/s) are addressed for the larger column (0.032 m, 6.5 m long). Figure A.6 shows the comparison for data at 5.4 m from the base of the column.

There is a very good agreement between experimental data and simulation results regarding the most probable value (mode) of the bubble velocity distributions (Figures A.6a and A.6d), for both flow conditions.

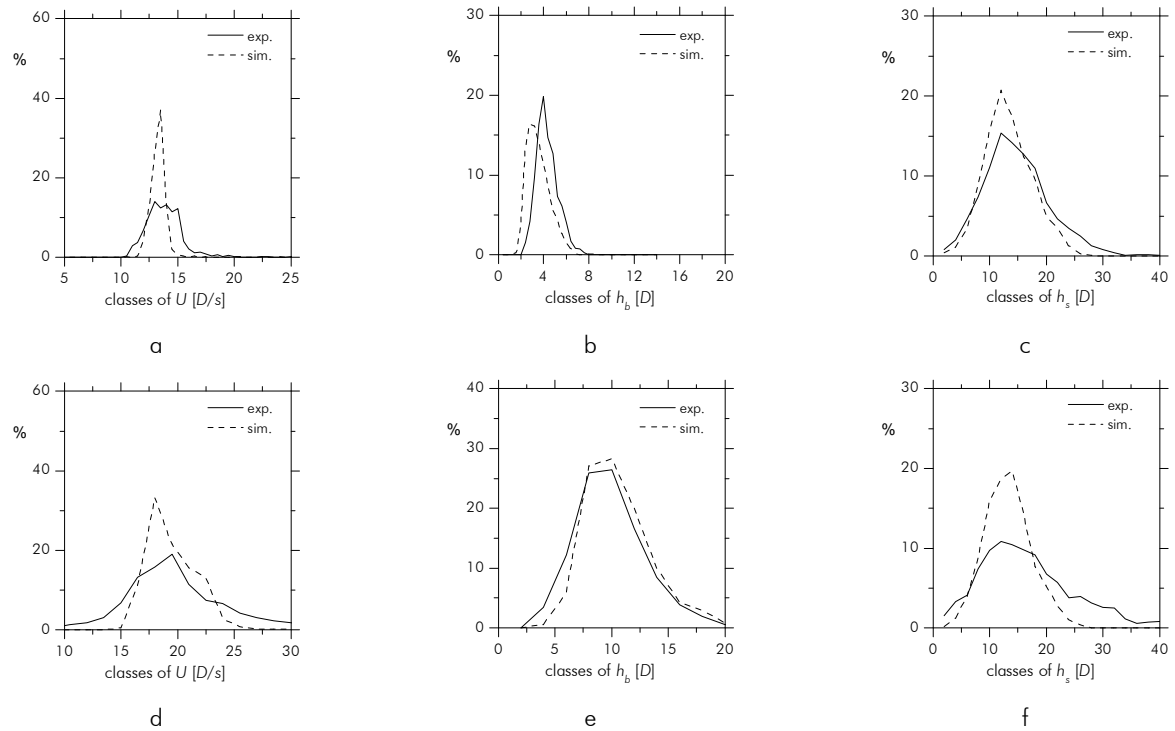

Figure A.6 – Frequency distribution curves: (a) bubble velocity, (b) bubble length and (c) slug length, for an experiment/simulation with $U_L \approx 0.10$ m/s and $U_G \approx 0.088$ m/s; (d) bubble velocity, (e) bubble length and (f) slug length, for an experiment/simulation with $U_L \approx 0.10$ m/s and $U_G \approx 0.26$ m/s; 0.032 m ID; vertical coordinate: 5.4 m

The corresponding standard deviations are, however, slightly different. The bubble length distributions from the simulations of both flow rate conditions represent the corresponding

experimental data reasonably well (Figures A.6b and A.6e). There is a slight underestimation, however, for the lower flow rate condition. The slug length distributions from the simulations of both flow conditions are in good agreement with the experimental data (Figures A.6c and A.6f). Notice in particular the matching between the experimental and the simulation data for the most probable slug length value.

Figure A.7 shows the comparison between experimental and simulation data for the narrower column (0.024 m, 10 m long), regarding again two different flow conditions ($U_L \approx 0.01$ m/s and $U_G \approx 0.41$ m/s; $U_L \approx 0.10$ m/s and $U_G \approx 0.63$ m/s). The simulations are based on estimates of U_B^{exp} according to Nicklin et al. (1962) correlation for co-current flow in turbulent regime (Eq. (A.2), with $C=1.2$ and $U_\infty=0.17$ m/s, after White and Beardmore (1962)). Focus is put on data at 6.88 m from the base of the column.

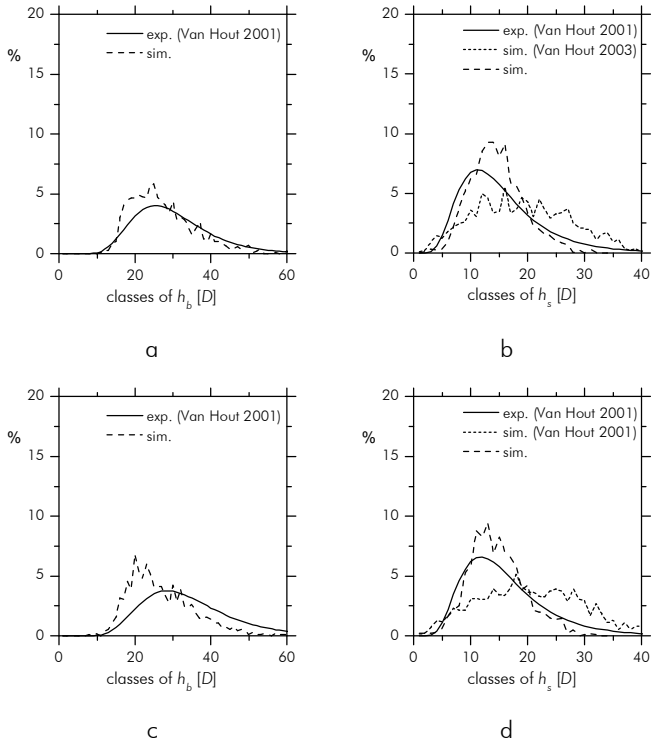

Figure A.7 – Frequency distribution curves of (a) bubble length and (b) slug length, for an experiment/simulation with $U_L \approx 0.01$ m/s and $U_G \approx 0.41$ m/s; (c) bubble length and (d) slug length, for an experiment/simulation with $U_L \approx 0.10$ m/s, $U_G \approx 0.63$ m/s; 0.024 m ID, vertical coordinate: 6.88 m

A very reasonable agreement between experimental data and simulation results is obtained, for both flow rate conditions, regarding the frequency distribution curves for bubble length (Figures A.7a and A.7c) and for liquid slug length (Figures A.7b and A.7d). The simulated frequency distribution curves from Van Hout et al. (2001), Van Hout et al. (2003) for the slug length variable are also shown in Figures A.7b and A.7d (the curves were drawn directly from the charts of the mentioned publications). From the analysis of these curves it can be concluded that a

better representation of the reported experimental data is obtained by using the simulator described in the present work.

In the light of the results discussed in this section, the proposed simulation approach emerges as a step towards a more accurate simulation of the slug flow pattern.

A.5.2 On the influence of the inlet slug length distribution

In a slug flow experiment, the characteristics of the flow pattern obtained at the column inlet depend on the type of gas injection system used. The gas injection systems influences, for instance, the mode and the standard deviation of the distributions of bubble length and liquid slug length obtained at that coordinate. However, the differences in the inlet distributions tend to dissipate along the column due to coalescence. Furthermore, the length of column along which the influence of the different inlet distributions (the entrance effects) can be observed is usually known as the entrance length of slug flow. Note that we do not follow the terminology of some researchers that relate the entrance length to the column length required to have fully developed slug flow. The entrance length concept adopted here (related to the dissipation of the entrance effects) is based on the idea that different inlet flow patterns evolve along the column to a single flow pattern. The column length required to have the single flow pattern is highly relevant, for instance, when choosing the vertical (column) coordinate at which to validate the simulation algorithm.

For the purpose of studying the dissipation of the entrance effects along the column, three similar simulations were performed for a 6.5 m long column (0.032 m ID). These differed only in the slug length distributions introduced at the column inlet. Three normal distributions centred on 2*D*, 5*D* and 8*D* were considered. Their evolution along the column was monitored at several observation points (in steps of 0.6 m). The frequency distribution curves of h_b and h_s obtained, for each simulation, at each observation point, were compared schematically. The maximum relative differences between those curves (focussing the average and the mode) are plotted against the vertical coordinate of the column in Figure A.8a. This figure confirms that the inlet differences dissipate along the column. Despite the differences in the inlet distributions, similar frequency distribution curves are obtained for vertical column positions above 65*D*, when $U_L \approx 0.10$ m/s and $U_G \approx 0.26$ m/s (accepting a maximal difference of 10%). Thus, 65*D* is the entrance length of the slug flow for the mentioned operating conditions (U_L and U_G). Extending the aforementioned approach to a set of increasing superficial gas and liquid velocities, one obtains the chart of Figure A.8b, showing the entrance length of slug flow for U_G and U_L in the range 0.10-0.50 m/s. For this range, the entrance length of slug flow varies between 50*D* and 70*D*. Note that the two vertical

coordinates at which the experimental data were collected (3.25 m and 5.40 m, i.e. 102*D* and 169*D*, respectively) are far above the mentioned entrance-length range. Thus, no entrance effects are likely to be affecting the experimental data collected. In addition, the fact that the simulation results above 70*D* are free from entrance effects (i.e. not dependent on the particular flow pattern characteristics at the column inlet), and that those results are in good agreement with the obtained experimental data (section A.5.1), is a further corroboration of the accurateness, robustness and usefulness of the proposed simulator.

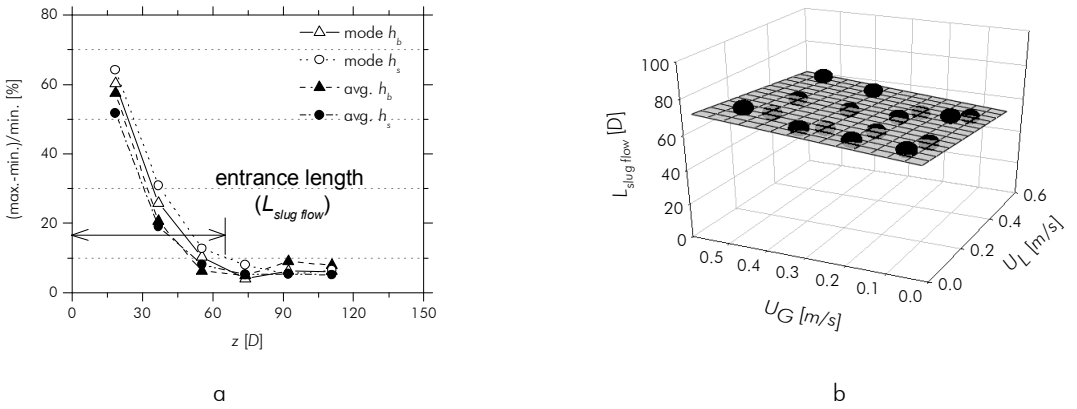

a b

Figure A.8 – (a) Maximal relative difference of the mode and average (h_b and h_s) along the column, for simulations with increasing average inlet slug lengths (2*D*, 5*D* and 8*D*), $U_L \approx 0.10$ m/s and $U_G \approx 0.26$ m/s; (b) entrance length of slug flow for simulations with U_L and U_G equal to 0.10, 0.23, 0.36 and 0.50 m/s; 0.032 m ID

A.5.3 On the gas expansion inside the column

A.5.3.1 Effect of gas expansion over bubble coalescence

A singular simulation was done in order to isolate the effect of the gas phase expansion over the flow development along the column. Non-distributed liquid slug lengths were considered at the inlet of the column and the bubble-to-bubble interaction was discarded. The former constrain assures that every liquid slug (and gas bubble) enters the column featuring equal length. Additionally, the fact that no bubble-to-bubble interaction is implemented in the upward movement of the bubbles guarantees that any evolution of the flow characteristics can be ascribed to the gas phase expansion. The simulation refers to a 6.5 m long column with 0.032 m internal diameter, equipped with a large cross-sectional tank at the column outlet. In Figure A.9, the length of bubbles (h_b) and liquid slugs (h_s) and the velocity of bubbles (U) are plotted against the column vertical coordinate, for a given instant after the start-up of a simulation.

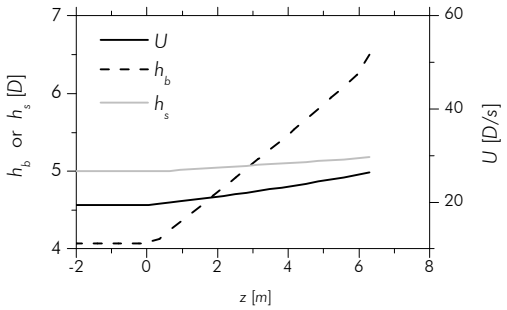

Figure A.9 – Bubble length, slug length and bubble velocity along the vertical coordinate of the column, for a given instant (simulation discarding bubble-to-bubble interaction and with constant values of bubble length, slug length and bubble velocity at the inlet)

The origin of the vertical coordinate (horizontal axis) is positioned at the base of the column. The expansion of the gas phase is computed only about that position. Above the column inlet, and due to the onset of the gas expansion, bubble and slug lengths as well as bubble velocity increase along the column.

Although the increase in the length of the bubbles (above inlet) can be directly related to the expansion of the gas phase, a deep analysis of all the effects influencing the flow pattern is required to fully interpret the variation of the liquid slug length along the column (increasing slightly). According to Eq. (A.18), the velocity of a bubble *i* flowing in the column has a contribution related to the expansion of the bubbles flowing below (last parcel of the right hand side of the equation). This means that the first bubble (from top to bottom), of a train of bubbles flowing in the column, has its velocity affected by the expansion of more bubbles than does, for instance, the 2nd bubble (flowing below the 1st). Consequently, this "extra" velocity, due to expansion, is higher for the 1st bubble than for the 2nd bubble, which is, in turn, higher than for the 3rd bubble, and so on. These ordered relations ($U_1 > U_2 > U_3$, …, clearly perceivable in Figure A.9) lead to the increase in the length of the liquid slugs as the train of bubbles flow upwards (see previous figure). This shows, therefore, that the gas expansion phenomenon slightly "opposes" to the merging of consecutive bubbles (coalescence) as it induces the increase (though smooth) in the length of the slugs. It is, nevertheless, a limited effect.

The fact that gas phase expansion has limited influence over the phenomenon of bubble coalescence points out a possible strategy for further assessing the correctness of the gas expansion algorithms proposed in section A.4.3. Under this assumption it is reasonable to expect that an approximate flow simulation, performed without gas expansion along the vertical coordinate, produces, at a given vertical coordinate, average flow parameters (such as bubble length, bubble velocity or liquid slug length) that are similar to those obtainable by a simulation featuring gas expansion. However, this matching is only likely to happen when the U_G estimate introduced in the approximate simulation (without gas phase expansion) is corrected for the

pressure at the vertical coordinate in question. To compute that, one must have information on the gas hold-up inside the column. For this purpose, the average gas hold-up was computed based on instantaneous gas hold-ups obtained at every second of the simulation including gas expansion. Three types of simulations were then performed: one considering gas expansion as described previously and two approximate approaches based on U_G estimates corrected for the mid- and top-column pressure, respectively. These two approaches are, ultimately, often implemented in many gas-liquid systems (e.g. Barnea and Taitel (1993), Hasanein et al. (1996), Coelho Pinheiro et al. (2000)). The simulations address the flow in a 6.5 m long column with 0.032 m internal diameter, equipped with a large cross-sectional tank at the column outlet. The comparison focuses on the average liquid slug length (Figure A.10a-b), bubble length (Figure A.10c-d) and bubble velocity (Figure A.10e-f), at two vertical coordinates in the column (3.25 m and 6.40 m, charts on the left and on the right, respectively). A superficial liquid velocity equal to 0.10 m/s and superficial gas velocities in the range 0.10-0.50 m/s were used.

As evident in the charts of Figure A.10a-b, all three types of simulations (with and without gas expansion) produce very similar average liquid slug lengths. Indeed, the maximal relative deviation between these approaches reaches no more than 3%, for both column vertical coordinates, and for the ranges of U_L and U_G studied. This is in agreement with the results of Figure A.9, as it confirms that the evolution of slug length variable is not strongly affected by gas expansion. Figure A.10c-d and Figure A.10e-f present similar comparisons focussing on the average bubble length and velocity. It is possible to observe that, for both variables and at the two vertical coordinates, the simulation including gas expansion produces average results very similar to those obtained for the approximate simulations based on U_G estimates at the pressure of the corresponding vertical coordinate. For instance, in Figure A.10c (data at the mid-column coordinate), the results of the simulation featuring gas expansion match those for the simulation based on U_G estimates corrected for the mid-column pressure. It is also possible to observe that, the simulations based on U_G values corrected for pressure other than that of the corresponding vertical coordinate, originate rather different estimates of the average bubble length and velocity. For the chosen vertical coordinates (and corresponding U_G estimates), deviations of up to 22% and 12% were obtained for bubble length and bubble velocity, respectively. This fact was expected since gas expansion is known to play an important role in the evolution of these variables.

The results discussed here confirm, as postulated previously, the correctness of the proposed gas expansion algorithms. They provide, in addition, further corroboration that the gas phase expansion does not have a pronounced effect over the coalescence of bubbles along the column.

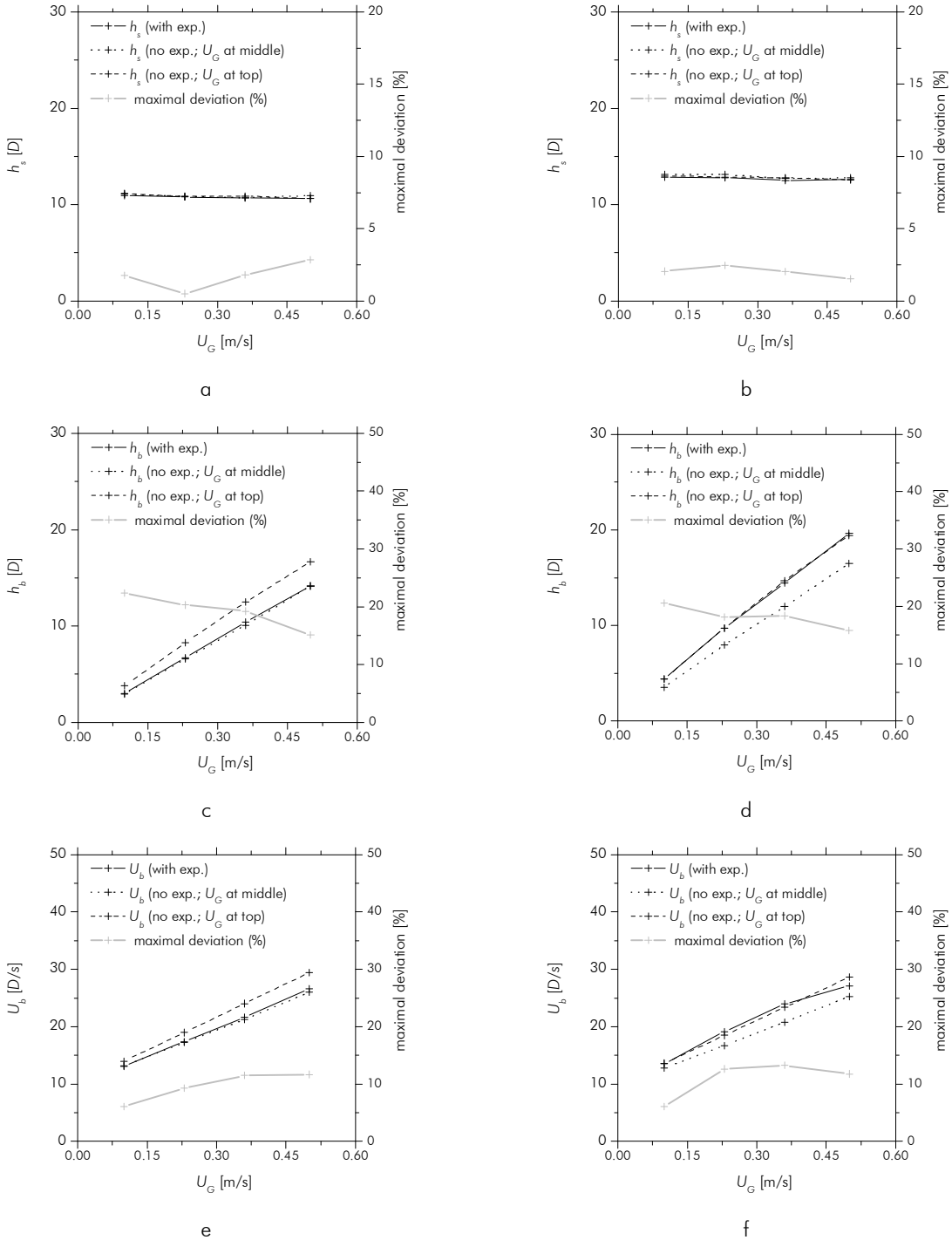

Figure A.10 – Average liquid slug length (a-b), bubble length (c-d) and bubble velocity (e-f) for simulations considering expansion (varying U_G) and discarding expansion (constant U_G equal to value at the middle or at the top of the column); $U_L \approx 0.10$ m/s and $U_G \approx 0.10$, 0.23, 0.36 and 0.50 m/s; column length: 6.5 m; outlet configuration: large tank; (a), (c) and (e) vertical coordinate: 3.25 m; (b), (d) and (f) vertical coordinate: 6.40 m

A.5.3.2 Relevance of gas expansion implementation in the assessment of flow parameters

As already discussed, it is possible to obtain reasonable average estimates of the flow parameters (such as h_b, U_b or h_s) even when simulating slug flow without gas expansion along the column, provided that the U_G value introduced in the simulation is corrected for the pressure at the vertical coordinate in question. This is, however a very unpractical procedure (when compared to the simulation including expansion along the column) since one simulation is required for every desired vertical coordinate. In addition, the correction of the U_G estimates for the pressure at a given vertical coordinate requires, as already mentioned, information on the average gas and liquid retention inside the column (in order to calculate the hydrostatic pressure at that coordinate). And still, this information may not be always available. Indeed, although gas hold-up values can be assessed, during a given slug flow experiment, by stopping the flow momentarily in order to measure the amount of liquid inside the column, this only provides instantaneous estimates of gas hold-up. Therefore, a correction of U_G based on such instantaneous (as opposed to average) gas hold-up estimate is accomplished with some degree of inaccuracy, which may result finally in the more or less inaccurate computation of the average flow parameters.

Finally, the implementation of the gas phase expansion along the column is a step towards a more accurate simulation of slug flow pattern. It enables a deeper study of the dynamic evolution of the flow and promotes a wider understanding of its governing rules.

A.5.3.3 Effect of the outlet configuration on the gas expansion rate

The expansion of gas bubbles along the column is a function of the hydrostatic pressure acting on the bubbles, which is, in turn, dependent on the coordinate of the liquid free-surface, among other parameters (see Eqs. (A.14) and (A.15)). Considering that the outlet configuration of the column influences the coordinate of the liquid free-surface (dampening effect), it is interesting to assess the extent of the influence of the outlet configuration over the gas expansion in the column. Three configurations are addressed: a column without a tank at the top (Figure A.11a), a column with a flat large cross-sectional tank at the top (Figure A.11b) and a column with a regular large cross-sectional tank at the top (Figure A.11c). These scenarios are discussed in the following sections.

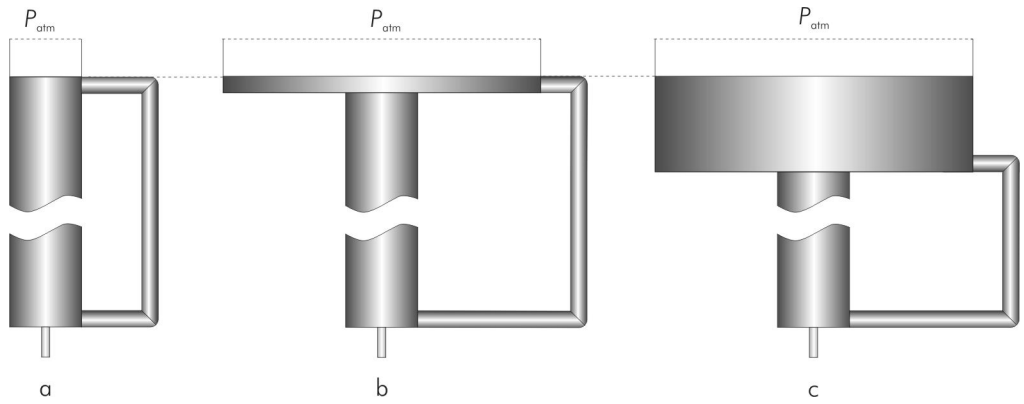

Figure A.11 – Column outlet configurations: (a) no tank, (b) flat large cross-sectional tank and (c) regular large cross-sectional tank

A.5.3.3.1 Column without a tank at the top (outlet)

The flow in a 6.5 m long column with internal diameter of 0.032 m was simulated considering superficial liquid and gas velocities (U_L and U_G) equal to 0.25 m/s and 0.36 m/s, respectively. Gas superficial velocity is given at ambient pressure. Gas expansion and bubble-to-bubble interaction is considered in the simulation. Focus is put on the evolution of the velocity of the first bubble along time. Notice that the so-called first bubble in the column changes every time a bubble reaches the liquid free-surface (2nd bubble becomes the new 1st bubble). The velocity of the first bubble (comprising and discarding gas expansion) is plotted against time in Figure A.12.

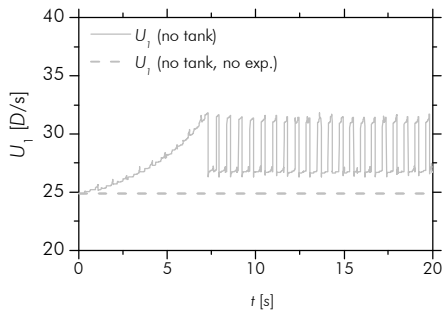

Figure A.12 – Values of the velocity of the first bubble along time for a simulation with $U_L \approx 0.25$ *m/s* and $U_G \approx 0.36$ *m/s*; without a tank at the column outlet

As expected, the velocity of the first bubble discarding the gas expansion contribution is constant and equal to the undisturbed upward bubble velocity as computed in Eq. (A.19). However, if the gas expansion contribution is considered, the evolution of the velocity of the first bubble is rather interesting. There is a continuous increase in U_1 in the first seconds of the simulation, followed by an oscillatory behaviour. The initial escalation of U_1 is related to the fact

that the simulation starts with the column full of liquid (no bubbles inside the column). As bubbles enter the column (increasing gas hold-up) the first bubble of the train is affected by the expansion of an increasing number of bubbles. Therefore, there is a continuous escalation of U_1 due to the increase in the last parcel of the right hand side of Eq. (A.18). This increase continues until the first bubble reaches the liquid free-surface. From that moment onward, an oscillatory behaviour is observed. In order to fully understand the causes of this behaviour special attention must be put in the evolution along time of other parameters as bubbles reach the liquid free-surface. Those parameters are the vertical coordinates of the liquid free-surface and of the nose of the first bubble, as well as the hydrostatic liquid height above the first bubble. These parameters are plotted against time in Figure A.13 (in the range 15-16.5 *s*).

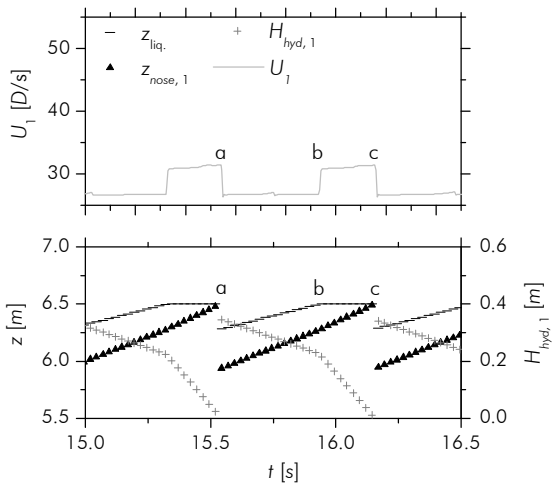

Figure A.13 – Plot of velocity and nose coordinate of the first bubble (U_1 and $z_{nose,\,1}$), hydrostatic liquid height above first bubble ($H_{hyd,\,1}$) and vertical coordinate of the liquid free-surface ($z_{liq.}$) along time, in the range 15-16.5 *s*; simulation with $U_L \approx 0.25$ *m/s* and $U_G \approx 0.36$ *m/s*; without a tank at the column outlet

Consider an instant ***a*** at which the first bubble of a train of bubbles reaches the liquid free-surface. At that instant, this interface, previously at 6.5 *m* (outlet coordinate) from the base of the column, drops instantly by an amount proportional to the height of the bubble exiting the column. Moreover, there is an "apparent" sudden drop in the coordinate of the nose of the first bubble, since the new first bubble (previously second bubble) is flowing somewhere below in the column. From that moment onward, the liquid free-surface will rise steadily due to the continuous entrance of gas and liquid in the column. This rise will continue until the liquid reaches again the outlet system (at 6.5 *m* from the base of the column; instant ***b***). At the same time, the new first bubble will rise in the column until it reaches the liquid free-surface (at instant ***c***). Considering that the hydrostatic liquid height above the first bubble is calculated as the difference between the liquid free-surface coordinate (z_{liq}) and the bubble nose coordinate ($z_{nose,\,1}$), it is obvious that this

parameter has different variation rates in time intervals ***a***-***b*** and ***b***-***c***. The movement of the liquid free-surface, in the time interval ***a***-***b***, accounts for this difference. As a direct consequence of the different variation rate of the pressure acting on the bubbles in these time intervals, different expansion rates occur. Indeed, the expansion of all bubbles flowing in the column between instants ***a*** and ***b*** is smaller than between instants ***b*** and ***c***. As a consequence, the expansion contribution for the velocity of the first bubble (but also for the remaining bubbles), in the former time interval is smaller than in the latter time interval. The aforementioned oscillatory behaviour of U_1 is, therefore, the result of the dynamic evolution of the liquid free-surface coordinate.

A.5.3.3.2 Column with a flat large cross-sectional tank at the top (outlet)

A large cross-sectional tank is often used at the top of the columns to assure proper separation of gas and liquid phases. Moreover, besides phase separation, such a tank has the advantage of strongly decreasing the oscillation of the liquid free-surface. Considering that the liquid free-surface oscillation originates considerable variations in the velocity of the bubbles inside the column (as discussed in the previous section), it is interesting to investigate if the dampening effect of a large cross-sectional tank affects also the evolution of the bubble velocity inside the column. For this purpose, the operating conditions addressed in the previous section were simulated again considering the existence of a flat large cross-sectional tank at the top of the column. The tank cross-sectional area is large enough so as to assure a practically constant liquid free-surface. The velocity of the first bubble (with and without gas expansion) is plotted against time in Figures A.14a and A.14b.

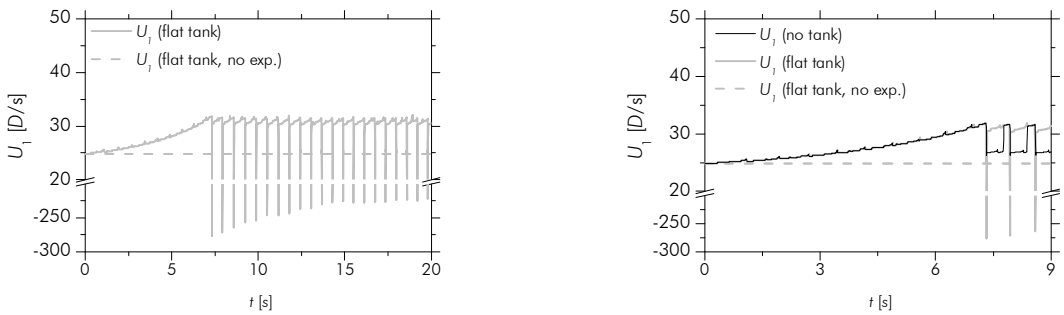

Figure A.14 – Values of the velocity of the first bubble along time for a simulation with $U_L \approx 0.25$ *m/s* and $U_G \approx 0.36$ *m/s*; (a) range: 0-20 s, flat tank data; (b) range: 0-12 s, no tank and flat tank data

As expected, a constant value is obtained when the gas expansion contribution is withdrawn from U_1. However, when focussing on the overall U_1 (including expansion contribution)

a puzzling result emerges. Although the evolution of U_1 is, most of the time, strongly dampened when compared to the same parameter for the no-tank scenario (see Figure A.14b), intriguing negative values of velocity are attained at every instant following bubble burst events (when bubbles reach the liquid free-surface). As before, a closer analysis of several parameters is required in order to shed light on this peculiar behaviour. These are the nose and rear coordinate of first and second bubbles, their velocities and lengths, and the corresponding hydrostatic liquid height. A short time range (15.0-16.5 s) is covered in Figure A.15.

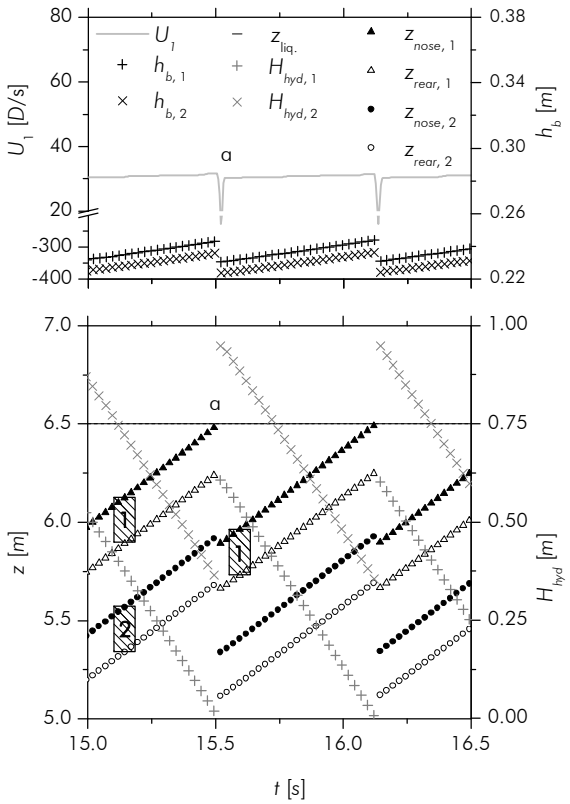

Figure A.15 – Plot of nose and rear coordinates of the first and second bubbles ($z_{nose,\,1}$, $z_{rear,\,1}$, $z_{nose,\,2}$ and $z_{rear,\,2}$), hydrostatic liquid height above first and second bubbles ($H_{hyd,\,1}$ and $H_{hyd,\,2}$), length of first and second bubbles ($h_{b,\,1}$ and $h_{b,\,2}$), velocity of first bubble (U_1) and vertical coordinate of the liquid free-surface ($z_{liq.}$) along time, in the range 15.0-16.5 *s*; simulation with $U_L \approx 0.25$ *m/s* and $U_G \approx 0.36$ *m/s*; with a large flat tank (0.01 *m* height) at the column outlet

For easier interpretation of the chart, both the first and second bubbles are depicted, at a given moment, in the chart. As these bubbles flow upwards in the column, the hydrostatic liquid height above them decreases and, accordingly, their lengths escalate. At instant **a**, the first bubble reaches the liquid free-surface and bursts. The previous second bubble becomes then the first bubble. As the volume of the bursting bubble is replaced, instantly, by liquid from the upper tank, there is a sudden increase in the pressure acting on the "new" first bubble, previously the second bubble. This abrupt escalation in pressure is the result of the equally abrupt change in the

hydrostatic liquid height acting on the bubble ($H_{hyd,1}^{\text{after } a} > H_{hyd,2}^{\text{before } a}$; note that despite the change in indexes these parameters refer to the same bubble). As a consequence of pressure escalation, bubble contraction, perceived as a decrease in bubble length, occurs ($h_{b,1}^{\text{after } a} < h_{b,2}^{\text{before } a}$, as evident in the upper chart of Figure A.15). This sudden bubble contraction, which obviously spans all bubbles in the column, occurs at every bubble burst event. Moreover, the extent of contraction decreases from the top to the base of the column, an expected behaviour since the variation of gas volume with pressure decreases as pressure escalates (see Eq. (A.15)). Given that as discussed previously (section A.4.3.3), bubble expansion results in an upward displacement of everything ahead of the bubble (the "extra" velocity due to expansion), bubble contraction, on the contrary, results in a downward displacement of the flow (a negative "extra" velocity). Indeed, a plunge of the gas and liquid inside the column occurs at every bubble burst event, resulting in the momentary negative bubble velocities shown in the charts of Figures A.14 and A.15. This plunge is very brief and a regular evolution of bubble velocity is obtained in the subsequent instants. Notice that these negative peaks in bubble velocities are related to the assumption of instantaneous column refilling (with liquid from the tank) at bubble burst events. In addition, the amplitude of these negative peaks must only be addressed in conjunction with the chosen simulation time increment, since the truly meaningful parameter is the plunging length of the first bubble (equal to $U_1 \times t_{\text{incr.}}$). Notice additionally that the instantaneous column refilling assumption, reasonable for low viscosity fluids (such as water for instance), might not be adequate if high viscosity fluids are to be considered. In that scenario, the overall evolution of the gas phase inside the column would result from the balance between gas phase contraction (more or less pronounced depending on the time required for column refilling), and the gas expansion related to the upward movement of the bubbles (due to the decreasing hydrostatic pressure). Parameters such as liquid viscosity and column diameter would play an important role in the aforementioned balance since they affect the time required for column refilling.

The use of a flat large cross-sectional tank at the top of the column assures a practically steady liquid free-surface and, most of the time, strongly dampened bubble velocities (and expansion rate). However, as a drawback, it brings about more or less pronounced instantaneous drops on bubble velocities (and expansion rate) at every bubble burst event. Nevertheless, the attainment of a steady liquid free-surface, often crucial in real applications (in which structural instabilities related to bubble bursting are undesirable, for instance), is, by itself, a strong incentive for the further development of the large tank solution. The use of an alternative tank configuration is discussed in the following section.

A.5.3.3.3 Column with a regular large cross-sectional tank at the top (outlet)

As an attempt to overcome the recurrent plunging of the flow at bubble burst events, an alternative tank configuration been tested. The tank cross-sectional area is similar but its height is considerably larger (0.5 m instead of the previous 0.01 m). It is hypothesised that by having a tank height higher than the length of the bubbles reaching the liquid free-surface, the pressure change inside the column due to bubble burst events should be less abrupt. For this purpose, the operating conditions addressed in the previous sections were simulated again acknowledging now the new tank configuration. The velocity of the first bubble (with and without gas expansion) is plotted against time in Figure A.16.

As expected, a constant value is obtained when the gas expansion contribution is withdrawn from U_1 (Figure A.16). Moreover, the recurring plunging of the flow, described previously for the flat tank configuration, is no longer present (no negative values of overall velocity). However, the evolution of the first bubble velocity is akin to the evolution for the no tank configuration (Figure A.16b). There is, as for that configuration, an intermittent oscillation between two major velocity values.

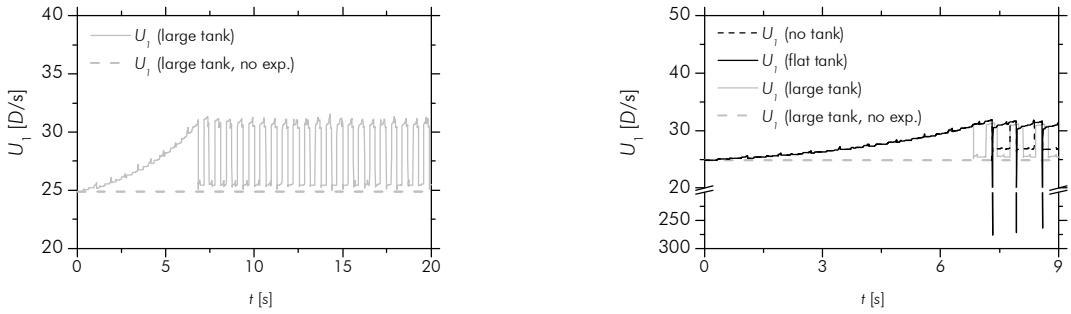

a b

Figure A.16 – Values of the velocity of the first bubble along time for a simulation with $U_L \approx 0.25$ *m/s* and $U_G \approx 0.36$ *m/s*; (a) range: 0-20 s, large tank data; (b) range: 0-12 s, no tank, flat tank and large tank data

As before, a closer analysis of some parameters is required to expound the reasons for this behaviour. These are the vertical coordinates of the nose and rear of the first bubble, in particular in the vicinity of the base of the tank (vertical coordinate $z_T=6$ *m*), and the hydrostatic liquid height above the second bubble, $H_{hyd,\,2}$. The variation of these parameters is plotted against time (in the range 15-16.5 *s*) in Figure A.17.

Three different time instants are relevant for understanding the oscillations of U_1: instant ***a*** referring to the moment at which a first bubble reaches the liquid free-surface (z=6.5 m); instants ***b*** and ***c*** referring to the moments at which the nose and rear of a "new" first bubble, respectively, reach the base of the tank (z=6.0 m). Notice that instant ***a*** is prior to instants ***b*** and ***c*** because,

after the burst of a first bubble at instant **a**, the previously second bubble, flowing somewhere below, becomes the "new" first bubble. Unlike the simulation with no tank at the top of the column, no major change in the velocity of the first bubble is observed when a bubble reaches the liquid free-surface (instant **a**, in Figure A.17).

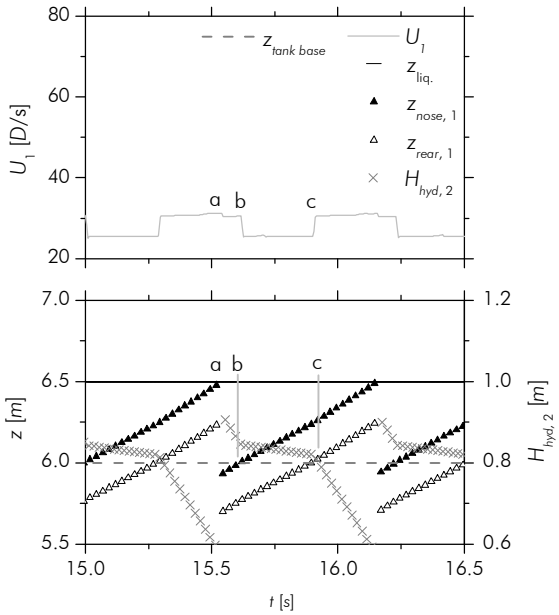

Figure A.17 – Plot of nose and rear coordinates and velocity of the first bubble ($z_{nose,\ 1}$, $z_{rear,\ 1}$, U_1), hydrostatic liquid height above second bubble ($H_{hyd,\ 2}$) and vertical coordinate of the liquid free-surface ($z_{liq.}$) along time, in the range 9-11 *s*; simulation with $U_L \approx 0.25$ *m/s* and $U_G \approx 0.36$ *m/s*; with a large tank at the column outlet (0.5 *m* height)

The large cross-sectional tank at the top of the column assures that the coordinate of the liquid free-surface remains practically unchanged at that event. Therefore, the evolution of the hydrostatic pressure acting on the "old" second bubble is fairly steady during the burst of the first bubble ($P_{hyd,2}^{\text{before a}} \approx P_{hyd,1}^{\text{after a}}$; as already mentioned, despite the change in indexes these parameters refer to the same bubble). Attention must be focused now on the evolution of the hydrostatic liquid height above the second bubble ($H_{hyd,\ 2}$), along time. The variation rate (slope) of this parameter between instants **a** and **b** is fairly constant (negative but almost constant). However, at instant **b** there is a sudden change in the variation rate (slope) of $H_{hyd,\ 2}$. Between instants **b** and **c** the first bubble is crossing the base of the tank and, as a consequence, the last parcel of the right hand side of Eq. (A.14) is smaller than before instant **b** ($\alpha_1 = 1$ before instant **b**, and decreasing from 1 to 0 between instants **b** and **c**). As a result, the variation rate (slope) of $H_{hyd,\ 2}$ in that time interval is less steep (than in the time interval **a**-**b**) and, consequently, the corresponding bubble expansion is smoother. The original variation rate of $H_{hyd,\ 2}$ is observed again as soon as the rear of the first bubble is above the tank base (after instant **c**, and until the next burst event; $\alpha_1 = 0$ in that time

interval). Notice that this analysis has been focused on the hydrostatic liquid height above the second bubble just for the sake of simplicity. Similar effects occur for all the bubbles in the column, although with different extent. Thus, because all bubbles in the column expand less when the first bubble of the train of bubbles is crossing the base of the tank, a smaller gas expansion rate is obtained inside the column during those periods, which result finally in the oscillation of the bubble velocities (and hence the oscillations in U_1).

By increasing the height of the outlet tank (for values higher than bubble lengths) one avoids the sudden pressure change at bubble burst events of the flat tank configuration, but continues to have pressure oscillation, though more gradual, as bubbles reach the base of the bank. The advantages of the regular large tank configuration (large in terms of cross-sectional area as well as height) are thus twofold: while it assures an almost steady liquid free-surface (which can be important for several practical applications), it prevents the flow plunging of the flat tank configuration. However, as already mentioned it does not avoid some degree of oscillation in the expansion rate of the gas phase.

A.5.4 On the gas hold-up inside the column

The retention of gas inside the column, usually termed gas hold-up, is one of the most important parameters for the hydrodynamic characterization of two-phase flows. It is defined as the fraction of gas inside the column and can be computed by v_G / v in terms of volume (or alternatively by H_G / H, in terms of the corresponding column equivalent height; note that $v_G = H_G S_c$). Considering that v_G escalates along the column as the gas phase expands, and that the rate at which this happens is influenced by the column outlet configurations, it is interesting to study how these parameters/phenomena interrelate. For this purpose two approaches are pursued: one addressing the effect of the column outlet configuration over the average value of gas hold-up and another assessing the relevance of the gas phase expansion in the estimation of average gas hold-up. The outcome of these approaches is discussed in the following sections.

A.5.4.1 Effect of the outlet configuration on the average gas hold-up

Several simulations were performed considering, as before, the flow in a 6.5 m long column with internal diameter of 0.032 m. Superficial liquid and gas velocities equal to 0.10, 0.23, 0.36 and 0.50 m/s were set. Every operating condition was simulated for each of the three outlet configurations described previously (see Figure A.11). The average gas hold-up obtained for simulations featuring no tank at the column outlet (Figure A.11a) is plotted against the superficial

liquid and gas velocities in Figure A.18. The average gas hold-up is based on several hundreds of instantaneous gas hold-up values obtained at every second of the simulations.

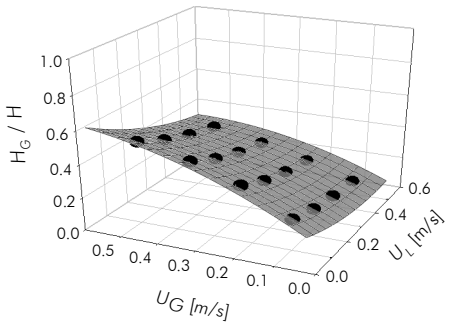

Figure A.18 – Gas hold-up for simulations with U_L and U_G equal to 0.10, 0.23, 0.36 and 0.50 m/s; no tank at the column top (Figure A.11a); column length: 6.5 m; surface fit equation:
$H_G/H = 0.59(U_L)^2 - 0.60U_L - 0.82(U_G)^2 + 1.31U_G - 0.53U_LU_G + 0.14$, r^2=0.998

As expected, gas hold-up escalates for increasing superficial gas velocity and for decreasing superficial liquid velocity. This derives from its definition (H_G / H) and from flow continuity. Moreover, similar behaviour is obtained for the remaining outlet configurations (flat and large tank). In Figure A.19 the average gas hold-up is plotted against U_G, for the three outlet configurations (no tank , flat tank and large tank) and U_L equal 0.10 m/s and 0.50 m/s (the extreme values of the range).

As perceivable in the chart of this figure, fairly similar gas hold-ups are obtained with the three outlet configurations for the highest superficial liquid velocity (U_L≈0.50 m/s). The deviation between the obtained gas hold-ups increases with U_G but reaches no more than 2%. However, this deviation increases for decreasing U_L. For instance, for U_L equal to 0.10 m/s, the deviation between the gas hold-ups obtained for the three outlet configurations reaches 6%. Moreover, and although not shown for the sake of simplicity, the maximum deviations (occurring for U_G≈0.50 m/s) are about 2, 3, 4 and 6% when U_L is equal to 0.50, 0.36, 0.23 and 0.10 m/s, respectively. These are nevertheless limited deviations, and match in particular the operating conditions leading to a higher gas fraction inside the column (i.e. high U_G / U_L ratio).

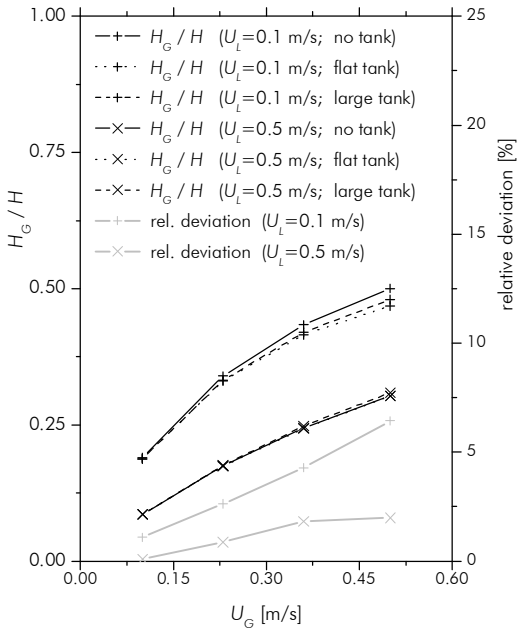

Figure A.19 – Gas hold-up for simulations with different column top configurations (no tank, flat tank and large tank); U_L≈0.10 and 0.50 m/s; U_G≈0.10, 0.23, 0.36 and 0.50 m/s; column length: 6.5 m

A.5.4.2 Relevance of gas expansion implementation in the assessment of gas hold-up

An attempt is made to gauge the relevance of the gas expansion in the computation of the gas hold-up. Following a strategy discussed previously, a comparison is made between three types of simulations: one including gas expansion and two others discarding gas expansion. For these approximate approaches, estimates of U_G are introduced in the simulations after correction for the pressure at the middle and at the top of the column, respectively. The three outlet configurations mentioned before were tested in each approach. The gas hold-up obtained for the large tank configuration is plotted against U_G in Figure A.20 (for U_L equal to 0.10 and 0.50 m/s).

The charts of this figure indicate that even when no gas expansion is considered in the simulation, it is still possible to compute the average gas hold-up with reasonable accuracy, provided that the estimate of U_G introduced in the simulator is corrected for the pressure at the middle of the column. Indeed, in that situation, the relative deviation between the gas hold-up of the simulations including expansion and the approximate approach (discarding expansion) is always smaller than 4%, for the ranges of U_G and U_L studied (0.10-0.5 m/s). Notice that the gas hold-up values (given in %) of both approaches differ less than 1 percentage point. However, when the estimate of U_G is introduced in the simulation at ambient pressure, higher gas hold-up deviations are obtained. For the ranges of U_G and U_L studied the relative deviations vary in the ranges 6-15% (U_L≈0.10 m/s) and 12-19% (U_L≈0.50 m/s). Notice that the relative deviations

decrease for increasing U_G and decreasing U_L (Figure A.20), i.e. for increasing gas hold-up. Nevertheless, the gas hold-up values of the two approaches differ just by 2-4 percentage points.

The previous approach was also implemented for simulations based on a longer column (20 m long). The results obtained for the large tank configuration are shown in Figure A.21.

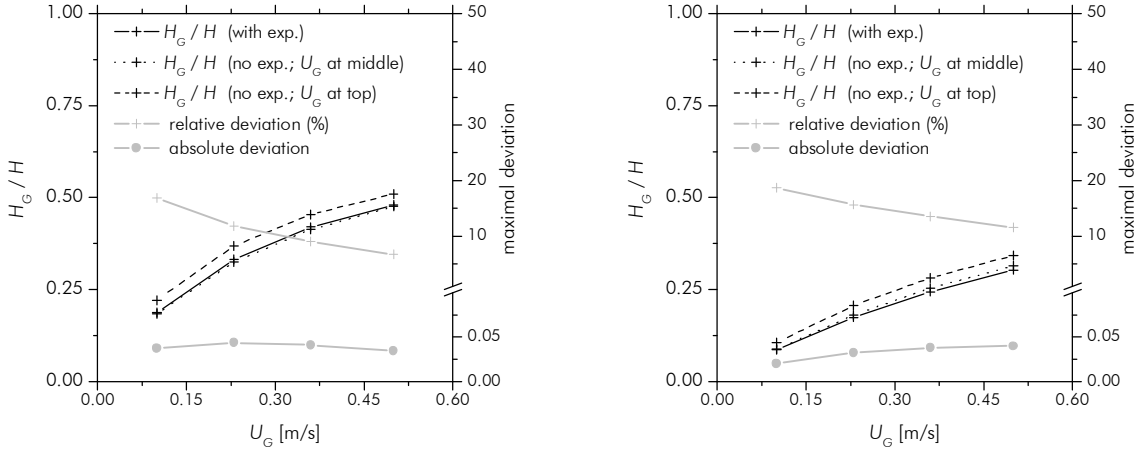

Figure A.20 – Gas hold-up for simulations considering expansion (varying U_G) and discarding expansion (constant U_G equal to value at the middle or at the top of the column); (a) $U_L \approx 0.10$ m/s and (b) $U_L \approx 0.50$ m/s; for $U_G \approx 0.10$, 0.23, 0.36 and 0.50 m/s; column length: 6.5 m; outlet configuration: large tank

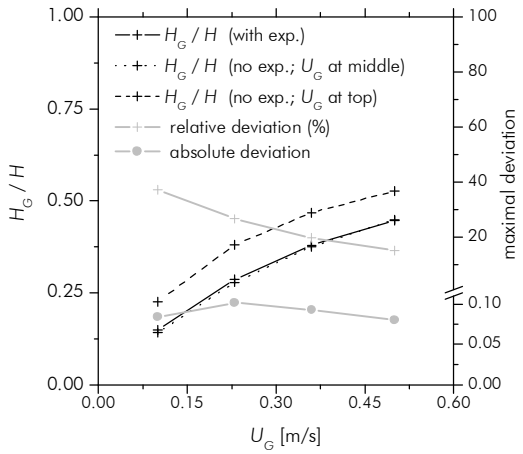

Figure A.21 – Gas hold-up for simulations considering expansion (varying U_G) and discarding expansion (constant U_G equal to value at the middle or at the top of the column); $U_L \approx 0.10$ m/s and $U_G \approx 0.10$, 0.23, 0.36 and 0.50 m/s; column length: 20 m; outlet configuration: large tank

As for the shorter column, a reasonable evaluation of the gas hold-up is obtained for simulations discarding the gas phase expansion provided that the U_G estimate is given at the mid-column pressure. For that situation, the relative deviations obtained are smaller than 5%.

Moreover, quite like for the shorter column, the corresponding gas hold-up values differ less than 1 percentage point. In opposition to this, quite significant relative deviations exist between the simulation including gas expansion and the approximate simulation, when U_G is used at the ambient pressure. These deviations vary in the range 16-37% (for $U_L \approx 0.10$ m/s and U_G in the range 0.10-0.50 m/s). Notice that for the same operating conditions, the deviations obtained for the 6.5 m long column are less than half of those obtained for the 20 m long column. It is therefore evident that as column length increases it becomes more and more inadequate to compute gas hold-up by the simpler approach discussed (no expansion along the column and U_G at ambient pressure).

The previous discussion was based only on the large tank configuration just for the sake of simplicity. Similar conclusions would derive from simulations based on the other outlet configurations.

A.6 Conclusions

A simulation study on the gas phase expansion and gas hold-up in co-current slug flow is reported. The simulations including gas expansion and approximate approaches are shown to produce very similar estimates of the average liquid slug length. Similar matching can be observed regarding the average bubble velocity and length, provided that the U_G estimates, used in the approximate approaches, are corrected for the vertical coordinate in question. In agreement with this, the gas phase expansion is shown to have reduced influence over the coalescence of bubbles (gas expansion slightly decreases coalescence).

The influence over the gas expansion rate of three alternative outlet configurations is discussed. The first, featuring no tank at the column outlet, brings along strong oscillations of the gas expansion rate and, consequently, of the bubble velocities. The second configuration, featuring a flat large cross-sectional tank at the column outlet, assures most of the time, a strongly dampened gas expansion rate (and hence bubble velocities) but, as a drawback, leads to recurrent plunging of the flow inside the column, at every bubble burst event. The third configuration, implying a regular large and high cross-sectional tank at the column outlet, prevents this latter phenomenon and stabilises the liquid free-surface. It does not avoid, however, some degree of oscillation in the expansion rate of the gas phase, much alike the one observed for the no tank configuration.

As expected, the average gas hold-up is shown to escalate with increasing U_G and decreasing U_L. The column outlet configurations are shown to have reduced effect over the average gas hold-up (deviations smaller than 6% for U_L and U_G in the range 0.10-0.50 m/s).

Approximate approaches based on U_G values corrected for the pressure at the middle of the column are shown to produce good estimates of the average gas hold-up (deviations smaller than 5%) for the ranges of U_L, U_G and H studied. Approximate approaches based on the U_G at ambient pressure are shown not to produce good estimates of the average gas hold-up, especially as column length increases.

A.7 Notation

Roman symbols

C	empirical coefficient	
D	column internal diameter	[m]
g	acceleration of gravity	[m/s^2]
h_b	length of gas bubble	[m]
h_s	length of liquid slug	[m]
H	height of gas and liquid inside the column	[m]
H_G	height of gas inside the column	[m]
$H_{hyd,\,i}$	hydrostatic liquid height above bubble i	[m]
n	number of bubbles	[#]
n_i	number of moles of air of bubble i	[mol]
P_{atm}	ambient pressure	[Pa]
$P_{hyd,\,i}$	hydrostatic pressure on bubble i	[Pa]
R	universal gas constant	[J/(K mol)]
S_b	bubble cross-sectional area	[m^2]
S_c	column cross-sectional area	[m^2]
T	temperature	[K]
t_i, t_{i+1}	consecutive time instants	[s]
U_b	bubble velocity	[m/s]
U_B	upward bubble velocity	[m/s]
U_G	superficial gas velocity	[m/s]
U_i	bubble i upward velocity	[m/s]
U_L	superficial liquid velocity	[m/s]
U_∞	upward bubble velocity in a stagnant liquid (drift velocity)	[m/s]
v	volume of gas and liquid inside the column	[m^3]
v_G	volume of gas inside the column	[m^3]
z	vertical coordinate along the column	[m]
z_T	vertical coordinate of the tank base	[m]
$z_{liq.}$	liquid free-surface coordinate	[m]

z_{nose}	vertical coordinate of bubble nose	[m]
z_{rear}	vertical coordinate of bubble rear	[m]

Greek symbols

α_i	parameter informing on the bubble positioning relative to the tank base	
Δh_i	expansion of bubble i	[m]
ρ	density of liquid	[kg/m^3]

A.8 Acknowledgments

The authors gratefully acknowledge the financial support of Fundação para Ciência e a Tecnologia through project POCTI/EQU/33761/1999 and scholarship SFRH/BD/11105/2002. POCTI (FEDER) also supported this work via CEFT.

A.9 References

Barnea, D. and Taitel, Y., 1993. A model for slug length distribution in gas-liquid slug flow. Int. J. Multiphas. Flow 19(5): 829-838.

Brown, R. A. S., 1965. The mechanics of large gas bubbles in tubes. I - Bubble velocities in stagnant liquids. CJChE 43: 217-223.

Campos Guimarães, R. and A. Sarsfield Cabral, J. (1997). Estatística, McGraw-Hill de Portugal Limitada.

Chouet, B., Dawson, P., Ohminato, T., Martini, M., Saccorotti, G., Giudicepietro, F., De Luca, G., Milana, G. and Scarpa, R., 2003. Source mechanisms of explosions at Stromboli volcano, Italy, determined from moment-tensor inversions of very-long-period data. J. Geophys. Res. 108(B1): 2019, doi:10.1029/2002JB001919.

Coelho Pinheiro, M. N., Pinto, A. M. F. R. and Campos, J. B. L. M., 2000. Gas hold-up in aerated slugging columns. Chem. Eng. Res. Des. 78(8): 1139-1146.

Collins, R., De Moraes, F. F., Davidson, J. F. and Harrison, D., 1978. The Motion of Large Gas Bubble Rising Through Liquid Flowing in a Tube. J. Fluid Mech. 28: 97-112.

Davies, R. M. and Taylor, G. I., 1950. The mechanics of large Bubbles rising through extended liquids and through liquids in tubes. Proc. R. Soc. Lond. A 200: 375-392.

Dumitrescu, D. T., 1943. Stromung an Einer Luftblase im Senkrechten Rohr. Z. Angeus. Math. Mec. 23: 139-149.

Fabre, J. and Liné, A., 1992. Modeling of two-phase slug flow. Ann. Rev. Fluid Mech. 24: 21-46.

Hasanein, H. A., Tudose, G. T., Wong, S., Malik, M., Esaki, S. and Kawaji, M., 1996. Slug flow experiments and computer simulation of slug length distribution in vertical pipes. AIChE Symposium Series 92(310): 211-219.

James, M. R., Lane, S. J., Chouet, B. and Gilbert, J. S., 2004. Pressure changes associated with the ascent and bursting of gas slugs in liquid-filled vertical and inclined conduits. J. Volcanol. Geoth. Res. 129(1-3): 61.

Nicklin, D. J., Wilkes, J. O. and Davidson, J. F., 1962. Two-phase flow in vertical tubes. Transactions of the Institution of Chemical Engineers 40: 61-68.

Seyfried, R. and Freundt, A., 2000. Experiments on conduit flow and eruption behavior of basaltic volcanic eruptions. J. Geophys. Res. 105: 23727-23740.

Sotto Mayor, T., Ferreira, V., Pinto, A. M. F. R. and Campos, J. B. L. M., 2006a. Hydrodynamics of gas-liquid slug flow along vertical pipes in turbulent regime. An experimental study. Submitted to International Journal of Heat and Fluid Flow.

Sotto Mayor, T., Pinto, A. M. F. R. and Campos, J. B. L. M., 2006b. An image analysis technique for the study of gas-liquid slug flow along vertical pipes - Associated uncertainty. In revision in Flow Measurement and Instrumentation.

Van Hout, R., Barnea, D. and Shemer, L., 2001. Evolution of statistical parameters of gas-liquid slug flow along vertical pipes. Int. J. Multiphas. Flow 27(9): 1579-1602.

Van Hout, R., Shemer, L. and Barnea, D., 2003. Evolution of hydrodynamic and statistical parameters of gas-liquid slug flow along inclined pipes. Chem. Eng. Sci. 58(1): 115-133.

White, E. T. and Beardmore, R. H., 1962. The Velocity of Single Cylindrical Air Bubbles Through Liquids Contained in Vertical Tubes. Chem. Eng. Sci. 17: 351-361.

B An image analysis technique for the study of gas-liquid slug flow along vertical pipes – Associated uncertainty[7]

B.1 Abstract

An image analysis technique for the study of continuous co-current gas-liquid slug flow, in vertical columns, is reported. The technique comprises the automatic analysis of a sequence of video frames with the purpose of object (bubbles) tracking and characterization (dimension, velocity, distance). Its applicability to continuous slug flow conditions (even for very large number of bubbles) and the high accuracy of the results are the main added value of the proposed technique. The evaluation of the uncertainty associated with the parameters measured is performed (following the *general uncertainty analysis approach*). Partial uncertainties are acknowledged in bubble boundary definition, time measurement and calibration procedure. Expressions are derived for the computation of the overall uncertainty of bubble velocity, bubble length and liquid slug length. Global relative uncertainties of 5%, 2.5% and 7%, were found, for these parameters. The uncertainty estimation supports the ongoing trend for the implementation of image analysis techniques for the study of slug flow pattern.

[7] Based on the paper by T. Sotto Mayor, A.M.F.R. Pinto and J.B.L.M. Campos, in revision in Flow Measurement & Instrumentation (FMI)

B.2 Introduction

The implementation of image analysis techniques for the study of phenomena is spanning to different fields of research, a natural consequence of its non-intrusiveness, but also a development promoted by the exponential evolution of hardware and software applications. Biphasic and multiphase flows are some of many areas that profited with the emergence of these techniques. Two-phase slug flow experiments, for instance, is a potential field of application of these new visualization strategies.

Slug flow studies have been performed using several experimental techniques, with more or less intrusive approaches (as in Pinto et al. (2001) or Van Hout et al. (2001), just to mention some, featuring pressure probes and optical fibre probes, respectively). Non-intrusive approaches have also been reported. Some examples refer to a visualization technique based on video recordings of the flow (Hasanein et al. (1996), with bubble length estimation achieved by direct comparison with on-site rulers), or describe an image processing procedure for the study of the motion of individual Taylor bubbles (Polonsky et al. (1999)). Other works (Van Hout et al. (2002)) report the application of the latter technique to continuous slug flow (although applicable only to a small number of bubbles). An experimental technique based on laser diodes and photo cells is also mentioned (Sousa et al. (2006)) as a tool for the study of the motion of individual Taylor bubbles. Although non-intrusive, this technique is not suitable for continuous slug flow operating conditions.

Gaining more and more adepts in the fluid mechanics research community, the image analysis techniques are providing solutions to tackle the experimental study of slug flow. As to support this ongoing trend, a detailed evaluation of the uncertainty associated to this measurement technique is needed.

The main goal of this work is to provide information concerning a straightforward and accurate image analysis technique, developed specially for the study of continuous gas-liquid slug flow, in vertical columns, and applicable for the measurement of a large number of bubbles (several thousands). Detailed assessment of the uncertainty associated to the parameters measured by this technique is performed. Focus is put on the propagation of the uncertainty of each measured variable over the overall uncertainty of typical flow parameters (bubble velocity, bubble length and liquid slug length).

B.3 Experimental set-up

The experimental apparatus is shown schematically in Figure B.1. Experiments were performed in an acrylic vertical column (6.5 m long). Water was used as flowing medium. The flow

was set and controlled by a peristaltic pump with damping chambers placed at the pump inlet and outlet to assure a continuous flow. A large open tank with a lateral outlet was mounted at the top of the pipe to minimise free-surface oscillations. The liquid flow rate was measured at the outlet of the tank, before and after each experiment. The liquid temperature was measured by a thermocouple placed inside the tank. Air from a pressure line was introduced laterally at the base of the column through a 3 mm internal diameter injector. The air flow rate was measured by calibrated rotameters.

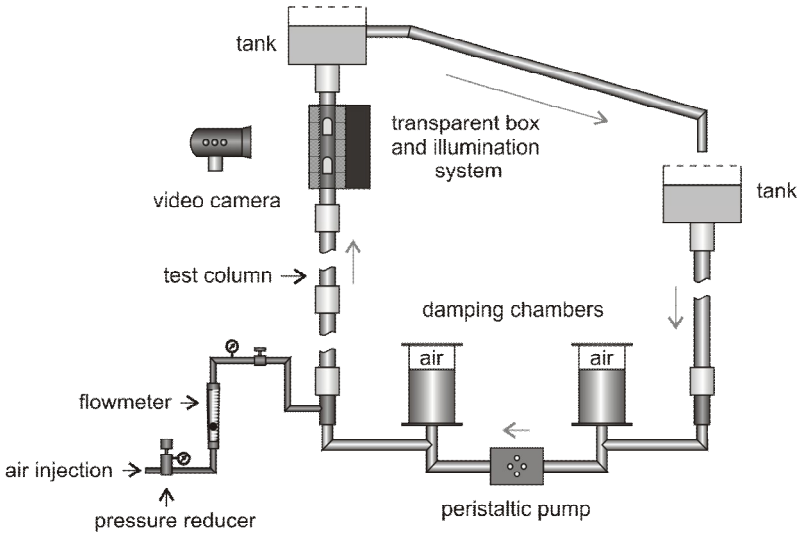

Figure B.1 – Experimental set-up

Images of slug flow around the vertical coordinate 5.4 m (from the base of the column) were recorded using a Canon digital video camcorder (model XM1) operating at a frequency of 25 Hz. A rectangular transparent acrylic box (1.2 m long) filled with water was fitted to the column at the measuring sections, in order to reduce image distortion and heating effects from the light source (Figure B.2).

Uniform illumination over the whole test sections was achieved by means of the illumination system illustrated in Figure B.2a. Two fluorescent lamps, equipped with an electronic ballast to avoid light scintillation problems (boosting scintillation frequencies to kHz range), were mounted inside an opaque box with a diffusive surface in front of the lamps for greater light uniformity. The illumination kit was placed in contact with the transparent acrylic box as illustrated in Figure B.2b. Both lateral faces as well as top and bottom sides of the acrylic box were covered with an opaque material in order to assure a single light source illuminating the column test-section.

Very short exposure times were chosen to assure "frozen" snapshots. Auto-focus was used to infer an adequate focal length for each experimental condition, followed by steady manual

focus during the experiments. This procedure avoided running the auto-tracking focus of the camera auto-focus system, whenever bubbles appeared in the field of view. A 90° rotation of the camera was chosen for better pixel resolution in the vertical coordinate, which is the main flow direction (the non-rotated camera field of view is 720 (width) x 576 (height) pixels). Different camera focal lengths were used according to the flow complexity and the average bubble and liquid slug dimensions (longer bubbles require a smaller image magnification whilst a more complex flow pattern calls for a larger magnification). Depending on the aforementioned balance, up to 0.6 m of pipe were captured in the camera field of view.

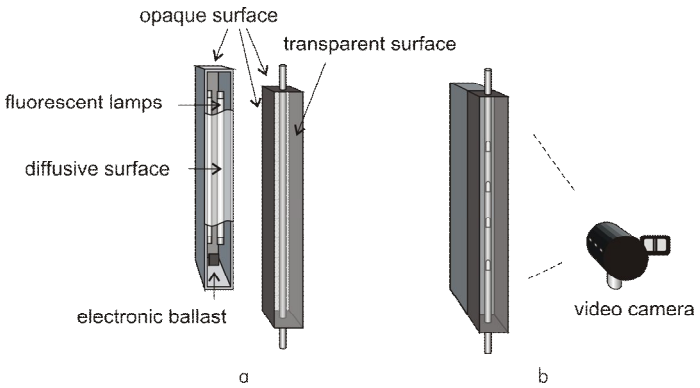

Figure B.2 – Schematic representation of the illumination system

B.4 Video processing – the image analysis

The recorded videos were transferred to a personal computer hard drive using video editing software (Adobe® Premiere). Raw videos were stored in the original acquired format (Microsoft DV) for further processing. For the sake of hard drive capacity, audio information was discarded in the recorded videos. Moreover, from the total field of view only the strip containing the test column was extracted and further processed (Figure B.3). This resulted in a considerable reduction in the size of stored information as well as processing time. Each video strip was processed using a MATLAB code specially developed for the purpose. The choice of a MATLAB environment as a video processing tool led to choosing Microsoft AVI codification for the output video format of the strips, since it is the only video format directly readable by MATLAB internal routines.

Notice that in Microsoft AVI format, a 30-minute video strip corresponds to about 4 GB of hard drive space. Considering that the direct analysis of such videos would cause RAM (random access memory) shortness problems, an extra step was implemented, before the video analysis, in order to further decrease the digital size of the videos: each video strip was split into 70 consecutive video files, using a general video tool together with automation Macro software.

Figure B.3 – Experimental frame: (a) full frame and (b) strip of frame

Each of these shorter video files was loaded into MATLAB workspace as a sequence of frames. Each frame corresponds to a snapshot of the camera field of view (a frame at each 0.04 s, corresponding to a frequency of 25 Hz). A sequential procedure was implemented to process each image frame. The outcome of every step of the procedure is shown in the images of Figure B.4, and briefly described below.

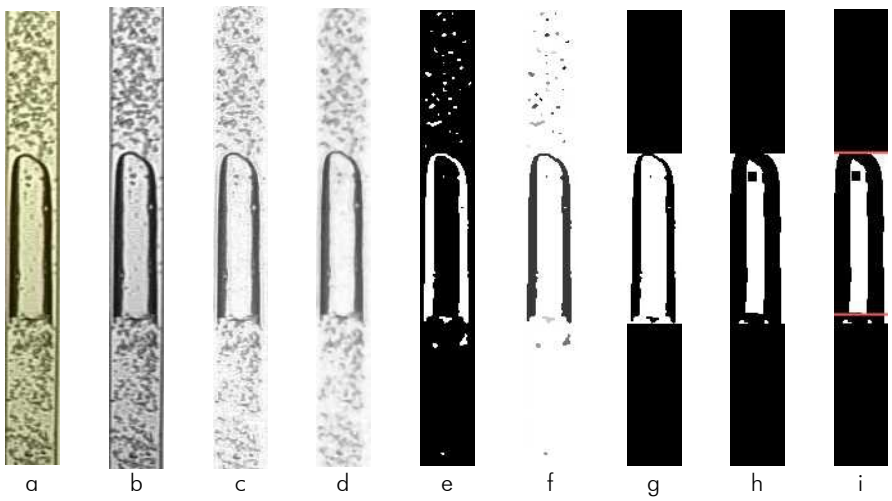

Figure B.4 – Sequential steps in the image process: (a) RGB image; (b) greyscale image; (c) after background subtraction; (d) after median filter; (e) after inversion and conversion to binary mode; (f) after labelling; (g) after object analysis; (h) after erosion; (i) bubble boundaries

Image loading

Each frame was loaded in 8 bits RGB (red, green and blue) colour format (Figure B.4a)

Image conversion

Each frame was converted from RGB to greyscale mode (Figure B.4b). The output image has 256 grey levels, ranging from 0 (black) to 255 (white). A greyscale version of the background image was also prepared. This background image is used for image contrast enhancements.

Image contrast enhancement

The subtraction of the background image (corresponding to a snapshot of the column with stagnant liquid and no gas flow) from the continuous flow image (with both liquid and gas) enhances its contrast. This procedure eliminates any information (or colour change) not related to the gas phase. The resulting image is shown in Figure B.4c.

Image Filtering

In order to remove or attenuate the image noise, a median filter was applied to the image (Figure B.4d). In this procedure, every image pixel is substituted by the median of its neighbour pixels. As a result, any eventual pixel outlier, i.e., pixels diverging considerably from the surrounding ones, are discarded. A slight decrease in image sharpness occurs.

Image conversion to binary mode

Conversion of a greyscale image to binary mode consists in a reduction to two of the number of grey levels of the original image: one corresponding to black (0) and another corresponding to white (1). This is accomplished by means of a threshold value, i.e., a pixel value (or luminosity) defining the transition between black and white colours. Once the threshold value (reference luminosity) is defined, an image simplification takes place: all pixels with luminosity values lower than the threshold value are considered black, while the remaining pixels are considered white. This operation creates images like the one depicted in Figure B.4e. In most experiments, a threshold value of 0.35 was used. See section B.8 for further details on the threshold value.

Image objects labelling

The above procedure created a black and white image that can be understood as a black background with white objects in foreground. These white objects were labelled using different grey levels to allow for easier observation of their positioning and dimension (Figure B.4f).

Object analysis I – Bubble nose definition

The objects in the image, easily perceived in the labelled representation (Figure B.4f), can be described in terms of their dimensions (width, length), their white area (estimate of the area of the white pixels), their square area (area of the smallest square comprising the object), etc. Each of these descriptions allows different analysis of the objects.

The aim of the algorithm is the tracking of Taylor bubbles moving upwards in a flowing liquid. As depicted in Figure B.4, Taylor bubbles flow through more or less aerated liquid slugs, depending on the liquid's physical properties, gas and liquid flow rates, column diameter, etc. In order to distinguish between Taylor bubbles and small bubbles flowing in the liquid slug, the length of the objects in the image was used as a sorting parameter. For this purpose, a minimum bubble length was defined to acknowledge the presence of Taylor bubbles. Depending on the flow complexity and average bubble length, a minimum bubble length ranging from 1*D* to 3*D* was used throughout the analysis of all experiments.

The use of object length as a sorting parameter allowed the immediate definition of the Taylor bubble nose as well as a rough estimate of the position of the Taylor bubble rear. This uncertainty is due to the oscillations in the bubble rear as Taylor bubbles flow in a column, and to the small bubbles travelling in the liquid wake. If bubble rear positioning was based on objects length, bubble length values would change considerably from frame to frame. Figure B.5 illustrates this problem. There is an obvious difference in the bubble length in consecutive frames.

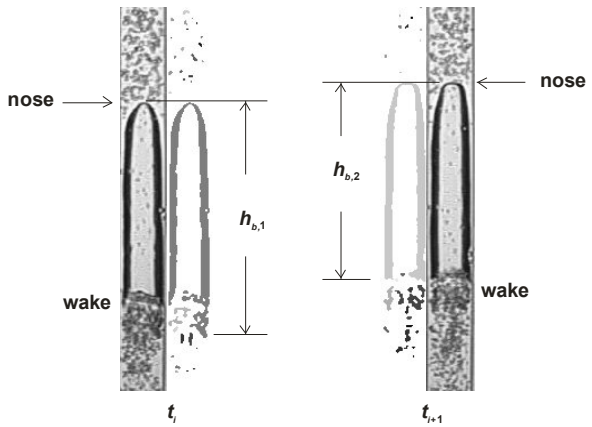

Figure B.5 – Representation of consecutive bubble images, with bubble boundaries based on simple object lengths

Image "Erosion"

Image erosion is a morphological image operation that changes every pixel in an image according to the values of its neighbouring pixels. More specifically, image erosion sets the value of every pixel in an image to the minimum value of its surrounding pixels. Thus, when a binary image (black and white pixels) undergoes erosion, there is a decrease in the area of the objects (in

white), since some white pixels in the extremity of the objects are set to black (minimum value of the surrounding pixels). This change in the area of the objects is easily recognised in Figure B.6d.

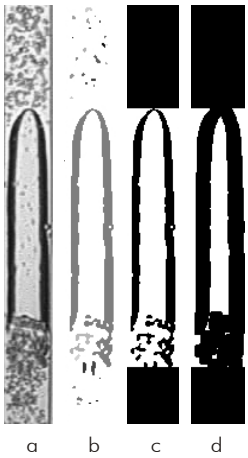

Figure B.6 – (a) image; (b) labelled version; (c) binary version and (d) binary eroded version

A *MATLAB* internal function (*'strel'*) was applied to define the surrounding area used for image erosion purposes. A flat, disk-shaped structuring element was used (type *'disk'*), with a 4 pixel radius. More details on this function can be found in The MathWorks (2002).

Object analysis II – Bubble rear definition

The erosion of the white objects allowed the isolation of the central white object (Figure B.6d), previously blended with the small objects in the bubble wake region. Notice that this object can easily be sorted from the remaining objects since it clearly has the largest white area. Analysing this central eroded object in detail, it can be seen that its lowest white pixel (at the base of the object) matches the beginning of the bubble wake region. Moreover, the upward movement, from frame to frame, of this lowest white pixel is noticeably smooth when compared to the movement of the lowest white pixel of the central non-eroded object (Figure B.6b). This indicates that by defining the position of the bubble wake region more accurately, the erosion procedure can facilitate the acquirement of more robust and coherent bubble length values (discarding the wake region). Figure B.7 depicts this approach.

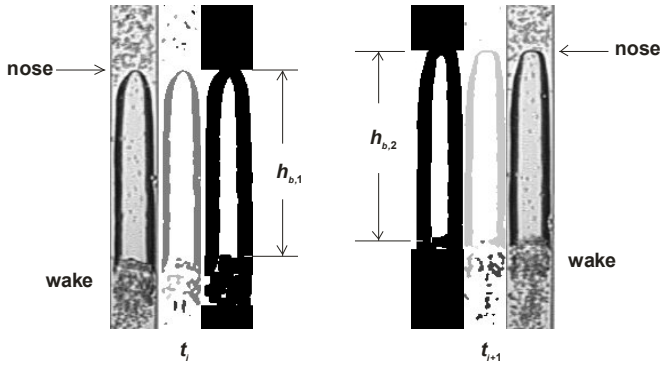

Figure B.7 – Representation of consecutive bubble images, with bubble boundaries based on object lengths and central area

B.5 Video processing – the data analysis

By determining the positioning and dimension of Taylor bubbles grabbed in every video frame it is possible to compile information about the flow pattern in slug flow experiments. Two different studies can be performed: one describing the flow pattern at a fixed column position (fixed-point data analysis), and another focussing on the bubble-to-bubble interaction as bubbles move along the column (moving-point data analysis).

B.5.1 Fixed-point data analysis

Figure B.8 depicts the camera's field of view in a slug flow experiment. Two imaginary reference lines, corresponding to 25% and 75% of the field of view height, were drawn (references 1 and 2, respectively). Bubbles are recognized when their noses cross the upper reference line.

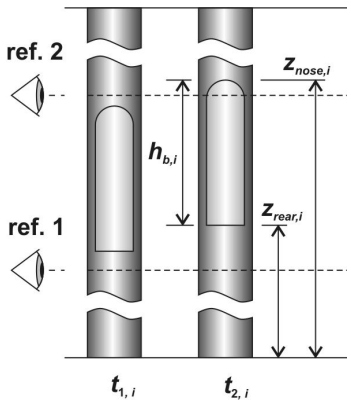

Figure B.8 – Representation of the camera field of view in fixed-point analysis, during the passage of a Taylor bubble

If $t_{1,i}$ and $t_{2,i}$ represent consecutive instants, prior and subsequent, respectively, to the passage of the nose of bubble i, through the upper reference line, the bubble velocity, U_i, is given by:

$$U_i = \frac{z_{nose,i}^{t_{2,i}} - z_{nose,i}^{t_{1,i}}}{t_{2,i} - t_{1,i}} \tag{B.1}$$

where $z_{nose,i}$ refers to the vertical coordinate of the bubble nose (measured from the base of the camera field of view). The bubble length is obtained directly from the position of its boundaries (nose and rear):

$$h_{b,i} = z_{nose,i}^{t_{2,i}} - z_{rear,i}^{t_{2,i}} \tag{B.2}$$

The liquid slug length ahead of bubble i, $h_{s,i-1}$, is computed from the coordinate of the rear of the previous bubble (bubble i-1) and the coordinate of the nose of bubble i:

$$h_{s,i-1} = z_{rear,i-1}^{t_{2,i}} - z_{nose,i}^{t_{2,i}} \tag{B.3}$$

The coordinate of the rear of bubble i-1, at instant $t_{2,i}$, can be predicted by:

$$z_{rear,i-1}^{t_{2,i}} = z_{nose,i-1}^{t_{2,i-1}} + (t_{2,i} - t_{2,i-1})U_{i-1}^{t_{2,i-1}} - h_{b,i-1} \tag{B.4}$$

where $t_{2,i-1}$ refers to the instant at which the nose of bubble i-1 crossed the upper reference line. In the above prediction, it is assumed that bubble i-1 has constant upward velocity between instants $t_{2,i-1}$ and $t_{2,i}$. This assumption is reasonable unless the bubble is coalescing, interacting or instantly accelerating or decelerating by the time it passes the upper reference line.

The above procedure must be implemented for each video frame to gather information about the characteristics of every bubble (regarding bubble length, velocity and liquid slug length). All variables mentioned above have pixel units (or pixel/s in the velocity case). To accomplish their conversion to real length units, the following correction must be computed:

$$variable\left[\text{m or m/s}\right] = variable\left[\text{pixel or pixel/s}\right]\frac{h_{cal.,m}}{h_{cal.,px}} \tag{B.5}$$

where $h_{cal.,m}$ and $h_{cal.,px}$ refer to the height of the calibration element in metres and pixels, respectively.

B.5.2 Moving-point data analysis

In the moving-point data analysis, the focus is put on bubble-to-bubble interaction. Hence, for higher accuracy, it is important to use an image magnification in which more than one Taylor bubble is visible in the camera field of view. In this scenario, the relation between bubble velocity and liquid slug length ahead of the bubble is achieved without using predictions to compute bubble boundary positioning as in the previous section. Figure B.9 depicts this situation.

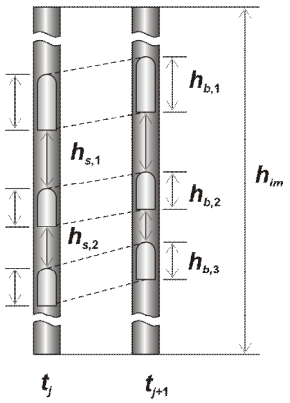

Figure B.9 – Representation of camera field of view in moving-point analysis

Consecutive instants t_j and t_{j+1} are chosen considering the requirement of frames with equal number of bubbles, and with all bubble boundaries inside the camera field of view (no bubbles entering or exiting the field of view).

Bubble velocities are calculated using the following equation, identical to Eq. (B.1), for every bubble in the chosen frames:

$$U_i = \frac{z_{nose,i}^{t_{j+1}} - z_{nose,i}^{t_j}}{t_{j+1} - t_j} \tag{B.6}$$

Bubble and liquid slug lengths are computed using the following equations:

$$h_{b,i} = z_{nose,i} - z_{rear,i} \tag{B.7}$$

$$h_{s,i-1} = z_{rear,i-1} - z_{nose,i} \tag{B.8}$$

Notice that, for *n* bubbles in a frame, only n-1 liquid slugs are computed. Additionally, the last two equations are applied to each pair of consecutive frames and, therefore, average values for each bubble and liquid slug length are calculated (from every two consecutive frames).

As referred to in the previous section, a correction must be computed to convert the aforementioned variables to real length (or velocity) units (see Eq. (B.5)).

B.6 Video processing – the error analysis

The methodology described in the previous sections allows the gathering of information on the variation of the positioning of bubble boundaries along time, which can be transformed in data about velocity of bubbles, length of bubbles and of liquid slugs. Considering that the acquisition of the initial data (positioning of bubble nose and rear and the time interval between consecutive frames) is accomplished within the precision and bias limits of the equipment used in the process, it is interesting to assess how these uncertainties propagate through the algebraic transformations, required for computing the final variables.

Consider generically a parameter *Y* computed algebraically by a function (the reduction equation) of *n* measured variables (y_1, …, y_n):

$$Y = f(y_1, y_2, \ldots, y_n) \tag{B.9}$$

If the uncertainty of each of the measured variables is represented by δy_1, …, δy_n, one can evaluate the uncertainty of parameter *Y* as follows (*general uncertainty analysis approach*):

$$(\delta Y)^2 = \left(\frac{\partial Y}{\partial y_1}\delta y_1\right)^2 + \left(\frac{\partial Y}{\partial y_2}\delta y_2\right)^2 + \ldots + \left(\frac{\partial Y}{\partial y_n}\delta y_n\right)^2 \tag{B.10}$$

The evaluation of the uncertainty of some slug flow parameters is described in detail in the following sections. Focus is put on the procedure *fixed-point data analysis* (section B.5.1), as it has, from the aforementioned two, the higher associated uncertainty (it requires the prediction of the positioning of bubble boundaries (as in Eq. (B.4)).

B.6.1 Bubble velocity

The velocity of the bubbles passing in a certain vertical coordinate (reference line) can be computed using Eq. (B.1), after rearranging according to Eq. (B.5):

$$U_i = \frac{z_{nose,i}^{t_{2,i}} - z_{nose,i}^{t_{1,i}}}{t_{2,i} - t_{1,i}} \frac{h_{cal.,m}}{h_{cal.,px}} \Leftrightarrow U = \frac{z_{nose,i}^{t_{2,i}} - z_{nose,i}^{t_{1,i}}}{\Delta t} \frac{h_{cal.,m}}{h_{cal.,px}} \tag{B.11}$$

According to the *general uncertainty analysis approach*, the uncertainty of the resulting variable (*U*) can be calculated as follows:

$$(\delta U)^2 = \left(\frac{\partial U}{\partial z_{nose}^{t_{2,i}}}\delta z_{nose}^{t_{2,i}}\right)^2 + \left(\frac{\partial U}{\partial z_{nose}^{t_{1,i}}}\delta z_{nose}^{t_{1,i}}\right)^2 + \left(\frac{\partial U}{\partial \Delta t}\delta \Delta t\right)^2 + \\ + \left(\frac{\partial U}{\partial h_{cal.,m}}\delta h_{cal.,m}\right)^2 + \left(\frac{\partial U}{\partial h_{cal.,px}}\delta h_{cal.,px}\right)^2 \tag{B.12}$$

where $\delta z_{nose}^{t_{1,i}}$, $\delta z_{nose}^{t_{2,i}}$, $\delta \Delta t$, $\delta h_{cal.,m}$ and $\delta h_{cal.,px}$ refer to the uncertainties of the corresponding measured variables. The five partial derivatives are expanded in the following equations. Notice that both sides of each expanded equation were divided by variable *U* or by its corresponding ratio (according to the reduction equation).

$$\left(\frac{1}{U}\right)\frac{\partial U}{\partial z_{nose}^{t_{2,i}}} = \left(\frac{\Delta t}{z_{nose,i}^{t_{2,i}} - z_{nose,i}^{t_{1,i}}}\frac{h_{cal.,px}}{h_{cal.,m}}\right)\frac{1}{\Delta t} = \frac{1}{\Delta z_{nose}} \tag{B.13}$$

$$\left(\frac{1}{U}\right)\frac{\partial U}{\partial z_{nose}^{t_{1,i}}} = \left(\frac{\Delta t}{z_{nose,i}^{t_{2,i}} - z_{nose,i}^{t_{1,i}}}\frac{h_{cal.,px}}{h_{cal.,m}}\right)\frac{-1}{\Delta t} = \frac{-1}{\Delta z_{nose}} \tag{B.14}$$

$$\left(\frac{1}{U}\right)\frac{\partial U}{\partial \Delta t} = \left(\frac{\Delta t}{z_{nose,i}^{t_{2,i}} - z_{nose,i}^{t_{1,i}}}\frac{h_{cal.,px}}{h_{cal.,m}}\right)\frac{-(z_{nose,i}^{t_{2,i}} - z_{nose,i}^{t_{1,i}})}{\Delta t^2} = \frac{-1}{\Delta t} \tag{B.15}$$

$$\left(\frac{1}{U}\right)\frac{\partial U}{\partial h_{cal.,m}} = \left(\frac{\Delta t}{z_{nose,i}^{t_{2,i}} - z_{nose,i}^{t_{1,i}}}\frac{h_{cal.,px}}{h_{cal.,m}}\right)\frac{(z_{nose,i}^{t_{2,i}} - z_{nose,i}^{t_{1,i}})}{\Delta t\, h_{cal.,px}} = \frac{1}{h_{cal.,m}} \tag{B.16}$$

$$\left(\frac{1}{U}\right)\frac{\partial U}{\partial h_{cal.,px}} = \left(\frac{\Delta t}{z_{nose,i}^{t_{2,i}} - z_{nose,i}^{t_{1,i}}}\frac{h_{cal.,px}}{h_{cal.,m}}\right)\frac{-(z_{nose,i}^{t_{2,i}} - z_{nose,i}^{t_{1,i}})h_{cal.,m}}{\Delta t\,(h_{cal.,px})^2} = \frac{-1}{h_{cal.,px}} \tag{B.17}$$

where Δz_{nose} is the pixel displacement of the nose of the bubble, between the consecutive instants t_1 and t_2 (when bubble passes the upper reference line). Eq. (B.12) can, thus, be rewritten in the form:

$$\left(\frac{\delta U}{U}\right)^2 = \left(\frac{\delta z_{nose}^{t_{2,i}}}{\Delta z_{nose}}\right)^2 + \left(-\frac{\delta z_{nose}^{t_{1,i}}}{\Delta z_{nose}}\right)^2 + \left(-\frac{\delta \Delta t}{\Delta t}\right)^2 + \left(\frac{\delta h_{cal.,m}}{h_{cal.,m}}\right)^2 + \left(-\frac{\delta h_{cal.,px}}{h_{cal.,px}}\right)^2 \tag{B.18}$$

By simplifying further, one obtains:

$$\left(\frac{\delta U}{U}\right)^2 = 2\left(\frac{\delta z_{nose}}{\Delta z_{nose}}\right)^2 + \left(\frac{\delta \Delta t}{\Delta t}\right)^2 + \left(\frac{\delta h_{cal.,m}}{h_{cal.,m}}\right)^2 + \left(\frac{\delta h_{cal.,px}}{h_{cal.,px}}\right)^2 \quad \text{(B.19)}$$

where δz_{nose} refers to the uncertainty of the bubble nose vertical coordinate, regardless of the time instant. Notice that the uncertainty of the latter variable is, obviously, similar, in different time instants. A final algebraic manipulation yields an expression for the relative uncertainty of the bubble velocity variable:

$$\frac{\delta U}{U}\left[\frac{\text{m}}{\text{m}}\right] = \sqrt{2\left(\frac{\delta z_{nose}}{\Delta z_{nose}}\right)^2 + \left(\frac{\delta \Delta t}{\Delta t}\right)^2 + \left(\frac{\delta h_{cal.,m}}{h_{cal.,m}}\right)^2 + \left(\frac{\delta h_{cal.,px}}{h_{cal.,px}}\right)^2} \quad \text{(B.20)}$$

Table B.1 shows the values of the parameters used in the computation of the uncertainty of bubble velocity variable.

Table B.1 – Values of parameters and absolute uncertainties in the calculation of bubble velocity uncertainty

parameter	units	value
Δz_{nose}	[pixel]	28.7
δz_{nose}	[pixel]	1
Δt	[s]	0.04
$\delta \Delta t$	[s]	1.25×10^{-4}
$h_{cal,m}$	[m]	0.18
$\delta h_{cal,m}$	[m]	0.0005
$h_{cal,px}$	[pixel]	221.5
$\delta h_{cal,px}$	[pixel]	2
$\delta U_B/U_B$	[(m/s) / (m/s)]	0.05019

Typical values of the parameters required for the computation of uncertainty were estimated as the average values of experiments with several superficial gas and liquid velocities (ranging from 0.1 m/s to 0.15 m/s). A typical bubble nose displacement of 28.7 pixels was considered. Moreover, 1 pixel uncertainty is considered in the determination of the bubble nose positioning (δz_{nose}; assumed equal to the maximum deviation between algorithm and operator predictions for bubble nose positioning, for a large number of frames). An image frame is grabbed every 0.04 s (25 Hz camera frequency; Δt=0.04s) with an uncertainty of 1.25×10^{-4} s (half of the frame exposure time: 1/4000 s; $\delta \Delta t$ = 0.5 x 1/4000 = 1.25×10^{-4} s). An 0.18 m calibration element was used with an uncertainty of 0.0005 m (half of the smallest scale interval: 0.001 m). A

2 pixel uncertainty is considered in the length of the calibration element, since its borders, in the calibration image, are defined by an operator). The aforementioned data results in a 5% uncertainty in the velocity of the bubbles.

B.6.2 Bubble length

The following equation provides the length of bubbles as a function of the position of their boundaries (the reduction equation; based on Eqs. (B.2) and (B.5)):

$$h_{b,i} = \left(z_{nose,i}^{t_{2,i}} - z_{rear,i}^{t_{2,i}} \right) \frac{h_{cal.,m}}{h_{cal.,px}} \Leftrightarrow h_b = \left(z_{nose} - z_{rear} \right) \frac{h_{cal.,m}}{h_{cal.,px}} \tag{B.21}$$

Following an approach similar to the one used for the bubble velocity variable, one obtains the uncertainty of h_b:

$$\left(\delta h_b\right)^2 = \left(\frac{\partial h_b}{\partial z_{nose}} \delta z_{nose} \right)^2 + \left(\frac{\partial h_b}{\partial z_{rear}} \delta z_{rear} \right)^2 + \left(\frac{\delta h_{cal.,m}}{h_{cal.,m}} \right)^2 + \left(\frac{\delta h_{cal.,px}}{h_{cal.,px}} \right)^2 \tag{B.22}$$

which yields, after rearrangement:

$$\frac{\delta h_b}{h_b} \left[\frac{\mathrm{m}}{\mathrm{m}} \right] = \sqrt{ \left(\frac{\delta z_{nose}}{h_b} \right)^2 + \left(\frac{\delta z_{rear}}{h_b} \right)^2 + \left(\frac{\delta h_{cal.,m}}{h_{cal.,m}} \right)^2 + \left(\frac{\delta h_{cal.,px}}{h_{cal.,px}} \right)^2 } \tag{B.23}$$

Table B.2 shows the values of the main parameters, considered in the computation of bubble length uncertainty.

Table B.2 – Values of parameters and absolute uncertainties in the calculation of bubble length uncertainty

parameter	units	value
δz_{nose}	[pixel]	1
δz_{rear}	[pixel]	5
h_b	[pixel]	225.4
$\delta h_b / h_b$	[m/m]	0.0245

A higher uncertainty is considered for the positioning of the rear of the bubble (5 pixels instead of 1 pixel). This figure was obtained taking the maximum deviation between algorithm and operator predictions for bubble rear positioning, for a large number of frames. A typical bubble

length value of 225.4 pixels is considered (as before, the average value of several experimental conditions). These uncertainties, together with those regarding the calibration procedure, result finally, in a 2.5% uncertainty, in the bubble length variable.

B.6.3 Slug length

The length of the liquid slugs can be computed by considering simultaneously Eqs. (B.1) -(B.4) and (B.5):

$$h_{s,i-1} = \underbrace{\left(z_{rear,i-1}^{t_{2,\,i-1}} - z_{nose,i}^{t_{2,i}} + (t_{2,i} - t_{2,i-1}) \frac{z_{nose,i-1}^{t_{2,i-1}} - z_{nose,i-1}^{t_{1,i-1}}}{\Delta t} \right)}_{h_s[\mathrm{px}]} \frac{h_{cal.,m}}{h_{cal.,px}} = h_s[\mathrm{px}] \frac{h_{cal.,m}}{h_{cal.,px}} \tag{B.24}$$

where h_s[px] refers to the length of the slug in pixel units. Following an approach similar to the one described in the previous sections one obtains an expression for the computation of the uncertainty of h_s, in real length units:

$$\frac{\delta h_s}{h_s}\left[\frac{\mathrm{m}}{\mathrm{m}}\right] = \frac{\sqrt{\left(\frac{h_{cal.,m}}{h_{cal.,px}}\right)^2 \left(\delta h_s[\mathrm{px}]\right)^2 + \left(\frac{h_s[\mathrm{px}]}{h_{cal.,px}} \delta h_{cal.,m}\right)^2 + \left(\frac{h_s[\mathrm{px}]\, h_{cal.,m}}{(h_{cal.,px})^2} \delta h_{cal.,px}\right)^2}}{h_s} \tag{B.25}$$

where δh_s[px] refers to the uncertainty of h_s in pixel units. This parameter is calculated as it follows:

$$\delta h_s[\mathrm{px}] = \sqrt{\left(\delta z_{rear}\right)^2 + \left(\delta z_{nose}\right)^2 + 2\left(U\delta t\right)^2 + 2\left(\frac{\Delta t_{bubble}}{\Delta t} \delta z_{nose}\right)^2 + \left(\Delta t_{bubble} \frac{\Delta z_{nose}}{\Delta t^2} \delta \Delta t\right)^2} \tag{B.26}$$

where Δt_{bubble} stands for the time interval required to have two consecutive bubble noses passing the reference line, δt is the uncertainty of variables $t_{2,i}$ and $t_{2,i-1}$ (obviously similar), and z_{rear} and z_{nose} refers to variables $z_{rear,i-1}^{t_{2,\,i-1}}$ and $z_{nose,i}^{t_{2,i}}$, respectively. Absolute uncertainties and typical parameter values, required for assessing the uncertainty of slug length variable, are shown in Table B.3:

As with Δt, variable t has an associated uncertainty equal to half of the typical exposure time (1/4000 s; δt = 0.5 x 1/4000 = 1.25x10^{-4} s). The uncertainties in the positioning of the bubble nose (δz_{nose}) and bubble rear (δz_{rear}) are estimated as in previous sections. The remaining typical parameters are estimated based on data of several experimental conditions. The aforementioned values result in a 7% uncertainty in the slug length variable.

Table B.3 – Values of parameters and absolute uncertainties in the calculation of slug length uncertainty

parameter	units	Value
δz_{rear}	[pixel]	5
δz_{nose}	[pixel]	1
δt	[s]	1.25E-04
$\delta \Delta t$	[s]	1.25E-04
Δt	[s]	0.04
Δt_{bubble}	[s]	1.121
Δz_{nose}	[s]	28.7
h_s	[pixel]	580.1
h_s	[m]	0.471
h_b	[pixel]	225.4
U	[pixel/s]	718.7
$\delta h_s/h_s$	[m/m]	0.0697

B.7 Conclusions

An image analysis technique for the study of continuous co-current gas-liquid slug flow, in vertical columns, is reported. The technique allows the straightforward measurement of several slug flow characteristics with almost no input from the operator (exception: calibration procedure). Specially built Illumination kit, together with image enhancements and custom made object tracking routines enable the thorough study of slug flow pattern, in continuous operation, by informing extensively on parameters such as bubble velocity, bubble length and liquid slug length.

The evaluation of the uncertainty associated to the parameters measured with the proposed technique is performed. The *general uncertainty analysis approach* is used to assess the propagation of the partial uncertainties (in bubble boundary definition, time measurement and calibration procedure) over the mentioned flow parameters. Relative uncertainties of about 5%, 2.5% and 7% were found, for bubble velocity, bubble length and liquid slug length, respectively. These low uncertainties support and advise the further implementation of image analysis techniques, as an important tool for the study of slug flow characteristics.

B.8 Appendix – On the threshold value

The conversion of a given greyscale image to binary mode requires the definition of the threshold value (see section B.4). Furthermore, the level of accuracy of the resulting binary image (i.e. the measure of how well the binary image represents the original greyscale image) is related, obviously, to the luminosity chosen for threshold. Consider Figure B.10a showing a frame of a slug flow experiment, right before the conversion to binary mode. The grey level profile along the middle cross-section of the frame is shown in Figure B.10b. The bubble contour (brighter areas of

the image) can easily be located in the grey level profile (two peaks of the curve). Furthermore, one can spot the gas-liquid interface by analysing the variation of the grey level index, namely around the main peaks of the profile. Thus, the gas-liquid interface can be detected by the steep variation of the grey level index, from about 0.2 to about 0.5 (Figure B.10b). It is interesting, however, to assess the sensitivity of the measured parameters (U, h_b and h_s) to the threshold value. For that purpose a sensitivity test was performed in which those parameters were obtained for a set of 10 Taylor bubbles, using different threshold values (0.25, 0.35 and 0.45). The parameters obtained were compared statistically, the results of which are shown, in brief, in Table B.4. The estimates of each measured parameter, obtained using the different thresholds, are fairly similar. Moreover, the standard deviation of the different estimates reaches about 1.2%, 1.3% and 1.9% of the corresponding average (for U, h_b and h_s, respectively; see Table B.4). This indicates that the estimates of these parameters are not particularly sensitive to the threshold value chosen for the binary conversion procedure, as long as it is in the range 0.25-0.45. As mentioned in section B.4, a threshold value of 0.35 was used for most experiments.

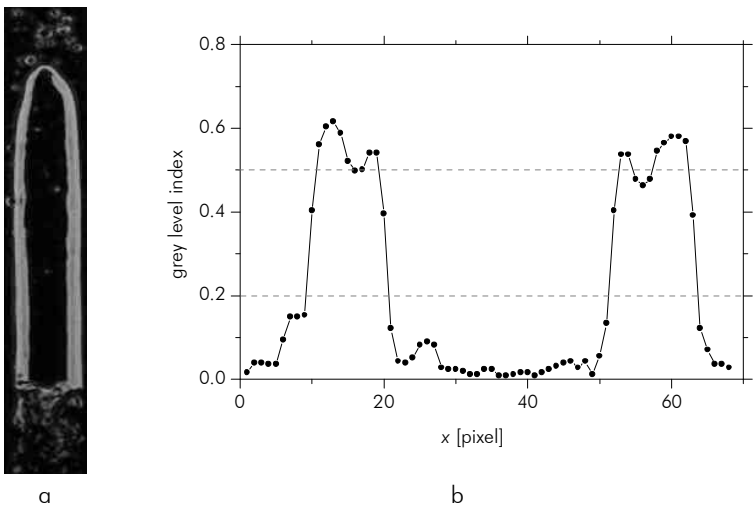

Figure B.10 – (a) Experimental frame before conversion to binary mode; (b) grey level profile along a cross-section of the experimental frame

Table B.4 – Standard deviation of the estimates of bubble velocity, bubble length and liquid slug length, obtained using threshold values of 0.25, 0.35 and 0.45 (for ensemble of 10 Taylor bubbles)

parameter	Stand. Dev. [% of avg.]
U	1.2
h_b	1.3
h_s	1.9

B.9 Acknowledgments

The authors gratefully acknowledge the financial support of Fundação para Ciência e a Tecnologia through project POCTI/EQU/33761/1999 and scholarship SFRH/BD/11105/2002. POCTI (FEDER) also supported this work via CEFT.

B.10 References

Hasanein, H. A., Tudose, G. T., Wong, S., Malik, M., Esaki, S. and Kawaji, M., 1996. Slug flow experiments and computer simulation of slug length distribution in vertical pipes. AIChE Symposium Series 92(310): 211-219.

Pinto, A. M. F. R., Coelho Pinheiro, M. N. and Campos, J. B. L. M., 2001. On the interaction of Taylor bubbles rising in two-phase co-current slug flow in vertical columns: Turbulent wakes. Exp. Fluids 31(6): 643-652.

Polonsky, S., Shemer, L. and Barnea, D., 1999. The relation between the Taylor bubble motion and the velocity field ahead of it. Int. J. Multiphas. Flow 25: 957-975.

Sousa, R. G., Pinto, A. M. F. R. and Campos, J. B. L. M., 2006. Effect of gas expansion on the velocity of a Taylor bubble: PIV measurements. Int. J. Multiphas. Flow 32: 1182-1190.

The MathWorks, I. (2002). Help files of "MATLAB: the language of technical computing".

Van Hout, R., Barnea, D. and Shemer, L., 2001. Evolution of statistical parameters of gas-liquid slug flow along vertical pipes. Int. J. Multiphas. Flow 27(9): 1579-1602.

Van Hout, R., Barnea, D. and Shemer, L., 2002. Translational velocities of elongated bubbles in continuous slug flow. International Journal of Multiphase Flow 28(8): 1333-1350.

C Slug Flow Simulator – A tool for the teaching and learning two-phase slug flow regime in vertical columns[8]

C.1 Abstract

As a step towards the learning-oriented approach, an attempt has been made to implement the use of a slug flow simulator (SFS), in the context of research assignments complementing traditional engineering lectures. This approach has been pursued on the Master course *Theoretical and Applied Fluid Mechanics,* at the Engineering Faculty of Porto University (Portugal). The goal is to engage students proactively in the learning process, so as to enrich their learning experiences and nourish knowledge retention. The main features of the simulator are presented (main windows, input parameters and monitored variables) and potential benefits of its use are discussed. A series of tasks with increasing complexity are proposed, covering both undergraduate and graduate levels.

[8] Based on the paper by T. Sotto Mayor, A.M.F.R. Pinto and J.B.L.M. Campos, accepted for publication in International Journal of Engineering Education (IJEE)

C.2 Introduction

Slug flow, a complex and irregular two-phase flow, occur in a variety of industrial and natural contexts. Some examples are pipeline transportation of hydrocarbons, chemical and nuclear reactors, geothermal power plants, membrane and crystallization processes, or even natural volcanic phenomena (such as the Stromboli volcano). Such a flow pattern is characterized by the intermittent and transient movement of elongated bullet-shaped gas bubbles (known as Taylor bubbles), separated by more or less aerated liquid plugs (known as slugs). The research on this topic already spans decades (Dumitrescu (1943), Nicklin et al. (1962), Collins et al. (1978), Fabre and Liné (1992), Pinto et al. (2001), Van Hout et al. (2001), Sotto Mayor et al. (2006a), Sotto Mayor et al. (2006b)) but several points still remain open, fuelling the curiosity of the scientific community.

Several Engineering Courses at both undergraduate and graduate level encompass two-phase flows (in particular slug flow). Subjects like Fluid Mechanics or Heat Transfer, taught to every Civil, Chemical or Mechanical Engineering student, include that topic. It is, thus, an issue traversing the background education of any engineering student.

The shift from the teaching-oriented to the learning-oriented paradigm, a must for the future of engineering education as stressed by Melsa (1997), advises teaching strategies that favour student involvement in the learning process. Student engagement promotes questioning, class attendance, grades and lasting interest on subjects (McKeachie (1994)). Hands-on activities are, undoubtedly, a potential promoter of student engagement. They enhance student participation in the learning process, along with augmenting student's self-esteem. Kresta (1998) reports 30-80% increase in the attendance of fluid mechanics seminars after implementation of hands-on demonstrations. Such proactive activities favour pear-to-pear interaction, teamwork, and cooperative strategies, valuable assets in real work environments (Melsa (1997)).

The advent of fast and robust computational platforms enabled the development of a variety of numerical and visualization tools (simulators) covering different topics. Computational fluid dynamics (CFD), for instance, is a field that profited greatly from the evolution of informatics systems. But even more confined approaches, regarding the simulation of specific phenomena/events, benefited from computational evolution. For instance, Higuchi (2001) reports several web-based simulations on fluid mechanics and aerodynamics. Moreover, a number of other contributions covering different topics exist (e.g. Palanki and Kolavennu (2003), Ramos et al. (2005)). Besides the numerical information, all these approaches provide the means to visualize the evolution of phenomena/events, so as to build up mental image representations. According to

Kolari and Savander-Ranne (2004), the visualization promotes students' apprehension and comprehension. It provides relevant representations of issues and helps students form visual interpretations of what concepts and abstractions mean. Simulators can therefore play a relevant role in lecture-like environments. While they bridge the traditional lectures and the hands-on real experiments, they also constitute a step towards the learning-oriented approach. Moreover, they make it possible to overcome some of the economical and portability issues often accounted for in real experiments.

The use of a user-friendly slug flow simulator (SFS) in a context of research assignments complementing traditional lectures is discussed in this chapter. Possible approaches and advantages of the use of such tool are addressed. The simulator is currently used in the Master's course *Theoretical and Applied Fluid Mechanics,* at the Engineering Faculty of Porto University.

C.3 The simulator

The learning-oriented approach, with its emphasis on student engagement, has been implemented in the Master's course *Theoretical and Applied Fluid Mechanics,* at the Engineering Faculty of Porto University. The traditional theoretical and laboratory lectures are complemented by several small research assignments based on the use of several simulation tools. One of such assignments, namely on the topic slug flow pattern, is based on the use of a slug flow simulator (SFS) developed by Sotto Mayor et al. (2006b) for vertical columns. The following sections outline the main features of the SFS. The aim is to give a general idea of the approach pursued for the development of a simulation tool on slug flow pattern. Other phenomena (two-phase flow or other) could be addressed in a similar way.

C.3.1 "Windows" to the phenomena

In order to study the evolution of the slug flow pattern along the column a set of "windows" to the phenomenon was developed. They are basically a set of horizontal and vertical "watchers" allowing the quantitative description of the flow pattern. Horizontal "watchers" compile two types of data: instantaneous and global. Instantaneous data (Figure C.1b) captures the characteristics of the bubbles inside the column, in a specific instant of time; it freezes the bubble motion and enables a detailed analysis of every bubble parameter (length, velocity and distance). Global data gather information on the bubbles crossing a certain column vertical coordinate during a slug flow experiment/simulation (Figure C.1a); it promotes a global assessment of the flow characteristics in a specific time interval.

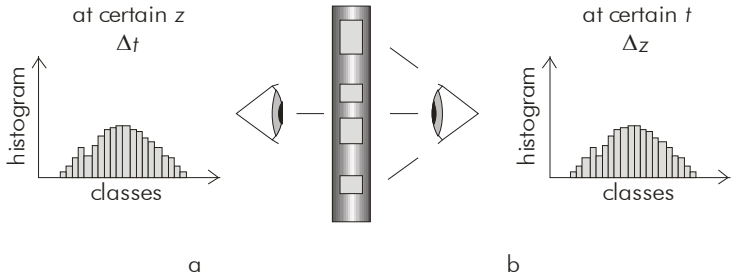

Figure C.1 – Example of the data compiled by horizontal "watchers": (a) global column analysis; (b) instantaneous column analysis

The *Slug Flow Simulator* allows numerous horizontal watchers (global type) to be established at any column vertical coordinate, with two different reference boundaries: bubble nose and bubble rear. The latter is relevant when studying long bubbles.

Vertical "watchers" focus on the coalescence inside the column. By counting the coalescence events occurring below, vertical "watchers" compile data describing the coalescence along the vertical column coordinate. An example of the output of this analysis is shown in Figure C.2. Several coalescence zones can be defined, featuring different occurrences of coalescence events (intense, average, rare and very rare). Direct analysis of this type of chart enables determination of the *Flow Stability Height* parameter, the vertical column coordinate above which almost no coalescence is observed.

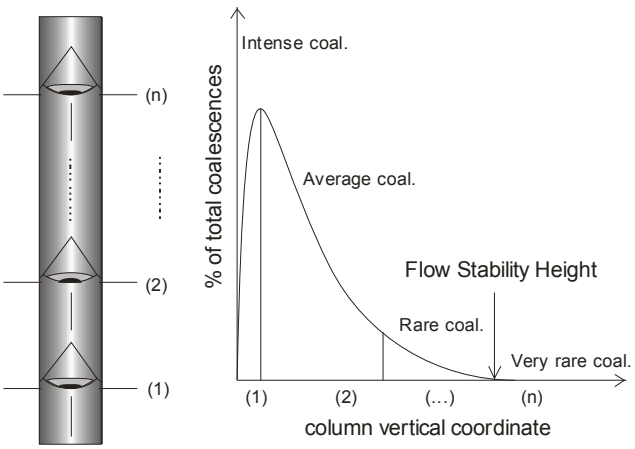

Figure C.2 – Example of the data compiled by vertical "watchers"

C.3.2 Main windows

The various windows of the slug flow simulator include the input of data (Figure C.3), the customization of the simulator (Figure C.4), the output of a slug flow simulation (Figure C.5), the input of simulations for comparison (Figure C.6) and the output of simulations for comparison (Figure C.7). Several parameters can be defined or controlled in each of these windows. The following sections describe this in more detail.

Input Data window

The main parameters regarding the simulation are defined in the Input Data window. Some examples are: column characteristics (height, diameter, and exit configuration), superficial gas and liquid velocities (U_G and U_L), fluid properties, number of slug units (sets of bubble + liquid slug) and type of distributions at the column inlet (for liquid slug length and U_G). Some other parameters related to the numerical simulation and resulting data are also defined here. The time increment of the simulation, the number and positioning of the horizontal watchers, and the time intervals for updating charts, grids and 2D flow picture are some examples. Note that by altering these time intervals the students can change the simulation rate. For instance, the simulation rate can be slowed down by setting the update of the 2D flow picture at very short time intervals.

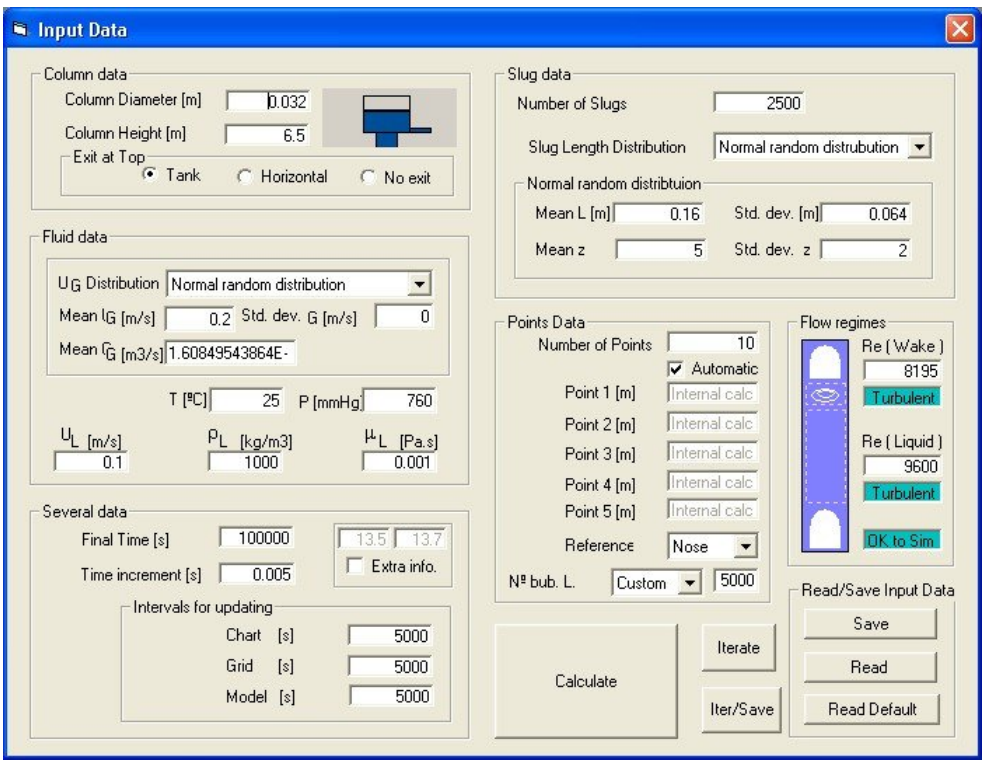

Figure C.3 – *Input Data* window

Depending on the specification of the superficial gas velocity (in terms of pressure), two different simulations can be performed: a straightforward simulation (*calculate* button) if U_G is given at the column inlet pressure, or an iterative procedure (*iterate* button) if U_G is given at the atmospheric outlet pressure. In this latter, several simulations must run sequentially until the required U_G is obtained at the outlet. More details on this subject can be found in Sotto Mayor et al. (2006b).

Options window

Several parameters concerning the numerical simulation and format of the output results are defined in the Options window. Some examples are: the phenomena acknowledged in the simulation (existence or absence of coalescence and gas expansion), the number of classes in the resulting histograms and the parameters whose variation along time is to be analysed in more detail.

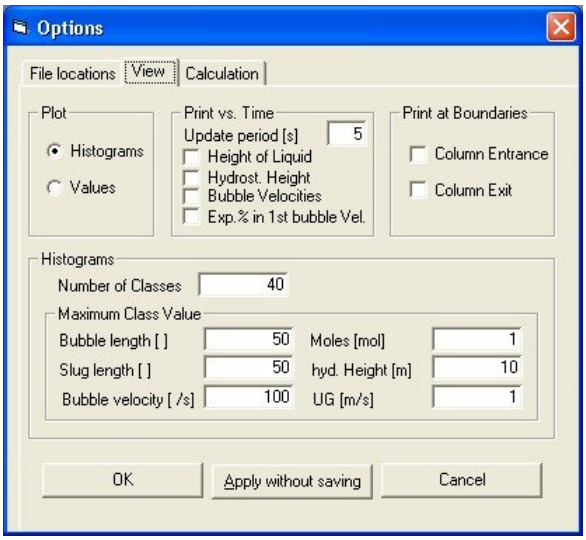

Figure C.4 – *Options* window (*View* Tab)

Simulation Results window

Two types of data visualization can be found in the *Simulation Results* window: graphical representation of several parameters and detailed numerical description of each parameter. The first type includes, for instance, charts and histograms of bubble velocity, bubble length and liquid slug length, or charts of coalescence plotted against the vertical coordinate of the column. Additionally, the 2D flow picture (on the lower right corner of Figure C.5), updated incrementally at the time interval defined in the *Input Data* window, enables a deeper and more realistic assessment of the development of the slug flow pattern. The second type of data visualization includes a set of 8 sheets featuring several numerical data describing the bubbles inside the column (regarding for

instance positioning, velocity and distance) and their motion over time. The content of these sheets is:

Sheet 1 – distributions at the inlet (characteristics of bubbles)

Sheet 2 – characteristics of bubbles inside the column at several points in time

Sheet 3 – characteristics of bubbles passing through several column coordinates

Sheet 4 – histograms at several column coordinates

Sheet 5 – detailed description of input data

Sheet 6 – reference data (such as experimental data) for comparison

Sheet 7 – evolution of coalescence events along the column

Sheet 8 – evolution of several flow parameters over time

The content of these sheets can be directly copied into any spreadsheet software for further processing.

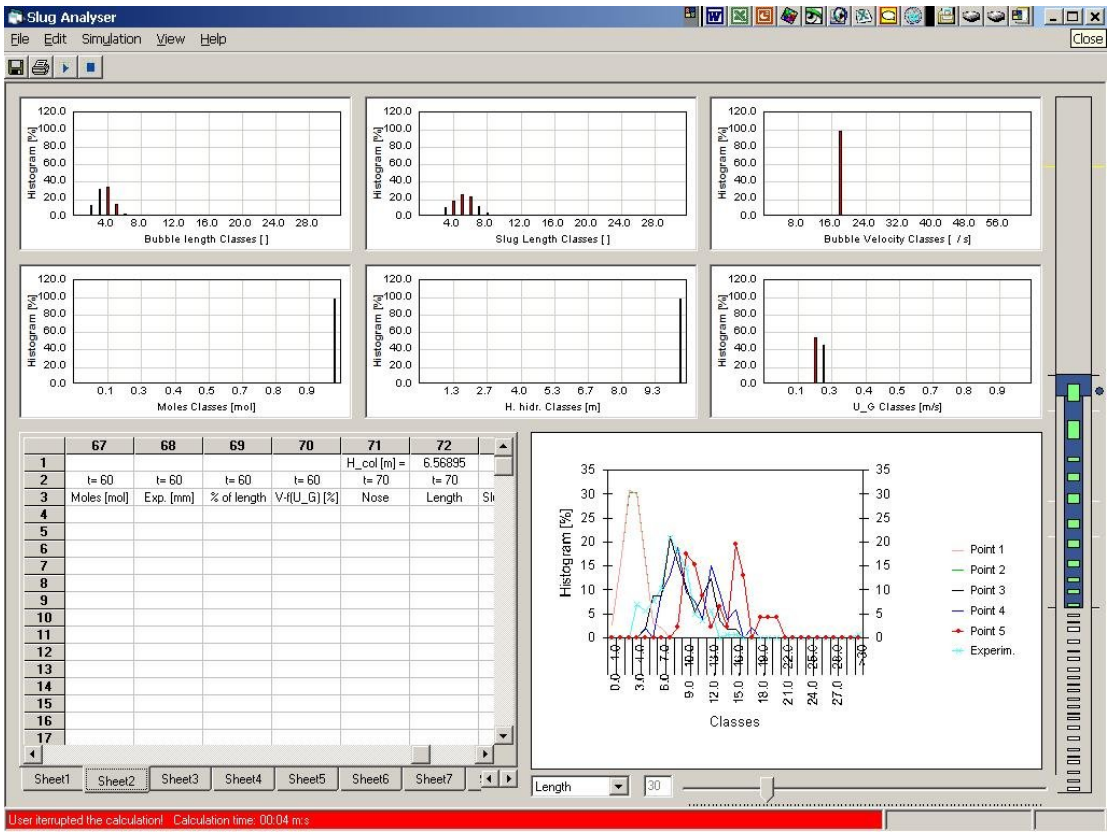

Figure C.5 – Main results of simulation routines

Compare Simulation Results window

After running several simulations, one can compare the resulting data in a straightforward way by using the *Slug Flow Simulator* comparing routines (Figure C.6). These allow an enormous

reduction in the time required for analysis since the data comparisons are automatically compiled and shown according to the aforementioned visualization strategies (numerically and graphically). Note that, besides the numerical information displayed in the several sheets of the output window, comparative study of the evolution of the distributions along the column is further boosted by having the mouse scroll wheel controlling the column vertical coordinate (P1, P2, …) displayed in the charts (as in Figure C.7, displaying data compiled at the 5th horizontal "watcher", P5).

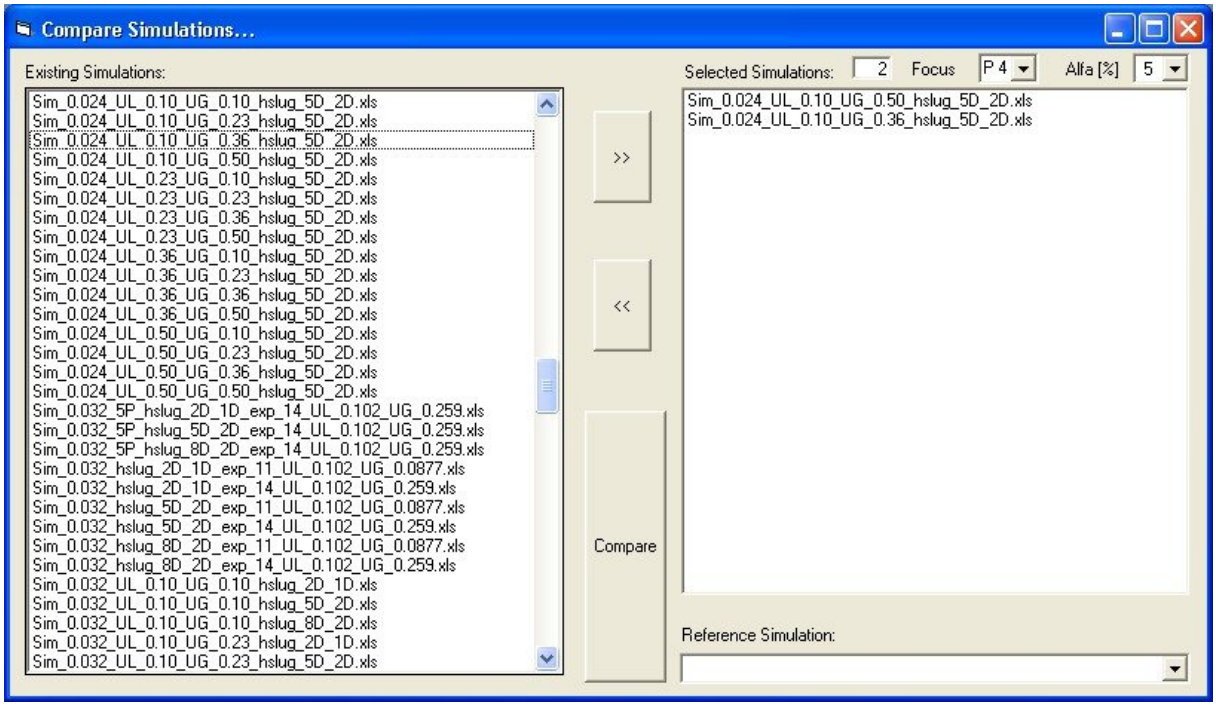

Figure C.6 – *Compare Simulations* window

This means, that by a single movement of the mouse scroll wheel, students can directly observe the evolution of the distributions of different simulation along the vertical coordinate. This possibility not only speeds up the comparisons but also promotes deeper comprehension of the dynamic evolution of the slug flow pattern.

As for the *simulation results* window, the numerical data resulting from the comparison of several simulations (shown in the sheets) can be easily exported into any spreadsheet software (such as Microsoft® Excel) for further processing.

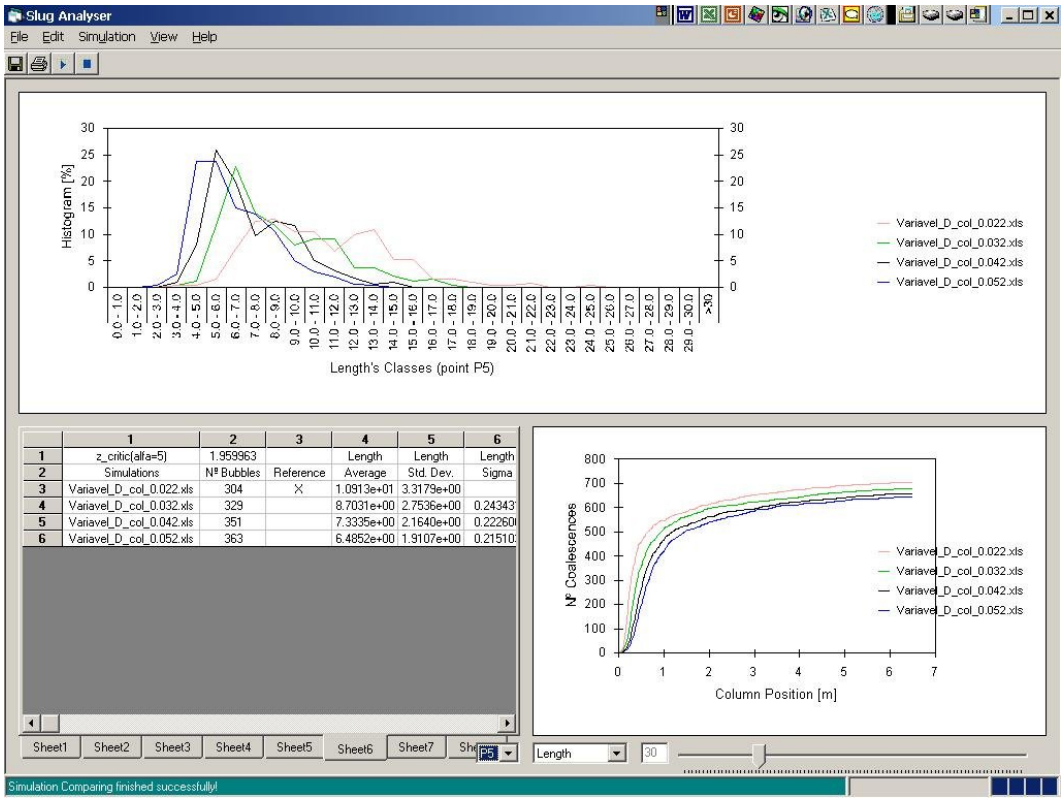

Figure C.7 – Main results of comparing routines

C.4 The approach

C.4.1 Research assignment – Series of tasks using the SFS tool

As already mentioned, several small research assignments based on the use of simulation tools are given to students as a complement to theoretical and laboratory classes. The use of a simulator (SFS) to demonstrate the slug flow pattern is discussed here. After lecturing students on the theoretical fundamentals governing such a flow pattern and introducing them to a real slug flow facility (6.5 m long/high; see Sotto Mayor et al. (2006a) for more details) a series of tasks with increasing complexity are given to the students. The aim is to go from a "worked-out" example (i.e. an example whose solution is shown worked out step-by-step, following Simon (1998)) to an "open" problem (an example whose solution is to be decided and investigated by the students). The tasks are summarized below.

1) To simulate slug flow pattern for a given set of input parameters;

A set of input parameters such as the ones in Figure C.3 are introduced in the SFS code. Upon completion of the simulation, the output data are compared with pre-obtained simulation results. Any difficulties arising while using the simulator should be overcome in this step.

2) To understand the use of histograms and the coalescence curves for the description of the flow pattern characteristics;

Different sets of input parameters can be tested freely by students. Changes over bubble length, slug length and bubble velocity are recorded by "reading" the histogram and coalescence curves.

3) To learn how to compare different simulation data using simulator internal routines;

After selecting the simulations to be compared in the SFS window shown in Figure C.6, their systematic comparison is performed using simulator internal routines. Figure C.7 gives an example of the resulting data (regarding, in this case, simulations for increasing internal diameters of the column).

4) To estimate adequate time increment and number of bubbles for representative flow pattern simulation;

The aim is for students to understand the notions of a grid test and a representative sample of bubbles. Regarding grid testing, several simulations with decreasing time increment are compared in order to determine the highest time increment producing accurate results. Using a similar approach, several simulations with increasing number of bubbles are compared in order to determine the smallest number of bubbles needed to obtain representative results. Figure C.8 shows an example of the latter.

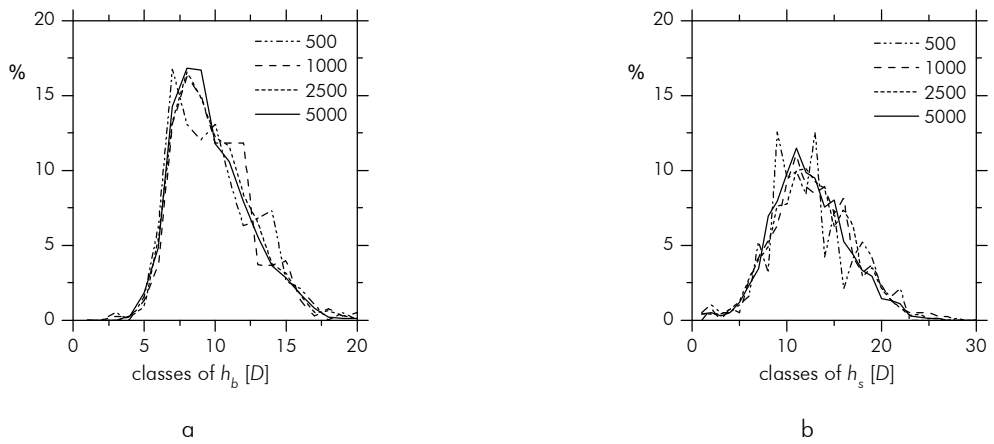

Figure C.8 – Frequency distribution curves of (a) bubble length and (b) slug length, for simulations with 500, 1000, 2500 and 5000 number of bubbles; 0.032 m ID; $U_L \approx 0.1$ m/s, $U_G \approx 0.26$ m/s

5) To study the effect of several parameters over the flow pattern;

The effect on the flow pattern of column length and superficial gas and liquid velocities is described. The students are expected to use the slug flow simulator systematically in order to determine the extent of the influence of each of these parameters on the flow pattern characteristics. Several simulations differing only on a single parameter can be prepared, and the resulting data can be compared using the custom-made routines. Figure C.9 displays bubble length data gathered under this strategy (regarding, in this case, the superficial gas velocity, U_G)

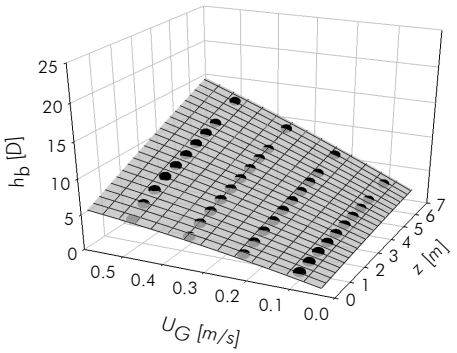

Figure C.9 – Evolution along the column of the most probable bubble length, for simulations with $U_L \approx 0.23$ m/s and $U_G \approx 0.10$, 0.23, 0.36 and 0.50 m/s

6) To study the influence of inlet parameter distributions on the results along the column;

The influence of initial distributions (of h_s for instance) on the evolution of the flow pattern along the column is studied. Comparing simulations featuring different inlet slug length distributions, students are expected to observe that initial differences tend to dissipate along the column. Figure C.10 illustrates this approach.

Figure C.10 – Frequency distribution curves of slug length at (a) inlet and (b) outlet (vertical coordinate: 5.4 m), for simulations with different inlet average slug length (2*D*, 5*D* and 8*D*); $U_L \approx 0.1$ m/s, $U_G \approx 0.26$ m/s; 0.032 m ID

7) To study the influence of different coalescence correlations on the evolution of the flow characteristics;

Several bubble-to-bubble interaction correlations are tested by students in order to assess the influence of interaction phenomena on the evolution of the flow. Using, for instance, correlations implying diverse bubble-to-bubble interaction for different distances (h_s), a chart like the one shown in Figure C.11 can be obtained, showing the evolution of bubble length and slug length parameters along the column. This approach highlights the influence of coalescence events in the evolution of these parameters.

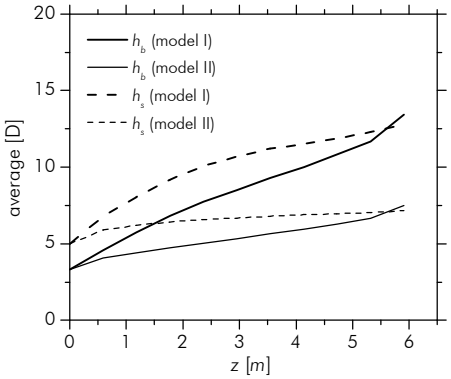

Figure C.11 – Evolution of bubble length and liquid slug length along the column, for simulations with different bubble-to-bubble interaction correlations; column height: 6.5 m; internal diameter: 0.032 m; $U_L \approx 0.1$ m/s and $U_G \approx 0.2$ m/s

The first three steps, while simple to accomplish, provide students with a basic understanding of the simulator and its features/outputs. The remaining steps aim at a deeper understanding of the flow pattern characteristics. Items 4 and 5 can be presented at undergraduate level, as they cover relatively simple notions/approaches. Items 6 and 7 should be presented at graduate level since require a more independent attitude and abstract approach from students. Regardless of the educational level, students' findings should be presented and discussed in writing as well as orally.

C.4.2 Remarks regarding the underlying pedagogy

Several authors argue that the majority of engineering students are visual learners (e.g. Kolari and Savander-Ranne (2002), Mourtos and Allen (2003)). This stresses the importance of integrating visualization into the process of teaching/learning (Kolari and Savander-Ranne (2004)). The use of the SFS tool for the study of slug flow is an attempt to address this.

Following the four-stage learning model proposed by Kolb (1984), the traditional theoretical lectures concern *Reflective Observation*. Ideally, it would be better to have the *Active Experimentation* and *Concrete Experience* stages grounded in real hands-on experiments. However, a 6.5 m height experimental facility poses serious scale, time and functional difficulties if experiments are to be performed by students, even under supervision. The use of a slug flow simulator is therefore the best feasible solution. While it overcomes the aforementioned difficulties it provides a *Concrete Experience* on the topic and enables *Active Experimentation* by the students. The oral discussions following students' presentations of the research assignment findings facilitate *Abstract Conceptualization*. From theoretical lectures to research assignments (pseudo hands-on experiments) and subsequent discussions, an attempt is made to cover all four stages of Kolb's learning model and, thus, to stimulate students' learning experiences. Stice (1987) reports considerable increase in the students' knowledge retention when Kolb's four stages are present in a pedagogical approach (90% retention), in comparison to when only the *Abstract Conceptualization* stage is present (20% retention).

C.4.3 Advantages of the research assignment based on the SFS tool

The advantages of implementing research assignments based on the use of simulators are twofold. There are pedagogical and practical benefits. Such student involvement is generally believed to enhance learning and skill development. Assuredly, the students' critical thinking and their ability to analyse and solve problems are substantially enhanced by a proactive and engaged attitude. Moreover, the necessary teamwork stimulates the development of cooperative strategies, which are ever more important in the increasingly competitive real work environment. Additionally, by diversifying the learning channels/opportunities, different learning styles can be accommodated and encouraged. It is also very important to support students as they progress from a simple worked-out problem to increasingly more complex problems and this helps to develop self-confidence, thus fostering the methodical approach one hopes to inspire in engineering students.

But there are other benefits of this via-simulation approach, particularly elimination of the cost, time and physical constraints related to experimental study of slug flow. Large and often expensive facilities, which usually constitute a serious obstacle to implementing slug flow experiments in laboratory classes, can be avoided. Slow-paced experiments (for instance with low superficial gas and liquid velocities) can be squeezed into one-hour lessons by avoiding the real-time conditions of the experimental work. Furthermore, the absence of physical constrains allows for broadening the operating conditions to ranges that would otherwise be impossible (for instance comprising a very long test column), thus enabling the study of eventual asymptotical behaviours.

And finally, by significantly reducing the time required for analysing results, a simulation tool like SFS avoids students' natural antipathy towards dense numerical data.

C.4.4 Outcome of the approach

The students' response to the use of SFS code was very positive. The motivation and engagement of all the research teams (groups of 3 or 4 students, in classes of up to 10 students) culminated in dynamic presentations/discussions on the topic. We believe that a deeper and lasting understanding of the flow governing rules emerged from this approach, which has stimulated us to widen the range of engineering topics addressed in this way.

C.5 Final remarks

This paper describes an attempt to complement traditional lectures with small research assignments based on the use of simulation tools. The use of the SFS code in the context of a research assignment on slug flow should be seen as more than a simple simulation task. All activities contained in the approach address different aspects of the learning process and aim at reinforcing students' learning experiences. It is an approach that could also be applied to other engineering topics at both undergraduate and graduate level.

C.6 Notation

Roman symbols

D	column diameter	[m]
h_b	bubble length	[m]
h_s	liquid slug length	[m]
t	time	[s]
U_G	superficial gas velocity	[m/s]
U_L	superficial liquid velocity	[m/s]
z	vertical coordinate	[m]

Greek symbols

Δt	time interval	[s]
Δz	column length interval	[m]

C.7 Acknowledgments

The authors gratefully acknowledge the financial support of Fundação para Ciência e a Tecnologia through project POCTI/EQU/33761/1999 and scholarship SFRH/BD/11105/2002. POCTI (FEDER) also supported this work via CEFT.

C.8 References

Collins, R., De Moraes, F. F., Davidson, J. F. and Harrison, D., 1978. The Motion of Large Gas Bubble Rising Through Liquid Flowing in a Tube. J. Fluid Mech. 28: 97-112.

Dumitrescu, D. T., 1943. Stromung an Einer Luftblase im Senkrechten Rohr. Z. Angeus. Math. Mec. 23: 139-149.

Fabre, J. and Liné, A., 1992. Modeling of two-phase slug flow. Ann. Rev. Fluid Mech. 24: 21-46.

Higuchi, H., 2001. Multi-level, interactive web-based simulations to teach fluid mechanics and aerodynamics from middle school to college levels. Int. J. Eng. Educ. http://www.ijee.dit.ie/OnlinePapers/WebBasedSimulationFiltered.html.

Kolari, S. and Savander-Ranne, C., 2002. Total integration and active participation in the learning process in textile engineering education. World Transactions on Engineering and Technology Education 1(2): 261- 274.

Kolari, S. and Savander-Ranne, C., 2004. Visualization promotes apprehension and comprehension. Int. J. Eng. Educ. 20(3): 484-493.

Kolb, D. (1984). Experiential learning: experience as the source of learning and development, Englewood Cliffs, N.J.: Prentice Hall cop.

Kresta, S. M., 1998. Hands-on demonstrations: an alternative to full scale lab experiments. J. Eng. Educ 87(1): 7-9.

McKeachie, W. J. (1994). Teaching tips: strategies, research, and theory for college and university teachers. Lexington, Massachusetts, DC Heath and Company.

Melsa, J. L., 1997. Trends in the engineering education in the USA. Comput. Control. Eng. J.: 209-214.

Mourtos, N. J. and Allen, E. L. (2003). Assessing the effectiveness of a faculty instructional development programme, part 2: teaching and learning styles. Proceedings of 6th UICEE Annual Conference on Engineering Education, Cairns, Australia.

Nicklin, D. J., Wilkes, J. O. and Davidson, J. F., 1962. Two-phase flow in vertical tubes. Trans. Inst. Chem. Engrs. 40: 61-68.

Palanki, S. and Kolavennu, S., 2003. Simulation of control of a CSTR process. Int. J. Eng. Educ. 19(3): 398-402.

Pinto, A. M. F. R., Coelho Pinheiro, M. N. and Campos, J. B. L. M., 2001. On the interaction of Taylor bubbles rising in two-phase co-current slug flow in vertical columns: Turbulent wakes. Exp. Fluids 31(6): 643-652.

Ramos, N. M. M., Delgado, J. M. P. Q. and De Freitas, V. P., 2005. Modeling and solving building physics problems using Matlab/Simulink. Int. J. Eng. Educ. 21(5): 784-789.

Simon, H., 1998. What we know about learning. J. Eng. Educ 87(4): 343.

Sotto Mayor, T., Ferreira, V., Pinto, A. M. F. R. and Campos, J. B. L. M., 2006a. Hydrodynamics of gas-liquid slug flow along vertical pipes in turbulent regime. An experimental study. Submitted to International Journal of Heat and Fluid Flow.

Sotto Mayor, T., Pinto, A. M. F. R. and Campos, J. B. L. M., 2006b. Hydrodynamics of gas-liquid slug flow along vertical pipes in turbulent regime. A simulation study. Submitted to Chemical Engineering Research and Design.

Stice, J. E., 1987. Using kolb's learning cycle to improve student learning. Eng. Educ. 77(5): 291-296.

Van Hout, R., Barnea, D. and Shemer, L., 2001. Evolution of statistical parameters of gas-liquid slug flow along vertical pipes. Int. J. Multiphas. Flow 27(9): 1579-1602.